Departamento de
Electrónica e Sistemas
UNIVERSIDADE DA CORUÑA

TESE DE DOUTORAMENTO

Testbed Design for Wireless Communications Systems Assessment

Autor **José Antonio García Naya**

Directores **Luis Castedo Ribas**, **Markus Rupp**

2010

D. Luis Castedo Ribas e D. Markus Rupp

CERTIFICAN

Que a memoria titulada "Testbed Design for Wireless Communications Systems Assessment" foi realizada por D. José Antonio García Naya baixo a nosa dirección no Departamento de Electrónica e Sistemas da Universidade da Coruña e remata a Tese que presenta para optar ó grao de Doutor.

A Coruña, xuño de 2010.

Asdo.: Dr. Luis Castedo Ribas
Director da Tese Doutoral
Catedrático de Universidade
Departamento de
Electrónica e Sistemas
Universidade da Coruña

Asdo.: Dr. Markus Rupp
Director da Tese Doutoral
Univ. Prof. Dr.-Ing.
Institute of Communications
and Radio-Frequency Engineering
Vienna University of Technology

Tese Doutoral: Testbed Design for Wireless Communications Systems Assessment

Autor: D. José Antonio García Naya

Directores: Dr. Luis Castedo Ribas e Dr. Markus Rupp

Data de defensa: 9 de setembro de 2010

Tribunal

Presidente: José Tomás Entrambasaguas Muñoz

Vogal 1:   Ana García Armada

Vogal 2:   Andreas Peter Burg

Vogal 3:   Sebastian Caban

Secretario: Carlos José Escudero Cascón

A meus pais e a Belén

Acknowledgements

First of all, I want to thank my professor Luis Castedo for his support on a scientific, financial and personal basis. This work would never have been possible without his effort. I also want to thank my co-advisor Dr. Markus Rupp for accepting me as a visiting student at the Vienna University of Technology. I owe him the possibility of experimenting with the Vienna MIMO Testbed, learning about measurements and, above all, enjoying the very nice views of downtown Vienna from the rooftops of the university buildings.

A large part of this work – summarized in Chapters 7 and 8 – would not have been possible without the invaluable collaboration and friendship of Sebastian Caban and Christian Mehlführer, from the Vienna University of Technology. They, together with the people from the MIMO-Lab (Aamir Habib, Dasa Bosanska, Michal Šimko, and Qi Wang), created an excellent atmosphere when I was far from home.

I also want to thank to all the members of the GTEC group at the University of A Coruña for their endless support on a personal as well as on a scientific basis. I owe much of this work to Francisco J. Vázquez and Miguel González (Chapters 5 and 6), Paula Castro (Chapter 9), Adriana Dapena (Chapter 4), Carlos Escudero, Óscar Fresnedo (Chapter 5) and, especially, to the initial testbed team: Luis Castedo, Miguel González, Héctor J. Pérez (Chapter 4), and Tiago Fernández. I would like as well to thank our secretary Cristina Ribao, who was always willing to help me with the tedious paperwork. Finally, my thanks to my colleague and friend Javier Rodas (Chapter 9) for helping me during the endless nights and weekends working in the CITIC lab.

My gratitude also goes to the people from the GTAS group at the University of Cantabria, Ignacio Santamaría, David Ramírez, Jesús Ibáñez, Jesús Pérez, and Javier Vía, for their collaboration in the results included in Chapter 4.

The work in Chapter 5 would not have been possible without the collaboration of Dr. Javier García Frías, from the University of Delaware.

I have to especially thank Belén, because of her infinite patience and invaluable support. I am absolutely sure I could not have completed this work without her.

Last, but not least, I would like to thank all my friends, especially Manu, who was always willing to help me overcome difficult situations during my life.

Finally, and most importantly, I want to thank my family, especially my mother Manuela and my father José Antonio.

Resumo

Dende que Marconi levou a cabo a primeira transmisión sen fíos en 1894, a investigación experimental estivo sempre vinculada ás comunicacións sen fíos. Hoxe en día, a dita investigación apóiase en simulacións por ordenador que soamente reflicten o contorno de simulación en vez do escenario real en que operan os sistemas sen fíos. Polo tanto, é axeitado avaliar os sistemas de comunicacións sen fíos en escenarios realistas, mantendo, ó mesmo tempo, o esforzo requirido en termos razoables. Entre as diferentes estratexias apropiadas para levar a cabo a devandita avaliación, as plataformas demostradoras *testbeds* constitúen unha solución sinxela e suficientemente flexible baseada no concepto de radio definida por software, en que soamente aquelas operacións que son fundamentais (normalmente a transmisión e a adquisición) son levadas a cabo en tempo real, mentres que as demais tarefas son implementadas en tempo diferido, utilizando linguaxes de programacin de alto nivel (por exemplo MATLAB) e operacións en punto flotante. Os testbeds constitúen unha solución axeitada en termos de custo, man de obra e coñecemento *a priori* e resultan axeitados para grupos de investigación pequenos e con poucos recursos, como é o noso caso.

Neste traballo presentamos o GTEC MIMO testbed, que é outro *testbed* sen fíos con múltiples antenas, baseado en módulos hardware comerciais dispoñibles no mercado. O hardware compleméntase cunha arquitectura software deseñada co obxectivo de facilitar a utilización do *testbed* así como de facer máis sinxelo o software necesario para o proceso de medición. Facendo uso do GTEC MIMO testbed, levamos a cabo varias campañas de medidas en interiores co obxectivo de explorar a viabilidade das técnicas de estimación cega da canle sen fíos en sistemas con codificación Alamouti; avaliar códigos de canle tecnolóxicamente punteiros como son os Serially-Concatenated Low Density Generator Matrix (SCLDGM); e avaliar a codificación analóxica conxunta da fonte e a canle.

Grazas á colaboración co Institute of Communications and Radio-Frequency Engineering da Vienna University of Technology, puidemos avaliar sistemas de comunicacións móbiles en escenarios urbanos e realistas utilizando o Vienna MIMO Testbed. Máis específicamente, avaliamos o rendemento de High-Speed Downlink Packet Access (HSDPA) medindo a taxa de transferencia (*throughput*) do enlace descendente da capa física de HSDPA e comparándoa coa capacidade estimada da canle así coma co máximo rendemento que se pode acadar, estimado segundo o estándar HSDPA.

Resumen

Desde que Marconi llevó a cabo la primera transmisión inalámbrica en 1894, la investigación experimental ha estado siempre vinculada a las comunicaciones inalámbricas. Hoy en día, dicha investigación se apoya en simulaciones por ordenador que sólo reflejan el entorno de simulación en vez del escenario real en el que operan los sistemas inalámbricos. Por lo tanto, resulta conveniente evaluar los sistemas de comunicaciones inalámbricas en escenarios realistas, manteniendo al mismo tiempo el esfuerzo requerido en términos razonables. Entre las diferentes estrategias apropiadas para llevar a cabo dicha evaluación, los *testbeds* constituyen una solución simple y suficientemente flexible que se basa en el concepto de radio definida por software, en el que sólo aquellas operaciones fundamentales (normalmente la transmisión y la adquisición) se llevan a cabo en tiempo real, mientras que las restantes tareas se implementan en tiempo diferido utilizando lenguajes de programacin de alto nivel (por ejemplo MATLAB) y operaciones en punto flotante. Los *testbeds* constituyen una solución adecuada en términos de coste, mano de obra y conocimiento *a priori*, resultando asequibles para grupos de investigación pequeños y con pocos recursos, como es nuestro caso.

En este trabajo presentamos el GTEC MIMO testbed, que es otro *testbed* inalámbrico con múltiples antenas y basado en módulos hardware comerciales disponibles en el mercado. El hardware se complementa con una arquitectura software diseñada con el objetivo de facilitar la utilización del *testbed* así como simplificar el software necesario para el proceso de medición. Haciendo uso del GTEC MIMO testbed, llevamos a cabo varias campañas de medidas en interiores con el objetivo de explorar la viabilidad de las técnicas de estimación ciega del canal inalámbrico en sistemas con codificación Alamouti; evaluar códigos de canal tecnológicamente punteros como los Serially-Concatenated Low Density Generator Matrix (SCLDGM); y evaluar la codificación analógica conjunta de la fuente y el canal.

Gracias a la colaboración con el Institute of Communications and Radio-Frequency Engineering de la Vienna University of Technology, hemos podido evaluar sistemas de comunicaciones móviles en escenarios urbanos y realistas utilizando el Vienna MIMO Testbed. Más específicamente, evaluamos el rendimiento de High-Speed Downlink Packet Access (HSDPA) midiendo la tasa de transferencia (*throughput*) del enlace descendente de la capa física de HSDPA y comparándola con la capacidad estimada del canal así como con el máximo rendimiento alcanzable estimado de acuerdo a las restricciones impuestas por el estándar HSDPA.

Abstract

Since Marconi succeeded in carrying out the first wireless transmission in 1894, experimental research has been always linked with wireless communications. Today, most wireless communications research relies only on computer simulations. Although computer simulations are necessary and recommendable for wireless systems evaluation, they only reflect the simulation environment rather than the actual scenarios in which wireless systems operate. Consequently, it is desirable to assess wireless communications systems in real-world scenarios while, at the same time, keeping the required effort within reasonable terms. Among the different strategies suitable for undertaking such assessment, the *testbed approach* constitutes a simple and flexible enough solution based on the software-defined radio concept in which only the fundamental operations (usually the transmission and the acquisition) are carried out in real-time, while the remaining tasks are implemented off-line in high-level programming languages (e.g. MATLAB) and using floating point operations. The testbed approach leads to a suitable solution in terms of cost, manpower and *a priori* knowledge, making them affordable for small research groups with scarce resources, as in our case.

In this work we introduce the GTEC MIMO testbed, which is just *another* multiple antenna wireless testbed based on commercial off-the-shelf hardware modules. We complement the hardware equipment with a software architecture designed to ease the utilization of the testbed as well as to simplify the software needed for the measurement process. Making use of the GTEC MIMO testbed we carried out several measurement campaigns in indoor scenarios with the objective of exploring the feasibility of blind estimation techniques of the wireless channel in Alamouti coded systems; assessing state of the art channel codes as the Serially-Concatenated Low Density Generator Matrix (SCLDGM); and evaluating analog joint source-channel coding.

Thanks to the collaboration with the Institute of Communications and Radio-Frequency Engineering at the Vienna University of Technology, we also assessed mobile communications systems in very realistic, outdoor, urban scenarios making use of the Vienna MIMO Testbed. More specifically, we evaluated the performance of High-Speed Downlink Packet Access (HSDPA) by measuring the actual throughput of the physical layer downlink and comparing it with the estimated channel capacity as well as with the estimated maximum attainable throughput according to the HSDPA standard.

Contents

List of Figures

Chapter 1

Introduction

In 1873, the Scottish theoretical physicist and mathematician James Clerk Maxwell formulated the laws that govern electromagnetism, based on the previous work of Kelvin. Hardly anybody believed Maxwell at that time. Later, in 1884, the self-taught English electrical engineer, mathematician, and physicist Oliver Heaviside reformulated Maxwell's equations in terms of electric and magnetic forces and energy flux. Finally, in 1887, the German physicist Heinrich Hertz succeeded in transmitting and receiving radio waves in a controlled laboratory environment. Surprisingly, Hertz seemed uninterested in the practical importance of his work. He stated that: "This is just an experiment that proves Maestro Maxwell was right – we have these mysterious electromagnetic waves that we cannot see with the naked eye; but they are there – I do not think that the wireless waves I have discovered will have any practical application." How wrong he was! At the beginning of 2000, mobile network operators in Europe were offered an auction of the 3G radio spectrum. They had to pay incredibly huge amounts of money for a small piece of the electromagnetic spectrum [250], originating the so-called "Telecoms crash".

The ability of electromagnetic waves to convey information was demonstrated by Nikola Tesla in 1894. However, the Italian inventor Guglielmo Marconi is widely recognized as the inventor of wireless transmissions. His first publicized radio experiment took place in 1898 from a boat in the English Channel to the Isle of Wight, while in 1901 his radio telegraph system sent the first radio signal across the Atlantic Ocean from Cornwall to Newfoundland[1].

Until 1918 all wireless transmissions were based on the Morse code. In 1918, the American electrical engineer Edwin Armstrong invented the superheterodyne receiver and, later on, the Frequency Modulated (FM) radio appeared. The first broadcast radio transmission took place at Pittsburgh, in 1920. Since then, the wireless communications idea has ben constantly investigated for practical implementation.

---

[1]Recently, research by professor Ángel Faus shows that the Spanish engineer Julio Cervera Baviera was also working on radio experiments in 1902 [4].

At that time, it was believed that error-free digital communication was only possible by increasing the signal-to-noise ratio to infinity or reducing the transmission rate to zero. However, in 1948 the American mathematician, electronic engineer and geneticist Claude Elwood Shannon, known as "the father of information theory", published his celebrated paper, "*A mathematical theory of communication*" [261]. In this paper, Shannon presented the so-called "Shannon capacity" (also known as "Shannon limit" or "Shannon–Hartley" formula) [261, 262] which relates, in a noisy channel, the channel capacity to the received signal-to-noise ratio. Shannon demonstrated that, with the appropriate channel code, it is possible to achieve error-free communications over a noisy channel with a finite bandwidth B and a finite signal-to-noise ratio γ if, and only if, the transmission rate R is lower than a certain value $C = B \log_2(1 + \gamma)$.

In 1992, Joseph Mitola published the paper "*Software radios-survey, critical evaluation and future directions*" [205], where he coined the term "software-defined radio". Although the software-defined radio concept was first proposed in 1991, software-defined radios have their origins in the defense sector since the late seventies, in both the U.S. and Europe. The SDR Forum [22] defines the software-defined radio as a "radio in which some or all of the physical layer functions are software-defined". The software-defined radio approach makes it possible to carry out most of the signal processing operations in the digital domain rather than using analog circuitry, constituting a cornerstone in the *testbed approach* for wireless communications research.

In 1996, the American telecommunications engineer Gerard Joseph Foschini introduced the idea of utilizing several antennas at both sides of a communication link, and thus Multiple-Input Multiple-Output (MIMO) systems were born [97, 98]. At the same time, Emre Telatar showed that the capacity of a MIMO system grows linearly with the minimum number of transmit and receive antennas, although the corresponding paper was not published until 1999 [280]. However, the origins of MIMO can be traced back to 1984, when Jack Winters, from Bell Laboratories, submitted a patent on wireless communications using multiple antennas. Later, in 1985, Jack Salz, also from Bell Laboratories, published a paper on MIMO based on Winters' research [255]. Finally, in 1993, Arogyaswami Paulraj and Thomas Kailath proposed the concept of spatial multiplexing using MIMO and, in 1994, the US Patent No. 5,345,599 was issued [231].

MIMO technologies promise greater coverage, higher data rates, and improved link robustness by adding a *spatial* dimension to the existing time, frequency, and coding dimensions. Consequently, MIMO technologies play a key role in the solutions devised – and those yet to be developed – to satisfy the enormous demand – in terms of high data rate and spectral efficiency – required by today's wireless communications systems. Internet has dramatically changed the way users worldwide share information, conduct business and seek entertainment, demanding broadband wireless access not only to provide faster web surfing and

quicker file downloads but to enable current and near-future multimedia applications such as real-time audio streaming, real-time video streaming, multimedia conferencing and interactive gaming. More and more services will be implemented requiring broadband connections everywhere, for example Voice over Internet Protocol (VoIP), High Definition TV (HDTV), or Video on Demand (VoD). This enormous growth in broadband access has caused an incredible explosion in the research activities related to wireless communications and current as well as future broadband applications. On the downside, users demand even cheaper and smaller devices with longer battery life and, thus, low power consumption. On the network operators' side, features such as cheaper network deployment, better spectral efficiency due to the enormous costs of the spectrum licenses and also low power consumption are much in demand. All these reasons drive a very active research in wireless communications with the aim of finding new techniques (channel coding, precoding, power adaptation, interference cancellation, etc.) as well as testing them in representative scenarios and at a reasonable cost.

Experimental research has always been related to wired and wireless communications. Today, it is commonly conjectured that computer simulations are sufficient for evaluating wireless communications systems. Although computer simulations are indeed necessary and recommendable for this purpose, they only reflect the simulation environment instead of the actual scenarios where the systems operate. Therefore, it is also desirable to evaluate wireless communications systems in realistic and representative scenarios, keeping the required efforts within reasonable limits. Different strategies can be followed to undertake such assessment tasks. Among them, the *testbed approach* constitutes a simple and at the same time flexible enough solution based on the software-defined radio concept in which only the fundamental operations are carried out in real-time. The remaining tasks are implemented in high-level programming languages using floating point operations executed by general-purpose processors. Such a concept fits perfectly with the needs for the experimental assessment of wireless communications systems, while keeping the costs, manpower and *a priori* required knowledge within reasonable limits, making testbeds affordable even for small research groups with scarce resources, as in our case.

In this work, we present a way of designing and implementing a MIMO testbed based on Commercial Off-The-Shelf (COTS) components. We not only focus on the hardware architecture but also on the testbed software design, so often ignored by research groups involved in the experimental assessment of wireless communications systems. We also carried out several measurement campaigns in indoor scenarios in which we have experimentally evaluated wireless communications systems such as the blind channel estimation techniques that help in improving the spectral efficiency by avoiding pilot symbols; the evaluation of state of the art capacity approaching channel codes such as Serially-Concatenated Low Density Generator Matrix (SCLDGM) codes; and even the evaluation of completely new approaches for wireless communications systems as, for example, those based on analog joint source-channel coding in

which analog transmissions are carried out making use of a digital system.

In principle, it could be thought that it is straightforward to obtain a flawlessly, fully-operational MIMO testbed after investing a certain amount of money and several months' work. Our experience in the development of the GTEC MIMO testbed showed us that this reasoning is completely wrong and very far from reality. Building a testbed not only requires *skilled* engineers, but also measurement equipment (spectrum analyzers, oscilloscopes); standard tools ranging from simple screw drivers to sophisticated RF equipment; and a very clear idea about the end purpose of the testbed, which is typically very difficult to achieve because members of the research community often demand a testbed for potentially measuring *everything*.

Thanks to the collaboration with the Institute of Communications and Radio-Frequency Engineering, Vienna University of Technology, Austria, we were also able to assess one of the most widely used mobile communications systems, High-Speed Downlink Packet Access (HSDPA), in very realistic, outdoor, urban scenarios making use of the Vienna MIMO Testbed [49]. We have evaluated the optimality of current mobile communications systems, such as HSDPA, by measuring the actual throughput of the physical layer downlink and comparing it with the estimated channel capacity as well as with the estimated maximum attainable throughput according to the standard requirements. We will see that there is still a lot to do to in order to approach the channel capacity.

1.1   Thesis Overview

This thesis is organized as follows. In Chapter 2 we address the problem of designing a MIMO testbed based on COTS hardware components, including the RF front-ends. We describe the typical components constituting a COTS-based testbed and how they are organized and configured in the GTEC MIMO testbed. We conclude the chapter showing that testbeds can be used for other purposes apart from that of evaluating wireless communications systems, for example in the development of real-time systems or in education.

Chapter 3 is dedicated to the software running on top of the testbed hardware. When we address the design and the development of the testbed software, our main requisite consists in providing an easy as well as effective way for researchers and/or students to interact with the testbed, even though they were not involved in its development. The result is a distributed multilayer software architecture that allows remote interaction with the testbed at an adequate level of abstraction. It also makes it possible to integrate heterogeneous hardware nodes into the testbed, as well as to extend the testbed to a multinode system for multiuser communications assessment. Additionally, such software architecture supports closed-loop MIMO measurements without requiring additional and expensive hardware.

We made use of the GTEC MIMO testbed to experimentally evaluate different wireless

communications systems and techniques. In Chapter 4 we address the problem of blind estimation of the MIMO wireless channel in the context of Alamouti coded systems. We do so to demonstrate the feasibility of avoiding the transmission of pilot symbols that do not convey information, thereby improving the spectral efficiency of the resulting system. In this chapter we review different strategies available in the literature to obtain low-complexity approaches that perform almost equal to standard channel estimation techniques. Our main contribution is the experimental evaluation of such blind MIMO channel estimation techniques in realistic indoor environments, with and without line of sight between the transmit antennas and the receive antennas. The results obtained are complemented with computer simulation results for comparison purposes.

In Chapter 5 we introduce the idea of joint-source channel coding and how such an approach can be implemented in a software-defined radio system. Our main contribution is the experimental evaluation – restricted to the single-antenna case – of state of the art analog joint-source channel coding schemes available in the literature in a realistic indoor environment. We compared the measurement results with those obtained by means of computer simulations over the Additive White Gaussian Noise (AWGN) channel, showing that, in the case of the experimental measurements, analog joint-source channel coding schemes achieve the Shannon limit, as in computer simulations.

Finally, in Chapter 6 we assess the capacity-approaching Serially-Concatenated Low Density Generator Matrix (SCLDGM) channel codes in indoor environments over a 4×4 MIMO wireless channel. We also propose a novel approach to help in achieving the channel capacity and consisting in not only adapting the transmit power value, the code rate or the modulation format, but also the channel code profile.

Chapters 7 and 8 contain the work carried out at the Institute of Communications and Radio-Frequency Engineering, Vienna University of Technology, Austria. In Chapter 7 we study the influence of the transmit antenna spacing and polarization on the throughput of standard-compliant High-Speed Downlink Packet Access (HSDPA) physical layer downlink transmissions. The measurements are carried out in a realistic, urban, rich-scattering scenario in downtown Vienna utilizing the Vienna MIMO Testbed. The results are complemented with three different bounds. The first two are the water-filling channel capacity and the unconstrained channel capacity (also known as mutual information in the literature), both assuming Gaussian input signals. Additionally, we also estimate the so-called functional capacity, which is defined as the channel capacity constrained by the inherent system losses imposed by the standard, representing the maximum attainable throughput.

Chapter 8 explores the utilization of antenna selection at the receiver side of a standard-compliant HSDPA communications system. We introduce the concept of antenna selection, the hardware implementation impairments and how they are overcome for the HSDPA case. Our main contribution is the proposal of a novel antenna selection criterion based on the

entire system design, including the receiver, rather than considering only the wireless channel. Additionally, we carried out a measurement campaign in a realistic, urban, rich-scattering scenario in downtown Vienna to evaluate the gains – in terms of HSDPA physical layer downlink throughput – that can be achieved when antenna selection is employed at the receiver in the downlink.

Finally, Chapter 9 is devoted to the conclusions and future work.

Chapter 2

MIMO Testbed Design Based on COTS Modules

In this chapter we introduce our approach for the experimental assessment of wireless communications systems with multiple antennas, namely the "GTEC MIMO testbed". Throughout this chapter we will focus on the hardware side and its technical features, while the software elements will be described in Chapter 3. This chapter is partly based on the publications [104, 106, 107, 111, 237, 240, 241, 271].

The rest of the chapter is organized as follows. In Section 2.1 we state the main motivations for the development of the GTEC MIMO testbed. The current version of the hardware testbed is briefly described in Section 2.2. Although the primary usage of the testbeds is the ability to experimentally evaluate the performance of wireless communications systems in realistic scenarios and at a reasonable effort, testbeds can be helpful in many other situations. As an example, in Section 2.3 we show that testbeds can be successfully utilized in the development of real-time prototypes as well as in educational environments. In Section 2.4 we discuss the future of testbeds, especially after the generalization of the software-defined radio concept [248] and the appearance of the GNU Radio [7]. Finally, Section 2.5 summarizes the main results of this chapter.

2.1 Motivation

In 1996, a new transmission concept consisting of using multiple antennas at each side of the radio link was proposed by Foschini [97, 98]. At the same time, Telatar demonstrated that the capacity of Multiple-Input Multiple-Output (MIMO) channels grows linearly with the minimum number of transmit and receive antennas. The latter work was published later, in 1999 [280]. The utilization of multiple antennas at both transmission and reception ends, also known as MIMO transmission systems, has received a great deal of interest from the

research community as well as from the wireless communications industry in recent years. Communication in wireless channels using MIMO technologies exhibits a superior performance in terms of spectral efficiency, reliability and data rate when compared to conventional single-antenna technologies. Existing and emerging standards for wireless communications such as IEEE 802.16 (WiMAX) [155, 156] or 3GPP UMTS LTE [29] support multiple antenna transmissions in their high-performance profiles.

In spite of their potential performance-enhancing capabilities, most of the research on MIMO technologies is based on theoretical studies. Typically, the expected gains of MIMO technologies are only shown under ideal conditions since most analyses rely on simulations reflecting only the simulation environment instead of the real-world wireless channel. Experimental evaluation of MIMO technologies in real-world scenarios is necessary to measure how these MIMO technologies perform over realistic, imperfect wireless channels. The experimental assessment of wireless communications systems not only takes into account the real multipath propagation in wireless channels, but also the implementation impairments so often ignored during the simulations. The main reason for the lack of experimental evaluation results is that measurement equipment is expensive, difficult to obtain and its set-up involves cumbersome, time-consuming tasks. Furthermore, the measurement equipment is not flexible enough when a multitude of transmission parameters are of interest (e.g. investigating the influence on performance of the transmit power, antenna spacing, antenna polarization, and multiuser interference). Last, but not least, it is difficult to carry out experimental evaluations in scenarios representative enough for the results to be treated as general statements. This is – perhaps too frequently – an insurmountable obstacle for the publication of experimental assessments in the literature.

Hardware implementations of wireless communications systems can be split into three groups [17, 45, 252]. The first of these is constituted by the so-called *demonstrators*, which are utilized to show specific technologies to prospective customers. For that reason, they are not meant to be flexible and scalable, but they require little time for their design and implementation. The second group is formed by *prototypes*. A prototype is a first full-scale and usually functional realization of a research concept. It often constitutes a preliminary stage where the system is implemented, debugged and subsequently implemented as a consumer product. Finally, the third set is constituted by *testbeds*, offering real-time transmission capabilities while data is (usually) generated and post-processed off-line.

Testbeds are generally used for research, resulting in requirements for scalability (e.g. the first version of the testbed is 2×2, the next version scales to 4×4 without having to buy everything again from scratch), modularity (e.g. replacing the RF front-ends to operate in a different spectrum band), and extendability (e.g. firstly, a single-user testbed with two nodes is built, then a multiuser testbed consisting of several nodes is constructed re-using the first two nodes).

The general idea of the MIMO testbed is to implement in real-time only those operations needed to transmit signals through the wireless channel and later acquire them for evaluation. The remaining operations are kept with the same level of complexity required by computer simulations. However, hybrid solutions can be devised in order to improve the measurement time or with the purpose of assessing time-critical systems (e.g. carry out closed-loop measurements in high-speed scenarios). As an example, a testbed can carry out some operations in real-time with the purpose of speeding up the measurement process. Usually, candidate signal processing operations to be implemented in real-time are those that operate at sample level, for example I/Q modulation, up-sampling, pulse-shape filtering, etc. An alternative, and frequently suitable, solution for those time-critical measurements is to use a quasi real-time approach [55, 56].

2.1.1   MIMO Testbed Requirements

Testbeds are often used to verify if a new signaling technique, a part of the physical layer of a communications standard, or even a complete standard system that has been proven useful by simulations is also valid in realistic wireless scenarios (indoor, outdoor or any combination of these). Testbeds can also contribute to improving the real-time hardware prototyping, helping to capture the hardware needs for real-time implementations, not only for the digital signal processing modules (mainly, Digital Signal Processors (DSPs) and Field Programmable Gate Arrays (FPGAs)) but also for the analogue Radio Frequency (RF) front-ends. Testbeds enable the requisites for the hardware used in the final real-time implementation to be captured. Consequently, evaluating performance with testbeds allows us to know whether a given technique is feasible from the real-time hardware and implementation requirements. Testbeds can also be used as a reference – in terms of the performance offered by the technique under development – for the real-time implementation.

Among the three different types of hardware implementations described above (demonstrators, prototypes and testbeds), testbeds present the following requirements that are seen as advantages from the wireless communications research point of view:

- **Flexibility**. Testbed hardware is often meant to be used for off-line processing. Only the signals are sent and acquired in real-time. This implies that testbed hardware is not subject to real-time restrictions even though the hardware must include some sort of real-time capabilities.

- **Modularity**. Usually, the minimum modularity found in a testbed is given by the separation between the digital side (up to the Digital-to-Analog Converters (DACs) and the Analog-to-Digital Converters (ADCs)) and the Radio Frequency (RF) front-ends. Sometimes, the digital hardware can be split into different modules performing specific operations: digital-to-analog and analog-to-digital conversions, digital up and

down conversion, signal buffering, etc. For the RF section it is possible to find custom ad hoc solutions or commercial products. Recently, commercial RF front-ends permit some degree of flexibility, for example allowing dual-band operation, RF carrier selection for each band or adjusting the gains at the transmitter power amplifier.

- **Scalability**. Due to the *enormous* costs and manpower required to set up a testbed from scratch, a common strategy consists in first developing a MIMO testbed with a *reduced* number of antennas (e.g. two transmit and two receive antennas). Next, the testbed can be used in several measurements to test it and to show its capabilities. In a later step, the testbed is scaled to support a greater number of antennas (e.g. 4×4). Consequently, it is desirable that the second evolution should only require more hardware to be added instead of replacing it entirely. Finally, the research team decides to start outdoor measurements and replaces the power amplifiers at the Transmitter (TX) end by new ones suitable for outdoor transmissions. All these evolutions should be carried out from the existing hardware, minimizing the new hardware needs.

- **High-level language development**. Bearing in mind that most of the processing tasks are carried out off-line, general purpose processors are adequate for processing the generated/acquired signals[1]. This allows the utilization of high-level programming environments (e.g. MATLAB, C/C++, Java) and the simplification of the implementation stages both in time and complexity. This feature also provides an additional degree of flexibility, because it is easy to change the implementation on the fly. Furthermore, a consequence of the off-line processing and the usage of high-level programming environments is that the operations are carried out in the floating-point domain instead of using fixed-point operations available for real-time devices. This permits the researcher to focus on the implementation rather than having to consider some other problems such as the arithmetic precision of the operations. Moreover, it is very typical to migrate existing simulation software to be able to assess the same techniques by testbed measurements. It is clear that this step is simplified when high-level languages are used for the experimental evaluation.

The SDR Forum [22] defines software-defined radio as a "radio in which some or all of the physical layer functions are software-defined". Even though the Software Communications Architecture [21] is the only result produced by the SDR Forum to date, the software-defined radio concept is well established in the literature [205–207, 248], and the resulting approach is suitable to be included in the testbed design. This implies that the testbed has some sort of flexibility such that the testbed may be configured – with the limitations imposed by the hardware – to support various air standards and waveforms, frequency bands, bandwidths, and

---

[1]Recently, the utilization of graphics processing units for signal processing and software-defined radio is being considered [11, 172, 259]
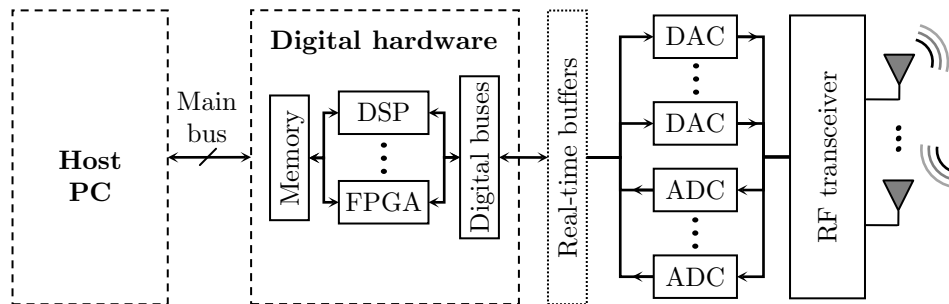
Figure 2.1: Block diagram of testbed hardware components including DSPs, FPGAs, real-time buffers, and RF transceivers.

modes of operation.

As shown in Figure 2.1, testbed hardware components can be classified into three groups according to their functionality. The first one is the host system – usually a Personal Computer (PC) –, which we will name "host PC". It is the equipment that allocates one or more boards containing the digital section of the testbed hardware. It also allocates additional hardware such as hard disk arrays for data storage, graphics processing units to speed up signal processing operations, etc. The second group is constituted by the digital hardware components, including non general purpose processors such as DSPs or FPGAs. Finally, the third group is formed by the RF front-ends. In the digital section, a bus termed *main bus* allows the data to be transferred from the host to the testbed hardware and vice-versa. Next, a set or just a single digital bus interconnects the digital hardware (DSPs, FPGAs, memory buffers, etc.) with the DACs and the ADCs. Note that the utilization of memory buffers accessible in real-time from the DACs and the ADCs is a suitable approach to avoid any kind of real-time signal processing.

With this basic configuration, it is possible to send samples coming directly from the main bus, convert them into the analog domain using the DACs and up convert them to the desired carrier RF using the RF front-ends. At the Receiver (RX) side, the signals are down converted by the RF front-ends, converted to the digital domain by the ADCs and then sent to the host through the main bus. Note that the main bottleneck in this scheme is the maximum data rate provided by the main bus, especially if there are no digital up and down converters available. In the most recent boards, by using PCI express or similar solutions it is possible to use the host memory as a buffer while samples are transferred in real-time through the main bus.

A first improvement of this basic scheme consists in incorporating a Digital Up Converter (DUC) before each DAC at the TX and a Digital Down Converter (DDC) after each ADC at the RX. These devices can either be dedicated elements or be implemented in an FPGA. Incorporating DUC and DDC into the MIMO testbed design, it is possible to transfer complex signals from/to the host, thus reducing both the transfer rate at the main bus and the software complexity. For MIMO operation, DUCs and DDCs must be fully synchronized. Additionally, another improvement consists in implementing some of the time-consuming sample-level tasks

in FPGAs (e.g. time and frequency synchronization).

2.1.2   Why COTS Modules?

Among the testbeds reported in the literature [27, 30, 34, 35, 42, 43, 49, 60, 65, 66, 69, 80, 82, 83, 86, 121, 131, 134, 162, 163, 169, 171, 172, 174, 175, 178, 179, 184, 185, 189, 195, 198, 204, 216–219, 223–225, 229, 234, 246, 249, 256, 275, 276, 290, 295–297, 300, 301, 304, 306, 310, 313], some are designed on the basis of Commercial Off-The-Shelf (COTS) modules found in the market. Some companies selling COTS modules are Ettus [3], GE Fanuc [6], Hunt Engineering [9], Innovative Integration [10], Lyrtech [15], Nallatech [18], National Instruments [19], Pentek [20], and Sundance Multiprocessor [23]. Some of these are focused on real-time hardware (e.g. Nallatech), whilst some offer an extreme modular solution in which even the digital section is divided into different modules containing distinct hardware elements (e.g. Nallatech or Sundance). Companies such as Sundance or Lyrtech offer both baseband modules as well as RF front-ends. Interestingly, only National Instruments offers an integrated solution including the hardware for the digital side and the well-known integrated development environment LabVIEW [14][2].

The GTEC MIMO testbed was designed on the basis of COTS modules due to the lack of previous experience in building similar solutions; time, money and manpower required for an ad-hoc solution; and the lack of test equipment required for the RF hardware.

2.2   GTEC MIMO Testbed

In this section we present the GTEC MIMO Testbed including its history (see Figures 2.2–2.4). We also explain in detail the different COTS modules used to construct the hardware of the testbed, leaving the description of the testbed software for the ensuing chapter. Finally, the performance offered by the testbed is shown by means of two constellation examples.

2.2.1   Brief History of the GTEC MIMO Testbed

The development of the GTEC MIMO Testbed began in 2005 when the Grupo de Tecnología Electrónica y Comunicaciones (GTEC) at the University of A Coruña together with the Grupo de Tratamiento Avanzado de la Señal (GTAS) at the University of Cantabria proposed the construction of a MIMO testbed for the experimental assessment of MIMO communications

---

[2]An example is the Hydra testbed [26], that utilizes the PXI-1045 chassis equipped with the PXI-8186 embedded PC, the PXI-5421 for the DACs, the PXI-5122 for the ADCs, and LabVIEW to implement the signal processing tasks as well as to configure and to control all hardware modules. Note, however, that the RF front-ends are not available from National Instruments.
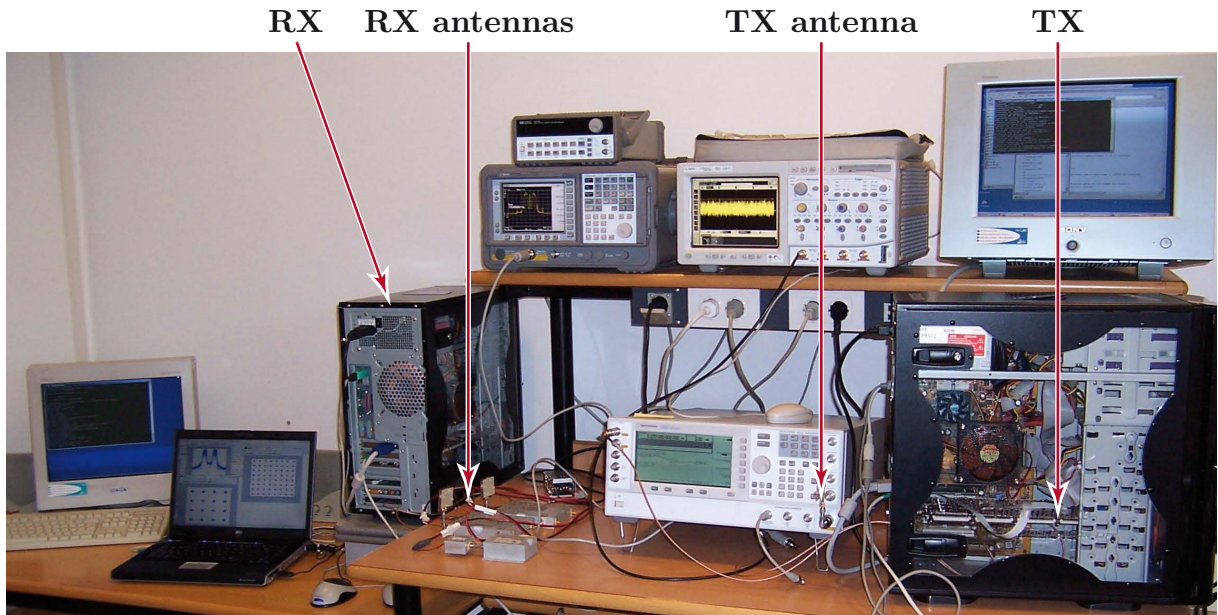
Figure 2.2: Picture of the first version of the testbed in a 1×2 configuration.

systems in the context of the MIMESIS project (TEC2004-06451-C05-01) funded by the Spanish Government.

The development of the first version of the testbed was split into the baseband part, implemented by the GTEC, and the RF front-ends, designed by the GTAS (see Figure 2.2). The integration of the baseband side of the testbed was based on COTS modules under the requisite of supporting a 4×4 MIMO half-duplex link with a bandwidth of 20 MHz. The second part was carried out by the GTAS. They used two Agilent E4438C vector signal generators for the up conversion stage, and two self-designed downconverters at 2.4 GHz. In a later step, the GTAS designed three downconverters at 5.2 GHz. The resulting testbed was 4×4 at the baseband side, 2×2 at 2.4 GHz, and 2×3 when operating at 5.2 GHz. Several measurement campaigns were successfully carried out with this testbed [104, 240, 241].

Later on, the GTEC started to build its own 2×2 testbed by re-utilizing the baseband side developed together with the GTAS, and replacing the previous RF modules by the new and promising Sundance SMT349 transceivers operating in the 2.4 GHz Industrial, Scientific and Medical (ISM) band (see Figure 2.3). Although we were able to carry out different experimental evaluations with this second version of the testbed [107, 237], such modules did not work as expected. When we bought another pair of SMT349 modules with the aim of scaling to a 4×4 testbed, we noticed that such modules could not be properly synchronized and we decided to cancel the upgrade based on such front-ends[3].

---

[3]The problems of the SMT349 front-end delayed the development of the 4×4 testbed about 12 months. As a consequence, a lot of money and time was lost. This kind of problem can be mitigated by following the advice given in [253], [55, Chapter 3, pp. 43], where some common pitfalls related to testbed design and implementation are analyzed. Finally, this kind of problem also explains the lack of experimental assessments in the literature compared to computer simulations and theoretical results.
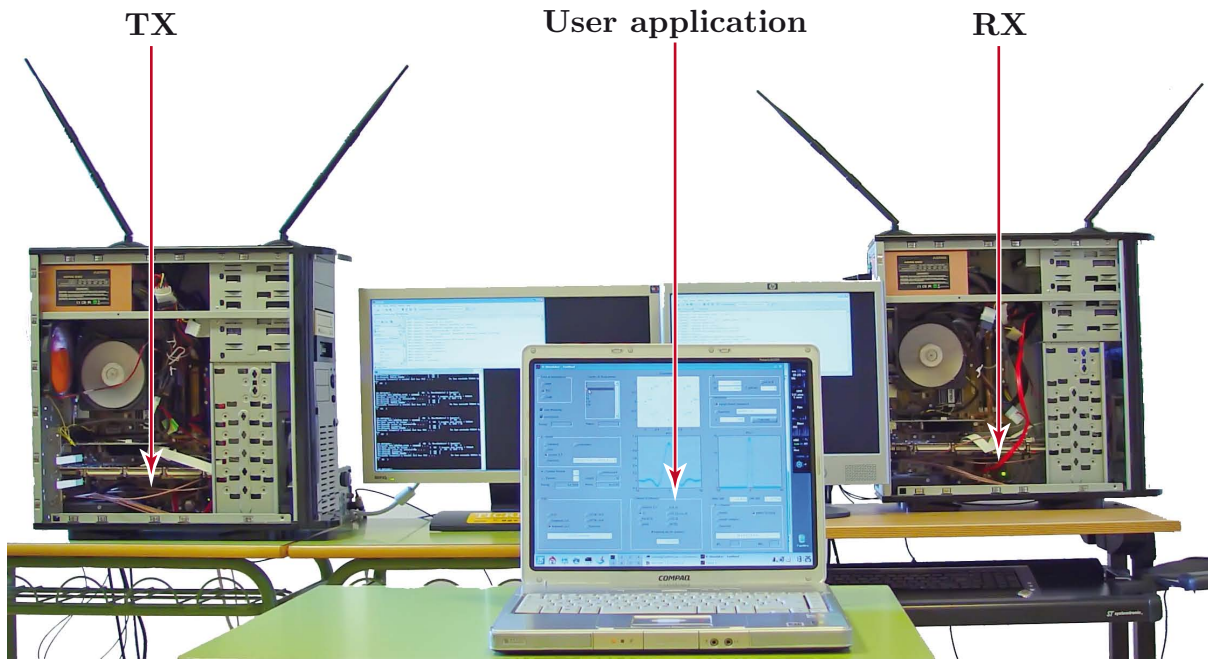
Figure 2.3: Picture of the second version of the testbed.

In 2008, after considering the past experience obtained from the development of the two previous versions of the testbed, we decided to completely redesign the GTEC MIMO testbed only re-utilizing the baseband hardware (see Figure 2.4). The design was conducted by the idea of simplifying the process required to experimentally assess a wireless system which has been simulated before, thus minimizing the need for additional requirements when migrating the simulation code to the testbed.

2.2.2 Digital Section of the GTEC MIMO Testbed

The GTEC MIMO testbed basically consists of two nodes (a TX node and a RX node), both externally controlled through standard Transmission Control Protocol (TCP) socket connections. Each node consists of a so-called host PC that allocates a Sundance SMT310Q PCI carrier board containing all baseband modules (also from Sundance) and providing interconnection with the host PC through the PCI bus. The PCI carrier board can allocate up to four different modules: DSP and FPGA for real-time processing and hardware configuration and control, real-time memory buffers, data acquisition modules containing DACs and ADCs, and even the RF front-ends. The number of possibilities for the configuration are enormous depending on the computational needs. However, such a high degree of freedom requires a considerable effort regarding the integration tasks, which is usually the biggest weakness of this kind of system.

In the case of the GTEC MIMO testbed, the two nodes use a master module providing basic processing capabilities by means of a Texas Instruments TMS320C6416 DSP running
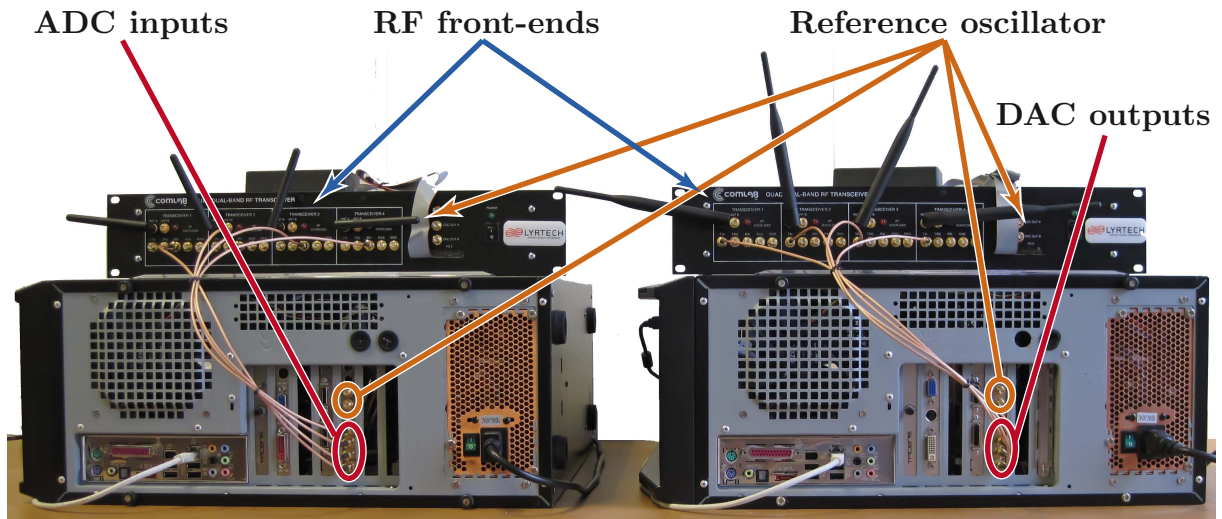
Figure 2.4: Picture of the third (current) version of the testbed.

at 600 MHz. It is also responsible for controlling the remaining modules of the carrier board. For this purpose, the master module employs a dedicated, low-rate, point-to-point control bus, which links the master module with each slave module. To be able to transfer data between modules, the master module has two ports of the so-called Sundance High-Speed Bus (SHB), a proprietary bus from Sundance allowing sustainable transfer rates of 400 MB/s through each port. Each slave module has at least two ports so as to be able to transfer data between the master and the slave modules or between slave modules. Such buses are shown in the schematic diagrams of Figures 2.6 and 2.8 for the TX and the RX carrier board, respectively.

Note that these Sundance modules do not implement any kind of DUC or DDC, thus the samples have to be sent to the DACs at the necessary sample rate. The SHB buses are capable of sustaining a sample rate of 100 Msample/s between the master module and each of the four DACs or the four ADCs. However, the DSP at the master module cannot sustain such rates when reading from the master module memory, making it impossible to directly transfer the samples between the master and the acquisition modules. To overcome this limitation, we make use of several buffers at both the TX and the RX sides. This way, at the TX, the signals are transferred off-line from the host PC to the master module. Next, they are stored in the 2 Msample buffers at the SMT370 modules. Finally, the DACs read the signals in real-time from the buffers. At the RX the same idea is utilized: the signals acquired by the ADCs are saved in real-time in two 256 Msample buffers per antenna. In a later step, the signals are transferred off-line from such buffers to the host PC through the PCI bus.
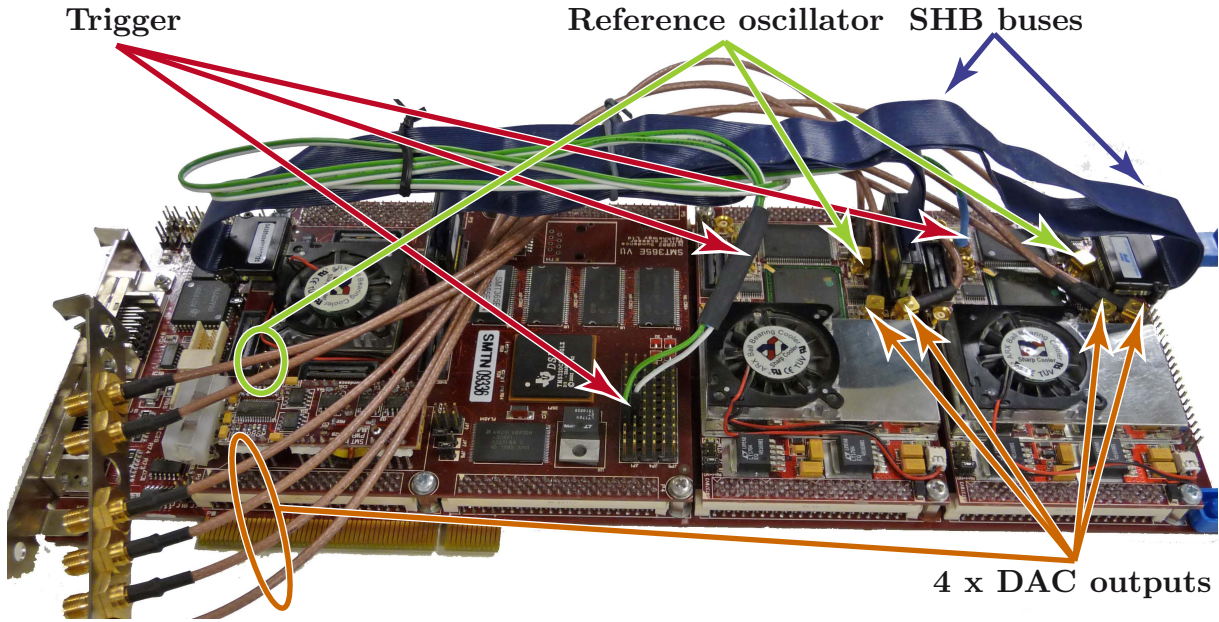
Figure 2.5: Picture of the baseband modules at the TX side.
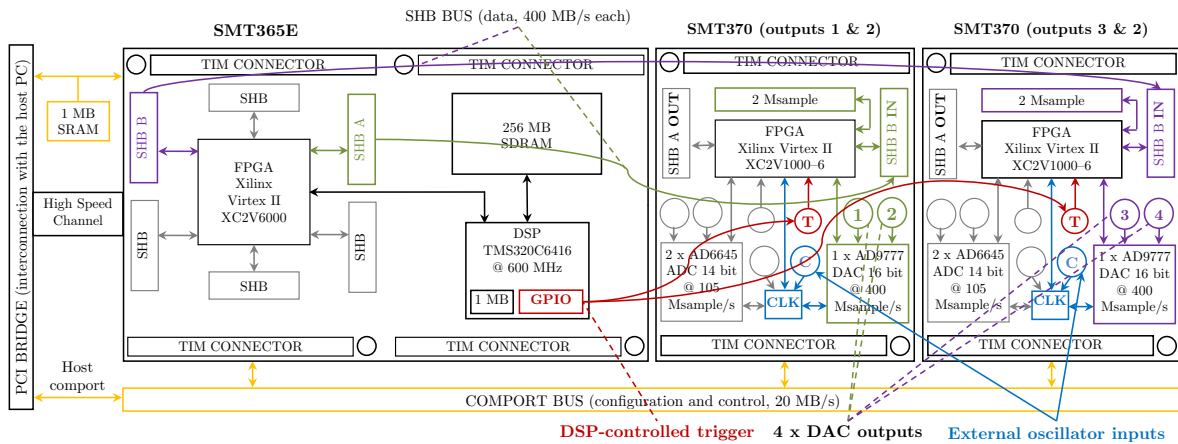
Figure 2.6: Detailed scheme of the baseband modules at the TX side.

2.2.3   The Transmitter

Figures 2.5 and 2.6 respectively show a picture and a schematic diagram of the TX carrier board containing three modules (from left to right): the processing module (SMT365E) and a pair of digital acquisition modules (SMT370), each containing a dual DAC (Analog Devices [2] AD9777) and two ADCs (Analog Devices AD6645). Only the dual DAC is used at the TX node. We implemented two mechanisms in order to be able to synchronize the four DACs in both time and frequency:

- A trigger controlled from the process running in the DSP of the master module. The trigger is attached to the general purpose input/output port of the DSP and to specific inputs at the SMT370 modules (see Figure 2.6). When the signals are ready to be transmitted (i.e. they are stored at the 2 Msample buffers in the SMT370), this process enables the trigger signal (see Figure 2.6) and the four DACs to start to transmit at the
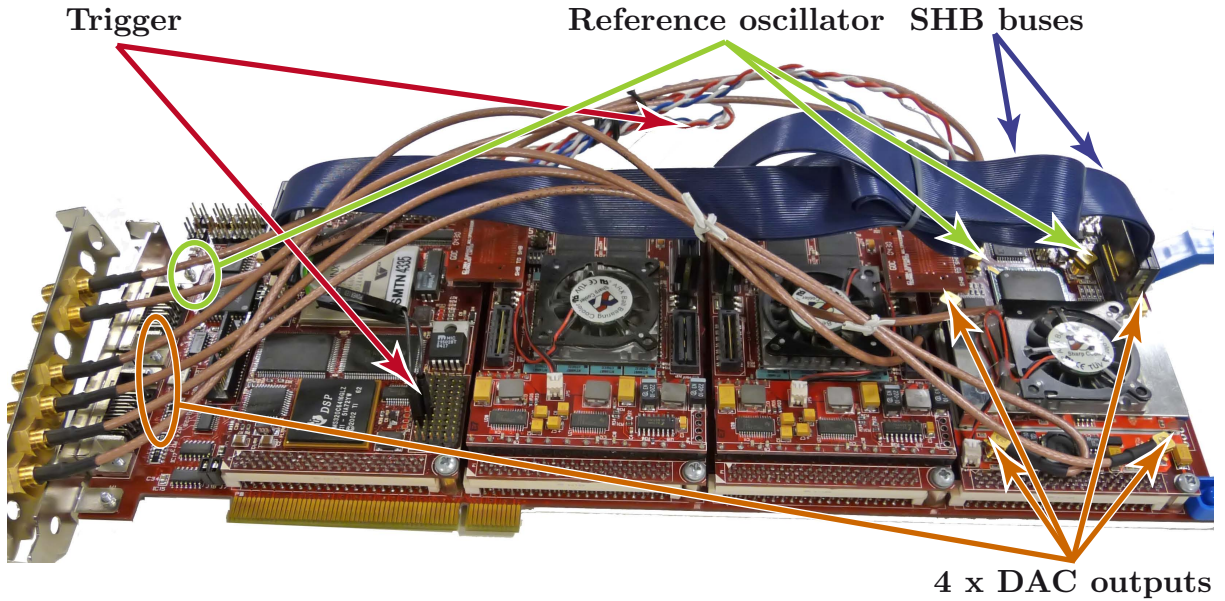
Figure 2.7: Picture of the baseband modules at the RX side.
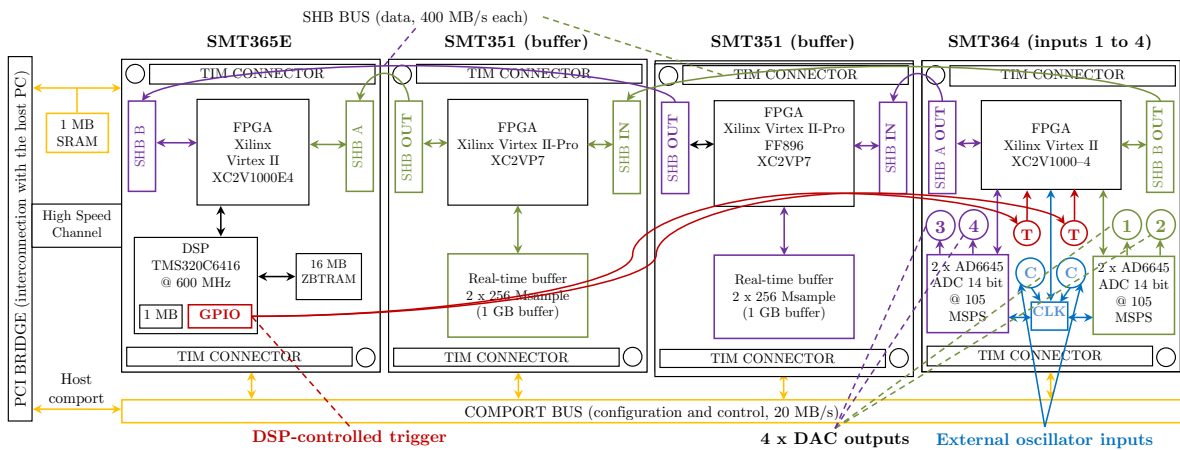
Figure 2.8: Detailed scheme of the baseband modules at the RX side.

same time.

- MIMO requires that all DACs be frequency-synchronized. For that purpose we configured both SMT370 modules to use an external reference oscillator. Note that it is guaranteed that all DACs are synchronized in frequency but not in phase. Therefore, experiments requiring fully-coherent TX and/or RX are not feasible with this hardware[4].

The two SMT370 modules are connected with the SMT365E master module through both the control bus and the SHB. The first one is utilized to send the configuration register values to the modules whereas the second one is employed to transfer the samples to the DACs.

- The signals are first acquired from the host PC through the PCI bus and stored in the 256 MB memory at the SMT365E master module. The PCI bus is connected to the SMT365E master module through the SMT310Q PCI carrier board using a bus that

---

[4]Typically, different phases at the TX and/or at the RX are compensated by the MIMO channel estimation.

Sundance termed as a high speed channel. Obviously, the maximum transfer rate of such a high speed channel is limited to the maximum transfer rate offered by the PCI bus, i.e. 133 MB/s.

- The signals are then transferred from the SMT365E memory to the corresponding 1 Msample per DAC buffers at the SMT370 modules.
- Finally, when the trigger is enabled, the signals are transmitted in real-time from those buffers to the DACs.

2.2.4   The Receiver

Figures 2.7 and 2.8 respectively show a picture and a schematic diagram of the RX carrier board containing four modules (from left to right): the processing module (SMT365), a pair of large real-time buffer modules (SMT351G), and a digital acquisition module (SMT364) containing four ADCs (Analog Devices AD6645). The SMT364 module is identical to the SMT370 but replacing the dual DAC by two additional ADCs. As at the TX side, the four ADCs are synchronized in both time and frequency by means of a trigger signal controlled by the DSP and a common external reference oscillator.

The sequence of steps followed to acquire the signals at the inputs of the ADCs to transfer them to the host PC is very similar to that for the TX:

- The trigger is enabled and the acquisition process starts. The signals at the inputs of the ADCs are converted to the digital domain.
- Each pair of ADCs uses a SHB port to send the samples to the corresponding SMT351G module in real-time. Note that each SMT351G module is connected through the SHB with a pair of ADCs of the SMT364 module.
- Once the acquisition has finished, the trigger is disabled and the process running in the DSP copies the data from the SMT351G buffers to the 16 MB memory of the SMT365.
- Finally, the DSP process transfers the data from the SMT365 memory to the host PC through the high speed channel and the PCI bus. Note that the size of the SMT365 memory is not a limitation for the maximum number of samples to be acquired because the samples are transferred off-line, on a block by block basis.

2.2.5   RF Front-Ends of the GTEC MIMO Testbed

Both TX and RX testbed nodes are equipped with a Quad Dual-Band RF front-end from Lyrtech [15]. The front-end is based on the Maxim [16] MAX2829 chip[5]. A photograph of

---

[5]The Maxim MAX2829 chip can also be found in front-ends such as Ettus XCVR2450, Sundance SMT911 or MORFAN [66].

SNR = 62.9 dB, EVM = −54.8 dB, BER = 0.0%
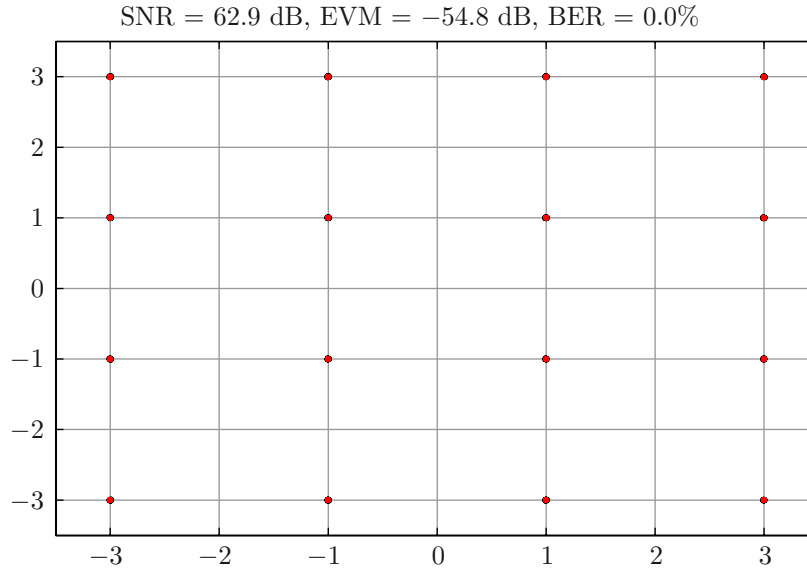
Figure 2.9: 16 QAM constellation (2 000 symbols) obtained when a DAC of the TX and an ADC of the RX are connected through a coaxial cable. The TX signal is plotted in red whereas the observations are in black.

SNR = 45.1 dB, EVM = −32.7 dB, BER = 0.0%
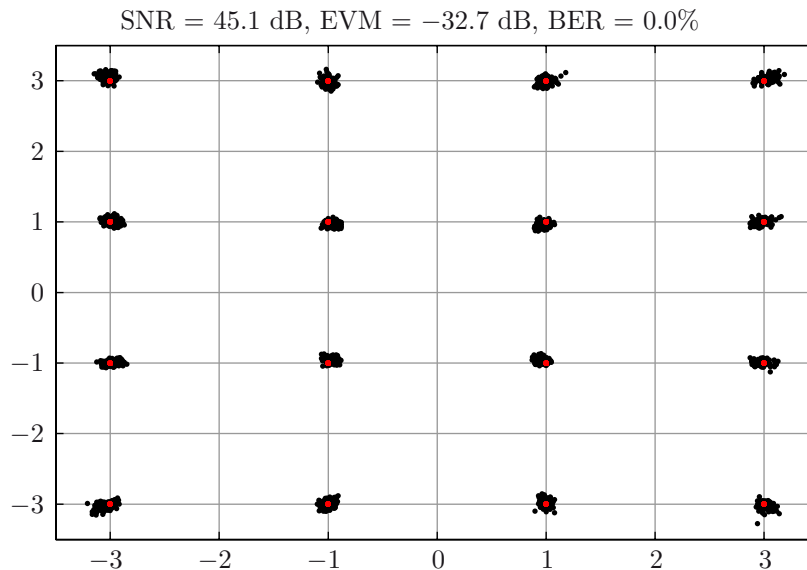
Figure 2.10: The same specifications as in Figure 2.9 when the Lyrtech Quad Dual-Band RF front-end is utilized and equipped with rod antennas [24].

the front-end is shown in Figure 2.4. These RF front-ends support both up and down conversion operations, and can radiate signals either at 2.4 GHz or at 5 GHz ISM bands with up to 40 MHz of bandwidth. Given that the RF front-end is a frequency agile radio [36], it can radiate at different carrier frequencies at the 2.4 GHz and at the 5 GHz ISM bands. More specifically, it can radiate from 2.4 to 2.5 GHz, and from 4.9 to 5.875 GHz. The front-end also incorporates a programmable variable attenuator to control the transmit power value. The attenuation ranges

from 0 to 31 dB in 1 dB steps.

The GTEC MIMO Testbed provides the same oscillator to TX and RX nodes, including the DACs, the ADCs, and the RF front-ends. Thus, the whole testbed is synchronized in frequency.

We tested the performance of the GTEC MIMO testbed evaluating acquired signal constellations when only the baseband section of the testbed is utilized (i.e. the DACs are directly attached to the ADCs through a coaxial cable), as well as together with the Lyrtech Quad Dual-Band RF front-end transmitting with rod antennas [24]. In both cases, the Agilent E4438C vector signal generator is used as the common reference oscillator. We generate the same signal for bog cases, consisting of a sequence of 2 000 16-QAM symbols (8 000 bits) that are pulse-shaped using a squared root raised cosine filter with 20 % roll-off and I/Q modulated at a carrier frequency of 5 MHz with both DAC and ADC sampling at 40 MHz. The resulting signal occupies 1.2 MHz of bandwidth. In the RF case, the RF carrier is equal to 5.62 GHz, with the TX and the RX spaced about 5 m apart. For the baseband case, the constellation showing the TX symbols and the RX symbols is shown in Figure 2.9, exhibiting an estimated Signal to Noise Ratio (SNR) equal to 62.9 dB and an Error Vector Magnitude (EVM)[6] of -54.8 dB, which gives a very good performance.

When the RF front-end is included, the Maxim MAX2829 constitutes a mid-performance commercial solution, offering a performance similar to that of general consumer devices such as laptops, or mobile phones. Therefore, the performance offered by the RF front-end as well as the impairments introduced are of a magnitude similar to that of conventional devices, thus making the testbed suitable for predicting the actual performance of typical *inexpensive* commercial equipment. For the RF case, the constellation showing the TX symbols and the RX symbols is shown in Figure 2.10, exhibiting an estimated SNR equal to 45.1 dB and an EVM of -32.7 dB, which gives a mid-performance result because of the loss in terms of EVM compared to the SNR. However, it is clear that the GTEC MIMO testbed is suitable to experimentally evaluate wireless communications systems as its performance is in the same order as that offered by commercial solutions and mainly limited by the RF front-end, which is based on a commercial chip.

2.3   Testbed Applications

Although testbeds are primarily meant for measurements, they can be used in a great variety of situations and environments, as shown below.

---

[6]The EVM is calculated according to [36, Chapter 1, pp. 27]

Real-Time Development

Methodologies covering the entire development process, from source code suitable for simulations and executed off-line to real-time implementations, as well as software tools according to these methodologies, are extremely scarce. One proposed methodology is the so-called rapid prototyping [166, 251, 252]. Based on our experience in the development of real-time prototypes [62, 89, 91, 92, 270, 272], we have also devised our own methodology that makes use of the testbed at different stages of the development cycle [271]. More specifically, the development starts with the production of a reference software implementation in e.g. MATLAB. At the beginning of the real-time development, the testbed can be used to transmit signals – using the reference software implementation – to the real-time RX without requiring that the real-time TX be ready to be used. Analogously, the testbed can acquire the signals transmitted by the real-time TX to check them using the reference software implementation. Moreover, the testbed can be used to explore the performance impact of a specific functionality in the real-time system without requiring the availability of the real-time implementation. For example, it can be used to evaluate the impact on the system throughput of a new channel estimator or a new channel code. Summarizing, the flexibility provided by the testbed is utilized to speed up the implementation of real-time prototypes as well as to improve the techniques used to test them.

Educational Environments

Commonly, testbeds are being developed at public research centers that often belong to different universities. Consequently, it is possible and desirable to take advantage of the investments in the testbed development to help teach students the basis of wireless communications (and many other disciplines around it). There are several contributions emphasizing the benefits of a tool like a testbed for education, e.g. [111, 243].

2.4 Future of the Testbeds

The lack of flexible and tunable RF front-ends is one of the major drawbacks limiting the flexibility of testbeds. Lastly, although new products have started to emerge in the market, they are constrained to the ISM bands and are not highly linear devices. Additionally, the digital section of the testbeds is still very expensive and almost unaffordable for small research groups. Investing more than 50K EUR in hardware plus the costs of test equipment such as oscilloscopes, spectrum analyzers, etc. plus the necessary cables, adapters, oscillators, and the necessary mechanical tools to properly work with the said hardware is not an affordable option for all research groups. Moreover, testbed development involves several areas of expertise, thus requiring engineers skilled enough to successfully set up the testbed. After all these expenses,
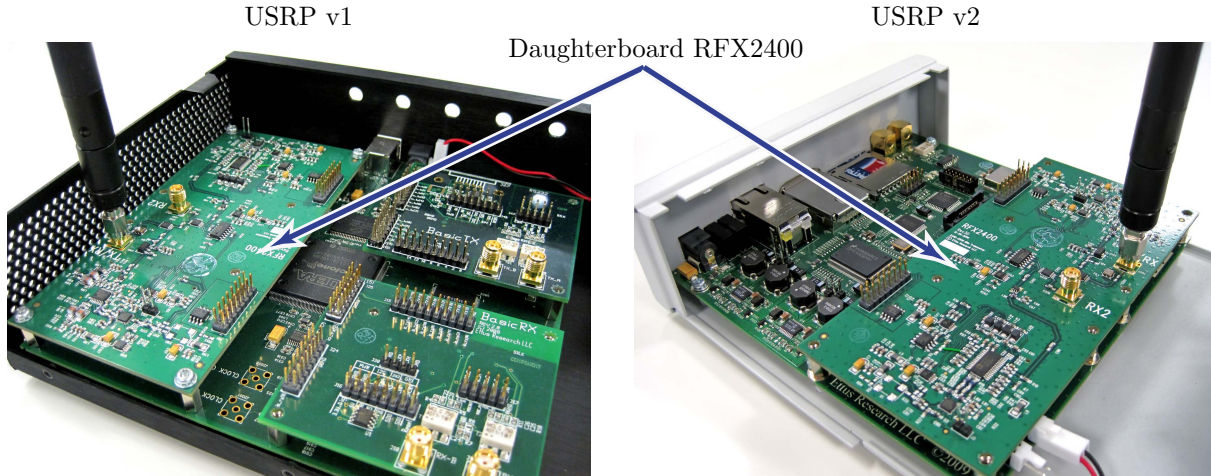
Figure 2.11: Pictures of the USRP and the USRP2, both equipped with the RFX2400 daughterboard that covers the 2.4 GHz ISM band.

measurement campaigns have to be carried out to produce valuable results with the testbed and, therefore, justify the investment.

With the advent of GNU Radio [7], a revolution in the software-defined radio technologies is foreseen that will greatly reduce development costs in terms of hardware, money, and manpower. GNU Radio is a free and open software toolkit for the development of software-defined radio systems (e.g. testbeds). GNU Radio provides the signal processing blocks for implementing reconfigurable software radios using the Universal Software Radio Peripheral (USRP). The USRP (and its successor, the USRP2) is a low-cost external device (see Figure 2.11) manufactured by Ettus Research LLC [3] and containing the digital hardware as well as pluggable RF front-ends named daughterboards. The available set of daughterboards covers a wide range of RF bands (from 50 MHz to 2.9 GHz, and from 4.9 to 5.85 GHz). Although Ettus claims that the designs of all daughterboards are free and open [5, 8], only the schematics are available for download.

Unfortunately, the GNU Radio approach presents some limitations to be overcome in the near future [247]. The USRP2 is still under development, which means that the hardware is already finished and available whereas the software is still not mature. Moreover, the MIMO capabilities of the URSP are very limited in the number of TX and RX antennas as well as in the maximum available bandwidth (8 MHz shared among all TX/RX antennas).

2.5 Conclusion and Criticism

In this chapter, we briefly defined the MIMO testbed concept in the context of wireless communications research. We also introduced our COTS-based GTEC MIMO testbed developed at the University of A Coruña. The GTEC MIMO testbed is just one of many approaches [27, 30, 34, 35, 42, 43, 49, 60, 65, 66, 69, 80, 82, 83, 86, 121, 131, 134,

162, 163, 169, 171, 172, 174, 175, 178, 179, 184, 185, 189, 195, 198, 204, 216–219, 223–225, 229, 234, 246, 249, 256, 275, 276, 290, 295–297, 300, 301, 304, 306, 310, 313]. Throughout this chapter we focused on the testbed hardware, providing detailed descriptions of the TX and the RX hardware modules and how they are interconnected. The performance of the GTEC MIMO testbed is similar to that offered by typical commercial devices, for example a laptop or a mobile phone. Therefore, the testbed is suitable for evaluating the performance of wireless communications systems in realistic, indoor scenarios. We also provided an overview of typical testbed applications, as in the development process of real-time prototypes or in education. Finally, we provided our particular vision of the future of the testbeds, placing special emphasis on the promising *new* GNU Radio platform.

The idea of constructing a testbed based on COTS modules is justified by the savings in time, manpower and the amount of *a priori* required knowledge and time. In practice, however, hardware modules are not correctly specified by the manufacturer, requiring more time for their correct set-up. Moreover, the manufacturer only provides integration examples for specific module configurations, and thus if your set-up requires a different configuration the corresponding software has to be implemented from scratch, as in our case. Fortunately, the Sundance hardware is bundled with the 3L Diamond software [1], which abstracts low-level details of the hardware components such as the interconnections through the SHB. As a positive consequence, we designed and implemented an Application Program Interface (API) based only on the 3L Diamond for dealing with every module type present in our hardware, thus allowing for any module combination without having to implement everything from scratch.

Another drawback of the Sundance hardware is that the firmware of the modules cannot be customized by means of high-level tools, as for example the Xilinx System Generator [25]. Finally, we make use of the agile feature of the RF front-end to generate channel realizations. However, a better solution would be to employ a system to move the RX antennas, as for example in [56].

Chapter 3

Distributed Multilayer Software Architecture for MIMO Testbeds

In this chapter we introduce the software architecture for the "GTEC MIMO testbed", complementing the hardware part presented in Chapter 2. This chapter is partly based on the publications [90, 105, 108, 110].

The software architecture of the GTEC MIMO testbed is based on well known solutions from the software engineering discipline. Such principles are introduced in Section 3.1 as are the basic elements of the software architecture designed for Multiple-Input Multiple-Output (MIMO) testbeds in general and particularized for the GTEC MIMO testbed. The software engineering concepts required to understand the architecture are described in Section 3.2, while the proposed architecture for MIMO testbeds is studied in Section 3.3. Making use of the proposed architecture, in Section 3.4 we define a closed-loop measurement procedure that is supported by the architecture, thus simplifying the implementation of measurement and evaluation software for the wireless communications system under study. As a result of a proper testbed software design, it is easy to build a testbed with more than two nodes. As an example, in Section 3.5 we present a multinode testbed obtained from the union of two independent testbeds. Finally, Section 3.6 is devoted to the conclusions and criticism.

3.1 Introduction

Based on the experience acquired in building and setting up the GTEC MIMO testbed [104, 106, 107, 237, 240, 241], as well as real-time prototypes that make use of the testbed [62, 63, 89, 91, 92, 270, 272], we can assert that once the testbed hardware is available and properly configured, the interface with the testbed becomes the main, and also frequently ignored, issue. It is convenient to provide at least a well documented Application Program Interface (API) to interact with the testbed, making it accessible and usable to the researchers. When a research

team decides to start the process of acquiring and/or constructing a new testbed, they need to take into account numerous aspects related both with the hardware and its technical features, and the extendability opportunities in the future [106, 253]. Usually, most of the efforts are devoted to the testbed set-up, which results in equipment that is hardly usable by those not involved in its development process.

As a result, the migration of an algorithm from a simulation environment to a testbed involves cumbersome low-level programming to access the hardware as well as a very detailed knowledge of the hardware. Unlike simulations, the experimental evaluation of wireless communications systems means having to deal with frequently ignored problems, as for example time and frequency synchronization and low-level signal processing operations such as pulse-shaping and matched filtering. All these issues make it more difficult to assess new MIMO communications systems in a testbed. For this reason, it is desirable to make the testbed accessible to researchers at a reasonable level of abstraction. This goal represents an important challenge due to the large number of heterogeneous technologies and development environments that have to be integrated together. However, if this challenge is met, the final result is a very attractive product for the user[1], who can focus on the development of new transmission techniques that can easily be translated to the testbed and later evaluated in realistic scenarios.

In this chapter we describe how to solve all the previously mentioned limitations by using a distributed multilayer software architecture. The proposed architecture is based on the software-defined radio concept [206, 207, 248] and enables the testbed to be easily accessible to its users by means of a suitable integration in the development environment they are using. Although all designs and results presented herein are particularized for the GTEC MIMO testbed, they are easily adaptable to most existing testbeds, even making the integration of heterogeneous testbed nodes possible in order to build a multinode testbed (more on this in Section 3.5).

Before continuing, we introduce the following software engineering concepts:

- **Software architecture**. The software architecture concept was first presented as a result of the research work conducted by Edsger Dijkstra in 1968. Subsequently, several research works focused on the problem of defining the gross structure of the software needed to implement a program or a computing system in general [112, 263]. The software architecture of a computing system models the structures of the system, which comprise software components, the externally visible properties of those components, and the relationships between them. Later on, the concept of pattern [101] – defined as an effective and reusable way to solve a non-trivial software problem – was also applied to the software architecture discipline [46, 47], resulting in the so-called *architectural patterns*.

---

[1]Throughout this chapter, a *user* is a researcher not involved in the testbed development and not familiarized with *low-level* signal processing tasks (e.g. synchronization).
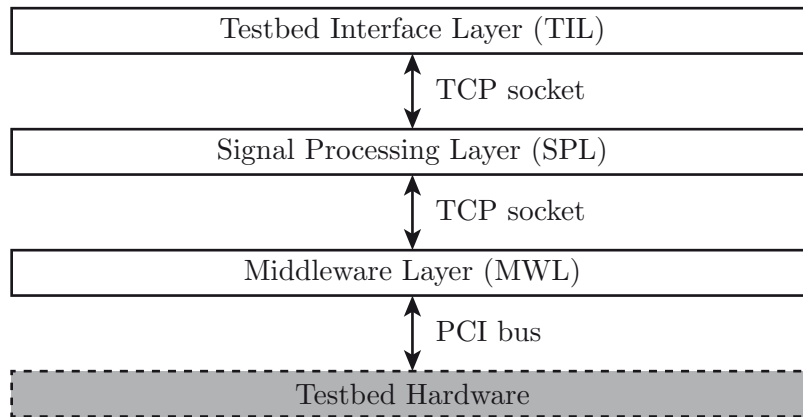
Figure 3.1: Basic scheme of the software architecture of the GTEC MIMO testbed.

- **Software layer**. The concept of software layer (also know as layer, tier or software tier) was generalized in [46] by means of the so-called *Layers* architectural pattern. Basically, a layer is a piece of software implementing a clearly defined set of functionalities and with a clearly defined interface to access it. A multitude of advantages are obtained from the utilization of the layers pattern in the design of a software architecture: the layer hides the technology used in its implementation to other layers in the system, being reusable in other systems and also physically separated from the system.

- **Distributed system**. Software systems are distributed when several parts (maybe layers) compounding the whole system are physically separated. It means that the entire system can be distributed among several processors. Note that testbeds often contain several processor types, e.g. general-purpose processors, graphics processing units, Digital Signal Processors (DSPs), Field Programmable Gate Arrays (FPGAs), micro controllers, etc. Systems are designed and implemented in a distributed way to take advantage of the different processors, thus speeding up the whole system and opening the door for parallelization.

According to the concepts defined above, we have designed and implemented a distributed and multilayer software architecture suitable for MIMO testbeds. The proposed software architecture (see Figure 3.1) consists of three different layers (from the lowest to the highest level):

1. **Middleware Layer (MWL)** is the lowest-level layer that interacts with the testbed hardware. It makes the testbed hardware accessible through standard Transmission Control Protocol (TCP) socket connections regardless of the hardware type utilized.

2. **Signal Processing Layer (SPL)** performs the necessary operations required to adapt the discrete-time signal sequences provided by the user into discrete-time signals suitable to be transmitted by the hardware. At the Receiver (RX), it is usual to perform signal processing operations such as time and frequency synchronization in case they are not carried out elsewhere. The SPL also incorporates a great variety of utility functions for

the users as well as a set of tests to check the correct functioning of the testbed hardware. Finally, the SPL implements the necessary functionalities for the measurement procedure explained in Section 3.4.

3. **Testbed Interface Layer (TIL)** is the highest-level layer and presents the testbed to the user at an adequate abstraction level. The TIL has to be specifically implemented for each programming environment. For example, if the user employs MATLAB, then a specific implementation of the TIL for MATLAB has to be developed. The main purpose of the TIL is to provide a simplified interface to access the testbed. This does not rule out the possibility of providing mechanisms to control the hardware in detail from the TIL. It is very important to emphasize that there is no business logic[2] in the TIL except that necessary for adapting the data format from the specific environment used by the SPL and vice-versa. The only requirement for the TIL to be implemented is the availability of a standard TCP socket library. The TIL can be seen as a *software wrapper* that avoids the direct utilization of plain socket interfaces to command the SPL.

The whole design and implementation of the proposed software architecture is carried out fulfilling the following requisites:

1. **Layers have to be decoupled as far as possible**. This is a fundamental concept in modern software design and structured programming. The key idea is not to replicate functionalities that are already present in another layer, which would be a symptom of a poor design. The basic premise is to design everything to be fully decoupled and reusable; and later on introduce some small violations of this principle only if they are strictly needed to increase the overall system performance.

2. **Each layer can be extended and/or customized** to be able to adapt it to meet future specifications and/or heterogeneous hardware environments. Consequently, each layer can be upgraded without reimplementing it again from scratch, which is frequently the only solution in case of monolithic, non-layered systems.

3. Finally, **layers should be distributable**, which means that they use remote connections to interact amongst themselves. On the one hand, this helps to ensure the decoupling and independence principles whilst, on the other hand, it allows the testbed to be remotely accessible from a host PC.

3.2   Technology Behind the Software Architecture

The field of computer engineering has encountered problems associated with complexity since its inception. The software architecture discipline focuses on the idea of reducing complexity

---

[2]In software engineering, the algorithms are termed the *business logic* to differentiate them from the rest of the code needed to perform input/output operations, data type conversions, etc.
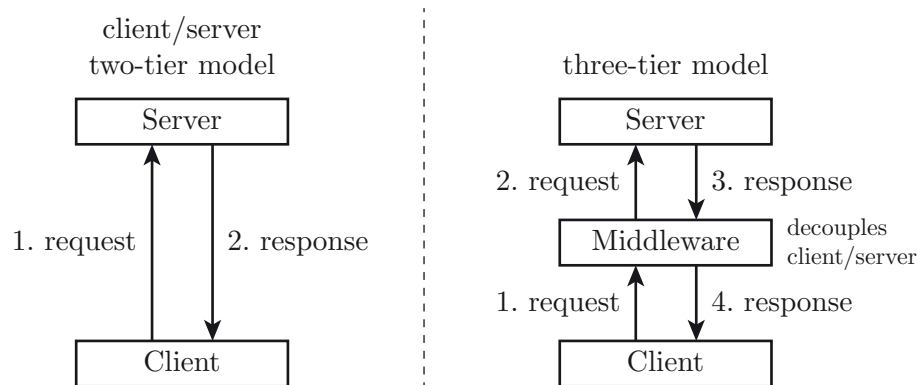
Figure 3.2: Software architecture models: client-server (left-hand side) and multi-tier (right-hand side).

through abstraction and separation. There are several kinds of software architectures, amongst which the most interesting for our work are the client-server architecture, which serves as the basis for most of the available architectures; the three-tier model; and finally, the most recent and advanced model-view-controller architecture.

3.2.1 Client-Server Software Architecture (Two-Tier Model)

Client-server (see left-hand side of Figure 3.2) describes the relationship between two computer processes in which one process (the *client*) makes a service request to another process (the *server*). Applications following the client-server architecture represent an evolution with respect to those called *monolithic*.

The basic operation mode for client-server applications consists in each instance of the client process sending requests to one or more connected servers. In turn, servers accept these requests, process them and return the requested information to the client. The basic client-server architecture considers only two types of host: clients and servers. Consequently, it is also known as the two-tier model. A special case of the two-tier software architecture arises when an instance simultaneously acts as a client or as a server, resulting in the peer-to-peer architecture.

3.2.2 Multi-Tier Software Architecture

The multi-tier software architecture represents a natural evolution from the client-server model towards a higher number of levels (see right-hand side of Figure 3.2). This is the reason why it is also known as the *n-tier software architecture*. Basically, the multi-tier software architecture is a client-server architecture consisting of more than two tiers, in which the inner tiers act simultaneously as client for one tier and as server for the other. The main difference with respect to the peer-to-peer model is that the tier order (its position or level in the multi-tier structure) does matter. An inner layer is also termed middleware because acts as an intermediary between

two adjacent tiers.

Note that the multi-tier software architecture, as well as the two-tier one, is a mechanism to design the physical structure of the system. Given one of the models, several degrees of freedom are still possible in the process of defining the logic structure of the system.

3.2.3   Tier Interconnection Mechanisms

In software architecture design there is still one open question: How are the messages sent from one tier to another? In principle, the way data is exchanged between two tiers is part of the architecture design, but in practice only the message types and their order are defined by using sequence diagrams, which leads to the definition of the interaction between all tiers. Messages can be transferred using plain socket connections or more elaborate mechanisms (e.g. CORBA, Java RMI or XML-RPC [266]). The different approaches have their own advantages and disadvantages and there is still no perfect system for message exchange. However, what is crucial is to use standardized mechanisms for message exchange, thus guaranteeing independence between tiers.

3.2.4   The Model View Controller Architectural Pattern

The Model View Controller (MVC) [46] is a pattern used in software engineering derived from the multi-tier software architecture. Successful use of the pattern leads to the isolation of the business logic from the user interface, allowing modifications in one layer without affecting the others. The controller collects user inputs, the model manipulates (and usually stores) application data, and the view presents results to the user. The MVC can be used as an architectural or design pattern. As an architectural pattern, it divides an application into three independent layers (similar to the right-hand side of Figure 3.2) that can be run in different computers: the presentation or user interface layer, termed the view; the business logic, called the model; and the so-called controller, an intermediate layer adapting the view to the model and vice versa.

3.2.5   Applying Software Engineering to MIMO Testbeds

In Chapter 2 we introduced the typical hardware architecture available in MIMO testbeds, showing that most manufacturers do not offer an integrated solution. Furthermore, we stress that this abstraction level is nowhere near sufficient and, consequently, a researcher not involved in the testbed development cannot directly interact with a communications system from the corresponding simulation code. In this chapter we have introduced standard architectural software models, starting with the well-known client-server model and finishing with the recently proposed model view controller, widely used in distributed, robust and efficient
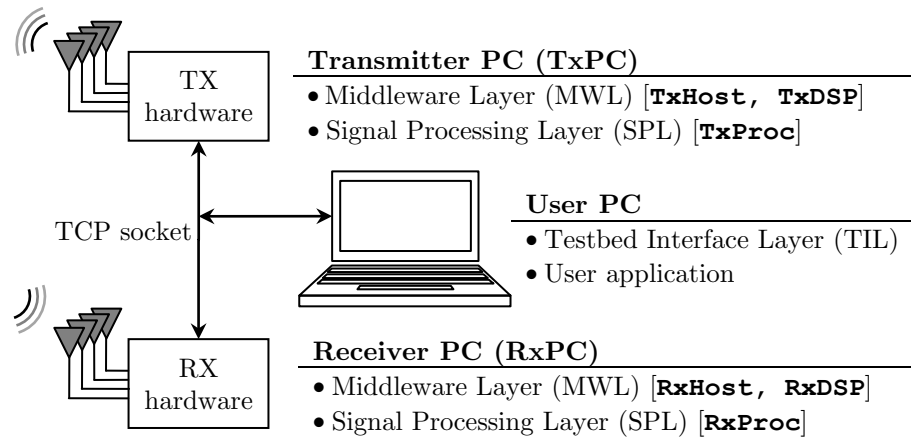
Figure 3.3: General scheme of the GTEC MIMO testbed showing the three different layers: MWL, SPL, and TIL. The corresponding name of the processes compounding each layer as well as the name of each *server* is shown in brackets.

applications. These architectural models serve as an inspiration to propose a novel software architecture useful for bridging the existing gap between the abstraction level offered by testbeds and that demanded by researchers and end users.

3.3 Software Architecture for MIMO Testbeds

Figure 3.3 shows the hardware organization of the GTEC MIMO testbed. It is constituted by two ordinary PCs hosting the testbed hardware, one for the Transmitter (TX) (called TxPC) and another one for the Receiver (RX) (named RxPC). The digital section of the testbed hardware is located inside the Personal Computers (PCs), whereas the Radio Frequency (RF) front-ends remain outside the PC case. All PCs are attached to the network.

In the rest of this section we assume the following:

1. The testbed consists of two nodes, the TX and the RX. In Section 3.5 we show that the software architecture can be extended to an arbitrary number of nodes.

2. It does not matter whether the testbed operates outdoors, indoors, outdoor to indoor or vice-versa. We assume that a network connection can always be established between the testbed nodes and the user PCs.

3. Testbed host PCs will use a standard operating system supporting remote operation from another PC attached to the network.

3.3.1 From the MIMO Testbed to the Multilayer Software Architecture

Figure 3.3 shows, next to the PC drawings, the names of the corresponding three layers of the proposed architecture, which are, from the lowest to the highest level, the MWL, the SPL, and

the TIL. The MWL and the SPL are divided into transmit and receive parts, while the TIL has just one instance running on the user PC. Actually, the TIL is just an API that has to be included with the user application (e.g. a simulation of a wireless communications system). The MWL is the only layer that has to be installed in the hardware PCs, while the rest of the software can be deployed in any machine attached to the network.

This is not an arbitrary proposal but a design inspired by the multi-tier and the model-view-controller software architectures. First of all, let us identify the use cases of our application. Basically, there is just one use case or action carried out by the user: transmitting a set of discrete-time sequences through the testbed and, consequently, through the wireless channel. Therefore, the layer corresponding to the view is the interface that provides access to the testbed, sending the sequences and getting back the acquired signals. This is what we term TIL, and it is the topmost layer of our software architecture. Note that several other use cases are included in the TIL, for example setting the TX gain, the RF carrier, and many more that may depend on the testbed hardware capabilities.

The controller plays a very important role in a system. It is responsible for obtaining the service requests from the view, adapting them and sending them to the model where the business logic resides. The results gathered are then sent back to the view to be presented to the user. Therefore, the controller plays the role of the middleware concept presented in the multi-tier software architecture. In the testbed system, the controller is called middleware and its functionality consists in controlling and configuring the hardware.

However, our architecture presents three major differences with respect to the model view controller and the multi-tier architectures:

- Adaptation of, for example, discrete-time sequences provided by the TIL as a request, both at the TX and at the RX sides, consists in performing different signal processing operations that can sometimes even be executed using different processor types. For instance, general-purpose processors, graphics processing units, FPGAs, or DSPs. It is thus necessary to put all these operations together and, consequently, the concept of SPLs arises. Therefore, the SPL is in charge of carrying out most of the signal processing operations needed between the MWL and the TIL.

- One of the reasons for using a multi-tier architecture jointly with the model view controller is the ability of the resulting application to be distributed among different machines. Therefore, different instances of the tiers run on different machines. However, in the testbed system there are two kinds of node: the TX and the RX. If a multi-node testbed is available, different TX and RX pairs will be distributed among different nodes. As a result, the MWL (and consequently the SPL) is split into two sides: the TX side and the RX side. They will be termed Tx MWL, Rx MWL, Tx SPL and Rx SPL, respectively. Additionally, they are also identified because the processes mapping the architecture design are also split into two sets, one for the TX and another for the RX.
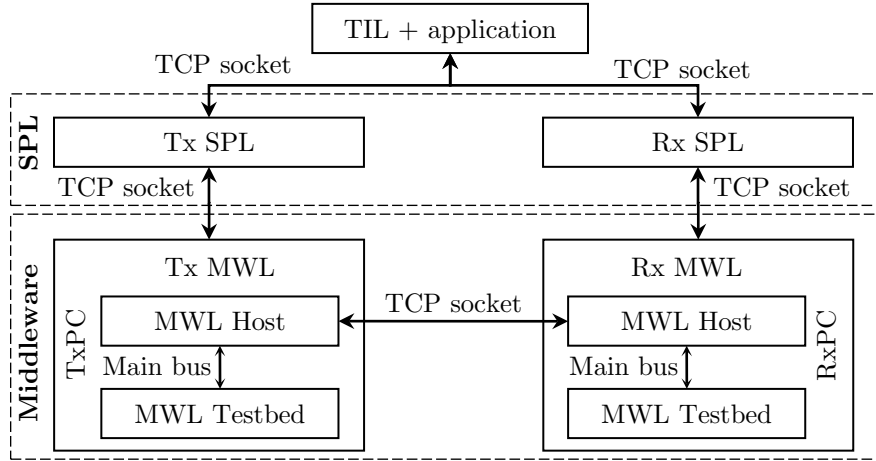
Figure 3.4: Basic structure of the distributed multilayer software architecture for MIMO testbeds. The three layers are shown: MWL, SPL, and TIL. Additionally, the testbed-hardware sub-layer in the MWL and the different interconnection mechanisms are included.

- Finally, another particularity present when adapting the model view controller and the multi-tier software architectures to the testbed software architecture is that the hardware is required to be attached to the host system by means of a bus (e.g. USB, PCI, PCIX, PCI Express, etc.). Consequently, it is not possible to use standard network connections through such buses, and the standard tools and techniques available for interconnecting layers are not applicable (except when a custom implementation is provided or when the hardware is attached through a network connection). These reasons motivated another division in the MWL, generating a *testbed-hardware* sub-layer (with its respective parts for the TX and the RX sides) responsible for dealing with hardware aspects as well as solving the bus connection issues with the host part of the MWL. Bearing in mind that in our testbed this sub-layer runs on the DSPs available at the TX and at the RX, the corresponding processes are named `TxDSP` and `RxDSP`, respectively.

3.3.2 Logical and Physical Designs of the Software Architecture

Figure 3.4 shows the basic structure of the proposed architecture. There are two sides, TX and RX, joined at the TIL, which has to hold connections with both sides of the SPL. All links between the different layer elements are implemented by means of standard socket connections. The exceptions are the links between the MWL sub-layers that use an ad hoc protocol over the existing main bus interconnecting the hardware and the host.

There are strong reasons for using standard socket connections instead of any other high-level mechanism (e.g. XML-RPC [266]). However, this does not imply that in some situations other connection types may be suitable. It is also possible to use different link types between different layers. For example, the TIL and the SPL can be connected using XML-RPC, thus
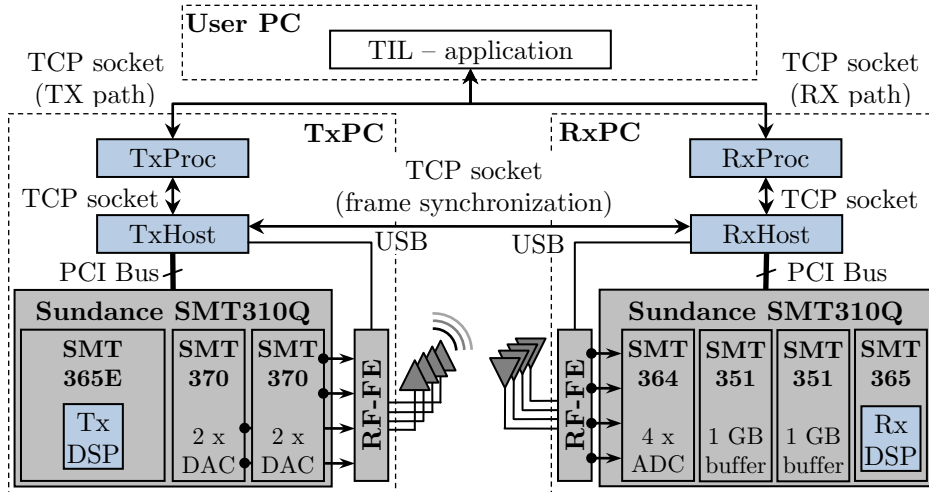
Figure 3.5: Testbed scheme containing the hardware and the software architecture deployment as well as the links between the components. The different processes are shown in blue, and are located in the usual place for a typical architecture deployment. The digital hardware sections of the testbed, as well as the RF front-ends, are shown in gray. Finally, the user application containing the TIL is in white. Note that TIL appears in white and not in blue because it is not a process but an API.

allowing total independence of the platform and full remote access. However, the ability of such high-level techniques to sustain high data rates and low latency connections is not the best. For these reasons, sockets offer sufficient flexibility while providing fast connections.

Figure 3.5 shows a block diagram of the hardware and the software of the GTEC MIMO testbed. Three main parts can be distinguished: the testbed hardware that allows us to transmit discrete-time signals over multiple antennas; the multilayer software architecture that makes the hardware accessible to the researchers at a high abstraction level; and the user application implemented employing the testbed capabilities and the architecture facilities. The lowest software level (i.e. the MWL) has to be installed in the same PC as the testbed hardware because it uses the system buses to communicate with the hardware. Otherwise, this restriction would not be applicable. The other two layers can be installed in any other available PC. In the typical deployment used for the GTEC MIMO testbed, the SPL is directly attached to the user application, thus avoiding additional latencies introduced by the socket connections, but preserving the structure in a decoupled way. Additionally, the SPL implements the measurement procedure that is accessible through the TIL, thus greatly simplifying the complexity of the software required for the evaluation of a communications system.

3.3.3 A Simple Transmission Example

In order to shed more light on the system architecture, we explain, step by step, the transmission of a single frame (see Figure 3.6). After the discrete-time sequences to be transmitted
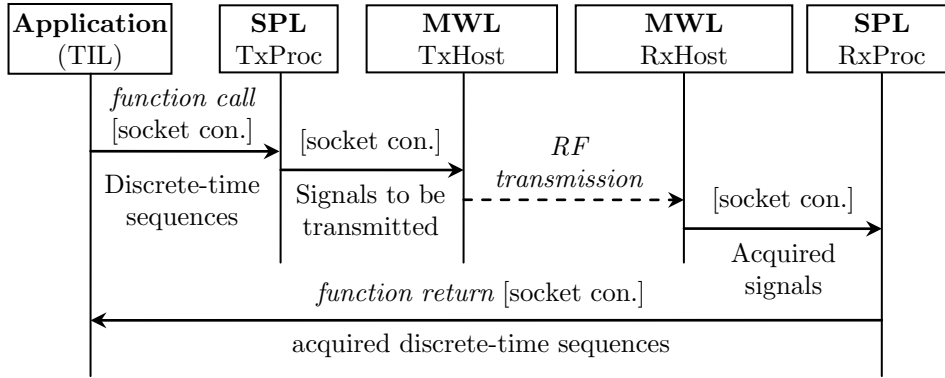
Figure 3.6: Frame transmission example, showing how a single frame transmission is carried out from the discrete-time sequences. For the sake of simplicity, the MWL is considered as a whole, even when it is actually divided into two sub-layers.

have been generated at the user application (e.g. the measurement program performing an experimental assessment of a wireless communications system), a function from the TIL is called, receiving the corresponding symbol vectors (one vector per transmit antenna) as the input parameter. These symbols are then sent to the SPL (`TxProc`) where they are converted (if necessary) to discrete-time signals ready to be transmitted by the hardware. Finally, such signals are subsequently sent to the MWL (`TxHost`). When both the TxPC and the RxPC are ready to complete a transmission, the signals are passed to the testbed hardware through the corresponding `TxDSP` process, to be transmitted by the antennas. At the RX side, the MWL (`RxHost`) acquires the signals stored in the hardware buffers by the `RxDSP`. Next, they are forwarded to the RX SPL (`RxProc`). At this moment, the TxPC and the RxPC are ready to process another frame while the acquired signals are converted into discrete-time sequences in the same format required by the end user. Finally, the discrete-time sequences are forwarded to the user application through the TIL, completing the transmission process.

3.3.4 Testbed Interface Layer

The TIL deals with the interaction between the testbed and the researcher (i.e. the end user). Basically, the TIL exposes the low-level layers of the software architecture by means of an API that supports the following functionalities (use cases):

- Configuring different hardware parameters. For example, the TX gain, the RX gain, or the RF carrier frequency.
- Transmitting up to four different discrete-time sequences (one sequence per TX antenna). By default, the frames are transmitted cyclically in a continuous way.
- Acquiring up to four different discrete-time sequences (one sequence per RX antenna). Note that the acquisition process is in no sense linked to the transmission, thus allowing for sequential acquisitions. This feature is useful when performing several acquisitions,

varying the TX power value.

- Complementing the two previous use cases, the TIL API also includes a function that carries out the whole process: transmission and acquisition of up to four discrete-time sequences. Therefore, a single function call is enough to carry out, on a block basis, all the steps needed to transmit and acquire a set of sequences.

The TIL API also supports the specification of the signal processing operations to be carried out by the SPL. If the researcher wants full control over the signals, then the SPL is merely a bypass. In this situation, the SPL adapts the sequences from the floating point domain to the format required by the Digital-to-Analog Converters (DACs). At the RX side, the samples coming from the Analog-to-Digital Converters (ADCs) are converted to the floating point domain. At the other extreme, the user provides complex-valued discrete-time sequences leaving the necessary low-level signal processing tasks (e.g. pulse-shaping, I/Q modulation and frame assembly at the TX side as well as the corresponding operations at the RX side, including time and frequency synchronization) to be carried out by the SPL. Consequently, the TIL supports different abstraction levels, leaving the researcher the freedom to specify which signal processing tasks will be carried out at the SPL.

3.3.5 Signal Processing Layer

The SPL is connected to both the TIL and the MWL (see Figures 3.4 and 3.5). It supports remote access and makes the other two layers platform-independent with respect to each other. This fact permits the SPL to be run in a PC cluster, dedicated machines with graphics processing units to speed up floating point operations, etc.

The SPL is physically mapped into two different processes that carry out the signal processing operations needed to link the TIL and the MWL. The first process (`TxProc`) receives the discrete sequences to be transmitted from the TIL and performs all necessary operations such as up sampling, pulse-shape filtering, I/Q modulation and frame assembly, in order to generate the discrete-time signals that will be sent to the MWL (`TxHost`). Similarly, the second process (`RxProc`) waits for the acquired signals from the MWL and performs the time and frequency synchronization operations followed by the demodulation, filtering and down sampling. The resulting vectors are sent to the TIL. A very important task carried out by the SPL is the conversion between fixed point and floating point domains. It is also important to emphasize that the SPL is designed and implemented by clearly separating its two main tasks: interconnection with the adjacent layers (i.e. TIL and MWL) and execution of the required signal processing tasks. Notice that depending on the type of sequences given to `TxProc`, not all operations will be required either at the TX or at the RX side.
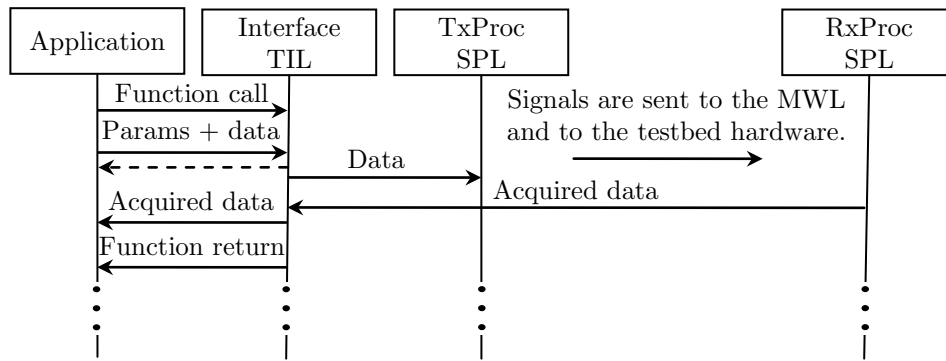
Figure 3.7: Sequence diagram describing the interaction between the user application, the TIL and the SPL.

3.3.6 Interaction between TIL, SPL and the User Application

Figure 3.7 shows a simplified version of the interaction between the user application, the TIL and the SPL. When the user application has generated the discrete-time sequences to be transmitted, the testbed calls a function in the TIL. Both sequences, as well as their type, are included as input parameters. Then, depending on the additional input parameters specified, the TIL offers the possibility of returning the control to the user application in order to continue executing other tasks while the signals are being transmitted and acquired. The TIL establishes a connection with the `TxProc` at the SPL and sends the transmit data. Next, depending on the mode of operation of the MWL, an interaction between the four processes compounding the MWL takes place. As a result, the signals are properly transmitted and then acquired by the MWL and transferred to the `RxProc` at the SPL. Finally, the acquired data is returned to the TIL to be accessible by the user application. If the user application received the control after calling the TIL, then the acquired sequences are not transferred to the TIL until the user application re-calls the TIL, but the MWL is ready to process more requests.

3.3.7 Middleware Layer

The MWL fills the gap between the testbed hardware and the SPL, allowing discrete-time signals to be transferred through the system bus and making the configuration of the whole testbed possible at a high level. The MWL supports several modes of operation:

- TX and RX nodes operate independently. Consequently, from the TIL the user decides when to transmit and when to acquire the signals. This allows multiple acquisitions of the same signals being transmitted cyclically, for example when the same frame is evaluated using different TX power values.
- The MWL can automatically synchronize the TxPC with the RxPC, thus each frame is transmitted and acquired once.

- The TX can broadcast a signal loaded into the real-time buffers in a cyclical way. This allows the signals to be monitored with external equipment or to be acquired by other receivers than the testbed RX.

- The RX can be configured to store up to 256 Msample per antenna before being transferred to the TIL. This feature can be used when acquiring long signals transmitted from a device possibly different from the testbed TX.

- Configuring and controlling all hardware elements, including the RF front-ends. Typical operations of this type include setting the TX power value or the RF carrier at both the TX and the RX. Some of these operations correspond to commands defined in the TIL.

The MWL is split into two different sub-layers (see Figures 3.4 and 3.5). The topmost sub-layer is responsible for establishing the network connections between the TX and the RX and with the SPL. The bottom sub-layer corresponds to the testbed hardware configuration and control software. Part of this sub-layer runs on the DSPs whereas the modules responsible for configuring and controlling the RF front-ends run on the host PCs. Figures 3.4 and 3.5 show the MWL with its two sub-layers plus the connections with adjacent layers.

The MWL is physically mapped into four different processes, two at the TX side and another two at the RX side. The first two, termed `TxHost` and `RxHost`, run respectively on the TxPC and the RxPC. They are implemented in standard C++ language and make use of the following connections:

- One connection between the `TxHost` and the `RxHost` processes. It is used to synchronize the TX and the RX, so the RX knows when the signal acquisition process has to start.

- Another connection is established between the `TxHost` and the `TxProc` processes and it is used to link the TX side of the MWL and the SPL layers.

- Analogously, there is also a connection between the `RxHost` and the `RxProc` processes.

- Finally, a pair of Universal Serial Bus (USB) connections are established between the `TxHost` and the TX RF front-end, and between the `RxHost` and the RX RF front-end. They are used to configure and control the RF front-ends from the TIL through the MWL.

The remaining two processes are the TX and the RX processes, which run on their respective DSPs available in the testbed hardware. Thus, the TX DSP process (`TxDSP`) performs data transfers through the PCI bus jointly with the `TxHost` process and configures and controls the hardware components at the TxPC. In the same way, the `RxHost` process and the RX DSP process (`RxDSP`) are responsible for transferring the data from the DSP side through the PCI bus, controlling and configuring the testbed hardware components.

The MWL design supports extendability in many senses. For instance, many transmitters and receivers can be linked by means of network connections. It is important to stress that since the hardware interfaces from the host side; from the software related to DSPs; and from

the software for controlling and configuring the RF front-ends are all developed as separate software modules, they can be replaced by implementations suitable for any other devices. For example, simply by replacing the hardware-dependent modules, the software architecture is already valid for a different testbed hardware (e.g. the USRP), and all previously implemented applications will work without any modification. Note that if the application makes use of a feature not supported by the replaced hardware, the application will be appropriately notified to deal with the problem.

3.4 Closed-Loop Measurement Procedure

Given the above-mentioned features offered by the testbed hardware together with the software architecture, we defined a complete closed-loop measurement procedure, described below. Such a procedure can be customized according to the requirements of the evaluation to be carried out. For example, if the communications system to be assessed does not require a closed-loop link, only control information is exchanged between the two nodes. The measurement procedure is implemented as an easy-to-use software template with the objective of simplifying the migration process from a simulation code to the analogous testbed code. Such software template is implemented on top of the TIL API.

Before starting a new measurement, the following parameters must be defined in the template:

- Number of TX and RX antennas.
- The set of RF carriers. In order to generate different channel realizations, we take advantage of the frequency agile capabilities of the RF front-ends. The front-ends support several RF carriers at both 2.4 GHz and 5 GHz Industrial, Scientific and Medical (ISM) bands, separated by about 1 MHz each.
- The set of TX power values. If the measurement is carried out varying the TX power value (correspondingly, the Signal to Noise Ratio (SNR) value), then the TX power of the signals is controlled at the TX RF front-end.
- The necessary signaling parameters, e.g. number of samples per symbol, etc. The number of parameters and their specific values depend on the signal processing operations to be performed by the SPL.
- Some other parameters have a default value that is valid in most cases. However, several testbed parameters are tunable without modifying the hardware or the software at all. For example, the sampling frequency of the DACs and the ADCs, or the size of the buffers at both TX and RX sides.

By default, the GTEC MIMO testbed employs a very simple but effective frame structure. It contains a Pseudo Noise (PN) sequence used for time synchronization followed by a *silence*, a

time interval in which no signals are transmitted; and, finally, the part of the frame generated by the evaluation software. The observed PN sequence is available at the RX side if needed. The measurement software automatically estimates the mean RX power of the signals as well as the mean Power Spectral Density (PSD) of the noise. Additionally, the SPL implements various tests to try to guarantee the correctness of the frame, i.e. that no other interferences have been received, or that the RF front-ends are working properly.

Once the above-mentioned parameters are defined, the measurement procedure consists basically of two loops plus several steps, as described below:

- An outer loop over the set of RF carriers.

    - An inner loop over the set of TX power values.

        * Several optional loops can be defined depending on the wireless communications systems to be measured and compared. At the innermost loop, the following steps are carried out:

            · The frame to be sent is assembled. It means that user code is executed in order to generate all blocks of symbol vectors to be transmitted. For example, if two different channel codes are compared, then, at this point, the two vector blocks (one for each channel code) are generated and sent to the SPL through the TIL.

            · A function is called, the transmission is carried out and the observations are returned. At this point, depending on the measurement type, the user code chooses between generating and transmitting new blocks according to the observations (i.e. closed-loop measurements) or skipping such steps and continuing with the next iteration. The user also selects between only varying the TX power on every iteration and also transmitting a new frame.

            · For each iteration, all intermediate results plus the observations are permanently saved in files. Therefore, the measurement can be paused – intentionally or not – and later resumed from the same point.

Once the measurement has finished, exactly the same code is used to perform the evaluation of the acquired data. Just changing the value of a parameter causes that, instead of the measurement, the evaluation is carried out. As a consequence, a simple look at the resulting code is enough to understand most of the measurement parameters. Therefore, the resulting script is also used as a sort of documentation for the measurement. Notice that there is no specific implementation for the feedback channel. Instead, all the software code needed for the TX and for the RX under evaluation is executed by *the same* process, and thus all information is already available at such a process.

RX node #3 (GTAS)   RX node #2 (GTAS)   RX node #1 (GTEC)   TX node (GTEC)
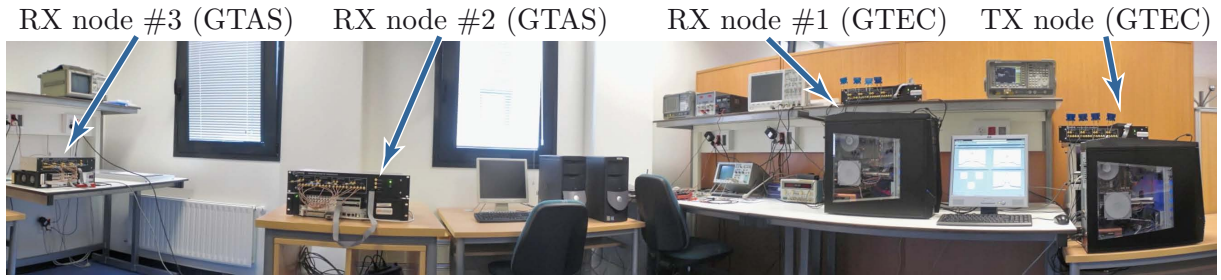
Figure 3.8: Panoramic picture of the multi-user testbed constructed with the two nodes of the GTEC MIMO Testbed plus two nodes of the testbed developed at the University of Cantabria.

3.5 Multi-Node Testbeds

Thanks to software architecture solutions like the one presented in this chapter, it is possible to build a multi-node testbed by joining two or more two-node testbeds. This approach is very interesting because it makes if possible for two or more research groups to construct a multi-user testbed without needing to replicate the testbed hardware. However, if the software design of each testbed has not been carried out carefully, the integration will involve a complete redesign and implementation of the new multi-user testbed. Consequently, a more intelligent and, therefore, cheaper solution consists in properly designing the software for each testbed, taking into account the scalability and flexibility requisites. This way, the integration task is reduced to a high-level implementation dealing with the TIL API – or similar interfaces according to each testbed design. Figure 3.8 shows a photograph of a demonstration of a multi-user testbed with four nodes with four antennas each. Two nodes are the from the GTEC MIMO testbed whereas the other two are from the testbed developed by the GTAS at the University of Cantabria. In such a set-up, a broadcast channel with one TX node and three RX nodes was measured.

3.6 Conclusion and Criticism

In this chapter we proposed a new distributed multilayer software architecture for MIMO testbeds focused on user access. The architecture fills the gap that currently exists between commercial hardware components and the most common abstraction level demanded by researchers. The architecture overcomes the limitations of implementing new algorithms directly on the testbed. Instead of using the low-level software interfaces typically provided by manufacturers, the architecture supplies a high-level interface access for testbeds. It releases researchers from need to know the details of the testbed hardware. For instance, they can easily test new algorithms without developing a completely new source code release specifically for the testbed, thus speeding up the implementation and test tasks by using a specific software template.

The key point for the multilayer architecture design is the use of ordinary network connections – or any other means of standardized communications mechanism – to link both software modules and hardware components. These connections are also useful for decoupling the software layers. Several advantages are obtained as a consequence of the multilayer software architecture.

The main advantage provided by the software architecture is that now the code implementing the communications system to be evaluated is in a single script or program, exactly as in a computer simulation. Therefore, it was trivial to implement a closed-loop system because the transmit signals, as well as the acquired observations, were examined by the same program, which applies the strategy to adapt the next blocks to be transmitted according to the conditions of the wireless channel. Moreover, a software template containing the steps of a simple but effective measurement procedure was provided.

However, the proposed software architecture penalizes the efficiency of the measurement, which is slightly reduced due to the interconnections among the layers. This problem is partially overcome by directly attaching the SPL to the TIL when both are implemented in MATLAB. Note that this is not a violation of the good software design principles, but an optimization of the architecture. The efficiency of the measurement process is also reduced due to the lack of an external hardware device to assist in the time synchronization process. Consequently, a large amount of data is acquired each time, of which a considerable amount is discarded after the time synchronization is carried out. An additional issue appears when the two sets of TX power values and RF carrier frequencies are required by the same measurement process. The problem is caused by the RF front-end, because an attenuation value is actually provided instead of specifying a TX power value and, for the same attenuation value, the resulting TX power value changes depending on the RF carrier utilized. This does not represent a problem if the measurement results are plotted with respect to the SNR (or a similar measurement unit, for example the E_b/N_0) because the SNR is estimated for every acquisition at the RX side. However, if the results are plotted over the TX power or the same TX power is required at the TX side regardless of the RF carrier utilized, then an additional calibration step is required at the TX side.

Chapter 4

Blind Channel Identification for Alamouti Coded Systems

In this chapter, we address the experimental evaluation of several blind channel estimation techniques making use of our multiple-antenna testbed and software defined radio implementations in MATLAB. This chapter is partly based on the publications [104, 107, 236, 237, 241] and is organized as follows.

In Section 4.1 a short introduction to Space-Time Block Codes (STBCs) is provided. Different channel estimation strategies suitable for Alamouti Orthogonal Space-Time Block Code (OSTBC) are described in Section 4.2 for the 2×1 Multiple-Input Multiple-Output (MIMO) case, and Section 4.3 for the 2×2 MIMO. In both cases, several channel estimation approaches are included as benchmarks and/or references. The description of the set-up, the procedures followed to measure the channel, and the results obtained – including computer simulation results – are explained in Section 4.4 for the 2×1 MIMO case and in Section 4.5 for the 2×2 MIMO case. Finally, Section 4.6 summarizes the main results of this chapter.

4.1   Introduction to Space-Time Block Codes

Since the pioneering work of Foschini and Telatar [98, 280], multiple-antenna systems have been considered in the literature to drastically improve the performance of wireless communications systems by adding a *spatial* dimension to the existing code, frequency and time dimensions [116, 221, 230, 311]. STBCs have emerged as good mechanisms to exploit spatial diversity in MIMO systems [115, 160]. STBC is very popular due to the work of Alamouti [31] and the later generalization by Tarokh [279], becoming one of the most famous MIMO transmission techniques and motivating a great variety of research [48, 51, 104, 107, 125, 127, 201, 202, 235–237, 241]. Other STBC schemes have been proposed for more than two transmit antennas, but they suffer from severe spatial rate losses [180, 279].

Among space-time coding schemes, OSTBCs are one of the most attractive because they are able to provide full diversity gain without any Channel State Information (CSI) knowledge at the Transmitter (TX), and this with very simple encoding and decoding procedures. The specific structure of OSTBCs makes it possible to convert the optimal Maximum Likelihood (ML) decoder into a simple linear Receiver (RX), which can be seen as a matched filter followed by a symbol-by-symbol detector. According to [102], such a linear RX maximizes the Signal to Noise Ratio (SNR) for each data symbol based on the CSI at the RX side. Moreover, it should be noted that from an information theory perspective, OSTBCs are far from being capacity approaching codes. Furthermore, as shown in [258], the specific signal structure introduced by OSTBCs causes, in general, a decrease in the Shannon capacity limit of the resulting MIMO channel. However, the Alamouti 2×1 OSTBC scheme is optimal.

As a rule, current wireless communications standards include pilot symbols in the definition of the TX signals. Consequently, the RX has to estimate the CSI by using supervised algorithms based on the transmission of pilot symbols. Such pilot symbols convey no information and, therefore, system throughput, spectral efficiency and transmit energy consumption are all penalized. The same reasoning holds true when acquiring the CSI for coherent detection of OSTBCs [220].

In the literature, several approaches for avoiding the limitations mentioned above have been studied. Representative examples are the Differential Space-Time Block Code (DSTBC) schemes [142, 153, 278] and unitary space-time modulation [141, 143]. Both approaches require no CSI knowledge at the RX. However, when these approaches are compared to the coherent ML receiver, which does employ channel estimates, they suffer performance losses. In the case of DSTBC, the method proposed in [153] presents a degradation of about $3\,\text{dB}$ compared to the coherent detector when channel estimates are not available. However, it is important to point out that the differential detection can approach the performance of the coherent detector within $2\,\text{dB}$, and within $1\,\text{dB}$ for the binary case and Bit Error Ratio (BER) values lower than 10^{-5} in Additive White Gaussian Noise (AWGN) channels (see [238, Chapter 5, pp. 276]). In the case of Rayleigh channels, such performance losses increase up to $3\,\text{dB}$ [238, Chapter 14, pp. 775]. When unitary modulation is employed and the ML detector is utilized, the performance losses with respect to the coherent detector are about $2\,\text{dB}$ [141]. Moreover, the complexity of the RX increases exponentially with the number of points in the unitary space-time constellation.

Blind channel estimation techniques can exploit the algebraic structure of OSTBCs while overcoming the limitations of DSTBC and avoiding the penalties introduced by pilot-aided channel estimation techniques. In the literature, there is a great variety of blind channel estimation proposals [44, 267]. Such proposals can be classified into two groups depending on whether they exploit the Higher-Order Statistics (HOS) or the Second-Order Statistics (SOS) of the acquired signals. HOS-based methods present two important drawbacks compared

to the SOS-based approaches: they demand high computational resources, and they require long streams of data for achieving accurate estimates. Consequently, SOS-based methods are preferable for practical implementations. In [260], a SOS-based method with reduced complexity for blind channel estimation using OSTBCs has been proposed. The resulting performance was evaluated using numerical examples, showing that it produces adequate channel estimations. Unfortunately, some OSTBCs – including the Alamouti code – present channel estimation ambiguities that have to be solved using, for instance, linear precoding at the TX or HOS-based methods.

In this chapter, different SOS-based channel estimation techniques [159, 235, 236] are presented, evaluated by means of computer simulations, and measured indoors. Such techniques avoid the channel estimation ambiguity problems introduced in [260]. From now on, the first and the second versions of the GTEC MIMO testbed are considered (more information about the testbed versions in Chapter 2, page 7). In all cases, DSTBC schemes as well as blind channel estimation methods based on the HOS of the acquired signals are evaluated as references for comparison purposes.

Throughout this chapter, we will assume a flat-fading MIMO channel model with n_T TX and n_R RX antennas. The $n_T \times n_R$ complex-valued channel matrix is

$$\overline{\mathbf{H}} = \mathbf{H}^T = \left[\overline{\mathbf{h}}_1 \cdots \overline{\mathbf{h}}_{n_R} \right] = \begin{bmatrix} h_{1,1} & \cdots & h_{1,n_R} \\ \vdots & \ddots & \vdots \\ h_{n_T,1} & \cdots & h_{n_T,n_R} \end{bmatrix},$$

where $h_{i,j}$ denotes the channel response between the i-th TX antenna and the j-th RX antenna, and $\overline{\mathbf{h}}_j$ contains the Multiple-Input Single-Output (MISO) channel response associated with the j-th RX antenna.

Let us consider an STBC transmitting M symbols during L time slots and using n_T antennas at the TX site. The transmission rate is defined as $R = M/L$ and the symbols of the n-th data block are denoted as $r_k[n]$, $k = 1, \ldots, M$. Depending on whether $r_k[n]$ is complex-valued or real-valued, the number of real symbols transmitted in each block is $M' = M$ for real-valued constellations, or $M' = 2M$ for complex-valued constellations. For an STBC, the n-th block of data can be expressed in terms of the transmitted real-valued symbols as

$$\mathbf{S}[n] = \sum_{k=1}^{M'} \mathbf{C}_k s_k[n], \ \mathbf{C}_k \in \mathbb{C}^{L \times n_T}, k = 1, \ldots, M',$$

where $\mathbf{C}_k$ are the STBC code matrices, and

$$s_k[n] = \begin{cases} \Re(r_k[n]) & ; k \leq M \\ \Im(r_{k-M}[n]) & ; k > M \end{cases}$$

are real-valued symbols. In the case of real STBCs, the code matrices $\mathbf{C}_k$ and, therefore, the transmitted matrix $\mathbf{S}[n]$ are real-valued.

The signal at the j-th RX antenna is given by

$$\mathbf{y}_j[n] = \mathbf{S}[n]\overline{\mathbf{h}}_j + \mathbf{n}_j[n] = \sum_{k=1}^{M'} \mathbf{w}_k(\overline{\mathbf{h}}_j)s_k[n] + \mathbf{n}_j[n], \qquad (4.1)$$

where $\mathbf{n}_j[n]$ is the complex-valued AWGN with variance N_0 and $\mathbf{w}_k(\overline{\mathbf{h}}_j)$ represents the combined effect of the STBC and the j-th channel, which is given by

$$\mathbf{w}_k(\overline{\mathbf{h}}_j) = \mathbf{C}_k\overline{\mathbf{h}}_j, \ k = 1,\ldots,M'.$$

Taking into account the isomorphism between complex-valued vectors $\mathbf{w}_k(\overline{\mathbf{h}}_j)$ and real-valued vectors $\tilde{\mathbf{w}}_k(\overline{\mathbf{h}}_j) = \left[\Re(\mathbf{w}_k(\overline{\mathbf{h}}_j))^T, \Im(\mathbf{w}_k(\overline{\mathbf{h}}_j))^T\right]^T$, we can define the real-valued extended code matrices

$$\tilde{\mathbf{C}}_k = \left[\begin{array}{cc} \Re(\mathbf{C}_k) & -\Im(\mathbf{C}_k) \\ \Im(\mathbf{C}_k) & \Re(\mathbf{C}_k) \end{array} \right]$$

such that

$$\tilde{\mathbf{w}}_k(\overline{\mathbf{h}}_j) = \tilde{\mathbf{C}}_k\tilde{\overline{\mathbf{h}}}_j, \ \tilde{\overline{\mathbf{h}}}_j = \left[\Re(\overline{\mathbf{h}}_j)^T, \Im(\overline{\mathbf{h}}_j)^T\right]^T. \qquad (4.2)$$

If the vectors $\tilde{\mathbf{y}}_j[n] = [\Re(\mathbf{y}_j[n])^T, \Im(\mathbf{y}_j[n])^T]^T$ and $\tilde{\mathbf{n}}_j[n] = [\Re(\mathbf{n}_j[n])^T, \Im(\mathbf{n}_j[n])^T]^T$ are defined, the above equation can be rewritten as

$$\tilde{\mathbf{y}}_j[n] = \sum_{k=1}^{M'} \tilde{\mathbf{w}}_k(\overline{\mathbf{h}}_j)s_k[n] + \tilde{\mathbf{n}}_j[n] = \tilde{\mathbf{W}}(\overline{\mathbf{h}}_j)\mathbf{s}[n] + \tilde{\mathbf{n}}_j[n],$$

where $\mathbf{s}[n] = [s_1[n],\ldots,s_{M'}[n]]^T$ contains the M' transmitted real symbols and $\tilde{\mathbf{W}}(\overline{\mathbf{h}}_j) = \left[\tilde{\mathbf{w}}_1(\mathbf{h}_j)\cdots\tilde{\mathbf{w}}_{M'}(\overline{\mathbf{h}}_j)\right]$. Finally, stacking all received signals into $\tilde{\mathbf{y}}[n] = \left[\tilde{\mathbf{y}}_1^T[n],\ldots,\tilde{\mathbf{y}}_{n_R}^T[n]\right]^T$, we can write

$$\tilde{\mathbf{y}}[n] = \tilde{\mathbf{W}}(\overline{\mathbf{H}})\mathbf{s}[n] + \tilde{\mathbf{n}}[n],$$

where $\tilde{\mathbf{W}}(\overline{\mathbf{H}}) = \left[\tilde{\mathbf{W}}^T(\overline{\mathbf{h}}_1)\cdots\tilde{\mathbf{W}}^T(\overline{\mathbf{h}}_{n_R})\right]^T$ and $\tilde{\mathbf{n}}[n]$ is defined analogously to $\tilde{\mathbf{y}}[n]$.

When $\overline{\mathbf{H}}$ is known at the RX, and assuming a Gaussian distribution for the noise, the coherent ML decoder is equivalent to minimize the following criterion [180]

$$\hat{\mathbf{s}}[n] = \underset{\mathbf{s}[n]\in\mathcal{S}}{\operatorname{argmin}} \left\|\tilde{\mathbf{y}}[n] - \tilde{\mathbf{W}}(\overline{\mathbf{H}})\mathbf{s}[n]\right\|^2$$

subject to the constraint that the elements of $\hat{\mathbf{s}}[n]$ belong to a finite set $\mathcal{S}$ and where $\|\cdot\|$ is the Euclidean norm. This is an NP-hard problem and optimal algorithms to solve it, such as *sphere decoding*, can be computationally expensive [78, 93, 116, 161]. Recently, it has been shown that such complex algorithms can be drastically speeded up by exploiting parallelism in Graphics Processing Units (GPUs) [259].

4.1.1 Orthogonal Space-Time Block Codes

In the case of OSTBC, the matrix $\tilde{\mathbf{W}}(\overline{\mathbf{H}})$ satisfies

$$\tilde{\mathbf{W}}^T(\overline{\mathbf{H}})\tilde{\mathbf{W}}(\overline{\mathbf{H}}) = \|\overline{\mathbf{H}}\|_F^2 \mathbf{I}, \tag{4.3}$$

where $\|\cdot\|_F$ denotes the Frobenius norm. Equation (4.3) reduces the complexity of the ML receiver to M' independent, parallel searches to find the symbols that are closest to the estimated signal

$$\hat{\mathbf{s}}_{\text{ML}}[n] = \frac{\tilde{\mathbf{W}}^T(\overline{\mathbf{H}})\tilde{\mathbf{y}}[n]}{\|\overline{\mathbf{H}}\|_F^2}.$$

In other words, the joint OSTBC-MIMO channel response vectors $\tilde{\mathbf{w}}_k(\overline{\mathbf{h}}_j)$ defined in Equation (4.2) can be seen as the ML equalizers.

The necessary and sufficient conditions for the code matrices C_k, $k = 1, \ldots, M'$ to satisfy Equation (4.3) are given by [180]

$$\mathbf{C}_k^H \mathbf{C}_l = \begin{cases} \mathbf{I} & ; k = l \\ -\mathbf{C}_l^H \mathbf{C}_k & ; k \neq l \end{cases}. \tag{4.4}$$

It is straightforward to prove that the conditions mentioned above must also be satisfied by the real extended code matrices.

$$\tilde{\mathbf{C}}_k^T \tilde{\mathbf{C}}_l = \begin{cases} \mathbf{I} & ; k = l \\ -\tilde{\mathbf{C}}_l^T \tilde{\mathbf{C}}_k & ; k \neq l \end{cases}.$$

As a consequence of Equations (4.3) and (4.4), the TX signals using an OSTBC satisfy $\mathbf{S}^H[n]\mathbf{S}[n] = \|s[n]\|^2 \mathbf{I}$.

The most popular OSTBC is the Alamouti code [31], which transmits $M = 2$ complex symbols in $L = 2$ time slots, so the code rate is $R = 1$. The n-th block of data for the Alamouti code is

$$\mathbf{S}[n] = \begin{bmatrix} r_1[n] & r_2[n] \\ -r_2^*[n] & r_1^*[n] \end{bmatrix}$$

and the corresponding code matrices are

$$C_1 = \begin{bmatrix} 1 & 0 \\ 0 & 1 \end{bmatrix}, \; C_2 = \begin{bmatrix} j & 0 \\ 0 & -j \end{bmatrix}, \; C_3 = \begin{bmatrix} 0 & 1 \\ -1 & 0 \end{bmatrix}, \; \text{and } C_4 = \begin{bmatrix} 0 & j \\ j & 0 \end{bmatrix}.$$

In this chapter we restrict the evaluation to the Alamouti code, thus the number of TX antennas is set to two. Additionally, we experimentally evaluate different channel estimation techniques for the Alamouti code in a 2×1 MISO or a 2×2 MIMO channel[1].

---

[1] When the measurements presented in this chapter were carried out, both first and second versions of the GTEC MIMO testbed employed only two TX and two RX antennas.

Nevertheless, current wireless communications standards make use of MIMO technologies. For example, IEEE 802.16e WiMAX or IEEE 802.20 and evolutions of third generation mobile communications systems such as Long Term Evolution (LTE) [29] support MIMO systems with two antennas and Alamouti coding due to cost and simplicity reasons [148, 155, 156].

4.2 2x1 Alamouti Channel Estimation

In this section we describe the channel estimation techniques used in both computer simulations and testbed measurements for the $2{\times}1$ Alamouti code. We start with the adaptation of the notation introduced in Section 4.1.1 for the case of the $2{\times}1$ Alamouti code. Next, we present a SOS-based blind channel estimation approach as well as two different HOS-based blind channel estimation techniques as a reference.

Starting from Equation (4.1), when the $2{\times}1$ Alamouti OSTBC is used the relationship between the vector of observations $\mathbf{x} = [x_1 \; x_2^*]^T$ and the vector of sources $\mathbf{s} = [s_1 \; s_2]^T$ is given by

$$\mathbf{x} = \mathbf{H}\,\mathbf{s} + \mathbf{n}, \tag{4.5}$$

where $\mathbf{H}$ is the $2{\times}2$ effective channel matrix resulting from coding the two channel coefficients according to the Alamouti code:

$$\mathbf{H} = \begin{bmatrix} h_1 & h_2 \\ h_2^* & -h_{1,}^* \end{bmatrix}, \tag{4.6}$$

where $\mathbf{n} = [n_1 \; n_2^*]^T$ is the AWGN. Note that $\mathbf{H}$ is an orthogonal matrix satisfying $\mathbf{H}\mathbf{H}^H = \mathbf{H}^H\mathbf{H} = \|\mathbf{h}\|^2\,\mathbf{I}_2$ where $\|\mathbf{h}\|^2 = |h_1|^2 + |h_2|^2$ is the squared Euclidean norm of $\mathbf{h}$.

Filtering a vector $\mathbf{x}$ with the matrix matched filter yields the following decision statistics

$$\mathbf{y} = \mathbf{H}^H\,\mathbf{x} = \|\mathbf{h}\|^2\,\mathbf{s} + \tilde{\mathbf{n}}, \tag{4.7}$$

where $\tilde{\mathbf{n}} = \mathbf{H}^H\,\mathbf{n}$ is the output noise vector, with the same statistical distribution as the input noise $\mathbf{n}$. It is apparent from Equation (4.7) that ML detection of s_1 and s_2 can be calculated by applying $\mathbf{y}$ to a pair of independent scalar slicers. Consequently, the correct detection of the transmitted symbols $\mathbf{s}$ requires an accurate estimation of the channel matrix $\mathbf{H}$ from the received data $\mathbf{x}$.

The channel estimation methods considered in this section are based on the computation of a $2{\times}2$ squared matrix $\mathbf{G}$ containing SOS or HOS of the acquired signals. The basic premise of the methods considered is that $\mathbf{G}$ has an algebraic structure with the form $\mathbf{H}\boldsymbol{\Delta}\mathbf{H}^H$ where $\boldsymbol{\Delta}$ is a diagonal matrix. Due to the orthogonal structure of $\mathbf{H}$, if the diagonal entries of $\boldsymbol{\Delta}$ are different, the channel matrix can be identified from the eigenvectors of $\mathbf{G}$ with a possible scaling and/or permutation.

4.2.1 SOS-Based Blind Channel Estimation

According to the signal model in Equation (4.5), the autocorrelation matrix of the observations can be written as

$$\mathbf{G}_{\mathrm{SOS}} = \mathrm{E}\left[\mathbf{x}\,\mathbf{x}^H\right] = \mathbf{H}\mathbf{R_s}\mathbf{H}^H + N_0\,\mathbf{I}_2, \tag{4.8}$$

where N_0 is the variance of the complex-valued noise and $\mathbf{R_s} = \mathrm{E}[\mathbf{s}\,\mathbf{s}^H]$ is the correlation matrix of the transmitted signals. Given that $\mathbf{H}$ is orthogonal, Equation (4.8) can be rewritten as the following eigenvalue decomposition:

$$\mathbf{G}_{\mathrm{SOS}} = \mathbf{H}\left(\mathbf{R_s} + \frac{N_0}{\|\mathbf{h}\|^2}\mathbf{I}_2\right)\mathbf{H}^H. \tag{4.9}$$

Notice that if the two transmitted sources have the same power, then $\mathbf{G}_{\mathrm{SOS}}$ is diagonal, and therefore $\mathbf{H}$ is not identifiable from an eigenvalue decomposition. To overcome this inconvenience, we unbalance the power of the transmitted sources as follows:

$$\mathrm{E}[|s_1'|^2] = \frac{2\sigma_s^2}{1+\gamma^2}, \ \ \mathrm{E}[|s_2'|^2] = \frac{2\gamma^2\sigma_s^2}{1+\gamma^2}, \tag{4.10}$$

where $0 < \gamma^2 < 1$ and s_1', s_2' are the new unbalanced sources. Note that the total mean power, σ_s^2, remains unchanged. Now, the eigenvalue decomposition of $\mathbf{G}_{\mathrm{SOS}}$ becomes:

$$\mathbf{G}_{\mathrm{SOS}} = \sigma_s^2\mathbf{H}\boldsymbol{\Delta}_{\mathrm{SOS}}\mathbf{H}^H, \ \ \boldsymbol{\Delta}_{\mathrm{SOS}} = \begin{bmatrix} \frac{2}{1+\gamma^2} + \sigma_h^2 & 0 \\ 0 & \frac{2\gamma^2}{1+\gamma^2} + \sigma_h^2 \end{bmatrix}, \ \sigma_h^2 = \frac{N_0}{\sigma_s^2\|\mathbf{h}\|^2}, \tag{4.11}$$

where $\boldsymbol{\Delta}_{\mathrm{SOS}}$ contains the eigenvalues of $\mathbf{G}_{\mathrm{SOS}}$. Thanks to the source power imbalance, matrix $\mathbf{H}$ is now identifiable from the eigenvectors of $\mathbf{G}_{\mathrm{SOS}}$ because $\boldsymbol{\Delta}_{\mathrm{SOS}}$ contains different eigenvalues.

Obviously, if the power of the two sources is unbalanced, the total channel capacity is lower than that of equally balanced sources. This is the price to be paid for making the SOS-based method applicable and taking advantage of its extremely low computational requirements.

4.2.2 HOS-Based Blind Channel Estimation

The orthogonal MIMO channel matrix $\mathbf{H}$ can be estimated blindly from the *eigendecomposition* of matrices made up of HOS of the received signals without the need to unbalance the power value of the sources. Indeed, for a 2×1 vector of observations $\mathbf{x}$, the 4-th order matrix of cumulants $\mathbf{G}_{\mathrm{HOS}}(\mathbf{M})$ is a 2×2 matrix, and its elements are given by

$$[\mathbf{G}_{\mathrm{HOS}}(\mathbf{M})]_{ij} = \sum_{k,\ell=1}^{2} \mathrm{cum}(\hat{x}_i, \hat{x}_j^*, \hat{x}_k, \hat{x}_\ell^*)m_{kl}, \tag{4.12}$$

where m_{kl} $k, l = 1, 2$, denote the entries of a 2×2 matrix $\mathbf{M}$, and the 4th-order cumulant is defined by the following equation:

$$
\begin{aligned}
\operatorname{cum}(\hat{x}_1, \hat{x}_2, \hat{x}_3, \hat{x}_4) = {} & \mathrm{E}[\hat{x}_1\hat{x}_2\hat{x}_3\hat{x}_4] - \mathrm{E}[\hat{x}_1\hat{x}_2]\mathrm{E}[\hat{x}_3\hat{x}_4] \\
& - \mathrm{E}[\hat{x}_1\hat{x}_3]\mathrm{E}[\hat{x}_2\hat{x}_4] - \mathrm{E}[\hat{x}_1\hat{x}_4]\mathrm{E}[\hat{x}_2\hat{x}_3].
\end{aligned}
\tag{4.13}
$$

For the particular case of zero-mean signals, the cumulant matrix admits the following decomposition [61]:

$$
\mathbf{G}_{\mathrm{HOS}}(\mathbf{M}) = \mathbf{H}\mathbf{\Delta}_{\mathrm{HOS}}(\mathbf{M})\mathbf{H}^H,
\tag{4.14}
$$

where $\rho_{4i} = \operatorname{cum}(s_i, s_i^*, s_i, s_i^*)$ is the kurtosis of the i-th source and $\mathbf{\Delta}(\mathbf{M})$ is a diagonal matrix given by

$$
\mathbf{\Delta}_{\mathrm{HOS}}(\mathbf{M}) = \operatorname{diag}(\rho_{41}\mathbf{h}_1^H\mathbf{M}\,\mathbf{h}_1, \ \rho_{42}\mathbf{h}_2^H\mathbf{M}\,\mathbf{h}_2).
\tag{4.15}
$$

Here, $\mathbf{h}_i$ is the i-th column of $\mathbf{H}$, i.e. $\mathbf{h}_1 = [h_1 \ h_2^*]^T$ and $\mathbf{h}_2 = [h_2 \ -h_1^*]^T$. Since for the Alamouti code the effective channel matrix is orthogonal, $\mathbf{H}^H$ diagonalizes $\mathbf{G}_{\mathrm{HOS}}(\mathbf{M})$ for any $\mathbf{M}$ provided that $\mathbf{\Delta}(\mathbf{M})$ contains different entries, i.e.

$$
L = |\rho_{41}\mathbf{h}_1^H\mathbf{M}\mathbf{h}_1 - \rho_{42}\mathbf{h}_2^H\mathbf{M}\mathbf{h}_2| \neq 0.
\tag{4.16}
$$

In particular, the approach proposed by Beres and Adve [39] considers the cases $m_{11} = 1$, $m_{12} = m_{21} = m_{22} = 0$, and $m_{11} = m_{12} = m_{21} = 0, m_{22} = 1$. Assuming that the transmitted signals have the same kurtosis, we obtain from Equation (4.16) the condition of identifiability of the channel matrix is $|h_1|^2 \neq |h_2|^2$.

As an extension of this approach, we propose to identify $\mathbf{H}$ by computing the eigenvectors of a linear combination of 4th-order cross-cumulant matrices. This can be obtained by using a matrix $\mathbf{M}$ with entries $m_{11} = 1, m_{12} = m_{21} = 0$ and $m_{22} = \lambda$, where λ is a real-valued parameter. From Equation (4.16), we conclude that this method allows $\mathbf{H}$ to be estimate when the following condition is satisfied:

$$
L = (1 - \lambda)(|h_1|^2 - |h_2|^2) \neq 0.
\tag{4.17}
$$

Thus, the channel is identifiable if $\lambda \neq 1$ and $|h_1|^2 \neq |h_2|^2$. In particular, we propose the utilization of $\lambda = -1$ since this choice provides a significant performance improvement with respect to the Beres and Adve approach [235].

Another way of estimating the mixing matrix consists in performing a simultaneous diagonalization of several fourth-order cumulant matrices, such the Joint Approximate Diagonalization of Eigenmatrices (JADE) algorithm [61]. This algorithm provides an excellent performance but, unfortunately, its computational cost is very high. From now on, the JADE algorithm will be employed solely as a benchmark for the blind channel estimation schemes.

4.3 2x2 Alamouti Channel Estimation

In this section we describe the channel estimation techniques utilized in both computer simulations and measurements for the 2×2 Alamouti code. First, we consider a conventional pilot-based supervised technique. Second, we describe a newly proposed SOS-based blind technique. Finally, a DSTBC approach used as a reference is introduced.

4.3.1 Pilot-Aided Channel Estimation

The pilot-aided channel estimation is based on the method explained in [220]. Basically, $n_T = 2$ pilot sequences are generated to be sent by the $n_T = 2$ TX antennas. During the n-th frame transmitted from antennas one and two, two pilot sequences are inserted, each one constituted by K symbols

$$\mathbf{S}^{\text{pilot}} = \begin{bmatrix} \mathbf{s}_1^{\text{pilot}} & \mathbf{s}_2^{\text{pilot}} \end{bmatrix} = \begin{bmatrix} s_{1,1} & s_{2,1} & \ldots & s_{K,1} \\ s_{1,2} & s_{2,2} & \ldots & s_{K,2} \end{bmatrix}^T.$$

The pilot sequences are designed to be orthogonal, thus allowing the independent estimation of the fading coefficient from each TX antenna to each RX antenna. Indeed, it is straightforward to show that the Least Squares (LS) estimate of the channel coefficient between the i-th TX antenna and the j-th RX antenna is given by

$$\hat{h}_{i,j} = \frac{\left(\mathbf{s}_i^{\text{pilot}}\right)^H \mathbf{y}_j^{\text{pilot}}}{\|\mathbf{s}_i^{\text{pilot}}\|^2},$$

where $\mathbf{y}_j^{\text{pilot}}$ is the acquired signal at the j-th RX antenna when $\mathbf{s}_i^{\text{pilot}}$ has been transmitted.

Note that the transmission of a pilot sequence causes a reduction in the spectral efficiency or, equivalently, a reduction in the effective transmission rate. For instance, if we transmit N_D data symbols and K pilot symbols during the n-th frame, the rate reduction factor associated to this technique is $N_D/(N_D + K)$.

4.3.2 SOS-Based Blind Channel Estimation

In the literature, different blind MIMO channel estimation methods for OSTBCs have been proposed. Among them, in this work we have chosen one described in [260]. The method is based only on SOS and is able to estimate the channel blindly (up to a real scalar ambiguity) for most of the existing OSTBCs when the number of receive antennas is greater than one [292]. However, some OSTBC schemes —including the Alamouti code— cannot be identified employing this method due to an additional ambiguity, which must be eliminated by resorting to other information (e.g. linear precoding, non-white source signals, reduced rate, TX antenna power unbalancing, etc.) [159, 235, 236, 260, 292, 293].

In this section, the method proposed in [260] is first summarized. Next, it is adapted for the Alamouti scheme using the method proposed in [159] to avoid the above-mentioned ambiguities.

By defining $\mathbf{R}_{\tilde{\mathbf{y}}}$ as the $2n_R L \times 2n_R L$ correlation matrix of the observations $\tilde{\mathbf{y}}[n]$ and given that $\mathbf{s}, \tilde{\mathbf{y}}$, and $\tilde{\mathbf{W}}$ are all real-valued, then

$$\mathbf{R}_{\tilde{\mathbf{y}}} = E[\tilde{\mathbf{y}}[n]\tilde{\mathbf{y}}^T[n]] = \tilde{\mathbf{W}}(\overline{\mathbf{H}})\mathbf{R}_s\tilde{\mathbf{W}}^T(\overline{\mathbf{H}}) + \frac{N_0}{2}\mathbf{I}, \tag{4.18}$$

where $\mathbf{R}_s = E[\mathbf{s}[n]\mathbf{s}^T[n]]$ is the correlation matrix of the sources and the method proposed in [260] is the solution to the following optimization problem

$$\hat{\overline{\mathbf{H}}} = \underset{\overline{\mathbf{H}}}{\operatorname{argmax}} \operatorname{Tr}\left(\tilde{\mathbf{W}}^T(\overline{\mathbf{H}})\mathbf{R}_{\tilde{\mathbf{y}}}\tilde{\mathbf{W}}(\overline{\mathbf{H}})\right) \text{ subject to } \tilde{\mathbf{W}}^T(\overline{\mathbf{H}})\tilde{\mathbf{W}}(\overline{\mathbf{H}}) = \mathbf{I}, \tag{4.19}$$

which is given by any channel matrix $\hat{\overline{\mathbf{H}}}$ with $\|\overline{\mathbf{H}}\|_F^2 = 1$ and satisfying

$$\operatorname{range}(\tilde{\mathbf{W}}(\hat{\overline{\mathbf{H}}})) = \operatorname{range}(\tilde{\mathbf{W}}(\overline{\mathbf{H}})), \tag{4.20}$$

equivalently $\tilde{\mathbf{W}}(\hat{\overline{\mathbf{H}}}) = \tilde{\mathbf{W}}(\overline{\mathbf{H}})\mathbf{Q}$, where $\mathbf{Q}$ is an orthogonal matrix.

In [293] it has been shown that Equation (4.19) can also be rewritten as the following Principal Component Analysis (PCA) problem

$$\underset{\hat{\bar{\mathbf{h}}}}{\operatorname{argmax}} \hat{\bar{\mathbf{h}}}^T \tilde{\mathbf{Z}}^T \tilde{\mathbf{Z}}\hat{\bar{\mathbf{h}}}, \text{ subject to } \|\hat{\bar{\mathbf{h}}}\|^2 = 1, \tag{4.21}$$

where $\hat{\bar{\mathbf{h}}}$ is the maximum eigenvector of $\tilde{\mathbf{Z}}^T\tilde{\mathbf{Z}}$, and the data matrix is defined as $\tilde{\mathbf{Z}} = [\tilde{\mathbf{Z}}[0]^T \cdots \tilde{\mathbf{Z}}[N-1]^T]^T$, $\tilde{\mathbf{Z}}[n]$ is

$$\tilde{\mathbf{Z}}[n] = \begin{bmatrix} \tilde{\mathbf{y}}_1^T[n]\tilde{\mathbf{C}}_1 & \cdots & \tilde{\mathbf{y}}_{n_R}^T[n]\tilde{\mathbf{C}}_1 \\ \vdots & \ddots & \vdots \\ \tilde{\mathbf{y}}_1^T[n]\tilde{\mathbf{C}}_{M'} & \cdots & \tilde{\mathbf{y}}_{n_R}^T[n]\tilde{\mathbf{C}}_{M'} \end{bmatrix},$$

and $\hat{\bar{\mathbf{h}}}$ is defined as

$$\hat{\bar{\mathbf{h}}} = \left[\hat{\bar{\mathbf{h}}}_1^T, \ldots, \hat{\bar{\mathbf{h}}}_{n_R}^T\right]^T.$$

Once the channel has been estimated, the transmitted signal is obtained as

$$\hat{\mathbf{s}}[n] = \tilde{\mathbf{Z}}[n]\hat{\bar{\mathbf{h}}}.$$

Ambiguity Problems

As we mentioned previously, for the particular case of Alamouti coding, this technique cannot be applied due to an ambiguity caused by Equation (4.20) [260]. Basically, this ambiguity

appears when there exists an estimated channel $\hat{\overline{\mathbf{H}}} \neq c\overline{\mathbf{H}}$ such that its associated equalization matrix $\tilde{\mathbf{W}}(\hat{\overline{\mathbf{H}}})$ spans the same subspace as $\tilde{\mathbf{W}}(\overline{\mathbf{H}})$. For the case of the 2×2 Alamouti OSTBC, this indeterminacy implies that the largest eigenvalue of $\tilde{\mathbf{Z}}^T\tilde{\mathbf{Z}}$ has a multiplicity of four [260, 292]. This means that the true channels $\overline{\mathbf{h}}_1$ and $\overline{\mathbf{h}}_2$ associated to the first and second RX antenna respectively belong to the subspace spanned by the four eigenvectors associated to the largest eigenvalue of $\tilde{\mathbf{Z}}^T\tilde{\mathbf{Z}}$.

Several attempts have been made to overcome this ambiguity by resorting to some form of precoding of the source signal [159, 260, 292, 293]. In this chapter we present two different ways of solving the ambiguity problems. The first is a simple method proposed in [159] and summarized in the ensuing paragraph. The second was described in Section 4.2.

It was proved that any OSTBC transmitting an odd number of real symbols (i.e. M' odd) is identifiable regardless of the number of RX antennas [32] [291, Chapter 8, pp. 102]. Therefore, any non-identifiable complex OSTBC can be made identifiable simply by transmitting one real symbol less per OSTBC block. Obviously, the transmission rate is reduced, but this rate penalty can be controlled by eliminating only one real symbol each B OSTBC blocks. In this case, the rate reduction factor is $(BM' - 1)/BM'$, which tends to one for $BM' \gg 1$. Finally, for a fixed number of transmitted OSTBC blocks there is a trade-off between the accuracy of the channel estimate and the rate reduction factor, an issue that has been discussed in [159].

4.3.3 Differential Space-Time Block Codes

An alternative to blind channel estimation methods that also avoids the need for CSI estimation is the use of differential schemes. However, it is well known that differential modulations suffer a degradation in performance compared to coherent detection. In this section, we briefly summarize the encoding and decoding procedures of 2×2 DSTBC. More details can be found in [180].

Encoding Algorithm

Let $\mathbf{X}[n]$ be a set of unitary matrices to be transmitted. In DSTBC schemes we transmit the matrices $\mathbf{T}[n]$, which are constructed as follows:

$$\mathbf{T}[n] = \mathbf{X}[n]\mathbf{T}[n-1],$$

with $\mathbf{T}[0] = \mathbf{I}$. A possible design for the matrices $\mathbf{X}[n]$ consists in using an OSTBC

$$\mathbf{X}[n] = \frac{1}{\sqrt{M}}\mathbf{S}[n],$$

where the normalization factor $1/\sqrt{M}$ is necessary to obtain $\mathbf{X}[n]\mathbf{X}^H[n] = \mathbf{I}$. Note that this particular choice of unitary matrices reduces the computational complexity of the detector.

Decoding Algorithm

If we transmit $\mathbf{T}[n]$, the received $L \times n_R$ matrix with the observations is

$$\mathbf{Y}[n] = \mathbf{T}[n]\mathbf{H} + \mathbf{N}[n] = \mathbf{X}[n]\mathbf{T}[n-1]\,\mathbf{H} + \mathbf{N}[n],$$

where $\mathbf{Y}[n] = [\mathbf{y}_1[n] \cdots \mathbf{y}_{n_R}[n]]$, and $\mathbf{N}[n]$ is defined analogously. The ML detection of $\mathbf{X}[n]$ from $\mathbf{Y}[n]$ and $\mathbf{Y}[n-1]$ amounts to maximizing the following cost function [180]

$$J\left(\mathbf{X}[n]\right) = \Re\left\{\mathrm{Tr}\left\{\mathbf{X}[n]\mathbf{Y}[n-1]\,\mathbf{Y}^H[n]\right\}\right\}. \tag{4.22}$$

For arbitrary unitary matrices $\mathbf{X}[n]$ this is a computationally expensive algorithm. However, using OSTBC matrices the detection of each symbol can be decoupled and the cost function to be maximized (Equation (4.22)) takes now the form

$$J\left(s_1[n], \cdots, s_{M'}[n]\right) = \sum_{k=1}^{M'} \left(\Re\left\{\mathrm{Tr}\left\{\mathbf{C}_k\mathbf{Y}[n-1]\,\mathbf{Y}^H[n]\right\}\right\} s_k[n]\right).$$

4.4 2x1 Alamouti Evaluation

This section describes the evaluation procedure as well as the set-up utilized to measured the schemes presented in Section 4.2. The evaluation is completed with computer simulation results.

4.4.1 Experimental Evaluation

Making use of the second version of the GTEC MIMO testbed, we tackle the problem of measuring the mean performance – in terms of BER vs SNR – of five different channel estimation schemes for the 2×1 Alamouti code: pilot-aided, Beres and Adve [39], JADE [61], the proposed SOS-based approach (Section 4.2.1), and finally the proposed HOS-based approach (Section 4.2.2).

Indoor Location – the Channel

We carried out two different experiments – named Experiments 4.1 and 4.2 – both at the UDC lab. In Experiment 4.1, the TX and the RX were at a distance of 5 m from each other, with a clear line of sight between them. The TX antennas were spaced about 30 cm apart in order to ensure a good spatial diversity. Note that such distance is easy to achieve in e.g. a laptop computer, by placing the two antennas on different corners of the lid. In Experiment 4.2, the TX and the RX were placed about 9 m from each other, with no line of sight between them. In all cases, the TX antennas and the RX antenna were typical rod antennas with a gain of 3 dB, similar to those utilized by WiFI access points [24].

Testbed Measurements

For the experimental evaluation, we chose to carry out narrowband (7 MHz of bandwidth[2]) 2×1 MISO measurements making use of the second version of the GTEC MIMO testbed. In our measurement approach, all signal processing operations were implemented in MATLAB. The data was generated off-line, transmitted in real-time through the wireless channel at a rate equal to 5 MBaud, and stored in the hard drives at the RX. In a later step, the measurement data was evaluated off-line. A different way – and probably offering the same results – of evaluating the above-mentioned methods would be to employ a channel sounder and then utilize the channel coefficients in a computer simulation.

Measurement Procedure

The transmission of a sequence of symbols (frame) involves the following steps:

- 1 000 symbols for each source (s_1 and s_2) are randomly generated according to a 4 QAM constellation.
- The 1 000 source symbols are coded according to the Alamouti code, resulting in 2 000 data symbols used to evaluate HOS-based channel estimation methods (balanced subframe).
- The same 1 000 source symbols are power unbalanced and coded with the Alamouti code, resulting in another 2 000 symbols utilized for the evaluation of the SOS-based methods (unbalanced subframe). Note that both unbalanced and balanced subframes present the same mean TX power value, but non-equally distributed between the two sources.
- The TX frame is assembled with the addition of a Pseudo Noise (PN) sequence used as a preamble for the frequency and time synchronization tasks, and the two subframes generated in the previous steps.
- The assembled frame is transmitted by the TX antennas through the wireless channel.
- At the RX the frame is acquired. Next, frequency and time synchronization operations are carried out with the purpose of guaranteeing the correctness of the acquired frame. If the frame is wrong, the frame is acquired again.
- Finally, the resulting observations are saved for subsequent evaluation.

The above procedure is repeated for different TX power values admitted by the TX equipment, avoiding saturation effects. In order to generate different channel realizations, the RX antenna is (manually) moved – avoiding significant changes in the path loss – and the whole process is repeated again. In total, each frame is transmitted 2 000 times at different TX power values and experiencing distinct channel realizations.

---

[2]Given the features of the scenario, 7 MHz of bandwidth is within the channel coherence bandwidth.
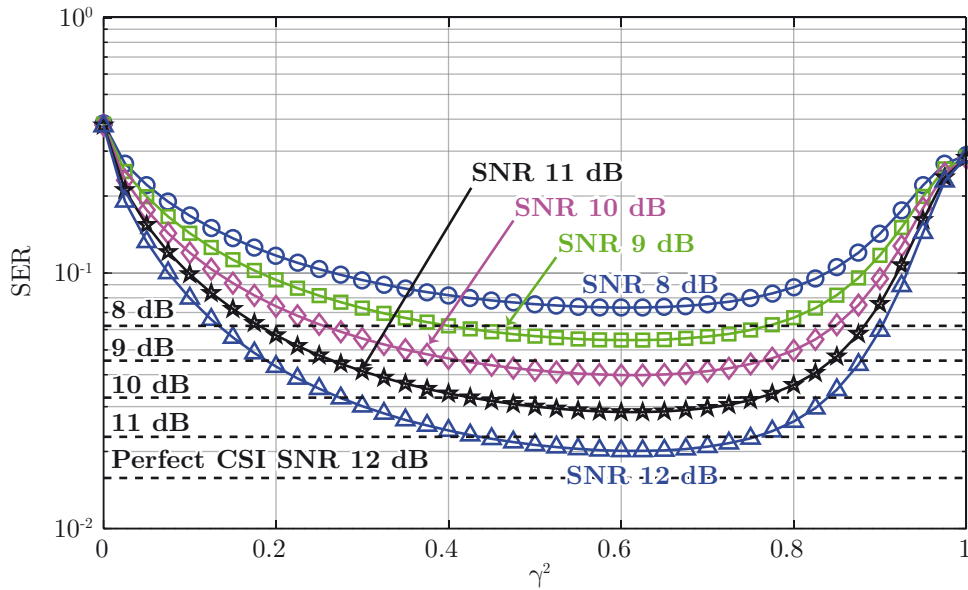
Figure 4.1: Computer simulations: SER versus γ^2 obtained with the SOS-based approach for 4 QAM signals and different values of SNR=σ_s^2/N_0. The horizontal dashed lines represent the SER obtained with perfect CSI.

Due to the limitations of the RF front-end utilized, it was not possible to vary the TX power value linearly to obtain different SNR values at the RX side. This inconvenience was overcome by estimating the SNR for each acquired frame jointly with the Symbol Error Ratio (SER) obtained by the corresponding channel estimation method. Next, the pairs constituted by the SNR with its corresponding SER are grouped and sorted with respect to the SNR. Finally, the mean SER for each group is estimated and the curves shown in Figures 4.4 and 4.5 are obtained.

4.4.2 Results

In this section the results obtained by means of computer simulations and measurements are presented.

Computer Simulation Results

The five different channel estimation methods to be measured are previously evaluated by means of computer simulations. The simulations randomly generate 4 QAM signals that are transmitted through Rayleigh-distributed randomly generated flat-fading channels affected by AWGN. We assume block fading, i.e. the channel remains constant during the transmission of a block of $K = 500$ symbols. The statistics in Equations (4.8) and (4.12) have been calculated by averaging over each block of symbols and the performance has been measured in terms of the SER.

We have evaluated the performance of the SOS-based approach for several values of γ^2.
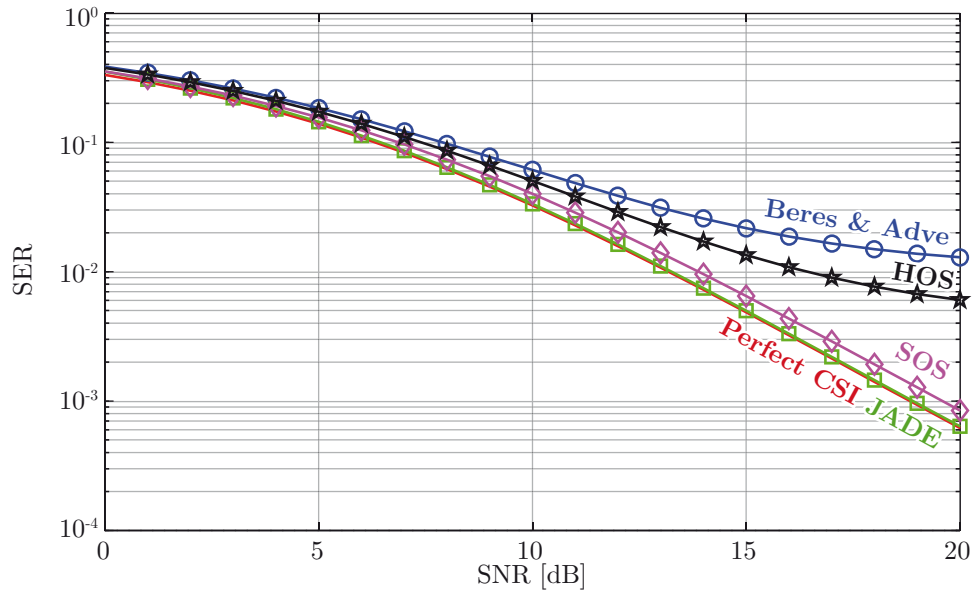
Figure 4.2: Computer simulation over Rayleigh-distributed flat-fading channel: SER versus SNR obtained with the different channel estimation methods, $\gamma^2 \approx 0.6$.

Figure 4.1 shows the SER versus γ^2 for SNR ranging from 8 to 12 dB. The autocorrelation matrix has been estimated with $K = 500$ symbols. Figure 4.1 also plots the SER obtained with perfect CSI knowledge at the RX (horizontal dashed lines). It is apparent that the SOS-based channel estimation approach fails for $\gamma^2 = 1$ because this case corresponds to sources with the same power. The same happens when $\gamma^2 = 0$, which corresponds to the extreme case in which only s_1 is transmitted. Note that the best performance is obtained with $\gamma^2 \approx 0.6$, and this value is used in the simulation results presented in Figure 4.2.

Figure 4.2 shows the SER with respect to the SNR for the five different channel estimation methods: JADE, Beres and Adve, the SOS-based approach with $\gamma^2 = 0.6$, and the HOS-based approach with $\lambda = -1$. The system performance with perfect CSI is also plotted as a benchmark. The SER curves were obtained by simulating data blocks of $K = 500$ symbols and by averaging the results for 10 000 different realizations. Note that the method proposed by Beres and Adve is outperformed by the HOS-based approach. However, notice the poor performance of HOS-based methods for SNR values greater than 10 dB compared to the SOS-based approach. The good performance of the SOS-based approach is apparent from Figure 4.2 since it only incurs a 0.5 dB loss in terms of the SNR needed to achieve the same BER with respect to the perfect CSI case, with only JADE performing better.

Measurement Results

In order to be able to use the SOS-based approach presented in Section 4.2.1, the optimum power unbalance factor γ^2 must be found. To this end, the SER is evaluated for different values of γ^2 using exactly the same set-up as for Experiment 4.1. The results are plotted in Figure 4.3
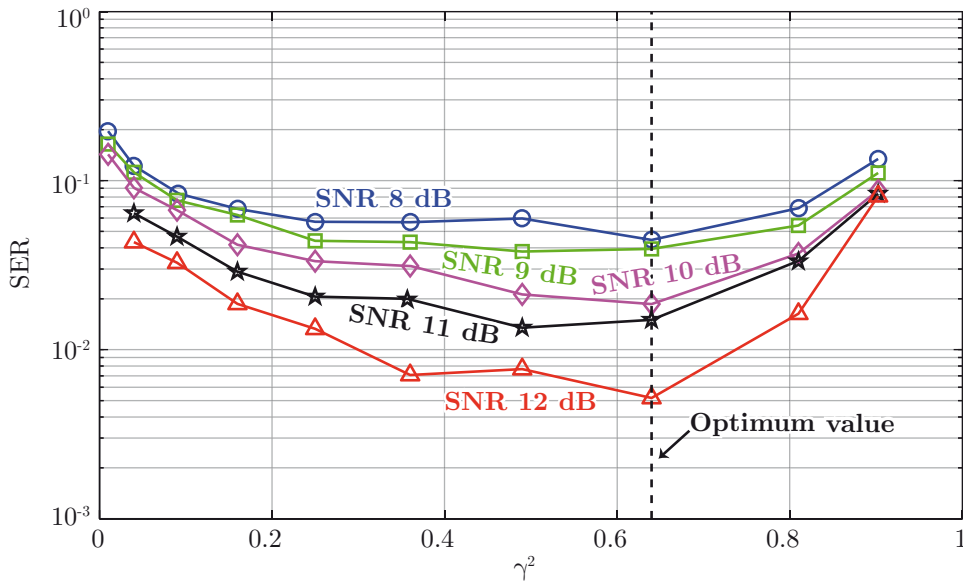
Figure 4.3: Experiment 1: performance of the SOS-based method as a function of γ^2.
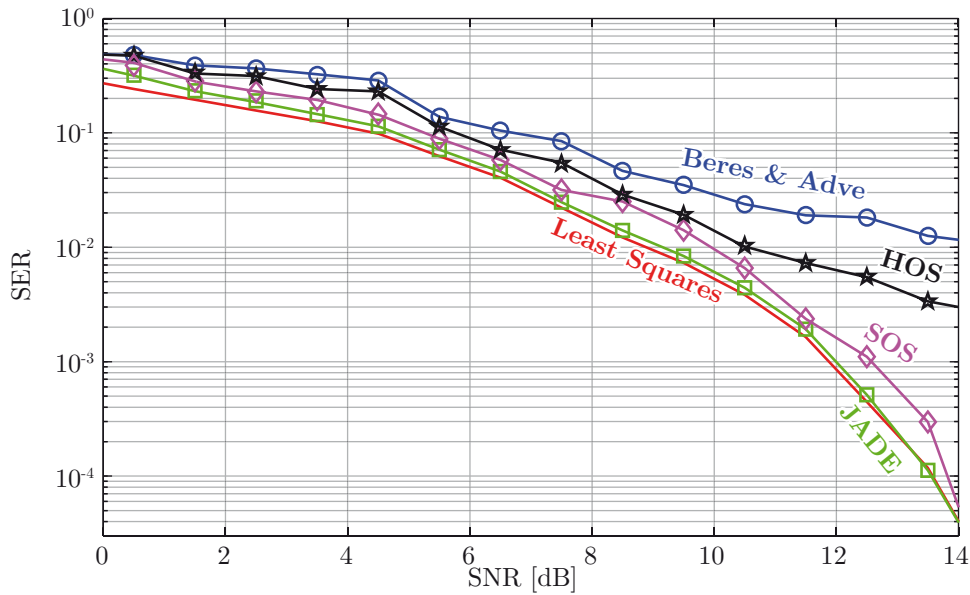
Figure 4.4: Experiment 4.1: SER performance versus SNR with clear line of sight.

and show that the optimal value is around $\gamma^2 = 0.64$. This value is in accordance with that obtained by simulations over an uncorrelated Rayleigh channel (see Figure 4.1). We set $\gamma^2_{\mathrm{opt}} = 0.64$ in the following measurements.

Figure 4.4 shows the measured SER versus SNR in Experiment 4.1 for the five different channel estimation methods: JADE, Beres and Adve, the SOS-based approach with $\gamma^2 = 0.64$, and the HOS-based approach with $\lambda = -1$. Notice that, similarly to computer simulation results, the JADE algorithm achieves the same performance as with LS estimation while the SOS-based only loses about 0.5 dB. Figure 4.4 also shows the poor performance of HOS methods since they present a floor effect for SNR values greater than 10 dB. Nevertheless, the performance of
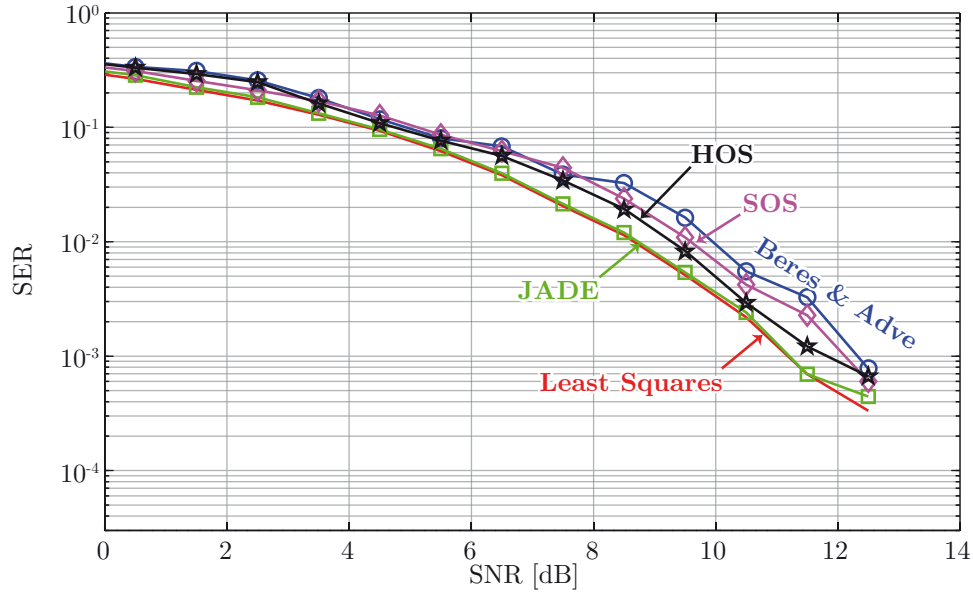
Figure 4.5: Experiment 4.2: SER performance versus SNR without line of sight.

the HOS-based method is better than that proposed by Beres and Adve [39].

Figure 4.5 shows the measured SER versus SNR in Experiment 4.2. Contrary to Experiment 4.1, both SOS-based and HOS-based methods perform adequately, exhibiting a loss in performance of less than 1 dB compared to the LS channel estimation. Again, JADE is the method that reveals the best performance whereas the HOS-based method proposed by Beres and Adve [39] performs the worst.

4.5 2x2 Alamouti Evaluation

This section describes the evaluation procedure as well as the set-up utilized to measure the schemes presented in Section 4.3. The evaluation is completed with computer simulation results.

4.5.1 Experimental Evaluation

Making use of the first version of the GTEC MIMO testbed, we carried out three different experiments – referred to as Experiments 4.3 to 4.5 – in two different locations to compare the 2×2 Alamouti code with pilot-aided channel estimation, using SOS-based blind channel estimation and, finally, employing the DSTBC as a reference. The measurements took place in two different indoor environments: the laboratory of the GTAS at the University of Cantabria and the laboratory of the GTEC at the University of A Coruña. From now on, the two locations will be respectively called "GTAS lab" and "GTEC lab". The results obtained are then compared with the DSTBC and with computer simulations for Rician and for Rayleigh

distributions of the wireless channels.

Testbed Measurements

We chose to carry out narrowband (1.4 and 7 MHz of bandwidth) multiple-antenna measurements making use of the first version of the testbed jointly developed by the Signal Processing Group at the University of Cantabria and the Electronic Technology and Communications Group at the University of A Coruña.

In the measurement approach, all signal processing operations were implemented in MATLAB. The data was generated off-line, transmitted in real-time over the wireless channel, and stored in the hard drives at the RX. In a later step, the measurement data was evaluated off-line.

Indoor Locations – the Channel

Experiments 4.3 and 4.4 took place at the GTAS lab whereas Experiment 4.5 was carried out at the GTEC lab. In Experiment 4.3 the TX and the RX were approximately at a distance equal to 2 m, with a clear line of sight between them. In Experiment 4.4 the TX was located farther away at a distance of approximately 10 m, with no line of sight. Finally, in Experiment 4.5, the TX and the RX were at a distance of 5 m, also avoiding line of sight.

Signaling Features

Each TX frame is composed of 63 preamble symbols for frame synchronization, 64 pilot symbols for channel estimation (for the pilot-aided technique), 1 000 Alamouti coded symbols, and 1 000 DSTBC coded symbols. For the preamble we used a PN sequence to facilitate frame synchronization and coarse symbol timing acquisition. Notice that this frame structure was selected for simplicity reasons and to ensure a fair comparison between all measured schemes. Each frame (containing the pilot symbols, OSTBC symbols, and DSTBC symbols) suffers the effects caused by *the same* channel realization.

The TX symbols are mapped to a 4 QAM constellation. Next they are pulse-shape filtered with a squared root raised cosine filter with 40 % roll-off. The symbol rate is 1 MBaud for the experiments 1 and 2, and 5 MBaud for the third one, thus the RF bandwidth is 1.4 and 7 MHz, respectively. The relatively low symbol rates and the corresponding frame durations guarantee that the channel coherence time is not exceeded whereas the channel remains frequency flat.

Measurement Procedure

The transmission of a sequence of symbols (frame) involves the following steps:
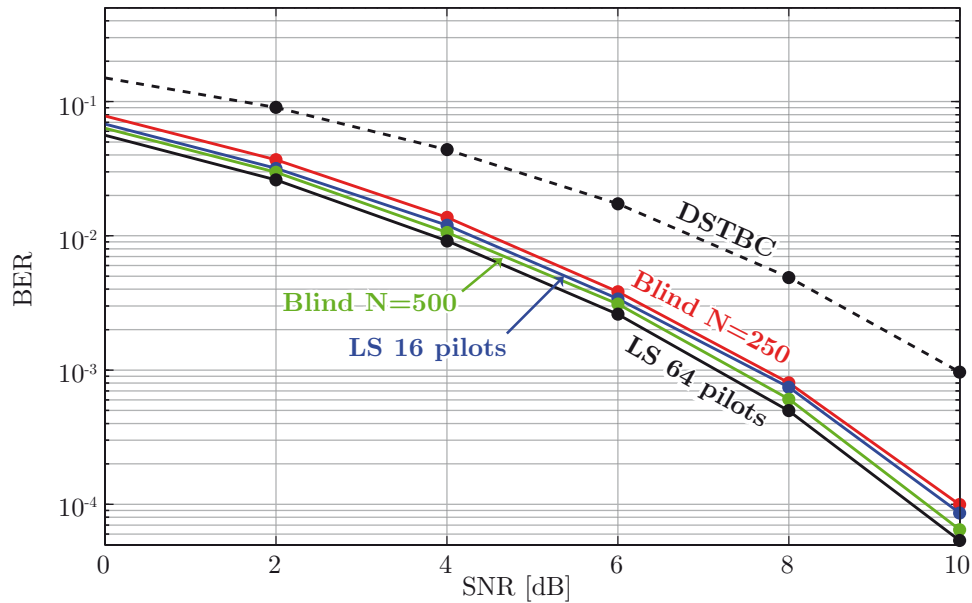
Figure 4.6: BER for the Rician simulation.

- A sequence of 500 4-QAM source symbols (1000 source bits) is randomly generated according to a uniform distribution.
- The sequence is coded using the Alamouti code to generate the first half of 1000 data symbols and utilizing the DSTBC to generate the second half of 1000 data symbols.
- The frame is assembled adding the preamble, the pilot symbols, and the two sequences of 1000 symbols each generated in the previous step.
- The assembled frame is transmitted by the TX antennas through the wireless channel.
- At the RX the frame is acquired. Next, frequency and time synchronization operations are carried out with the purpose of guaranteeing the correctness of the acquired frame. If the frame is wrong, a re-acquisition is requested to the TX.
- Finally, the resulting observations are saved for subsequent evaluation.

The above steps are repeated for several TX power values (see the abscissas of Figures 4.8–4.10). The whole process is repeated 200 times in order to average the BER over different channel realizations. Note that the coherence time of the channel is longer than that required for the transmission and acquisition of the frames for all required TX power values.

4.5.2   Results

In this section the results obtained by means of computer simulations and measurements are presented.
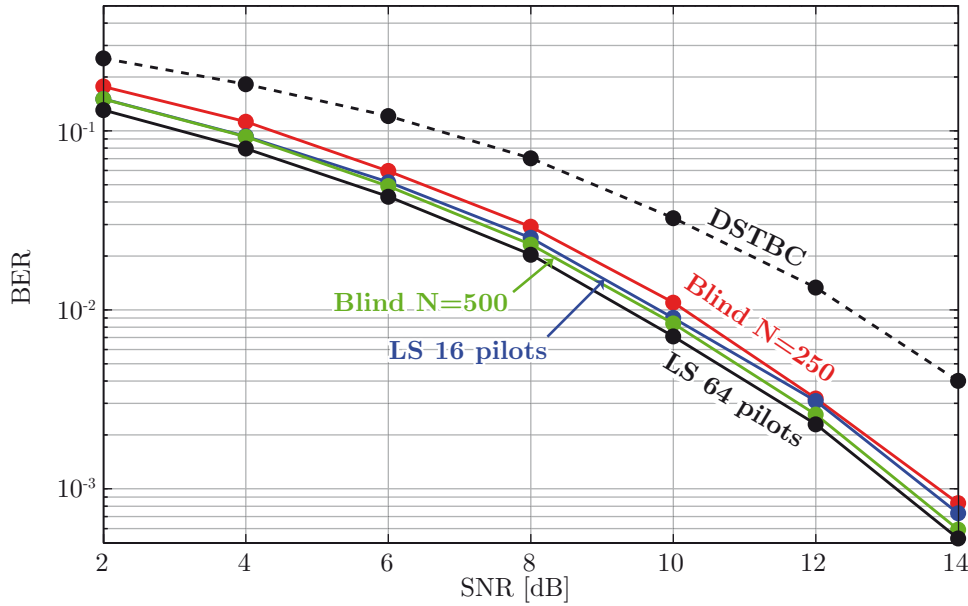
Figure 4.7: BER for the Rayleigh simulation.

Computer Simulation Results

Computer simulation results are presented in Figures 4.6 and 4.7 for a Rayleigh and a Rice channel model with a Rice factor of 3 dB. From Figures 4.6 and 4.7 it can be seen that in both cases the LS channel estimation with 16 pilot symbols performs similarly to the blind method with $N = 250$. The same reasoning is valid for the LS with 64 pilot symbols and the blind method with $N = 500$. As expected, the DSTBC approach presents a loss of 3 dB in terms of the required SNR to achieve the same BER.

Measurement Results

Figures 4.8–4.10 show the results for the three different experiments in the two different locations (GTAS lab and GTEC lab). In these figures we compare:

- The Alamouti scheme with pilot-aided channel estimation, labeled as 16 or 64 pilots according to the number of pilot symbols used to estimate the channel. Note that 64 pilot symbols are always transmitted, hence two different BER curves are obtained using either 16 or 64 pilot symbols.
- The Alamouti scheme with blind channel estimation, labeled as Blind (B10-NX), where 10 is the number of Alamouti blocks in which one real symbol is eliminated to avoid the channel estimation ambiguity and X is the number of blocks that we used to estimate the channel matrix. The results are evaluated when half ($N = 250$) or the whole ($N = 500$) data sequence is used for the channel estimation.
- Finally, the DSTBC BER curve is shown as a reference.
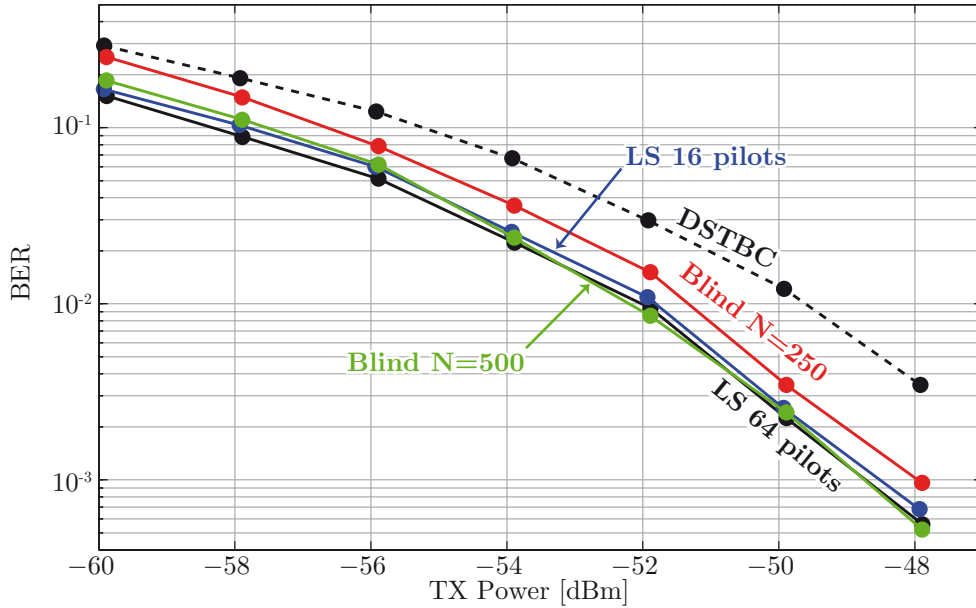
Figure 4.8: Experiment 4.3: BER vs TX power value (clear line of sight, GTAS lab).

Method	Rate
LS with 64 pilot symbols	0.9398
LS with 16 pilot symbols	0.9843
Blind (B10-N250)	0.9750
Blind (B10-N500)	0.9750

Table 4.1: Rate for the different channel estimation methods.

It is important to note that both channel estimation methods (pilot-aided and blind) that we use for coherent detection incur a rate penalty (see Table 4.1).

As can be seen from Figures 4.8 and 4.9, the blind technique with N = 500 blocks practically achieves the same performance as the pilot-aided method with 64 pilot symbols. This improvement is achieved at the expense of a moderate increase in computational cost, since the blind technique has to obtain the main eigenvector of a 8×8 correlation matrix for this particular set-up. On the other hand, we also observe the expected 3 dB loss for the DSTBC in terms of the TX power value needed to achieve the same BER. Additionally, the pilot-aided method with 16 pilot symbols loses about 0.4 dB with respect to the same technique when 64 pilot symbols are employed. Note that we do not use more than 64 pilot symbols because channel estimation using more pilot symbols does not improve the performance of the system.

In the case of blind channel estimation, if we use a lower number of blocks for channel estimation, the estimate of the correlation matrix deteriorates causing a degradation of the BER. More specifically, if we use N = 250 instead of N = 500 blocks, the loss in TX power value is about 0.9 dB. However, the use of a reduced number of blocks for blind channel estimation
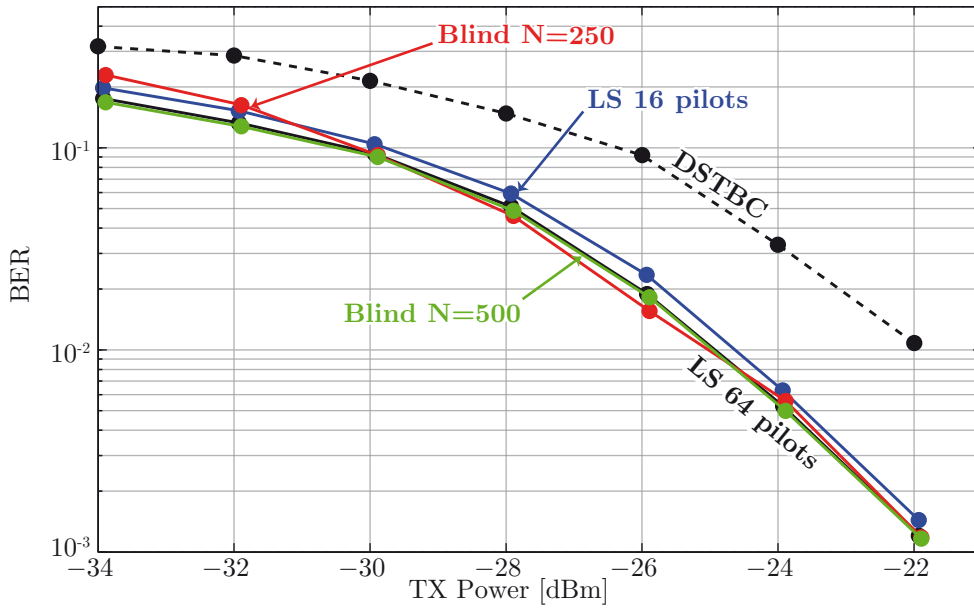
Figure 4.9: Experiment 4.4: BER vs TX power value (non line of sight, GTAS lab).
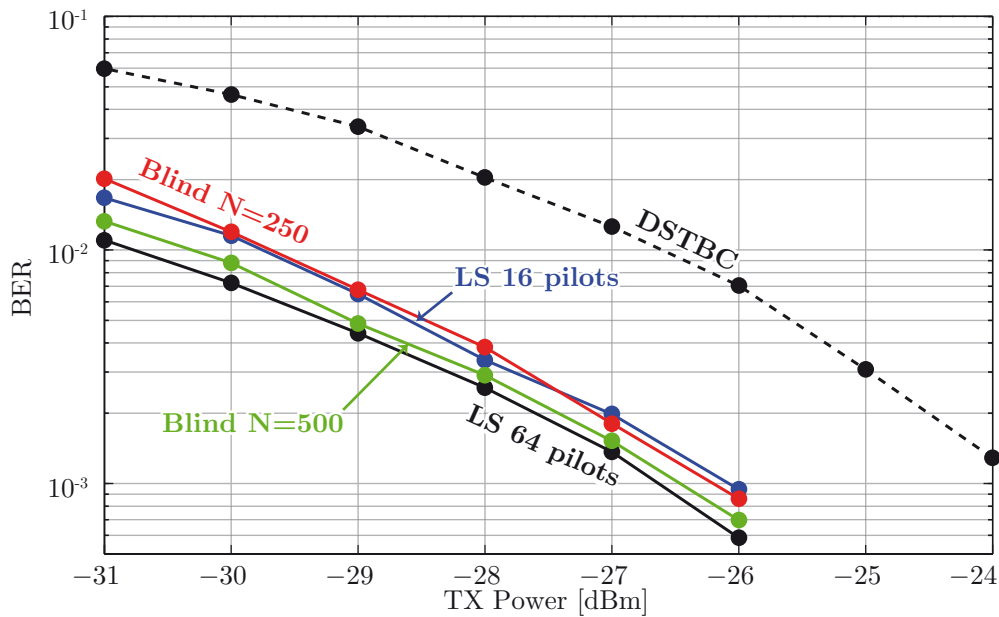
Figure 4.10: Experiment 4.5: BER vs TX power value (non line of sight, UDC lab).

permits the use of shorter frames, which is crucial when channel coherence time is short.

In Experiment 4.5 a higher transmission rate (5 MBaud) is set, obtaining the curves plotted in Figure 4.10. These results are very similar to those obtained for Experiment 4.4 since there is no clear line of sight (as in Experiment 4.4). Although carried out in a different scenario and with a different rate, the results in Figure 4.10 confirm the conclusions obtained for Experiments 4.3 and 4.4.

Finally, it can also be seen that the computer simulation results shown in Figures 4.6 and 4.7 are reasonable approximations for the behavior observed in the non-line of sight and line of sight scenarios, respectively. Regarding the behavior of the different OSTBC transmission

techniques, the conclusions jointly derived from the experiments and from the simulations are consistent. Despite the similarities, there are also some differences between the experimental (see Figures 4.8–4.10) and the simulated curves. For instance, the diversity gain estimated as the slope of the BER curve at large TX power values is not the same. This may be due to the fact that the actual channel is not exactly Rayleigh nor Rice. Furthermore, the simulations also assume uncorrelated channels, but this is not true in practice [48, 51]. Finally, frequency and timing synchronization errors are also included in the experimental curve. Additionally, the curves from the measurements plot the BER respect to the TX power value, whereas in the simulations the SNR is employed. The fact of using the TX power value instead of the SNR in the measurement curves motivated the inclusion of the DSTBC as a reference.

4.6 Conclusion and Criticism

In this chapter, four different blind channel estimation schemes, namely JADE, the Beres and Adve method, an SOS-based approach and an HOS-based approach, were evaluated by computer simulations and by testbed measurements (Experiments 4.1 and 4.2). A pilot-aided LS channel estimation as well as the JADE algorithm were also measured as benchmarks. Both simulations and realistic experiments in LOS and NLOS scenarios show that the SOS-based estimation suffers from a loss of less than 1 dB compared to the perfect CSI (or the LS) case. Given the low computational requirements demanded by the SOS-based approach, it exhibits an excellent tradeoff between channel estimation accuracy and computational complexity.

The performance of several 2×1 as well as 2×2 MIMO-STBC systems was also measured in different realistic indoor scenarios using a 2×2 MIMO testbed operating at 2.4 GHz. In particular, Alamouti code for two RX antennas with coherent and non-coherent demodulation was measured. Two different channel estimation methods have been considered: a conventional pilot-aided technique and an SOS-based blind algorithm. We have presented the results obtained from three different experiments (Experiments 4.3 to 4.5). In all cases, the blind channel estimation provides a performance – in terms of BER – similar to that exhibited by pilot-aided estimation. On the one hand, such blind methods reveal a slight increase in the effective data rate and a moderate increase in the computational complexity of the detector. On the other hand, the DSTBC evaluated as a reference presents, as expected, a penalty of about 3 dB with respect to coherent schemes.

The measurement results presented in this chapter (Experiments 4.1 to 4.5) were carried out using the first versions of the GTEC MIMO testbed. If we repeated the measurements again, then we would modify the measurement procedure in such a way that we could present the results with respect to the SNR as well as with respect to the TX power value. We would also provide confidence intervals for the resulting curves to show the accuracy of the measurements.

Chapter 5

Analog Joint Source-Channel Coding in Indoor Environments

In this chapter we address the feasibility of the practical implementation of the analog joint source-channel coding based on a software-defined radio approach. We carry out indoor measurements in a representative scenario making use of our testbed in order to evaluate the performance of such analog coding methods. This chapter is partly based on the publications [151, 152].

The remainder of the chapter is organized as follows. In Section 5.1 a brief introduction to the analog joint source-channel coding approach is provided, emphasizing the benefits of this approach with respect to traditional digital systems. A detailed explanation of the basis of the analog joint source-channel coding is given in Section 5.2, in which the encoder and the decoder for 2:1 systems are also studied. The description of the set-up as well as the procedure followed to measure the analog coding techniques are described in Section 5.3. The results obtained – including computer simulation results – are presented in Section 5.4. Finally, Section 5.5 summarizes the main results of this chapter.

5.1   Introduction

From a theoretical perspective, it is well known that a digital system based on separation between source and channel coding is optimal for digital communications in many channel environments, such as in Additive White Gaussian Noise (AWGN) channels [261]. However, the complexity of such systems can be very high when they are designed to perform close to the Shannon limit. For that purpose, digital systems make use of capacity-approaching channel codes (e.g. turbo codes, Low Density Parity Check (LDPC) codes or Serially-Concatenated Low Density Generator Matrix (SCLDGM) codes). Such codes introduce a very high encoding and decoding complexity, thus demanding a large amount of computational resources. Furthermore,

any capacity-approaching code requires the transmission of long codewords. Consequently, significant delays are introduced in the communication link. Moreover, full redesign of the digital system is required whenever we want to change the code rate or the distortion target.

Interestingly, analog communications are optimal under some circumstances. For instance, direct transmission of uncoded Gaussian samples over AWGN channels is optimal because Gaussian sources are perfectly matched to Gaussian channels [113, 120]. Notice that these schemes perform analog compression at symbol level. Consequently, they do not demand high computational resources neither do they require the transmission of long blocks of data, thus making them very attractive for applications based on software-defined radio.

Despite the initial work that has investigated possible schemes based on analog transformations aimed at perfectly matching sources with channels [72, 99, 138, 139, 242], research in this area has just started. Furthermore, the actual performance of these schemes over real physical scenarios has never been analyzed to date. In this chapter, we make use of the third version of the GTEC MIMO testbed to assess the actual performance of analog joint source-channel coding in indoor scenarios. Moreover, while implementing and measuring such methods, we address the problems that analog compression schemes pose in practice. First, the Peak-to-Average Power Ratio (PAPR) of the transmitted signals can be very high, so careful normalization of the transmitted signals is needed to prevent performance degradation due to the limited resolution of the Digital-to-Analog Converter (DAC) and the Analog-to-Digital Converter (ADC). Second, the transmitted signals in analog compression schemes are parameterized according to the Signal to Noise Ratio (SNR), so it was necessary to implement a closed-loop software-defined radio system. Although an open-loop system would be much simpler to implement, it would limit the attainable performance with analog joint source-channel coding. This is similar to digital systems that approach capacity in a wireless channel, which also use a closed-loop to adapt both transmit power and transmit rate according to the channel response.

5.2   Analog Joint Source-Channel Coding

We consider the analog transmission of discrete-time continuous-amplitude sources over an AWGN channel. At the Transmitter (TX), N independent and identically-distributed (iid) source symbols are encoded into K channel symbols, resulting in an $N : K$ system. Such symbols are then transmitted through an AWGN channel with noise variance N_0. At the Receiver (RX), these symbols can be decoded using either a Maximum Likelihood (ML) or a Minimum Mean Squared Error (MMSE) approach.

The distortion between a source symbol vector $\mathbf{x} = [x_1, x_2, \ldots, x_N]^T$ and a decoded symbol vector $\hat{\mathbf{x}} = [\hat{x}_1, \hat{x}_2, \ldots, \hat{x}_N]^T$ is calculated according to the Mean Squared Error (MSE), defined
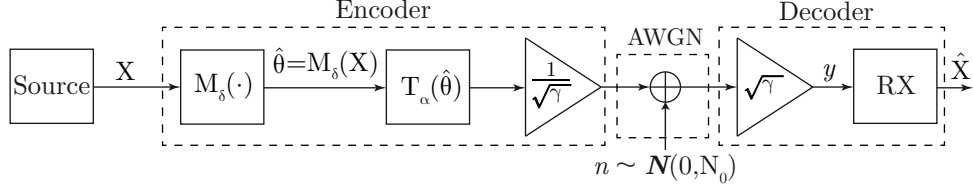
Figure 5.1: System model for the N:1 bandwidth compression scheme.

as

$$\text{MSE} = \frac{1}{N}E\left[\|\mathbf{x} - \hat{\mathbf{x}}\|^2\right] = \frac{1}{N}\sum_{i=1}^{N}E\left[|x_i - \hat{x}_i|^2\right],$$

where $E[\cdot]$ denotes the expectation operator.

Consequently, the performance of the system can be measured in terms of the output Signal-to-Distortion Ratio (SDR) with respect to the SNR, where SDR is defined as

$$\text{SDR} = 10\log\left(\frac{1}{\text{MSE}}\right).$$

Given N and K, the so-called Optimal Performance Theoretically Attainable (OPTA) is calculated by equating the rate distortion function to the AWGN channel capacity [40]

$$\frac{N}{10}\text{SDR} = N\log\left(\frac{1}{\text{MSE}}\right) = K\log\left(1 + \frac{1}{N_0}\right) = \text{OPTA}, \tag{5.1}$$

where the transmitted symbols are normalized to unit mean power. The OPTA represents the theoretical limit for the system performance given in terms of the achievable SDR.

5.2.1 Encoder

Figure 5.1 shows the block diagram of an N:1 analog joint source-channel coding system where the source generates blocks of B iid symbols from a Gaussian distribution that are encoded into B/N channel symbols. Without loss of generality, we assume a Gaussian distribution with zero mean and unit variance for the source, and that the mean transmit power is equal to one.

A particular type of parameterized space-filling continuous curves, called spiral-like curves, are used to encode the $X = (x_1, x_2)$ Gaussian samples. These curves were proposed for transmission of Gaussian sources over AWGN channels by Chung and Ramstad [72, 138, 242]. For the case of 2:1 compression (i.e. N=2), they are formally defined as

$$\begin{cases} x_1(\theta) = \text{sign}(\theta)\dfrac{\delta}{\pi}\theta\sin\theta \\ x_2(\theta) = \dfrac{\delta}{\pi}\theta\cos\theta \qquad\qquad \text{for } \theta \in \mathbb{R}, \end{cases} \tag{5.2}$$

where δ is the distance between two neighboring spiral arms, and θ is the angle from the origin to the point $X(\theta) = (x_1(\theta), x_2(\theta))$ on the curve. Note that in the curve described above (Equation (5.2)) there is a one-to-one correspondence between the angle θ and each pair of
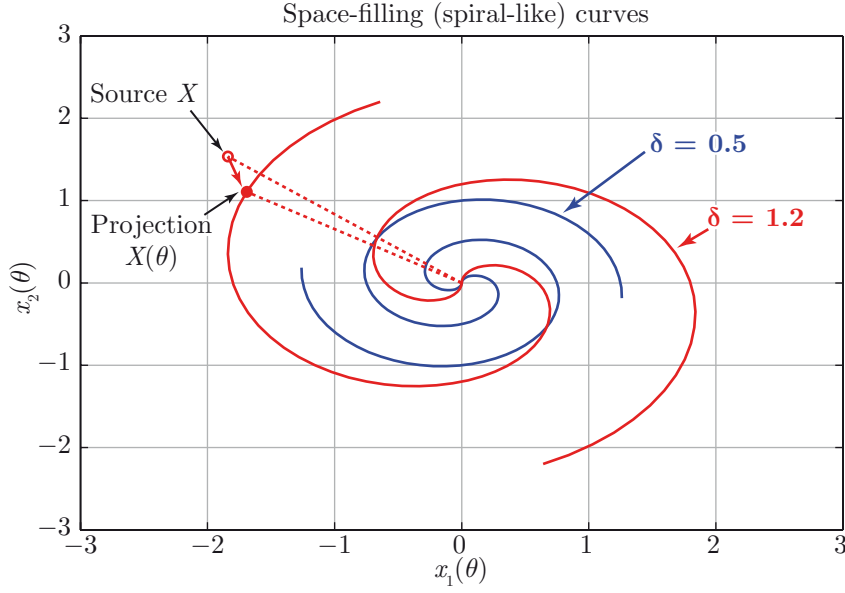
Figure 5.2: Space-filling (spiral-like) curves for $\delta = 0.5$ and $\delta = 1.2$. Additionally, an example of how a source point X is mapped to a point $X(\theta)$ in the curve is shown.

Gaussian samples – i.e. the point $(x_1(\theta), x_2(\theta))$ on the curve, so that the curve gradually fills in the whole two-dimensional space as the absolute value of θ grows. As a consequence, a mapping function called M_δ is utilized to project (map) each pair of Gaussian source samples $X = (x_1, x_2) \in \mathbb{R}^2$ onto the curve defined in Equation (5.2). Such a projection consists in finding the closest point to X on the spiral (see an example in Figure 5.2). The angle from the origin to that point on the spiral, $\hat{\theta}$, will be the channel symbol for x_1 and x_2, i.e.

$$\hat{\theta} = M_\delta(X) = \arg\min_\theta \left\{ \left(x_1 \pm \left(\frac{\delta}{\pi} \right) \theta \sin\theta \right)^2 + \left(x_2 - \left(\frac{\delta}{\pi} \right) \theta \cos\theta \right)^2 \right\}. \tag{5.3}$$

Since our goal is the minimization of the MSE, the bi-dimensional space has to be filled by the spiral in the best possible way for every SNR value. On the one hand, by changing the δ value, we manage to optimize this matching and to improve the system performance. On the other hand, it is possible to achieve higher compression rates (i.e. N:1) by extending Equation (5.2) to generate more complex curves [95, 96].

The next step consists in defining an invertible function of $\hat{\theta}$ – with the corresponding normalization factor to ensure the transmit power constraint. In [72, 138, 139], the invertible function $T_\alpha(\hat{\theta}) = \hat{\theta}^\alpha$, with $\alpha = 2$ was proposed. However, as shown in [152], the system performance can be improved if α and δ are jointly and numerically optimized for each SNR value. Therefore, the channel symbol is $T_\alpha(\hat{\theta})/\sqrt{\gamma}$, where $\sqrt{\gamma}$ is the normalization factor. To sum up, the received symbol y at the decoder can be expressed as

$$y = T_\alpha(M_\delta(X)) + n\sqrt{\gamma}.$$

5.2.2 Decoder

Most of the work on space-filling curves has focused on ML decoding and high SNR values. In general, in the high SNR regime, ML decoding results in a performance very close to the theoretical limit. However, ML decoding does not perform well for low SNR, and even in the case of high SNR is not optimal. The case of MMSE decoding was first mentioned in [72]. In [151, 152] quasi-optimal MMSE decoding and optimization for all SNR values is proposed. In this section, we describe both ML and MMSE decoding.

ML Decoding

Given a received symbol y, the ML estimate is obtained as the source pair $X = (x_1, x_2)$ belonging to the curve and satisfying

$$\hat{X}_{\mathrm{ML}} = \arg\max_{X \in \text{ curve}} \{p(y|X)\} = \{X | X \in \text{ curve and } T_\alpha(M_\delta(X)) = y\}. \qquad (5.4)$$

ML decoding is equivalent to first applying the inverse function $T_\alpha^{-1}(\cdot)$ to the received symbol y (i.e. $\hat{\theta}' = T_\alpha^{-1}(y)$), and then performing inverse mapping on $\hat{\theta}'$ according to Equation (5.2).

MMSE Decoding

Given a received symbol y, MMSE decoding is performed at the RX to calculate an estimation of the corresponding source symbol. Optimal MMSE decoding can be expressed as

$$\hat{X}_{\mathrm{MMSE}} = E\{X|y\} = \int X\,p(X|y)dX = \frac{1}{p(y)} \int X\,p(y|X)p(X)dX, \qquad (5.5)$$

where the mapping function $M_\delta(\cdot)$ is used to obtain the conditional probability $p(y|X)$. Note that the integral in Equation (5.5) can only be calculated numerically via Monte Carlo integration because $M_\delta(\cdot)$ is discontinuous and highly non-linear. To do so, X is firstly discretized using a uniform step and a mapped value is calculated for each discretized point according to Equation (5.3). As a result, we obtain a discretized version of $p(y|X)$. Next, $p(X)$ is also computed for each point, and thus the calculation of the integral is reduced to multiplicative and additive operations. Since the discretization of $p(X)$ does not depend on the received symbol, it is calculated once off-line and stored in the decoder.

5.2.3 N:K Compression Systems

The proposed analog system can be easily modified to adapt the compression rate from N:1 to N:K, N and K satisfying $K < N < 2K$, as shown in Figure 5.3. Now, blocks of $c_1 + c_2$ source symbols are generated at the transmitter: c_1 symbols are sent through a 1:1 uncoded system and the rest are encoded into $c_2/2$ channel symbols using a 2:1 system. Since the total
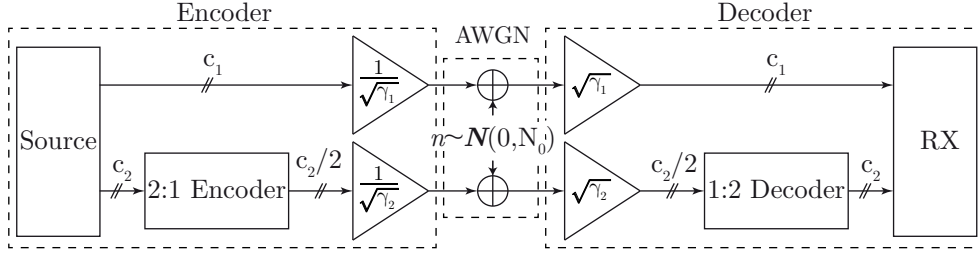
Figure 5.3: Proposed system model for $N{:}K = (c_1 + c_2)/(c_1 + c_2/2)$ bandwidth compression.

number of symbols transmitted through the channel is $c_1 + c_2/2$, the overall compression rate is $N/K = (c_1 + c_2)/(c_1 + c_2/2)$. By properly choosing c_1 and c_2, any arbitrary compression rate between 1:1 and $N{:}K$ can be achieved as long as the condition $K < N < 2K$ is fulfilled. The total average transmit power per channel symbol should be constrained to one, but the power invested to transmit the c_1 uncoded symbols and the $c_2/2$ coded symbols can differ as long as the total power constraint is satisfied. For this reason, we added a power allocation module to the encoder that decides how much power is allocated to each sub-system in order to achieve the best performance.

Optimal Power Allocation

Defining $p \in (0, 1)$ as the fraction of the total transmit power allocated to the 1:1 sub-system, the power for transmitting each channel symbol is:

$$\frac{1}{\gamma_1} = \frac{(c_1 + c_2/2)p}{c_1}$$

in the 1:1 sub-system, and

$$\frac{1}{\gamma_2} = \frac{(c_1 + c_2/2)(1 - p)}{c_2/2}$$

in the 2:1 sub-system. Since the 1:1 uncoded sub-system is optimal, according to Equation (5.1) we have

$$\frac{1}{D_1} = 1 + \frac{(c_1 + c_2/2)p}{c_1 \, N_0},$$

where D_1 is the distortion per source symbol transmitted by the 1:1 uncoded sub-system. Assuming that the 2:1 non-linear mapping is near-optimal we can write:

$$\frac{1}{D_2} = G \left(1 + \frac{(c_1 + c_2/2)(1 - p)}{N_0 \, c_2/2} \right)^{\frac{1}{N}},$$

where D_2 is the distortion per source symbol transmitted by the 2:1 sub-system, and G is a constant that represents the gap between the actual performance of the 2:1 sub-system and the theoretical limit. For the case of Gaussian sources, the gap is below $1\,\mathrm{dB}$ in the whole SNR region and thus we can consider $G = 10^{(-\frac{1}{10})}$.

Consequently, the total average distortion is

$$\overline{D} = \frac{c_1 D_1 + c_2 D_2}{c_1 + c_2},$$

and the resulting output SDR

$$\text{SDR} = 10\log\frac{1}{\overline{D}} = 10\log\frac{c_1 + c_2}{c_1 D_1 + c_2 D_2}.$$

Note that given c_1, c_2, and N_0, $\overline{D}$ is a function of p, thus the optimal power allocation strategy is to calculate the value of p that minimizes $\overline{D}$. The optimum values for γ_1 and γ_2 are the following

$$\gamma_1 = \frac{c_1}{(c_1 + c_2/2)p_{opt}}, \gamma_2 = \frac{c_2/2}{(c_1 + c_2/2)(1 - p_{opt})}, \tag{5.6}$$

where $p_{opt} \in (0,1)$ has to be optimized for different compression ratios and different SNR values.

5.3 Experimental Assessment

Making use of the third version of the GTEC MIMO testbed we tackle the problem of measuring the mean performance – in terms of SDR – of the analog joint source-channel coding described in Section 5.2 in a typical indoor environment (specifically, an office). The results measured are then compared with both the OPTA and the results obtained from computer simulations.

5.3.1 Closed-Loop Set-up

We chose to carry out narrowband single-antenna measurements for simplicity reasons and because we already had prior experience in similar experiments [90, 108, 110, 237, 241]. It was necessary to implement a feedback channel from the TX to the RX to obtain a closed-loop set-up. This is because in a simplex system such as this one, the SNR is estimated at the RX side and is afterwards fed back to the TX in order to select the optimum δ value. There is more on how we have implemented the feedback channel in Chapters 2 and 3. Note that although the testbed is 4×4 MIMO-capable, we only make use of a single TX antenna and a single RX antenna.

The measurement approach is based on software-defined radio principles, and all signal processing operations were implemented in MATLAB. The data was generated off-line, transmitted in real-time over a wireless channel, and stored in the hard drives at the RX. In a later step, the measurement data obtained is evaluated off-line. Given the specific features of the signals obtained after the analog joint source-channel coding (e.g. the high PAPR and the limited resolution of the DAC and the ADC), it is very important to carry out experiments
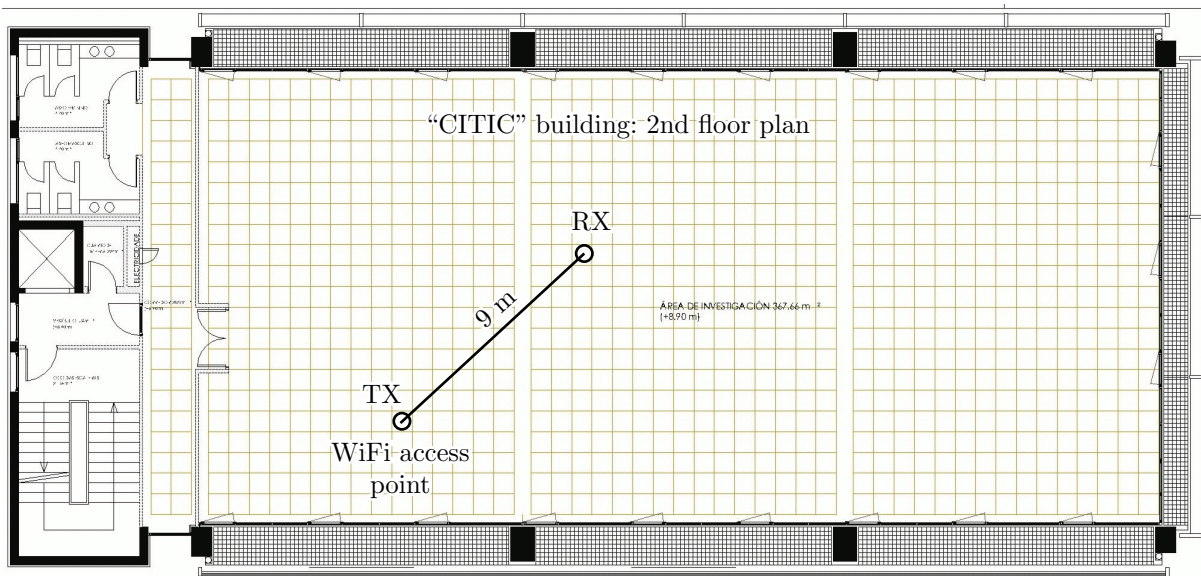
Figure 5.4: Plan of the second floor of the "CITIC" building.

using the hardware testbed to take into account the possible distortions introduced by the ADC, the DAC, and the power amplifier. Unrealistic results may be obtained if the real-time channel is replaced with a simulated channel whose coefficients have been obtained from a channel sounder. More specifically, effects like those caused by the high PAPR of the transmitted signals would not be taken into account in a realistic way.

5.3.2   A Typical Indoor Environment – the Channel

We evaluated experimentally the performance of the analog joint source-channel coding in an office, with direct line of sight between the TX and the RX antennas (see Figure 5.4). The TX antenna was placed on a table immediately adjacent to a WiFi access point of the public wireless network at the University of A Coruña. The RX antenna was placed on a table used by one of the employees in the office, thus emulating the actual position that a desktop or a laptop computer would occupy. The TX and RX antennas were approximately 9 m apart.

In order to incorporate greater realism into the measurements, we used standard rod antennas with a gain of 3 dB [24]. These antennas are similar to those employed in WiFi access points that operate at 5 GHz.

5.3.3   Quantization of the Transmitted Signals

One of the major hindrances that has to be taken into account when implementing analog joint source-channel coding in a software-defined radio testbed is the elevated PAPR of the transmitted signals. For the correctness of the measurements, it is important to ensure that each generated sequence has the same mean transmit power value. In order to guarantee such a constraint we have implemented the following procedures:

- After the encoding stage, the resulting channel symbols are normalized to ensure that the whole sequence – including the uncompressed symbols – always has a mean power equal to one. This normalization is performed independently of the rate and the power allocation scheme utilized.

- Once the channel symbols have been converted to discrete Intermediate Frequency (IF) signals, they have to be quantized according to the 16 bits of resolution of the DAC. Given the high PAPR of the resulting signals, we have determined, by means of computer simulations, the maximum absolute value that a channel symbol can reach – including all possible rates and power allocation schemes, this turning out to be approximately equal to 8.8. Consequently, it is very easy to compute the maximum scale factor for each generated sequence, ensuring the transmit power constraint as well as guaranteeing that no clipping effects are introduced either by the DAC or by the ADC.

5.3.4 Measurement Procedure

The transmission of a sequence of symbols involves the following operations:

- The TX obtains the estimated SNR from the RX, which has performed the estimation based on the previously transmitted frame.

- Based on the estimated SNR value, the TX selects the optimum value of δ, generates a new Gaussian sequence, and encodes it using the selected δ value.

- If a scheme with power allocation is being measured, then the TX computes the values of γ_1 and γ_2 based on the estimated SNR and distributes the total TX power accordingly.

- The entire transmitted sequence is normalized to ensure a transmit power value equal to one. The resulting normalization factor has to be sent to the RX to perform the inverse operation before decoding. Note that when power allocation is used, the normalization factor is included in the parameters γ_1 and γ_2. Now these two values have to be sent to the RX instead of the normalization factor.

- Next, the sequence is pulse-shape filtered, scaled, and I/Q modulated.

- The transmit frame is assembled. In addition to the encoded signal, a preamble and a training sequence is included. These are needed for time and frequency recovery, and to equalize the channel at the RX, respectively.

- The assembled frame is then transmitted through the wireless channel.

- At the RX, the channel is estimated using the Least Squares (LS) approach. Next, the SNR is estimated[1] and fed back to the TX. Finally, the observed sequence is saved for subsequent evaluation.

---

[1] In order to guarantee the accuracy of the SNR estimation, the RX estimates the Power Spectral Density (PSD) of the noise during the time intervals when no signals are transmitted.

	Source	Coded	Uncoded	Total I/Q	Frame	Transfer rate
Rate	symbols	symbols	symbols	symbols	duration (ms)	(symbol/s)
2:1	7 200	3 600	0	1 800	0.9	$8 \cdot 10^6$
10:6	7 200	2 880	1 440	2 160	1.1	$6.55 \cdot 10^6$
10:9	7 200	720	5 760	3 240	1.6	$4.5 \cdot 10^6$

Table 5.1: Transfer rates according to the code rate. Frame overheads are not included.

Note that although our testbed has four RX antennas, it is not possible to evaluate four different transmissions simultaneously because each RX antenna sees a different SNR, thus making it impossible to transmit the same sequence encoded using different values of δ.
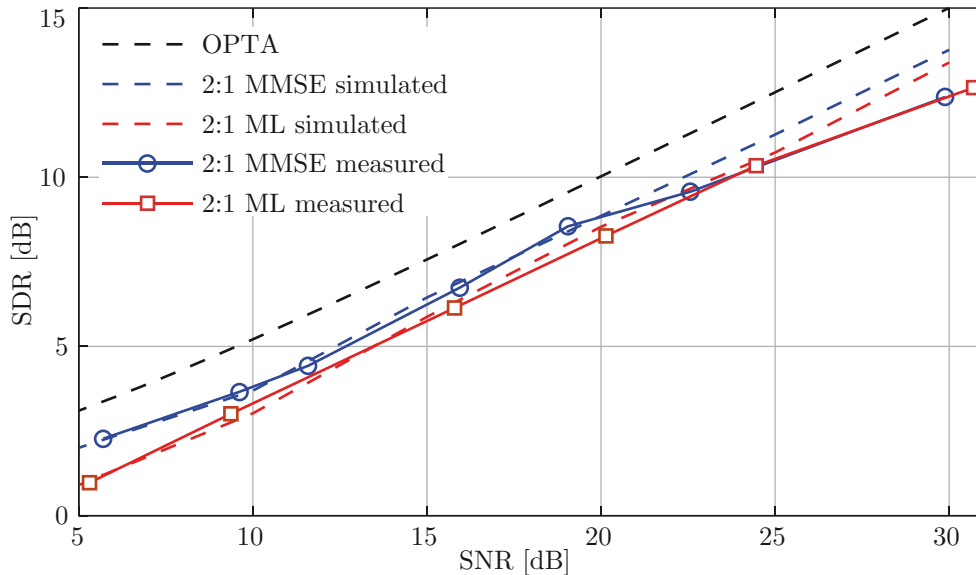
Figure 5.5: Experiment 5.1: 2:1 scheme: OPTA, simulated SDR and measured SDR, both for ML and MMSE decoders.

Signaling Features

All frames have the same structure: a Pseudo Noise (PN) sequence made up of 100 symbols (preamble), 16 pilot symbols, and 7 200 source symbols that are encoded according to one of the three possible compression rates considered, i.e. 2:1, 10:6, or 10:9. Each pair of channel symbols is mapped to a complex I/Q symbol. We use a symbol period of $T_s = 20$ samples per symbol, with the sampling frequency of both the DAC and the ADC fixed to 40 Msample/s. The symbols are pulse-shape filtered using a squared root raised cosine filter with 20 % roll-off, resulting in a 2.4 MHz occupied bandwidth at the carrier frequency of 5.605 GHz. Table 5.1 shows the resulting transfer rates for the three different compression rate values, and the number of coded and uncoded symbols (i.e. the channel symbols) obtained when 7 200 source symbols
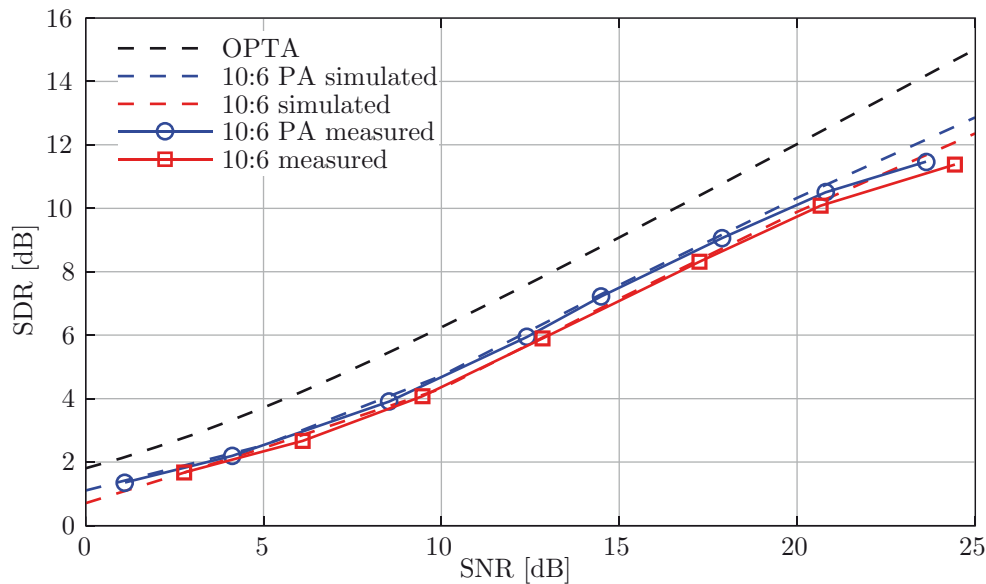
Figure 5.6: Experiment 5.2: 10:6 scheme: OPTA, simulated SDR with and without power allocation (PA), and measured SDR with and without power allocation (PA).

are used. Additionally, the number of I/Q symbols that compose the transmit frame, and the frame duration, are indicated. Note that Table 5.1 does not include the overheads due to preamble, pilot symbols, and normalization values.

5.3.5 Experimental Evaluation

We have assessed the SDR of the transmitted sequences with the MMSE RX with rates 2:1, 10:6, and 10:9; and with the ML RX with rate 2:1. For the 10:6 and the 10:9 cases, two schemes are evaluated. The first transmits the whole sequence with the same mean power value, whilst the second uses the power allocation scheme defined in Section 5.2.3. In total, six different schemes are measured. In order to produce the curves shown in the ensuing section, each scheme is measured at different TX power values to obtain different SNR values. We repeated the experiments 100 times, which resulted in approximately 6 000 different realizations.

Note that in order to achieve relatively low SNR values (≈ 5 dB) while keeping the complexity of the synchronization tasks in reasonable terms, we boost the preamble such that the mean power of the acquired preamble is significantly larger than that of the rest of the frame.

5.4 Results

Figures 5.5–5.7 present the results obtained for the rates 2:1, 10:6, and 10:9, respectively. For the 10:6 and the 10:9 cases, the SDR is measured with and without the power allocation (PA) scheme. For the 2:1 case, both ML and MMSE receivers are evaluated. Notice that in the
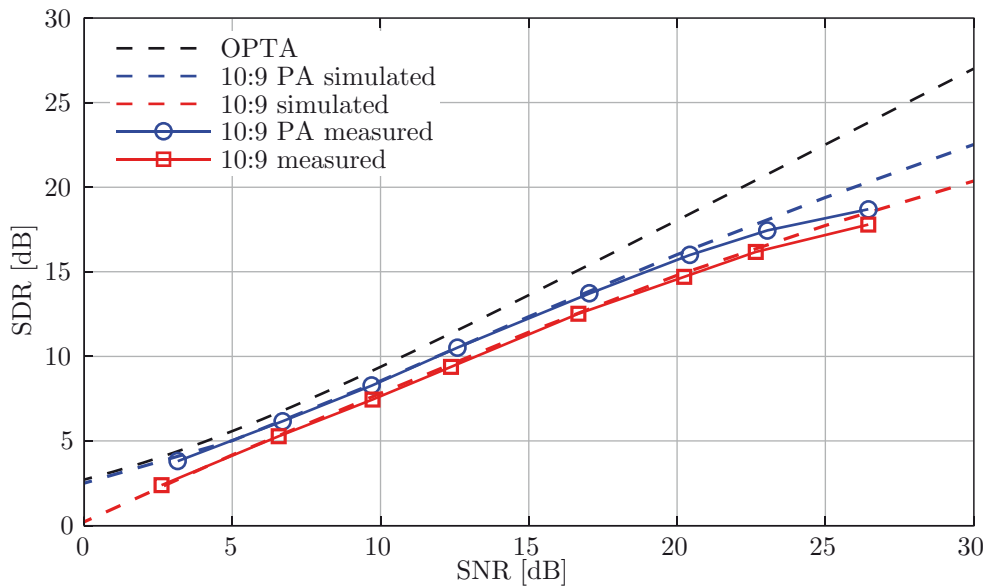
Figure 5.7: Experiment 5.3: 10:9 scheme: OPTA, simulated SDR with and without power allocation (PA), and measured SDR with and without power allocation (PA).

2:1 case there is no possibility of including a power allocation scheme because all transmitted symbols are coded symbols. Also note that the parameters to be optimized are different for the ML, for the MMSE and for the MMSE with power allocation.

For comparison purposes, in all graphs we have included the OPTA curve as well as the corresponding SDR curves when the six different schemes are simulated using an AWGN channel model. In all cases, the abscissas and the ordinates of Figures 5.5–5.7 respectively show the SNR and the SDR values expressed in decibels.

All graphs in Figures 5.5–5.7 clearly show that the measurement curves perfectly match the simulated ones for SNR values below 20 dB. When the SNR is greater than 20 dB, the SDR curves exhibit saturation effects. Such effects are mainly caused by the limited number of resolution bits of the DAC (16 bits in this case), and also by the high PAPR of the transmitted signals. Looking at Table 5.1, and at the graphs mentioned above, it is interesting to see how the SDR increases as the transfer rate decreases, as expected.

5.5   Conclusion and Criticism

Recently, analog joint source-channel coding has been introduced as a means of achieving near-optimum performance for high data rates with very low complexity. However, no experimental evaluation proving its feasibility in practical applications has previously been carried out. In this chapter, we have described a software-defined radio implementation of a practical wireless communication system that uses analog joint source-channel coding. We have used this software-defined radio implementation to carry out closed-loop narrowband single-antenna

measurements in a typical and very realistic indoor scenario, which has forced us to take into account the problems that analog joint source-channel coding schemes pose in practice. The results obtained showed that the analog joint source-channel coding measurements perfectly matched those originally reported by simulations in AWGN channels for SNR values below 20 dB, thus clearly demonstrating the feasibility of these analog compression schemes in real environments. For SNR values above 20 dB there is a performance degradation caused by the limited number of resolution bits of the DAC (16 bits in this case), and also by the high PAPR of the transmitted signals.

When implementing these schemes in a practical system, a feedback channel is needed to send the SNR value to the TX end. Additionally, training sequences are needed for channel estimation, and a normalization factor (or a pair of values if the power allocation scheme is utilized) has to be sent from the TX to the RX. More research is needed to determine the exact overhead introduced by the required pilot symbols and normalization factors.

Chapter 6

Serially-Concatenated LDGM Codes in Indoor Environments

Modern wireless systems consider closed-loop wideband Multiple-Input Multiple-Output (MIMO) transmissions to attain very high throughput over frequency selective wireless channels. To exploit the potential of closed-loop transmission, Adaptive Modulation and Coding (AMC) is employed. AMC consists in adapting the modulation format and code rate to approximate the transmission rate to the instantaneous channel capacity. However, AMC does not take into account a key characteristic of the channel such as its EXtrinsic Information Transfer (EXIT) function, which has a major influence on performance when turbo iterative detection is employed at the Receiver (RX). In this chapter we introduce EXIT-based Adaptive Coding (EAC), an adaptive transmission scheme based on matching the Forward Error Correction (FEC) EXIT function to that of the instantaneous MIMO channel realization. We perform adaptation on both transmit power and the FEC code profile with the aim of best fitting the channel capacity to the transmission rate as well as the EXIT characteristic of the used FEC to that of the overall MIMO channel.

The remainder of the chapter is structured as follows. In Section 6.1 we introduce the so-called Serially-Concatenated Low Density Generator Matrix (SCLDGM) channel codes, an approximation to obtain capacity-approaching channel codes suitable for MIMO systems. In Section 6.2 we present EAC. The details of the experimental set-up as well as the measurement procedure to assess the SCLDGM channel codes and the EAC are explained in Section 6.3. The results obtained are presented and analyzed in Section 6.4. Finally, Section 6.5 is devoted to the conclusions and criticism.

6.1 Introduction

The development of channel codes able to approach the theoretical capacity limits has been a very active area of research during the last decade [261]. The basic premise of the so-called capacity-approaching channel codes is to produce long, random-like codewords that resemble the idea of random coding introduced by Shannon. Two well-known examples of such an idea are the turbo codes [41] and the Low Density Parity Check (LDPC) codes [100, 193]. More specifically, in [73] it has been reported that for the binary input Additive White Gaussian Noise (AWGN) channel, the LDPC codes approach the channel capacity within a small fraction of a decibel when long codewords are utilized. LDPC codes also exhibit a good performance when transmitting over AWGN or Rayleigh Single-Input Single-Output (SISO) channels [149].

The utilization of turbo and LDPC codes for transmission over MIMO channels has been studied in [144, 150, 187, 188, 281]. Unlike turbo codes, the main problem of using LDPC codes is their significant complexity in the encoding process. In order to avoid this problem, several subclasses of LDPC codes have been reported in the literature. Among them, in this chapter we will focus on the so-called Low Density Generator Matrix (LDGM) codes [192], whose generator matrix is large and random as well as sparse. Due to their poor minimum distance, LDGM codes can only attain an arbitrarily low error probability by reducing the rate to zero. In other words, LDGM codes present a high error floor, and thus the Bit Error Ratio (BER) decreases very slowly as the E_b/N_0 increases. This problem meant that LDGM codes were initially discarded in favor of LDPC codes. However, LDGM codes exhibit a very good convergence threshold. Consequently, LDGM codes are still useful when they are combined with techniques to reduce such an error floor, for example when an outer code is used to correct the residual errors at the output of the inner LDGM code [103]. Given that the number of errors per block to be corrected is very low, a high-rate code is sufficient to correct such errors. Interestingly, the performance of high-rate LDGM codes is quite good, and they are therefore good candidates to be serially concatenated with an inner LDGM code with a rate close to the desired final rate. The resulting scheme is termed Serially-Concatenated Low Density Generator Matrix (SCLDGM), which yields to a channel coding approach with a good convergence threshold and, at the same time, keeps the error floor low enough for practical SISO and MIMO applications [103, 122–124, 126, 287–289, 312].

It has been demonstrated that SCLDGM codes perform very well for the case of AWGN and Rayleigh channels [126] as well as for MIMO systems [289]. However, there are no experimental evaluation results on the performance of such SCLDGM codes in realistic scenarios. In this chapter we present measurement results carried out with the GTEC MIMO testbed in a realistic indoor scenario with the objective of showing the performance of the SCLDGM codes. Additionally, and based on the measurement results, we propose a novel technique to approach capacity similar to AMC, but taking also into account the turbo iterative
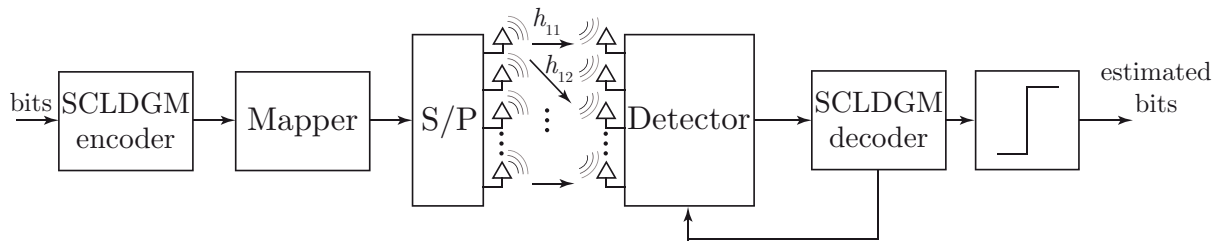
Figure 6.1: Block diagram of the SCLDGM code in a MIMO system.

detection and decoding performed at the RX side. Hereafter, we present two different experiments. In the first we evaluate experimentally the performance of SCLDGM codes non-optimized for the specific wireless channel in which they are measured. In the second experiment, we explore the performance gains that can be obtained when the FEC EXIT function of the code (hereafter referred to as EXIT funtion) is also adapted to match that of the wireless channel. In both cases, we consider a 4×4 MIMO system in indoor environments.

Figure 6.1 shows an example of a coded MIMO system. At the Transmitter (TX), the source bits are encoded, mapped to constellation symbols and passed to a spatial multiplexer, which distributes the modulated symbols to the n_T TX antennas. Each signal, with an average energy E_s, travels to each of the n_R RX antennas through different wireless channels, affected by distinct fading coefficients. From now on, we consider this scheme for the experimental evaluation of SCLDGM codes.

6.2 EXIT-based Adaptive Coded MIMO transmission

When a feedback channel between the TX and the RX is available, closed-loop MIMO schemes are the best choice for maximizing capacity. Adapting transmissions to the instantaneous channel conditions is crucial for exploiting the capacity of time-varying wireless channels.

AMC constitutes a practical mechanism to exploit the potential of closed-loop transmission (see [59] and references therein). For that purpose, AMC adapts the modulation format and the code rate with the aim of approaching the instantaneous capacity of a time varying channel. Several modern wireless standards make use of AMC, such as IEEE 802.16 WiMAX [155, 156], High-Speed Downlink Packet Access (HSDPA) [28], or LTE [29]. In the case of WiMAX and LTE, AMC is combined with Coded Orthogonal Frequency Division Multiplexing (COFDM) to provide very high data rates over frequency-selective channels. In addition, multiple antennas at both TX and RX sides are also employed to benefit from the capacity increase related to MIMO systems [280].

However, AMC does not take into account the turbo iterative detection and decoding usually performed at the RX to obtain dramatic performance improvements over conventional non-iterative reception. In this case, the key for maximizing performance and, therefore,

approaching the channel capacity, is to use an FEC with an EXIT function matched to that of the channel (including the overall effect of the modulator, the channel and the detector) [126, 287, 289].

Given that Gray mapping is used, AWGN and Rayleigh fading SISO channels exhibit an EXIT function that is approximately flat regardless of the constellation used [287, Chapter 3, pp. 43]. This makes turbo iteration at the RX unnecessary, and the use of an FEC optimized for the AWGN channel is the optimum choice. However, this is no longer true when transmitting over MIMO channels [287, Chapter 4, pp. 64], where employing an FEC optimized for the AWGN channel results in large performance losses with respect to an FEC optimized for the particular TX-RX antenna configuration and channel realization.

This motivates us to introduce EAC, an adaptive transmission scheme aimed at better exploiting the capacity of MIMO channels by matching the EXIT function to that of the instantaneous MIMO channel realization. For simplicity reasons, in our formulation of EAC we consider that the FEC rate and the modulation format are fixed. Therefore, only the TX power is adapted to ensure that the channel capacity is large enough to support the transmission rate. However, adaptation of modulation format and code rate can additionally be considered to obtain a higher flexibility or better ease of implementation.

While FEC rate can be easily modified by puncturing a given mother code, it is not clear how to modify a given code to change its EXIT function. However, this inconvenience does not prevent us from employing EAC in practice. In order to overcome this limitation, we resort to using different profile codes, each with a different EXIT function. Although in a practical system we can consider only a small number of different profile codes, we will see that this suffices to explore the feasibility of the proposed EAC scheme.

6.3   SCLDGM Experimental Evaluation

In this section we explain the measurement set-up and procedure for the experimental evaluation of SCLDGM codes in a 4×4 MIMO channel (Experiment 6.1) as well as for EAC 4×4 MIMO transmissions (Experiment 6.2). The scenario for the evaluation is the same, even though the measurements were not carried out simultaneously. Only small differences are found in the set-up and the measurement procedure employed in both experiments. For this reason, we explain the experimental evaluation together. Next, we particularize the results for each experiment in the ensuing sections.

Making use of the third version of the GTEC MIMO testbed we tackle the problem of measuring the mean performance – in terms of the BER with respect to the E_b/N_0 – of the SCLDGM codes in a 4×4 MIMO channel. Additionally, the estimated capacity of the wireless channel – in terms of the minimum E_b/N_0 required for a transmission with an arbitrarily low

error probability – is provided assuming no channel knowledge at the TX side.

6.3.1 Closed-Loop Set-Up Emulation

We chose to carry out narrowband 4×4 MIMO measurements using the third version of the GTEC MIMO testbed for simplicity reasons and because all the necessary equipment was already available. Although experimental evaluation of the adaptation of the channel code profile as well as the TX power (Experiment 6.2) requires a closed-loop communications system, we carried out the experiments avoiding the implementation of the feedback channel. Given that we have considered four different profiles for Experiment 6.2, we can transmit all of them together in the same physical frame, so that they experience the same wireless channel[1]. In both experiments, the TX power adaptation is carried out by always transmitting with the highest TX power value supported by the testbed and, during the evaluation, artificially generated Gaussian noise is added to the acquired sequence to obtain a desired E_b/N_0 value. This approach presents several advantages with respect to the closed-loop equivalent wireless system:

- *The best* channel code profile is selected by simple inspection of the performance results, without implementing any kind of mechanism for the profile adaptation in the testbed code.
- It is possible to evaluate any mechanism of adaptation without measuring again, and it is possible to compare the results with the optimum adaptation.
- Assuming that the whole frame duration – including all profiles measured – is shorter than the channel coherence time, it is possible to transmit every profile through *the same* wireless channel realization, thus guaranteeing a fair comparison between the profiles.
- Assuming that the thermal noise present in the real system is Gaussian, adding the necessary noise artificially enables small E_b/N_0 values (from 1 to 7 dB) to be reached in small steps (0.25 dB) without including practical errors that the testbed would introduce at such E_b/N_0 levels (e.g. time and frequency synchronization degradation). At the same time, the experimental evaluation process is speeded up because the additional artificial noise is added in the digital domain during the evaluation stage instead of requiring the transmission and evaluation of the signals at different TX power values.

In our measurement approach, the data was generated off-line, transmitted in real-time over a wireless channel, and stored at the hard drives at the RX. In a later step, the measurement data obtained is evaluated off-line using a cluster of Personal Computers (PCs).

---

[1]Note that the coherence time of the channel is longer than the frame length.

6.3.2 A Typical Indoor Environment – the Channel

We evaluated experimentally the performance of the SCLDGM codes and the EAC scheme in an office, with direct line of sight between the TX and the RX antennas (see Figure 5.4, page 74). The TX antennas were placed on a table immediately adjacent to a WiFi access point of the public wireless network at the University of A Coruña. The RX antennas were placed on a table used by one of the employees in the office, thus emulating the actual position that a desktop or laptop computer would occupy. The TX and RX antennas were approximately 9 m apart, while the spacing between the four TX and the four RX antennas was equal to 7 cm.

In order to incorporate greater realism into the measurements, we used standard rod antennas with a gain of 3 dB [24]. These antennas are similar to those employed in WiFi access points that operate at 5 GHz.

6.3.3 Measurement Procedure

The transmission of one codeword (Experiment 6.1) or a set of four codewords (Experiment 6.2), each one generated according to a different EXIT function, involves the following operations:

- One or the four off-line generated codewords are assembled in the same physical frame containing a preamble for the synchronization as well as 20 pilot vectors (a vector contains one symbol per TX antenna; thus, 80 pilot symbols are used in total).
- Each TX frame is normalized to ensure that it is transmitted using the same energy.
- The whole frame is upsampled to 20 samples per symbol, pulse-shape filtered using a squared root-raised cosine filter with 20 % roll-off and, finally, I/Q modulated to be sent to the Digital-to-Analog Converters (DACs).
- The frame is transmitted through the $4{\times}4$ MIMO wireless channel.
- At the RX, time and frequency synchronization operations are carried out.
- Next, using the preamble, the noise Power Spectral Density (PSD) N_0 as well as the Signal to Noise Ratio (SNR) are estimated[2]. To ensure that the frames are being acquired at an adequate SNR level, if the estimated SNR is less than a preset threshold value (e.g. 30 dB), the frame is discarded and a new acquisition takes place.
- Once the frame has been correctly acquired, it is matched-filtered, I/Q demodulated, and decimated to obtain the complex-valued observations.
- The observations are then stored in the hard drives of the RX, and subsequently moved to the cluster of PCs for their evaluation.

---

[2]Usually, both N_0 and the SNR are estimated just after the Analog-to-Digital Converters (ADCs) and also after the digital filter (typically a squared root-raised cosine). This task is carried out thanks to the functionalities provided by the signal processing layer introduced in Chapter 3.

In order to obtain different realizations of the wireless channel we make use of the agile feature of the GTEC MIMO testbed Radio Frequency (RF) front-end. After the transmission of a frame is completed (with a single or four codewords), the RF front-end switches to another carrier frequency, and all steps are repeated. In our measurement, we have used 20 different carrier frequencies from 5.2 GHz to 5.745 GHz.

Frame Structure

All transmitted frames have the following structure:

- A Pseudo Noise (PN) sequence made up of 100 symbols plus a small silence (with a duration of 50 symbols) that is used as a preamble for time and frequency synchronization as well as for the estimation of the noise PSD and the SNR.
- 20 pilot vectors for the channel estimation at the RX side. Given that each vector contains four pilot symbols – one for each TX antenna – this results in 80 pilot symbols transmitted in total.
- A single codeword (Experiment 6.1) or four codewords (Experiment 6.2) are added to the frame. Each codeword is built from 8 000 uncoded bits that are coded using a SCLDGM code with rate 1/2 and mapped to a 4 QAM constellation. Thus, 8 000 symbols are transmitted in total, 2 000 symbols per antenna.
- The whole frame is upsampled and filtered with a symbol period of T_s = 20 samples per symbol, with the sampling frequency of all DACs and ADCs fixed to 40 Msample/s. Taking into account the 20 % roll-off, this results in 2.4 MHz of occupied bandwidth. Each codeword takes 8 000 symbols × 20 samples per symbol, resulting in 160 000 samples per codeword, which turns into a frame duration of 160 000 samples/40 Msample/s = 4 ms, and a transfer rate of 2 Mbit/s, without taking into account the overheads introduced by the preamble and the pilot symbols.

6.3.4   Experimental Evaluation

Evaluation Stage

During the evaluation stage, the MIMO detector utilized is a Maximum Likelihood (ML) List Sphere detector [144] with a list of 32 candidates, whereas for the MIMO channel estimation we use two different algorithms:

- The Maximum Likelihood Expectation-Maximization (ML-EM) channel estimation method [81], [287, Chapter 6, pp. 104] employing 20 pilot vectors.
- The Least Squares (LS) channel estimation from 20 pilot vectors (only for Experiment 6.1).

- The LS channel estimation that makes use of all observed vectors. The channel matrix obtained with this method is only utilized to estimate the channel capacity, but not for performance evaluation.

Once the complex-valued observations are ready for evaluation, for each channel realization a different *observed frame* has been obtained as a result of the measurement process. Each observed frame is made up of one (Experiment 6.1) or four (Experiment 6.2) subframes depending on the experiment carried out. For all subframes of a given channel realization, the following steps are performed:

- The variance of the noise N_0, as well as the energy-per-bit E_b of each subframe, are estimated from the values provided by the measurement results. Notice that the amount of energy consumed by the transmission of pilot symbols is also included in the estimated E_b/N_0 value.
- The *instantaneous* capacity of the channel is estimated – in terms of the minimum E_b/N_0 value required for a transmission with an arbitrarily low error probability – assuming no other channel knowledge different from the E_b/N_0 at the TX side.

Next, the mean capacity of the wireless channel is obtained by averaging all instantaneous capacity values.

In order to average the BER for different E_b/N_0 values (the ordinates in Figures 6.2–6.4), a set of 200 different Gaussian noise sequences is generated for each E_b/N_0 (the noise sequences are reused among different channel realizations). Taking into account the estimated value for N_0, the variance of the Gaussian noise sequences is calculated accordingly.

Next, for each triple constituted by a channel realization, a noise sequence and an E_b/N_0 value, a complete evaluation process takes place with the aim of obtaining the mean BER. Therefore, a different pair (E_b/N_0, BER) is obtained for each pair formed by a noise sequence and a channel realization. Consequently, to obtain the pair (E_b/N_0, BER), turbo iterative evaluation is performed from the observations corresponding to a channel realization and the 200 noise sequences for a given E_b/N_0 value. In an iterative way, the detection, the channel estimation and the decoding processes are carried out:

- A single iteration is performed in the channel estimator.
- Another single iteration of the ML List Sphere detector is executed.
- With the obtained result, 10 iterations of the SCLDGM decoder are carried out.
- All the above is repeated 10 times, resulting in 100 iterations in total per pair (E_b/N_0, BER).
- Finally, the mean BER value is obtained (the abscissas in Figures 6.2 and 6.3). Analogously, the mean BLock Error Ratio (BLER) value is calculated (the abscissas in Figure 6.4).
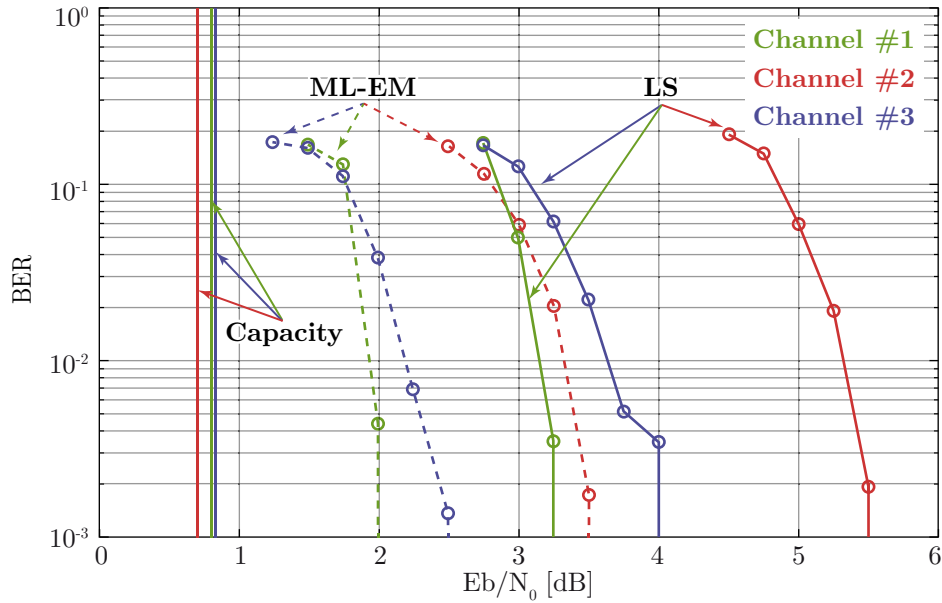
Figure 6.2: Experiment 6.1: BER and capacity over E_b/N_0 for three different channel realizations. For each channel realization, two BER curves are plotted, one when the channel estimator is the LS, and another when it is the ML-EM.

6.4   Results and Discussion

6.4.1   Experiment 6.1

The objective of Experiment 6.1 is to evaluate experimentally the performance of SCLDGM codes that have not been optimized for the 4×4 MIMO wireless channel in which they are measured because at the the time of measurement, the said wireless channel is unknown.

Experiment 6.1 consists of three different measurements carried out on different days. Thus, they experienced a different wireless channel but using exactly the same frames to be transmitted, i.e. the EXIT function of the SCLDGM code is the same. The results are shown in Figure 6.2, in which three different *representative* channel realizations are plotted together with the corresponding channel capacity. The results are presented for the ML-EM channel estimator as well as for the LS channel estimator. Note that the utilization of the ML-EM leads to a gain – in terms of the E_b/N_0 needed to achieve the same BER – ranging from 1 dB to 2 dB. Interestingly, the distance between the ML-EM curve and the channel capacity varies considerably for different channel realizations. Distances of 1.2 dB, 2.8 dB and 1.7 dB are found for channel realizations #1, #2 and #3, respectively. This result motivated us to investigate the impact of the EXIT function adaptation on the performance of the channel code in a specific channel realization, which leads us to Experiment 6.2, presented in the ensuing subsection.
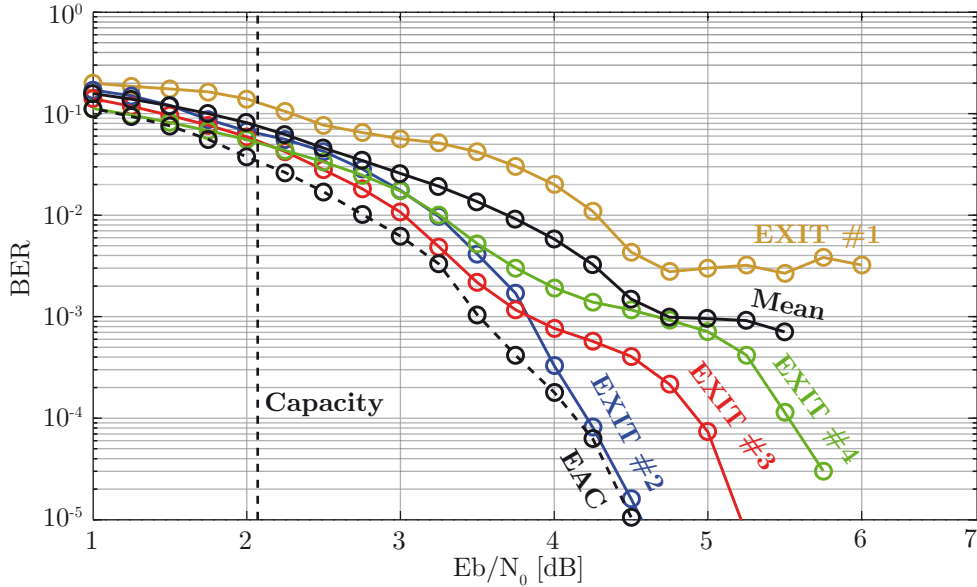
Figure 6.3: Experiment 6.2. BER of the four different code profiles as well as when EAC is applied.
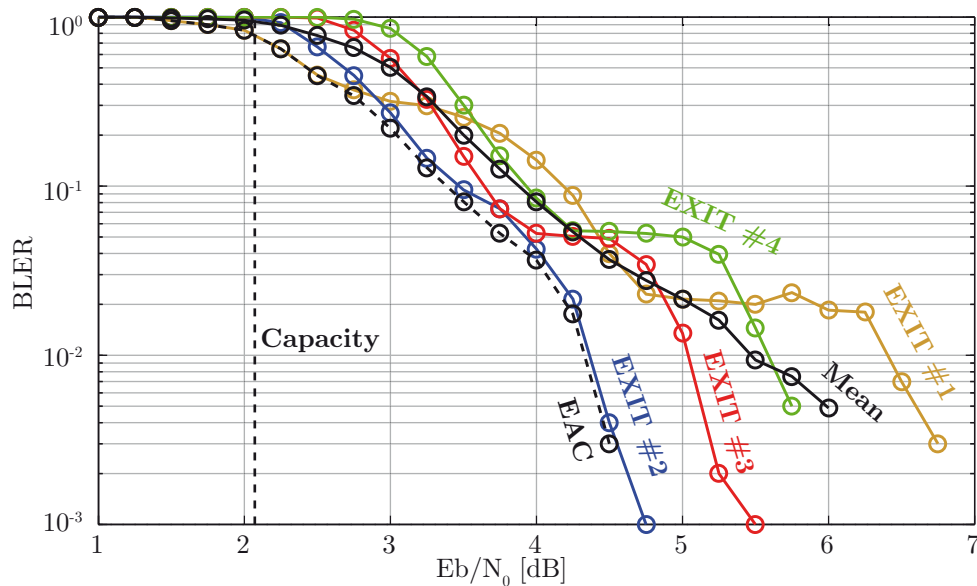
Figure 6.4: Experiment 6.2. BLER of the four different code profiles as well as when EAC is applied.

6.4.2 Experiment 6.2

In this experiment we estimate the mean performance – in terms of the BER and the BLER with respect to the E_b/N_0 – of four different profiles of the SCLDGM channel code (see Table 6.1 for the specification of the four profiles), all of them experiencing *the same* perturbation caused by *the same* wireless channel realization. Additionally, the estimated capacity of the wireless channel – in terms of the minimum E_b/N_0 required for a transmission with arbitrarily low error probability – is provided assuming no channel knowledge at the TX side. The objective of these experimental measurements is to show the feasibility of EAC together with TX power adaptation to approach channel capacity.

Profile name	Total rate	Outer code rate	$d_u^{f_1}$	$d_u^{f_2}$	$d_{p^1}^{f_2}$
EXIT #1	0.5	0.9797	3	6	73
EXIT #2	0.5	0.9863	3	5	34
EXIT #3	0.5	0.9793	4	4	23
EXIT #4	0.5	0.9662	3	3	13

Table 6.1: Specification of the four different code profiles of the SCLDGM code. According to the notation employed in [289], $d_u^{f_1}$, $d_u^{f_2}$, and $d_{p^1}^{f_2}$ correspond to the variable node degrees; the outer code rate is the rate of the outer code (an LDGM) while the total rate of the SCLDGM is 0.5 for all profiles.

Figures 6.3 and 6.4 respectively show the results in terms of the BER and the BLER with respect to the E_b/N_0. In each graph, the following curves are plotted:

- The colored curves labeled as "EXIT #1", "EXIT #2", "EXIT #3" and "EXIT #4", respectively, correspond to the BER (in the case of Figure 6.3) and to the BLER (in the case of Figure 6.4) for the four different channel code profiles and averaged over the different channel realizations and noise sequences. Consequently, these four curves show the mean performance of each code profile for the same channel realizations.

- The black curve labeled as "Mean" shows the mean BER (in the case of Figure 6.3) and the mean BLER (in the case of Figure 6.4) of the four different code profiles. In other words, this curve represents the mean performance of the four code profiles.

- The black dashed curve labeled as "EAC" shows the BER (in the case of Figure 6.3) and the BLER (in the case of Figure 6.4) corresponding to the case in which for every channel realization the code profile exhibiting the minimum BER (BLER) is selected for every E_b/N_0 value. Next, the obtained BER (BLER) values are averaged over all channel realizations.

- Finally, the mean capacity of all channel realizations is obtained in terms of the E_b/N_0 value needed to carry out error-free transmissions given the configuration employed (4 QAM symbols and code rate of 1/2).

In Figure 6.3 the results are shown in terms of the BER. In this case it is clear that code profile #1 works the worst for all E_b/N_0 values. For E_b/N_0 values less than 2.25 dB the best profile is #4, whilst for E_b/N_0 values between 2.25 dB and 3.75 dB the best profile is #3. Finally, for E_b/N_0 values greater than 3.75 dB the best profile is the #2. Note that the performance offered by the EAC system always outperforms – on average – the performance offered by every profile independently. This means that for every E_b/N_0 region, the best code is always chosen, thus maximizing the performance offered by the four profiles. At a BER value of 10^{-5}, the distance between the EAC curve and the capacity is about 2.5 dB. A very similar value is achieved at the same BER value for profile #2. It is straightforward to see that profile #2

achieves the best performance in general because the other three profiles present a considerable error floor (profile #1) or a worse convergence threshold (profiles #3 and #4).

In Figure 6.4 the results are shown in terms of the BLER. Note that the performance of the profiles as well as the EAC is very different from that offered for the BER case. Thus, depending on the metric to be maximized (BER or BLER in this case), the profile offering the best performance is a different one. However, the results in Figure 6.4 show that, similarly to Figure 6.3, profile #2 achieves the best performance in general for E_b/N_0 values greater than 2.8 dB. For a BLER value of 10^{-3}, the distance to the capacity is also about 2.5 dB.

The so-called "Mean" curves for both BER and BLER show the expected performance when the code profile is randomly chosen, i.e. when there is no *a priori* knowledge about the channel. Note that the improvement offered by the EAC is more than 1 dB in both cases. This improvement is measured at 10^{-3} for the BER, and at 10^{-2} for the BLER. For smaller BER and BLER values, the floor effect exhibited by profiles #2, #3, and #4 excessively penalizes the mean performance.

6.5 Conclusion and Criticism

In this chapter we assessed the performance of Serially-Concatenated Low Density Generator Matrix (SCLDGM) channel codes over MIMO channels using the GTEC MIMO testbed in indoor scenarios. The evaluation reported that the EXIT function of the channel code can significantly influence the final performance exhibited by the channel code. This result motivated us to introduce the so-called EXIT-based Adaptive Coding (EAC) as a means of help to approach the channel capacity. The EAC can also be used together with AMC to ease the practical implementation of the resulting communications system. The results obtained showed that the EAC enabled the performance offered by a set of code profiles (four in this case) to be maximized without any *a priori* knowledge of either the channel or the EXIT function. However, the quantitative attainable gain strongly depends on the measured wireless channel, which means that if all code profiles perform close to the optimum, then the mean performance will be the same regardless the code profile selected.

Furthermore, the results obtained assume a *perfect* TX power adaptation, which is still not possible in practical wireless communications systems. Consequently, we would have to subtract the losses of the TX power adaptation from the obtained gain due to the EAC adaptation. Moreover, we have assumed an *ideal* EAC adaptation, which is still an open question to be answered. Therefore, we can assert that EAC is a very promising technique that can help in improving wireless communications systems, but much research is still needed for it to become useful for practical implementations.

Chapter 7

Antenna Spacing in HSDPA Systems

In this chapter we study the influence of transmit antenna spacing and polarization on the throughput of standard-compliant High-Speed Downlink Packet Access (HSDPA) physical layer downlink transmissions. We complement the results with three different bounds. The first two are the water-filling channel capacity and the unconstrained channel capacity (also referred to as mutual information in the literature). Both assume Gaussian input signals and both are bounds intrinsic to the wireless channel that do not depend on the specific signaling scheme employed. Additionally, the so-called functional capacity – consisting in the unconstrained channel capacity constrained by the inherent system losses imposed by the standard – is also provided. The functional capacity is a very important practical bound because it represents the maximum attainable system throughput. This chapter is based on the publications [54, 56, 202, 203].

The remainder of this chapter is structured as follows. In Section 7.1 the investigation hereafter presented is introduced. A general overview of the state of the art of HSDPA and antenna spacing is provided in Section 7.2. In Section 7.3, the theoretical performance bounds estimated directly from the channel coefficients are studied in detail. The measurement set-up is explained in Section 7.4, including a description of the Transmitter (TX) and the Receiver (RX) antennas as well as the measurement scenario. The measurement procedure as well as the way in which the throughput is calculated from the measurement data is described in Section 7.5. A detailed discussion of the obtained results is provided in Section 7.6. Finally, Section 7.7 is devoted to the chapter's conclusions and criticism.

7.1   Motivation

The demand for multimedia wireless communications supporting higher and higher transfer rates is continuously growing today at an explosive pace. A common trend found in many current mobile communications standards (e.g. HSDPA [28], WiMAX [155, 156] or LTE [29])
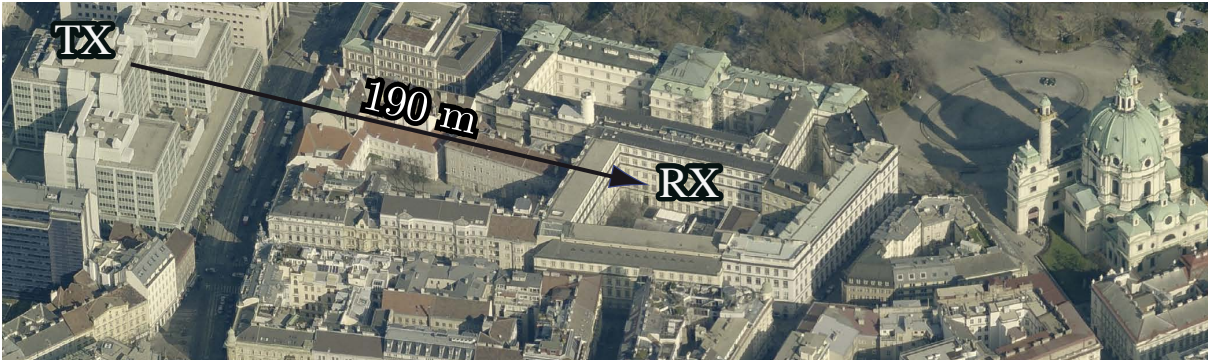
Figure 7.1: Scenario overview, TX antennas mounted on a roof, RX antennas employed inside an office.

to achieve such extensively demanded high-rate transmissions is the adoption of Multiple-Input Multiple-Output (MIMO) technologies. However, the inclusion of multiple antennas at the base station side leads to an increase in its size because multiple elements have to be placed immediately adjacent to each other. For example, when two antennas are used at the base station, cross or equally polarized antennas can be utilized.

When equally polarized antennas are used, the question is to what extent the throughput of a communications system changes as a result of antenna spacing. It is well known that the correlation between different propagation paths reduces the channel capacity. A general statement accepted by the research community affirms that placing the antennas *far* apart from each other results in an increase of the maximum available diversity. Moreover, it is often conjectured that the greater the TX antenna spacing, the better the radio link performance. Although this phenomenon is well understood in terms of quality, the question remains open for exact quantitative behavior.

In this chapter we answer this question using the Vienna MIMO Testbed [49] to directly measure the mean closed-loop physical layer downlink throughput of 2×2 HSDPA [28] at 2.5 GHz (including the HSDPA pilot structure [200, Chapter 3]) in a realistic, urban, outdoor scenario (see Figure 7.1) for equally polarized TX antennas at variable antenna spacings as well as for cross polarized TX antennas. In the measurements we employ realistic TX and RX antennas (see Figures 7.2 and 7.3) and cross polarized antennas at the RX. Notice that in the experimental evaluation we only measure a single, isolated HSDPA downlink. Additionally, we estimate the water-filling channel capacity and the unconstrained channel capacity. Finally, we also calculate the functional capacity based on the capacity constrained to the requirements imposed by the standard (pilot and synchronization channels, precoding vectors, etc.).

7.2 State of the Art

High-Speed Downlink Packet Access (HSDPA)

The HSDPA transmission mode [28] was introduced in Release 5 of the Universal Mobile Telecommunications System (UMTS) to provide high data rates to mobile users. This is achieved by employing techniques such as fast link adaptation, fast Hybrid Automatic Repeat reQuest (HARQ), and fast scheduling. MIMO HSDPA was standardized in Release 7 of UMTS and is capable of increasing the maximum downlink data rate by spatially multiplexing two independently coded and modulated data streams. Additionally, channel-adaptive spatial precoding is implemented at the base station. The standard defines a set of precoding vectors of which one is chosen on the basis of a precoding control indicator feedback obtained from the user equipment. Two different MIMO HSDPA modes are defined: the Transmit Antenna Array (TxAA), which utilizes two antennas to transmit a single stream, and the Double Transmit Antenna Array (D-TxAA), in which one or two streams (whichever leads to a higher throughput) are transmitted using two antennas.

In the literature, there are theoretical publications that study specific details of the HSDPA physical layer [28], as for example HARQ [79], receive antenna diversity [176], equalizer architectures [137, 186], Radio Frequency (RF) hardware impairments [269], or link adaptation [222]. Remarkably, only [194] presents results in terms of physical layer throughput including link adaptation, but restricted to Single-Input Single-Output (SISO) transmissions.

Apart from simulations, HSDPA was also evaluated experimentally. In [177], the throughput performance of a SISO HSDPA system is simulated on the basis of so-called drive test measurements. An experimental evaluation of a MIMO HSDPA multiuser detector is provided in [256]. The impact of distributed antenna systems on HSDPA performance in indoor environments is studied in [158]. Additionally, throughput measurement results of a SISO HSDPA system are presented in [145]. Also, a non standard-compliant MIMO HSDPA system was measured in [245]. Finally, MIMO HSDPA closed-loop throughput measurements are presented in [54, 56, 109, 203]).

Antenna Spacing

The effects of antenna spacing, both at the TX and at the RX sites, have been studied for a long time. The earliest measurement campaigns carried out in outdoor scenarios date from the seventies [183, 244]. In these measurements, the correlation coefficient of the incoming signals with respect to antenna spacing was investigated. More recent measurements examined this effect in indoor-only scenarios [88, 157, 173], in outdoor-to-indoor scenarios [196], and in outdoor-only scenarios [233, 309].

The impact of antenna spacing on channel capacity has been measured in a variety of

scenarios and conditions, including indoor scenarios [157, 164], outdoor scenarios [71, 164, 265], reverberation chambers [170], and using virtual antenna arrays [197]. These measurement results were complemented with theoretical analyses in [70, 264, 283, 294] and the references therein.

The influence of antenna spacing on the Bit Error Ratio (BER) was also theoretically investigated [87, 190], measured indoors [48, 50], and measured outdoors [154, 285].

Recently, the influence of antenna spacing on the throughput of an Orthogonal Frequency-Division Multiplexing (OFDM) transmission was studied in [282] by using sounded channel coefficients in a simulation. Similarly, [165] investigates the throughput difference between equally and cross polarized TX antennas. Notably, except for [154, 282], all the references cited above do not employ base station antennas similar to those currently in use in mobile cellular networks. Furthermore, except for [282], none of the references found relates TX antenna spacing to the closed-loop physical layer throughput of a standard-compliant, multiple antenna mobile communications system such as 2×2 MIMO HSDPA.

7.3 Theoretical Performance Bounds

In this section, we define the theoretical performance bounds for the throughput results presented further on. These bounds are obtained from the channel coefficients estimated from the data collected during the measurements [200, Chapter 3]).

Given an $n_R \times n_T$ MIMO channel, the time-dispersive channel of length L_g taps between the n_T-th TX and the n_R-th RX antenna can be defined as:

$$\mathbf{g}(n_R, n_T) = \begin{bmatrix} g_0(n_R, n_T) & \ldots & g_{L_\mathbf{g}-1}(n_R, n_T) \end{bmatrix}^T.$$

Utilizing the N_DFT point Fourier transform $\mathbf{DFT}\{.\}$, the channel can be translated into the frequency domain as $\mathbf{h}(n_R, n_T) = \mathbf{DFT}\{\mathbf{g}(n_R, n_T)\}$, resulting in N_DFT frequency flat channels. The MIMO channel matrix of the k-th frequency bin can then be written as

$$\mathbf{H}_k = \begin{bmatrix} \mathbf{h}_k(1,1) & \ldots & \mathbf{h}_k(1, n_T) \\ \vdots & \ddots & \vdots \\ \mathbf{h}_k(n_R, 1) & \ldots & \mathbf{h}_k(n_R, n_T) \end{bmatrix}, \ k = 1, \ldots, N_\mathrm{DFT}. \tag{7.1}$$

7.3.1 Unconstrained Channel Capacity

The unconstrained channel capacity calculation of a frequency selective MIMO channel [59, 232, 239] depends on whether the TX is considered informed or not. When the TX is not informed, i.e. no channel knowledge except the receive Signal to Noise Ratio (SNR) is available at the TX side, we compute the so-called unconstrained channel capacity (also referred to as

mutual information in the literature) [98, 140, 280, 299]. This capacity, averaged over all N_{DFT} frequency bins, is given by:

$$I = \frac{B}{N_{\text{DFT}}} \sum_{k=1}^{N_{\text{DFT}}} \log_2 \left\{ \det \left(\mathbf{I}_{n_R} + \frac{p_{\text{TX}}}{\sigma_n^2} \mathbf{H}_k \mathbf{H}_k^H \right) \right\}, \tag{7.2}$$

where B is the total occupied bandwidth (4.68 MHz for HSDPA[1]); $\mathbf{H}_k$ represents the MIMO channel matrix defined in Equation (7.1); $\mathbf{I}_{n_R}$ is the identity matrix with the same dimension as the number of RX antennas, n_R; p_{TX} is the TX power value at the base station; and σ_n^2 is the noise variance.

Next, let us consider the Singular Value Decomposition (SVD) [214] of the MIMO channel at frequency bin k [200, Chapter 3]:

$$\frac{1}{\sigma_n} \mathbf{H}_k = \mathbf{U}_k \mathbf{\Sigma}_k \mathbf{V}_k^H,$$

$$\mathbf{\Sigma}_k = \operatorname{diag} \left\{ \sqrt{\lambda(1,k)}, \sqrt{\lambda(2,k)}, \dots \sqrt{\lambda(M,k)} \right\},$$

where $\lambda(m,k)$, $m = 1, \dots, M$, with $M = \min(n_R, n_T)$, are the singular values of $\mathbf{H}_k/\sigma_n$. The optimum capacity-achieving, frequency-dependent precoder at the TX is given by the unitary matrix $\mathbf{V}_k$, whereas the optimum RX filter is given by $\mathbf{U}_k^H$. When both are employed, the MIMO channel is separated into $M = \operatorname{rank}(\mathbf{H}_k)$ independent SISO channels, each with a gain of $\sqrt{\lambda(m,k)}$. The resulting unconstrained channel capacity is obtained by optimally distributing the available TX power over all $M = \min(\mathbf{H}_k)$ sub-channels and frequency bins. The optimum power distribution $p(m,k)$ is the solution to the following optimization problem:

$$C = \max_{p(m,k)} \frac{B}{N_{\text{DFT}}} \sum_{m=1}^{\min(n_R,n_T)} \sum_{k=1}^{N_{\text{DFT}}} \log_2 \left(1 + p(m,k)\lambda(m,k) \right)$$

$$\text{subject to} \sum_{m=1}^{\min(n_R,n_T)} \sum_{k=1}^{N_{\text{DFT}}} p(m,k) = N_{\text{DFT}}, \tag{7.3}$$

where the second part in Equation (7.3) is a TX power constraint that ensures an average TX power equal to the number of frequency bins. The power distribution $p(m,k)$ maximizing Equation (7.3) can be calculated by using the water-filling algorithm described in [232, 239]. Consequently, the capacity obtained in Equation (7.3) is termed as water-filling channel capacity, or simply, water-filling capacity.

---

[1]In HSDPA, the channel bandwidth is 5 MHz, whereas the transmit chip stream is transmitted at a rate of 3.84 MChip/s and filtered with a root-raised cosine filter with 22 % roll-off factor. This leads to a total occupied bandwidth of 4.68 MHz.

7.3.2 Functional Capacity

The so-called *functional capacity* or *achievable throughput* is a function of the MIMO channel and the precoding matrix defined by the HSDPA standard[2]. Therefore, the functional capacity can be viewed as the capacity of the channel as it is defined by the standard. When multiple antennas are used at the TX side, HSDPA defines a precoding matrix $\mathbf{W}$ made up of the scalars $w_0 = 1/\sqrt{2}$ and $w_1 \in \{(1+j)/2, (1-j)/2, (-1+j)/2, (-1-j)/2\}$. From now on, we consider two standard-compliant HSDPA transmit modes:

- Transmit Antenna Array (TxAA). This transmission mode uses two TX antennas to transmit a single stream of data. The precoding matrix is defined as: $\mathbf{W}_{\mathrm{TxAA}} = [w_0 \; w_1]^T$, where the signal at the first TX antenna is always weighted by the same scalar constant w_0, whereas the signal at the second TX antenna is weighted by w_1, which is selected with the purpose of maximizing the Signal to Interference and Noise Ratio (SINR) [199]. Therefore, there are four possible precoding matrices in the TxAA mode.

- Double Transmit Antenna Array (D-TxAA). In this mode, either one stream or double-stream – whichever leads to a higher physical layer throughput – is transmitted by the two TX antennas. The corresponding precoder is a unitary matrix such that the precoding vectors corresponding to the two TX antennas are orthogonal:

$$\mathbf{W}_{\mathrm{DTxAA}} = \begin{bmatrix} w_0 & w_0 \\ w_1 & -w_1 \end{bmatrix}.$$

In the D-TxAA mode there are four possible precoding matrices when double-stream is employed. When single-stream is transmitted, then the precoding matrices are the same as in the TxAA mode.

From the expressions for the unconstrained MIMO mutual information defined in Equation (7.2) and taking into account the precoding matrices defined for the two HSDPA transmission modes, the functional capacity is obtained as [200, Chapter 3, pp. 58]:

$$C_{\mathrm{f}} = \max_{\mathbf{W} \in \mathcal{W}} \frac{B_{\mathrm{s}}}{N_{\mathrm{DFT}}} \sum_{k=1}^{N_{\mathrm{DFT}}} \log_2 \det \left(\mathbf{I}_{n_R} + \frac{p_{\mathrm{data}}}{\sigma_n^2} \mathbf{H}_k \mathbf{W} \mathbf{W}^H \mathbf{H}_k^H \right), \qquad (7.4)$$

were $\mathcal{W}$ is the set of all possible precoding matrices; B_{s} corresponds to the HSDPA chip rate of 3.84 MHz[3]; p_{data} is the TX power at the base station, including the losses imposed by the HSDPA system; $\mathbf{W}$ is the precoding matrix; and σ_n^2 is the noise variance.

It is important to emphasize that when HSDPA operates in the D-TxAA mode and two data streams are transmitted, the precoding matrix $\mathbf{W}$ is unitary ($\mathbf{W}\mathbf{W}^H = \mathbf{I}_2$) and the functional

---

[2]The concept of functional capacity is presented in [33].

[3]In HSDPA the chip rate is equal to 3.84 MChip/s. Next, the data stream is filtered with a root-raised cosine filter with 22 % roll-off, resulting in an occupied bandwidth $B = 4.68$ MHz.

capacity defined in Equation (7.4) is now equal to the capacity defined in Equation (7.2) with $B = B_s$ and $p_{\mathrm{TX}} = p_{\mathrm{data}}$.

Estimated water-filling capacity, unconstrained capacity and functional capacity can be found in [254] for urban as well as for alpine scenarios.

7.4 Measurement Set-up

The goal of the experimental set-up described below is to examine the impact of base station TX antenna spacing and polarization on the mean closed-loop physical layer downlink throughput of a 2×2 HSDPA standard-compliant transmission in the specific small-scale fading scenario shown in Figure 7.1.

7.4.1 Closed-Loop Set-up

We employ closed-loop quasi-realtime testbed measurements as the hardware is readily available and we have past experience with similar experiments and set-ups [49, 50, 56, 200]. In this measurement approach, all possible transmit data blocks are generated off-line in MATLAB, but only the required data is then transmitted over the wireless channel, which is altered by moving the RX antennas. The feedback calculation – mandatory for closed-loop HSDPA – is performed instantly in MATLAB in approximately 40 ms (less than the channel coherence time). The received data itself is not evaluated in real-time but off-line using a cluster of Personal Computers (PCs). Results for the scenario measured are automatically obtained using the same program that has already controlled the complete measurement procedure and documentation. More details about the measurement procedure can be found in [56].

7.4.2 An Urban Outdoor Environment – the Channel

We consider a realistic, non line of sight scenario in downtown Vienna, Austria (see Figure 7.1). The TX antennas are placed on the roof of a tall building immediately adjacent to existing base station antennas of other mobile phone operators (see Figure 7.2), making the measurement results obtained very realistic and representative for a mobile communications system. The RX antennas are placed in a small office at a distance of approximately 190 m (see Figure 7.3). The estimated root mean square delay spread for this rich scattering scenario is $0.5\,\mu$s.
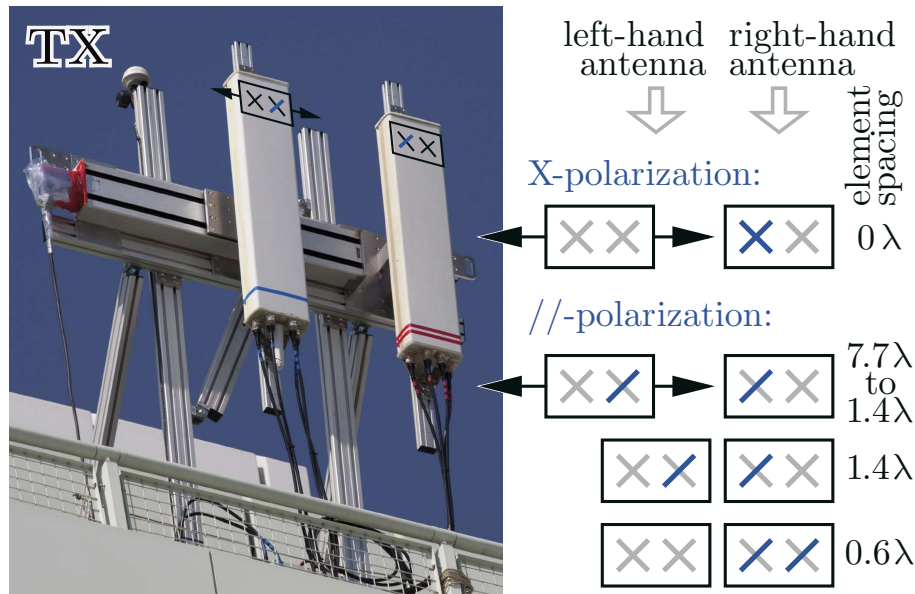
Figure 7.2: A two-element base-station antenna consisting of a moveable 2X-pol antenna (left-hand) and a fixed 2X-pol antenna (right-hand). Only two antenna elements are simultaneously excited from all eight available elements.

7.4.3 Realistic Antennas

A Two-Element Flat Panel Antenna at the Base Station

At the base station (see Figure 7.2), we employ two KATHREIN 800 10629 [13] 2X-pol panel antennas with a half-power beam width of 80°/7.5° and a total down tilt of 16° (10° mechanical + 6° electrical). Each 2X-pol antenna consists of two cross polarized antennas spaced by $0.6\,\lambda$ (λ=12 cm, the wavelength at our carrier frequency of 2.5 GHz). Only two of the eight possible elements are excited at the same time to obtain a two-element base station antenna with a variable element spacing from $0.6\,\lambda$ to $7.7\,\lambda$, for equal polarization, and $0\,\lambda$ for cross polarization. Using two ordinary X-pol antennas instead of two 2X-pol antennas would have only allowed us to measure down to an element spacing of $1.4\,\lambda$ rather than $0.6\,\lambda$ because at that point the two antennas touch each other.

Two Printed Monopole Antennas at the RX

At the receiver site, we utilize two printed monopole antennas [168] that can be integrated into a mobile handset or a laptop computer. We employ differently polarized antennas to obtain robust measurement results that approximate to reality. As shown in Figure 7.3, we measure different RX antenna positions (x,y) in an area of $3\,\lambda\times3\,\lambda$ to average over small scale fading and to avoid large scale fading effects. Because the antennas point in different directions, they experience a different average path loss. This effect is averaged out by rotating the antennas (Φ) during the measurement.
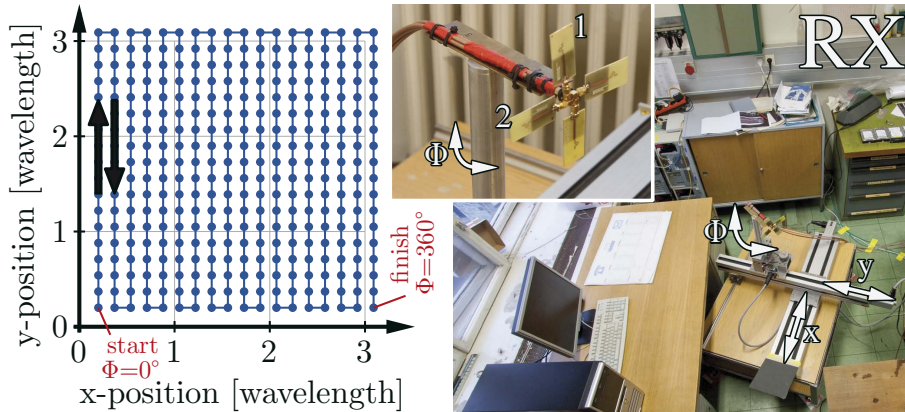
Figure 7.3: The RX employing two (1,2) moveable (x,y) and rotatable (Φ) printed monopole antennas. The other two printed monopole antennas shown are not used.

7.4.4 Standard-Compliant MIMO HSDPA transmissions

We transmit standard-compliant HSDPA data frames (including the standard-compliant pilot structure [200, Chapter 3]) encoded for a Category 16 user equipment [28]. Three different 2×2 MIMO HSDPA modes plus a 1×2 Single-Input Multiple-Output (SIMO) transmission mode are measured:

- **One stream mode (TxAA)**. As commented in Section 7.3.2, the Transmit Antenna Array (TxAA) mode with transmit diversity uses strongly quantized precoding to increase the SINR at the user equipment. In this transmission mode, the data rate of a Category 16 user equipment can be adjusted between 68.5 kbit/s and 12.779 Mbit/s [28].

- **One-or-two stream mode (D-TxAA)**. The so-called Double Transmit Antenna Array (D-TxAA) is downwardly compatible with TxAA and equals TxAA when the SINR at the user equipment is low. At larger SINR values, D-TxAA switches to dual stream mode and transmits two independently coded HSDPA data streams. Thus, in TxAA, a single stream is always transmitted and in D-TxAA, either single stream or double stream transmission – whichever leads to a higher physical layer throughput [199] – is performed. In this transmission mode, the data rate of a Category 16 user equipment can be adjusted between 68.5 kbit/s (lowest rate of single stream transmission) and 27.952 Mbit/s (highest rate of double stream transmission) [28].

- **Dual stream mode**. In addition to the standard compliant modes defined above, we also implemented a mode – non existent in the standard – that behaves like D-TxAA, but consistently forces the TX to use two streams, regardless of the SINR estimated at the RX. This mode has been devised to improve understanding of the findings reported in Section 7.6. In this mode, the data rate of a Category 16 user equipment can be adjusted between 4.581 Mbit/s and 27.952 Mbit/s.

- **SIMO HSPDA**. We measure 1×2 SIMO HSDPA as a reference in order to obtain concomitant observations that can be utilized to enhance the precision of the 2×2 results
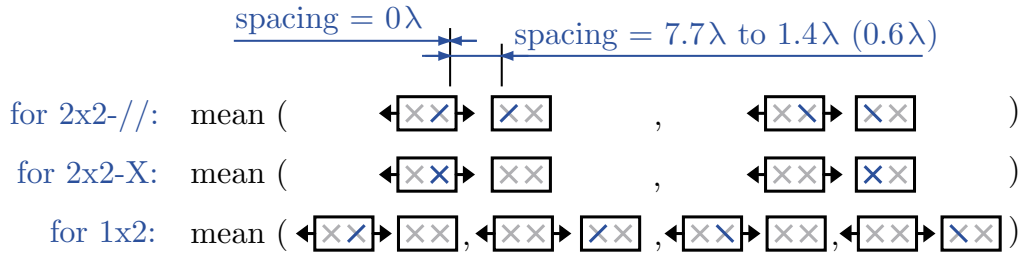
Figure 7.4: Ensuring a fair comparison between $2{\times}2$ HSDPA with cross polarized and equally polarized TX antennas as well as with the $1{\times}2$ HSDPA.

measured over antenna spacing.

7.5 Inferring the Mean Scenario Throughput

When comparing the throughput obtained with the set-ups that use equally polarized TX antennas spaced from $1.4\,\lambda$ to $7.7\,\lambda$ with that obtained when cross polarized TX antennas are employed, the main problem is that these transmissions use different antenna elements and, thus, exhibit greatly different (up to $4\,\text{dB}$) average path loss. This problem can be overcome by averaging the throughput measured at different antenna elements, as shown in Figure 7.4. In other words, to measure, for example, the throughput of the TxAA mode with equally polarized TX antennas, we average two measurements, one exciting two of the equally polarized elements, and the other exciting the remaining two equally polarized elements. We use well known statistical techniques explained, for example, in [77, 84, 94] to infer the mean throughput performance of the urban scenario as described below (*the technical terms are given in italics in brackets*):

1. We measure the HSDPA modes to be compared (*grouping, comparison*) in random order (*randomization*) immediately after each other over the same channels (*blocking*) equally often (*balancing*).

2. We measure all the above at 12 different TX antenna spacings (see Figure 7.2) when equally polarized TX antennas are used (*one-factor-at-a-time experiment*). When cross polarized TX antennas are employed, TX antenna spacing is $0\,\lambda$.

3. We measure all the above at 11 different transmit power levels (*12×11 full factorial design*).

4. We measure all the above at 324 different RX antenna positions, as shown in Figure 7.3 (*systematic sampling*).

5. We evaluate all measured throughput values off-line and average them (best estimator for the mean having no other knowledge, *plug-in principle*) over the RX antenna positions to obtain the mean scenario throughput.

6. We use the correlation between the 2×2 and the 1×2 throughput values (*concomitant observations* that we define to be constant over the TX antenna spacing) to enhance the precision of the 2×2 results measured over TX antenna spacing. This step is necessary because when we compared the 1×2 with the 2×2 throughput curves with respect to antenna spacing, we discovered that they were highly correlated, thus the fluctuations of the curves were caused by the different antenna positions and not only by the antenna spacing.

7. We extract the channel coefficients from the measurements to calculate the water-filling capacity, the unconstrained capacity and the functional capacity (see Section 7.3).

8. Finally, we calculate the 99% confidence intervals for the mean (BC_a *bootstrap algorithm* [84]) to gauge the precision of the results shown in Figure 7.5.
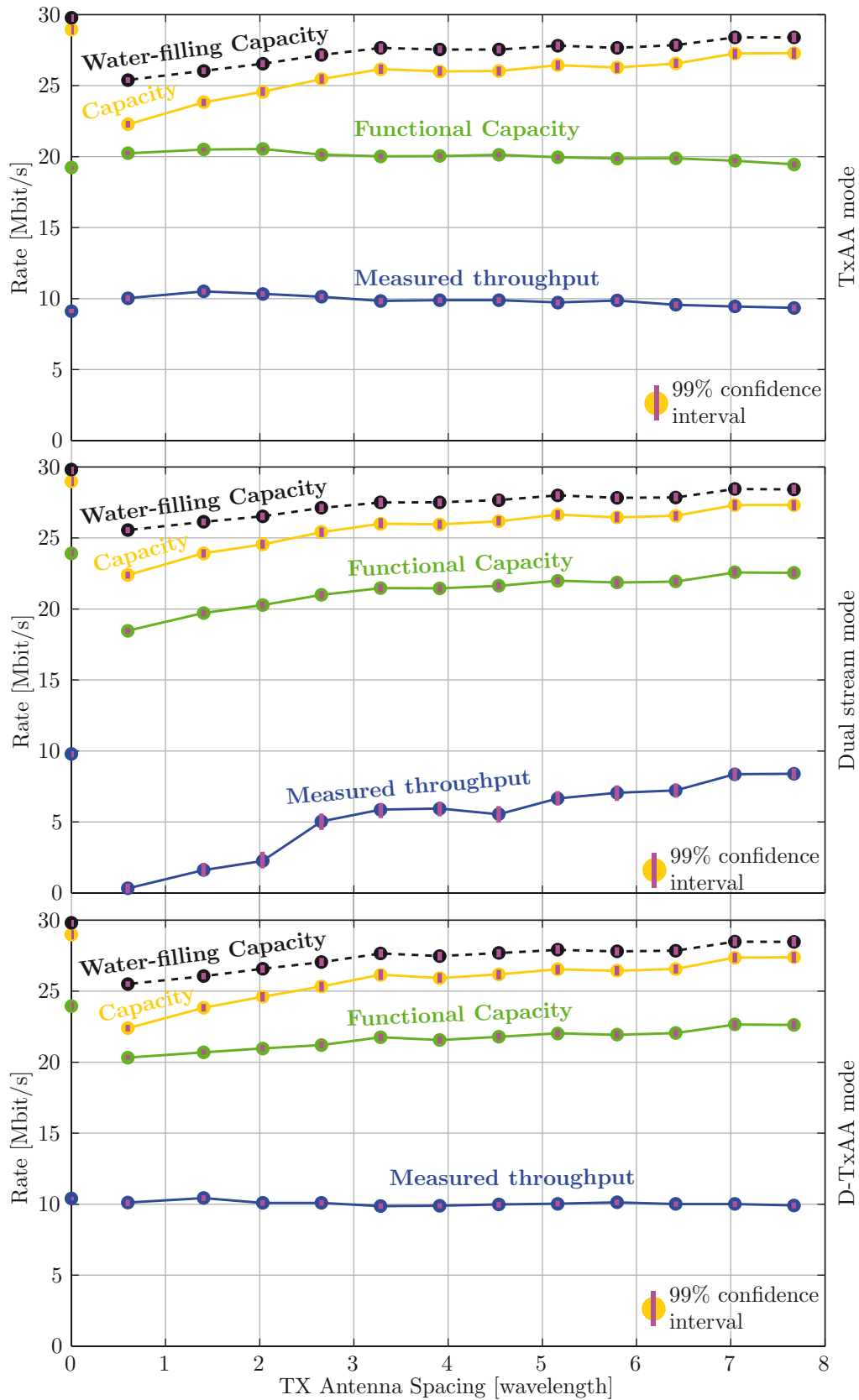
Figure 7.5: Water-filling capacity, capacity, functional capacity, and measured throughput of the closed-loop 2×2 MIMO HSDPA physical layer over TX antenna spacing at a TX power value of 24.6 dBm for the TxAA, the dual stream, and the D-TxAA modes.

7.6   Measurement Results

In the experiment carried out we conclude that for a constant TX power, the 2×2 MIMO and the 1×2 SIMO throughput values are correlated (correlation coefficient 99 %-confidence-interval=[0.87, 0.98], linear regression coefficient 99 %-confidence-interval=[0.79, 1.24]). However, the 1×2 throughput should not change over antenna *spacing* (as there is only one TX antenna) but does change over antenna *position* because the antenna positions are different. The basic idea is to define the SIMO throughput to be constant over TX antenna spacing (the *concomitant observations*) and use the correlation between the SIMO and the MIMO throughput to enhance the precision of the measured MIMO throughput over TX antenna spacing. The resulting curves are shown in Figure 7.5

   Figure 7.5 show the results for the three HSDPA modes measured: TxAA, D-TxAA, and the non-standard dual stream mode. In each graph, the dots at $0\,\lambda$ correspond to the results measured with cross polarized TX antennas, whereas the curves ranging from $0.6\,\lambda$ to $7.7\,\lambda$ correspond to the results measured with equally polarized TX antennas. Each of the three graphs in Figure 7.5 show, from bottom up, the measured throughput, the functional capacity, the capacity and, finally, the water-filling capacity. All curves also show the 99 % confidence intervals for the mean.

   Note that the water-filling capacity and the capacity are (apart from the measurement uncertainty expressed via the confidence intervals) equal for all three HSDPA transmission modes because they only depend on the channel. The functional capacity differs among the three modes because its computation is different depending on the precoding vectors (see Equation (7.4)). Note that in the non-standard mode in which two streams are consistently transmitted, the precoding matrix $\mathbf{W}$ in Equation (7.4) is unitary and, thus, the functional capacity is just a scaled version of the capacity.

7.6.1   Discussion of the Results

From now on, we discuss the main results that can be deduced from Figure 7.5.

Equally vs. Cross Polarized TX Antennas

We observe that the curves corresponding to the equally polarized TX antennas converge towards the cross polarized ones for large values of the TX antenna spacing. This is an expected result because as the TX antenna spacing increases, the transmission paths become more and more uncorrelated. Obviously, cross polarized antennas lead to uncorrelated transmission paths. Given that we are using cross polarized RX antennas, greatly spacing or cross polarizing the TX antennas leads to nearly uncorrelated transmissions. This is especially noticeable in the

throughput of the non-standard dual stream mode, which offers the best performance when cross polarized antennas are used.

Unconstrained Capacity

Looking at the water-filling capacity curves as well as the capacity curves, both increase with TX antenna separation, as expected. The maximum values of both bounds are achieved when cross polarized TX antennas are employed.

Functional Capacity

Only in the non-standard dual stream mode is the functional capacity a scaled version of the capacity, as explained above. Moreover, the capacity of the TxAA mode decreases slightly with TX antenna separation. This is because the TxAA mode restricts the channel to a set of four possible precoding vectors. Thus, the beamforming is reduced to only four possible weights, which explains the loss in performance when the TX antenna spacing increases. When cross polarized TX antennas are used, these effect is even more noticeable. In the D-TxAA mode, the functional capacity curve is obtained by the maximization of the corresponding functional capacity curves for the TxAA and the non-standard dual stream modes. Consequently, for short TX antenna spacings, the dominant functional capacity is that of the TxAA mode, whereas as the TX antenna spacing increases, the D-TxAA mode offers a better potential performance, thus becoming the dominant factor in the functional capacity curve.

Throughput

Because of the above-mentioned reasons, the throughput curves of the TxAA mode and the non-standard dual stream mode are approximately scaled versions of the functional capacity curve. On the contrary, in the D-TxAA mode, the throughput stays more or less constant over the TX antenna spacing. This is because, at short TX antenna spacings, the TxAA performs better while at larger spacings the TxAA mode is compensated by the dual stream mode. However, it is very remarkable that the non-standard dual stream mode performs so poorly for most of the TX antenna spacing values. The reason is that the lowest possible rate defined for the dual stream case leads to a throughput of 4.581 Mbit/s. Therefore, in order to use the non-standard dual stream mode, we would need better channel conditions.

It is important to stress the enormous gap that exists between the functional capacity and the actual observed throughput. Moreover, such throughput curves are obtained when using expensive, state of the art RF hardware, and represent an upper bound for the throughput typically attainable when low-cost receivers are employed. Also notice that the gap between the capacity and the functional capacity curves in the D-TxAA mode increases with the TX

antenna spacing.

Finally, it is clear that the throughput of both TxAA and D-TxAA standard modes remains approximately constant with respect to the TX antenna spacing. Consequently, this makes it possible to build smaller base stations because the TX antennas can be placed very close together when they are equally polarized. Additionally, we must emphasize that future improvements of HSDPA should focus on reducing the gap between the functional capacity and the throughput, which is by far more relevant than the impact of TX antenna spacing.

7.7 Conclusion and Criticism

In this chapter, the influence of TX antenna spacing and polarization on the closed-loop throughput of 2×2 Multiple-Input Multiple-Output (MIMO) High-Speed Downlink Packet Access (HSDPA) was investigated by means of testbed measurements. The measurement campaign was carried out in a realistic, urban, outdoor scenario in downtown Vienna employing cross polarized antennas at the receiver. Using the channel coefficients extracted from the measurement data, we were able to estimate the water-filling channel capacity, the unconstrained channel capacity and the functional capacity.

In general, the results showed the existence of a large gap between the actual throughput and the functional capacity, which means that the wireless communications system is far from taking advantage of all the potential throughput provided by the wireless channel. This difference is also more significant than that from the TX antenna spacing. In the two standard HSDPA modes analyzed, the resulting throughput remains approximately constant over TX antenna spacing, thus opening the door for small base station construction.

The gap mentioned above between the measured throughput and the functional capacity is explained in [203], and in [200, Chapter 3]. Basically, there are three main causes of throughput losses. First, the rate-matched turbo code specified by HSDPA is not optimal, particularly at high code rates when a Maximum A-Posteriori (MAP) decoder is utilized. Second, the Linear Minimum Mean Square Error (LMMSE) equalizer employed in the HSDPA RX represents a low-complexity and cost-effective solution, but it is also not optimal. In the literature there are potentially better solutions, for example the LMMSE-MAP [303]. Finally, the third cause of throughput loss is due to the large delay spread present in the urban scenario, leading to a large inter-code interference.

Chapter 8

Antenna Selection in HSDPA Systems

When measuring the High-Speed Downlink Packet Access (HSDPA) physical layer throughput at the same Transmitter (TX) power value but at different Receiver (RX) antenna positions, it was found that the throughput varies greatly depending on antenna position and polarization. Therefore, we decided to carry out measurements with the aim of evaluating the impact of antenna subset selection techniques on the system throughput. This chapter is partly based on publications [52, 109, 199].

The remainder of the chapter is structured as follows. First, in Section 8.1, the antenna selection concept is introduced in general. An overview of the state of the art is also provided together with the motivation of the work included in this chapter as well as our contribution to the antenna selection topic. In Section 8.2, a receive antenna selection overview is provided and our throughput-based antenna selection criterion is introduced. Next, important and frequently ignored hardware implementation aspects are dealt with in Section 8.3. We also explain how the considered criterion overcomes the limitations imposed by antenna selection. Next, in Section 8.4 the measurement results are presented and discussed. Finally, Section 8.5 is devoted to our conclusions and criticism.

8.1   Introduction

The utilization of Multiple-Input Multiple-Output (MIMO) technologies is continuously growing due to the drastic increase in the channel capacity and the enormous improvement in the communications link reliability [280]. Despite these advantages, MIMO has been slow to be adopted in practical wireless systems. Currently, MIMO technologies are available in HSDPA [28], WiMAX [155, 156], and LTE [29].

One of the main reasons for the slow introduction of MIMO technologies in commercial wireless systems is the necessary increment in complexity and hardware costs. While antenna elements are cheap and usually small, each one requires a complete Radio Frequency (RF)

chain including low-noise amplifiers, frequency down-converters, Analog-to-Digital Converters (ADCs), filters, and so on. Unfortunately, RF hardware is expensive compared to digital hardware and does not follow Moore's law [215]. Furthermore, introducing new hardware consumes more energy, which is very inconvenient for today's hand-held mobile devices. Nevertheless, these limitations can be overcome to a large extent by using Antenna Subset Selection (ASS).

The basic idea of ASS consists in capturing all the potential diversity offered by a full $n_\mathrm{T} \times n_\mathrm{R}$ MIMO system simultaneously employing only $l_\mathrm{T} \times l_\mathrm{R}$ complete RF chains ($l_\mathrm{T} < n_\mathrm{T}$ and $l_\mathrm{R} < n_\mathrm{R}$). ASS adaptively chooses a specific subset from all available antennas based on the so-called *selection criterion*. Therefore, the performance of the resulting wireless communications system will mostly depend on such ASS criterion.

Interestingly, in a great variety of scenarios, ASS systems can achieve the same diversity gains as full-complexity systems while considerably reducing system complexity. On the downside, ASS suffers from a loss in array gain (mean RX Signal to Noise Ratio (SNR) gain) but this loss can be mitigated by adequate preprocessing in the RF domain [210, 213, 273, 274, 308].

8.1.1 State of the Art

In addition to the first publications on ASS [181, 182], a considerable amount of research has been reported in the literature with ASS as the main topic (see [68, 76, 114, 118, 128–130, 136, 208, 209, 226, 228, 257, 268, 286, 305, 307, 314] and references therein). Most of the published work usually assumes perfect knowledge of the channel at the TX and at the RX sides under the assumption of a flat fading channel model with independent and identically-distributed (iid) fading at each antenna. In [209], the problem of channel frequency selectivity is jointly addressed with some practical issues such as channel estimation errors and hardware non-idealities. The ASS at the RX side is extensively studied in [117, 119, 133, 135, 191]. Besides the general ASS overview, [132, 298] deal with the ASS problem at both the TX and the RX sides. As mentioned before, most of the available literature addresses the problem from a theoretical point of view and rarely focuses on common practical issues such as antenna coupling effects, noisy estimates of the channel, or hardware non idealities. However, some studies focus on more realistic channel models and consider the ASS problem for frequency-selective channels when frequency-domain equalizers are used (see [298], and references therein), or when only noisy channel estimates are available [37, 38]. Another interesting advantage of ASS is given by its potential to reduce the complexity of MIMO-OFDM precoded systems [227], including the case with limited-feedback [226, 228], as well as when it is combined with spatial multiplexing [136].

In order to take advantage of the diversity available in the MIMO link, there is also a certain

amount of previous work on ASS based on the maximization of channel capacity [211, 212]. In recent years, MIMO-OFDM systems have become very popular due to their ability to exploit the benefits from both MIMO and Orthogonal Frequency-Division Multiplexing (OFDM) systems. For this reason, ASS has also been studied in such systems. More specifically, research work has been reported on indoor environments and based on existing wireless communication standards [74, 75, 277, 284].

Despite all the previous work, very little attention has been paid to real scenario measurements and/or selection criteria taking into account the effects of practical implementations. In [147], an ASS implementation applied to IEEE 802.11a is presented, in which indoor measurements and polarization antenna experiments were carried out. In [277], the performance of TX and RX ASS for MIMO-OFDM based on measured, correlated, indoor and frequency selective channels is studied in depth. The results obtained are compared with those computed using the TGn [85] channel model. The comparison reports that the capacity gain predicted from the simulated channels is significantly lower than that achievable with real channels. The study also provides useful information about the antenna effects. ASS has also been analyzed in the context of the IEEE 802.11n standard [67]. Finally, [213] emphasizes a complete list of practical issues related to ASS, e.g. RF preprocessing, ASS training, RF mismatch, non-idealities in selection or the ASS in OFDM systems. Additionally, an analysis of capacity in indoor scenarios based on measurements is provided.

8.1.2 Our Contribution

We propose a new ASS criterion specifically suited for, but not limited to, HSDPA [28, 146] [200, Chapter 3]. The criterion considers the entire system design rather than only using the channel state information. The ASS criterion is based on the post-equalization Signal to Interference and Noise Ratio (SINR) for every RX antenna subset, and the subset leading to the highest SINR is chosen. As the SINR is mapped into the physical layer throughput by means of a look-up table [199] [200, Chapter 3, pp. 56], maximizing the SINR also leads to throughput maximization.

With the purpose of showing the performance of the proposed ASS criterion in real scenarios, we carried out measurements in a realistic, urban, outdoor scenario making use of the Vienna MIMO Testbed [49]. The results are presented in terms of HSDPA physical layer throughput. The main difference between our measurement approach [53, 56] and typical simulations reported in the literature is that not all individual Single-Input Single-Output (SISO) links of the full MIMO system offer the same average gain. On the contrary, they exhibit significant differences, thus resulting in a great difference in performance depending on the antenna subset selected. To illustrate such differences, HSDPA throughput is plotted in Figure 8.1 over different RX antenna positions in an area of $3\lambda \times 3\lambda$, keeping the TX power
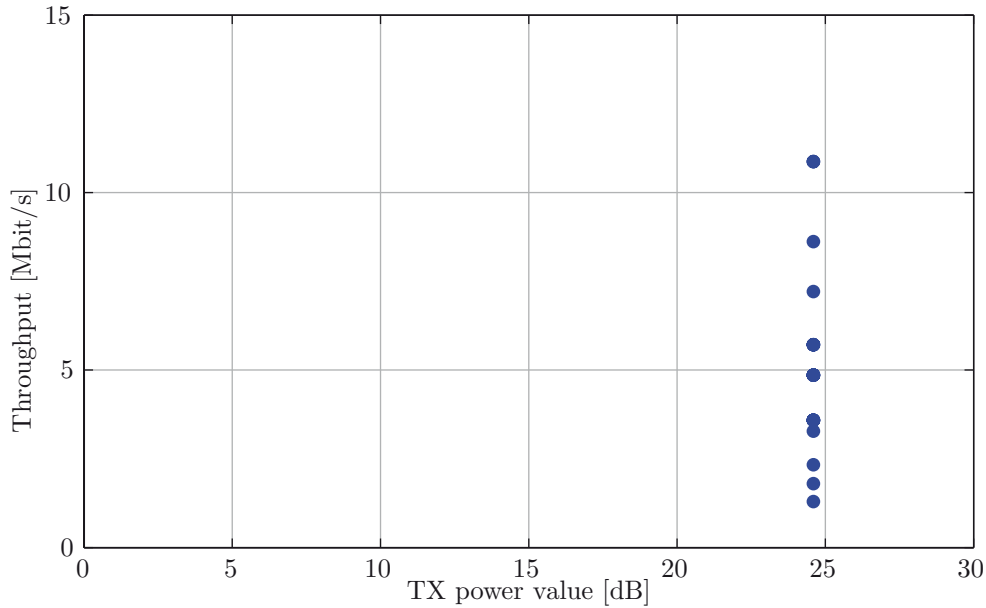
Figure 8.1: HSDPA throughput measured over different RX antenna positions while keeping the TX power value fixed.

value fixed. Note the high variability of the throughput depending on the RX antenna position. Such variability is mainly due to antenna polarization effects and makes the scenario especially suitable for ASS.

8.2   Receive Antenna Selection

Diversity via multiple RX antennas is a direct extension of traditional diversity ideas. The receiver sees several versions of the transmit signal, each one experiencing a different fade and noise. The classic extension of selection combining to RX ASS consists in choosing the l_R RX antennas with the largest SNR among the n_R available. Therefore, it is necessary to know all individual branch SNRs, which can be accomplished by means of sounding the full MIMO channel in a time-multiplexed manner. When more than one antenna is selected, Maximum Ratio Combining (MRC) can be performed among l_R out of n_R antennas. Using this approach, ASS can extract most of the diversity of the full system without requiring all n_R RF chains.

When the wireless channel has sufficient degrees of freedom, the data streams transmitted from multiple antennas can be separated, thus leading to parallel data paths. The capacity of the radio channel under these conditions (the channel matrix is full-rank) grows with $\min(n_T, n_R)$, that is, linearly with the minimum number of antennas [280]. In a multiple antenna system with n_T TX and n_R RX antennas, the complex-valued channel matrix $\mathbf{H}$ is of dimension $n_R \times n_T$. When ASS is employed at the RX, a subset of l_R out of n_R antennas is selected. It is straightforward to see that the equivalent problem consists in building a channel matrix $\tilde{\mathbf{H}}$ with dimensions $l_R \times n_T$ from the full channel matrix $\mathbf{H}$. The selection requires sounding all

possible paths using the available l_R RF chains at the RX, requiring $\lceil \frac{n_R}{l_R} \rceil$ sounding operations. Next, the selection criterion has to be applied by exhaustive searching among all $\binom{N_r}{l_R}$ different receive antenna combinations. For example, selecting one out of four receive antennas requires four sounding operations and evaluating the selection criterion four times, whereas selecting two out of four receive antennas involves only two sounding operations but six evaluations of the selection criterion. Consequently, there is a tradeoff between the total number of TX or RX antennas with respect to the number of available RF chains and the latency required to sound the full MIMO channel from the available branches. There is also another tradeoff in terms of costs. The greater the number of RF branches (l_R), the more expensive the final system is, whereas greater throughput can be achieved.

8.2.1 Antenna Selection Based on the System Throughput

In the literature, different selection criteria have been reported based on specific properties of the wireless channel such as channel capacity or eigenvalue spread. However, most of these ASS methods do not consider the entire wireless system, including the RX. For example, eigenvalue-based or capacity-based selection methods are based only on the coefficients of the wireless channel. Besides the channel coefficients, an optimum selection criterion for a specific transmission system like HSDPA has to consider the properties of the transmit signals and the RX. Therefore, we propose the utilization of analytic expressions of the post-equalization SINR as the criterion to select the RX antennas subset. The SINR is directly obtained from the estimated wireless channel and can be mapped to the physical layer throughput by a look-up table [199] [200, Chapter 3]. In [199] [200, Chapter 3] it is shown that maximizing the SINR also leads to throughput maximization. Notice that this ASS criterion is not only limited to HSDPA. It can be used whenever it is possible to describe the physical layer throughput by means of analytic expressions that depend on the channel coefficients and the implemented RX type.

8.3 Hardware Aspects of Antenna Selection

Ideal hardware is widely considered in the ASS literature. Nevertheless, when taking into account the actual features of the hardware, the promised gains of ASS are smaller. Special attention should be paid to the RF switch. *Ideal* switches do not deteriorate the receiver noise figure and work instantaneously, without any delay. However, these features cannot be completely fulfilled in practice. The attenuation of typical switches varies between a few tenths of a decibel and several decibels, depending on the switch size and the required switching speed. In addition, typical settling times of RF switches are in the order of microseconds, corresponding to a duration of several symbols in current wireless communications systems.

The losses caused by the RF switches at the RX side are difficult to compensate. One possible approach consists in installing the switch after the low-noise amplifier, but this requires as many low-noise amplifiers as RX antennas, thus reducing the benefits provided by ASS in terms of costs and power consumption. Note also that HSDPA is an interference-limited system and not a noise-limited system. This means that although the RX noise figure suffers some deterioration caused by the switch insertion loss, the final system throughput will not be significantly degraded. On the other hand, the switching time does degrade the system throughput because during the switching time no signals can be acquired.

From the hardware point of view, sequentially sounding the full MIMO channel is a challenging task. It can take a long time for the full MIMO channel to be acquired, especially in systems in which base stations do not continuously broadcast pilot symbols. Until the full MIMO channel state information becomes available, antenna selection cannot be used. Typically, this leads to a loss in spectral efficiency. Fortunately, the base stations in HSDPA are always transmitting pilot channels. Therefore, the user equipment is able to continuously perform channel sounding over the n_R RX antennas even though no data is being received. As soon as the user equipment is notified by the base station of a new incoming data block, it can use the previously obtained channel information to select the optimum antenna subset. However, this *instantaneous best throughput selection* requires the channel to be approximately constant over several subframes (a few milliseconds). If the channel changes faster faster than this, the antennas can be selected according to the average throughput of the last subframes (in the order of hundreds). Unfortunately, continuously sounding the wireless channel consumes energy that may be not affordable by a handheld device. Consequently, a tradeoff must be reached between the accuracy of the channel estimate and the energy invested in the channel sounding stage. Therefore, investing less energy in sounding the channel will lead to a noisy estimation of the channel that could lead to a suboptimal subset selection, thus degrading the performance. Fortunately, there are publications in the literature reporting that ASS is quite robust to imperfect channel estimations (e.g. [273]).

8.4 Experimental Assessment of Antenna Selection

The measurements we present in this chapter were carried out using the Vienna MIMO Testbed [49] in a realistic, urban, outdoor scenario (see Figure 8.2). The details of the steps followed to carry out the measurements, as well as the details of the testbed setup, can be found in [52]. An example of the wireless communications system exemplarily measured in this work is a laptop with four RX antennas and two RF chains located in an office and connected to the base station unit.
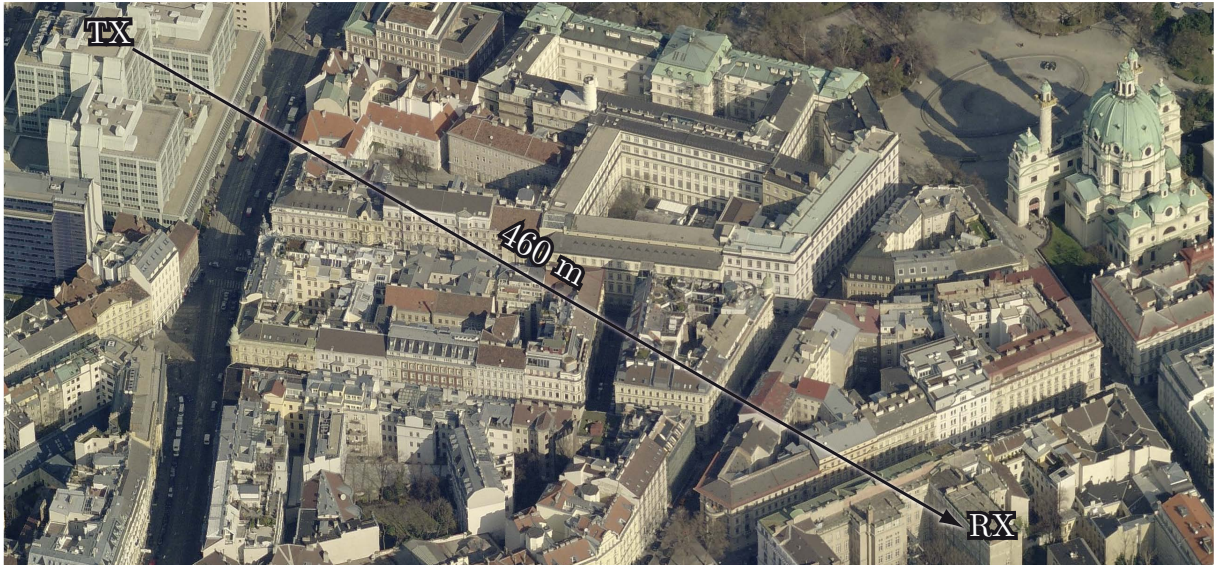
Figure 8.2: Locations of the TX (base station) and the RX in downtown Vienna.
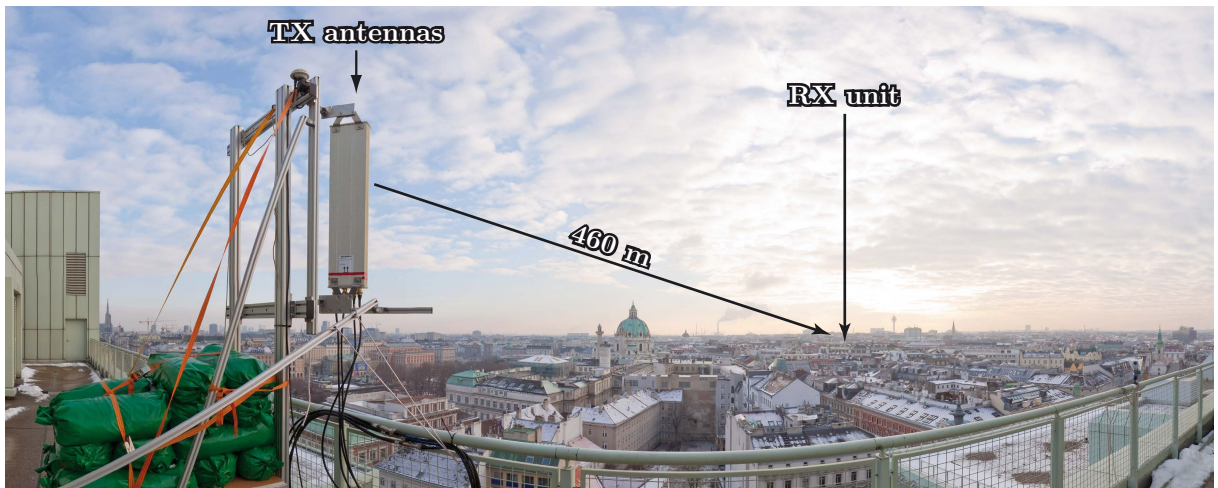
Figure 8.3: Picture of the scenario showing the antennas at the TX side.

8.4.1 The Testbed and the Scenario

We estimate the mean HSDPA throughput when using ASS in a non line-of-sight, urban scenario featuring rich scattering (see Figures 8.2–8.4). At the base station, we employ a Kathrein 800 10543 [12] 2X-pol base station panel antenna ($2\times\pm45°$polarization, half-power beam width $58°/6.2°$, down tilt $6°$). The TX is placed on the roof of a tall building in downtown Vienna (see Figure 8.2). The RX antennas are located at an approximate distance of 460 m inside an office room (see Figure 8.4). These RX antennas are moved by using a fully automated $XY\Phi$ positioning table (in an area of $3\lambda\times3\lambda$) to automatically generate many small scale fading channel realizations (see Figure 8.4). The RX antennas are printed monopole elements [167, 168] that were designed according to the generalized Koch pre-fractal curve with a resonation frequency equal to 2.7 GHz and bandwidth greater than 400 MHz. A picture

Figure 8.4: Photograph of the scenario at the RX side. The testbed RX is shown as well as the four
printed monopole RX antennas [167, 168] mounted on the XYΦ positioning table.

of such antennas is shown on the right-hand side of Figure 8.4.

8.4.2 HSDPA ASS Experimental Assessment

The experimental evaluation of ASS in HSDPA is carried out using one TX antenna (see
Figure 8.5) or two TX antennas (see Figure 8.6). In both cases, the results are measured using
all four RX antennas and are presented when one, two or all four RX antennas are selected.
Obviously, no selection is performed at all when the four RX antennas are utilized. For both
cases (one and two TX antennas), the mean throughput of HSDPA physical layer is evaluated
employing the following antenna subset selections:

- All four RX antennas are used, thus no selection is performed at all. This case is measured
  to obtain an upper bound for the throughput. The signals acquired by the four RX
  antennas are combined by means of an MRC in order to maximize the RX gain.
- Two RX antennas are selected out of the four RX antennas available.
- A single RX antenna is selected out of the four.

Therefore, given that one or two TX antennas can be used together with three different
subset selections at the RX, we evaluate six different cases. For the four cases in which two RX
antennas or a single RX antenna is selected, the following selection criteria are evaluated:

- **Instantaneous best selection**. For each channel realization created by moving the RX
  antennas, the RX antenna combination (one or two RX antennas) offering the highest
  throughput is chosen in accordance with the SINR expressions calculated in [199]. Notice
  that the measurements are carried out acquiring the signals simultaneously from all
  four RX antennas, regardless of the mode being measured. Consequently, during the
  evaluation stage it is possible to evaluate the RX antenna combination offering the best

throughput for each channel realization. This selection criterion is an upper bound for the HSDPA physical layer throughput when ASS is performed at the RX side and the channel is known for every realization.

- **Best Average Selection**. The HSDPA throughput is estimated for every RX antenna combination (one or two RX antennas), and for every channel realization. Next, the estimated mean throughput for every antenna combination over all channel realizations is calculated. Finally, the combination offering the highest throughput is chosen, which corresponds to the mean throughput obtained with this criterion. Note that this approach is especially suitable when the channel coherence time is short compared to the frame duration.

- **Worst Average Selection**. Analogously to the best average selection introduced above, after the estimation of the mean throughput for each antenna combination, the antenna combination leading to the worst throughput is chosen. This selection criterion corresponds to the worst possible case, even worse than selecting the antennas randomly, thus constituting a lower bound for the antenna selection performance.

8.4.3   Measurement Results and Discussion

Measurement results are plotted for the case in which one TX antenna is used (Figure 8.5) and when two TX antennas are employed (Figure 8.6). In each figure, three different sets of curves are plotted (from top down):

- The first set plots a single curve for the case in which all four RX antennas are employed (i.e. no selection). In the graphs in Figures 8.5 and 8.6, this set is labeled as "SIMO 1×4", or "MIMO 2×4". The curves are in black.

- The second set corresponds to the case in which two out of four RX antennas are selected. In the graphs in Figures 8.5 and 8.6, this set is labeled as "SIMO 1×2 (out of 4)", or "MIMO 2×2 (out of 4)". The curves are in red.

- Finally, in the third set a single RX antenna is selected out of four, the resulting curves are plotted in blue and labeled as "SISO 1×1 (out of 4)", or "MISO 2×1 (out of 4)" in Figures 8.5 and 8.6.

For the second and third cases, three different curves are plotted, corresponding to the three different selection criteria. The topmost dashed curve shows the mean throughput when the instantaneous best selection is performed. The two bottom curves respectively plot the mean throughput for the best and for the worst average selection criteria.

Note that the 15 to 30 dBm transmit power region is the most adequate for comparing the different throughput curves. For higher transmit power values, no higher modulation and coding schemes are available in HSDPA to exploit the channel capacity and, therefore, saturation occurs.
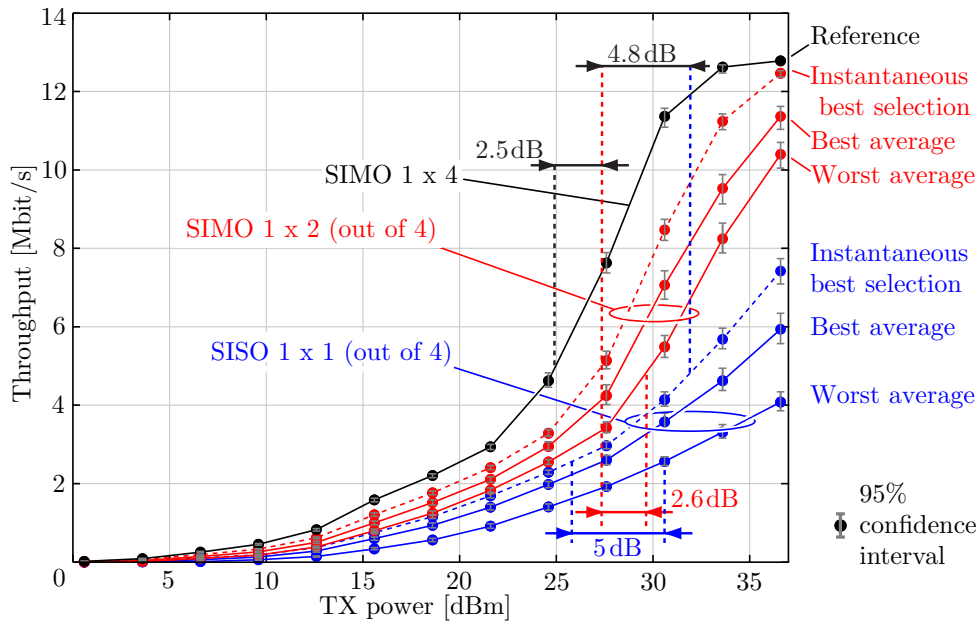
Figure 8.5: Estimated mean HSDPA throughput when ASS is used with a single TX antenna.

We estimate the precision of the measurement by means of bootstrapping methods [77, 84, 94]. In both throughput graphs (Figures 8.5 and 8.6), the dots represent the inferred mean throughput; the gray vertical lines, the 95 % confidence intervals for the mean; and the corresponding horizontal lines, the 2.5 % and the 97.5 % percentiles. Note that the RX antenna position remains unchanged while measuring the two schemes with one and two TX antennas at different TX power levels. This leads to smooth curves and relative positions of the curves that are more accurate than the confidence intervals for the absolute positions might suggest.

From the results presented in Figure 8.5 we can obtain the following conclusions:

- The difference between the SIMO 1×4 full system curve and the SIMO 1×2 instantaneous best selection – in terms of the TX power value needed to achieve the same throughput value – is about 2.5 dB. This can be explained by the additional array gain of the four RX antenna system.

- The SIMO 1×2 scheme presents a TX power gain of up to 4.8 dB with respect to the SISO 1×1 system. This is due to the array gain offered by the 1×2 system and, additionally, due to the ability to exploit all available diversity.

- The maximum observed gain offered by ASS is about 2.6 dB for the SIMO 1×2 scheme, and about 5 dB for the SISO system. Such a gain comes from the difference between the "instantaneous best selection" and the "worst average selection" curves.

From the results shown in Figure 8.6 for the case of two TX antennas, the following points should be noticed:

- The difference between the MIMO 2×4 full system and the MIMO 2×2 instantaneous best selection is in the order of 2.5 dB.
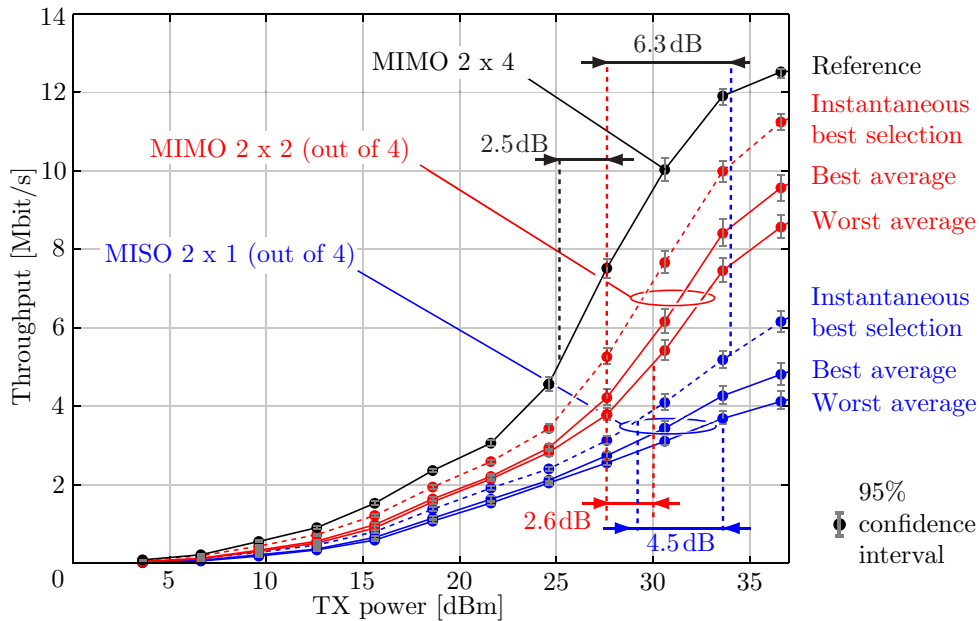
Figure 8.6: Estimated mean HSDPA throughput when ASS is used with two TX antennas.

- The MIMO 2×2 scheme presents a gain of up to 6.3 dB with respect to the MISO 2×1 system.

- Finally, the maximum observed gain offered by ASS is about 2.6 dB for the MIMO scheme, and about 4.5 dB for the MISO system.

8.5 Conclusion and Criticism

In this chapter, a new antenna Antenna Subset Selection (ASS) criterion applicable to HSDPA, as well as other mobile communications systems, was introduced. The criterion takes into account the entire system design and is based on the SINR expressions describing the behavior of the whole link – including the RX – instead of using only channel state information. We stressed the suitability of ASS to HSDPA-like systems because it enables most of the implementation issues exhibited by ASS to be overcome. With the aim of evaluating the performance of such ASS criterion, we carried out measurements in a realistic, outdoor, urban scenario with non line-of-sight between the TX and the RX. The results were presented in terms of the HSDPA physical layer downlink throughput and show significant throughput gains when ASS is used. Such gains are especially remarkable when only one RX antenna is selected out of the four available, in which case they vary from 5 dB to 4.5 dB when one or two TX antennas are used, respectively. It is also worth noting the enormous gain obtained when two RX antennas are selected instead of only one. More specifically, such gains are equal to 4.8 dB, when one TX antenna is used, and up to 6.3 dB in the case of two TX antennas. Finally, the maximum achievable gains resulting from ASS implementation range from 2 to 5 dB, depending on the number of TX antennas and the number of selected RX antennas. Finally, notice that

the instantaneous best selection criterion is affected by the settling time required by the RF antenna switch. Consequently, the corresponding instantaneous best selection curves should be corrected accordingly.

Chapter 9

Conclusions and Future Work

The main objective of this work is to demonstrate the feasibility of the experimental assessment of wireless communications systems in indoor as well as in outdoor environments. In Chapter 2 we analyze different approaches to obtain a *measurement device* suitable for the experimental evaluation of wireless communications systems. Among the existing options, we choose to develop a testbed called GTEC MIMO testbed for several reasons such as, for example, flexibility, modularity, scalability and high-level language development features exhibited by testbeds in contrast with other measurement solutions. Given the lack of resources (money, manpower, etc.) available in our research group, we decided to build the testbed based on Commercial Off-The-Shelf (COTS) hardware components. The GTEC MIMO testbed is just another testbed approach among others [27, 30, 34, 35, 42, 43, 49, 60, 65, 66, 69, 80, 82, 83, 86, 121, 131, 134, 162, 163, 169, 171, 172, 174, 175, 178, 179, 184, 185, 189, 195, 198, 204, 216–219, 223–225, 229, 234, 246, 249, 256, 275, 276, 290, 295–297, 300, 301, 304, 306, 310, 313]. In Chapters 4 to 6 we show that the GTEC MIMO testbed is suitable for experimental evaluation of multiple antenna, closed-loop wireless communications systems in indoor scenarios. We also show that testbeds can be helpful in activities other than wireless systems assessment; for example, in the development of real-time wireless communications systems or in education.

While in Chapter 2 we only focus on the hardware aspects of the GTEC MIMO testbed, in Chapter 3 we address the problem of the testbed software design in general. We start the chapter by introducing several fundamental concepts from software engineering and how they are applied to the testbed case. As a result, a distributed multilayer software architecture focused on user access is obtained. The architecture fills the gap that currently exists between commercial hardware components and typical abstraction levels provided by the software interfaces included with such hardware components. The objective is to facilitate the experimental assessment of wireless communications systems that have been previously evaluated by means of computer simulations. Therefore, such software architecture releases the researchers from the necessity of knowing low-level details of the testbed hardware as well

as the cumbersome low-level programming required by such hardware elements. The key point of the software architecture is the utilization of connection mechanisms (e.g. ordinary network connections) to decouple hardware elements from the lowest-level software layer as well as one software layer from another. Additionally, given that different problems are addressed at different abstraction levels (layers), the software architecture brings greater flexibility, modularity and extendability, taking into account future upgrades of the testbed (e.g. adding more nodes to the testbed). From the researcher's point of view, the source code required to perform the assessment of a wireless communications system is a single script or program, exactly as in a computer simulation, thus keeping the complexity of the evaluation at a similar level to that required for computer simulations. Therefore, it is very easy to implement a closed-loop system because the transmit signals, as well as the acquired observations, are examined by the same program that decides the strategy for adapting the next blocks to be transmitted. Moreover, the software architecture provides several utility functions to configure and control the fundamental testbed parameters (e.g. transmit power value, carrier frequency, etc.) and it also incorporates a software template reflecting a measurement procedure that can be tuned according to the evaluation needs. Such a measurement procedure supports closed-loop evaluation, *controlled* channel realizations by modifying the Radio Frequency (RF) carrier frequency to be used by the transmitter and the receiver and configuration of the transmit power value, all provided by an easy-to-use Application Program Interface (API) built on top of the software architecture.

Chapters 4 to 6 address the experimental evaluation of different wireless communications systems, showing the feasibility of our COTS-based GTEC MIMO testbed, including the multilayer software architecture. Chapter 4 tackles the problem of improving the spectral efficiency of Multiple-Input Multiple-Output (MIMO) systems, specifically Alamouti coded systems, avoiding the use of pilot symbols to estimate the wireless channel. Instead, three blind channel estimation strategies are proposed to estimate the mixing matrix of an Alamouti coded system. In particular, we assess a low-complexity scheme based on second order statistics suitable for 2×2 MIMO systems. Such a strategy is evaluated in several indoor scenarios as well as by means of computer simulations. In all cases, the performance of the method is similar to that offered by standard Least Squares (LS) channel estimation algorithm. Additionally, we evaluate two different methods suitable for 2×1 Alamouti coded systems. The first is also based on second order statistics of the acquired signals, while the second is based on high order statistics. Again, the performance of such methods is evaluated by means of computer simulations and experimentally using the GTEC MIMO testbed. The results show that the performance of the method based on second order statistics is very close (within a decibel in terms of the required Signal to Noise Ratio (SNR) to achieve the same Bit Error Ratio (BER)) to that offered by the well-known Joint Approximate Diagonalization of Eigenmatrices (JADE) algorithm or non blind solutions such as LS estimation. The main advantages of all proposed

approaches are, on the one hand, the gain obtained in terms of spectral efficiency and, on the other hand, the low computational complexity exhibited by such methods compared to that offered by existing solutions (e.g. the JADE algorithm).

Chapter 5 is dedicated to the experimental evaluation of analog joint source-channel coding in single antenna, narrowband, closed-loop indoor environments. The idea of analog source-channel coding was recently introduced as a means of achieving near-optimum performance for high data rates and with very low complexity in contrast to the state of the art channel coding schemes (e.g. Low Density Parity Check (LDPC) or Serially-Concatenated Low Density Generator Matrix (SCLDGM) channel codes) that require the utilization of iterative receivers and thus exhibit very high computational complexity. The feasibility of the analog joint source-channel coding approach was demonstrated by means of computer simulations. In Chapter 5 we show the feasibility of implementing such an approach in software-defined radio systems. The experimental evaluation has forced us to take into account the problems posed by analog joint-source channel coding in practice. First, the Peak-to-Average Power Ratio (PAPR) of the transmitted signals can be very high, so careful normalization of the transmitted signals is needed to prevent performance degradation due to the limited resolution of the Digital-to-Analog Converters (DACs) and Analog-to-Digital Converters (ADCs). Second, the transmitted signals in analog compression schemes are parametrized in accordance with the Signal to Noise Ratio (SNR), so it is necessary to carry out a closed-loop evaluation. As we carry out single-antenna measurements, we directly compare the experimental results with those obtained by means of computer simulations in Additive White Gaussian Noise (AWGN) channels. Additionally, we estimate the Optimal Performance Theoretically Attainable (OPTA) curve based on the estimated SNR values. The results show that the analog joint source-channel coding measurements perfectly match those originally reported by simulations in AWGN channels for SNR values below 20 dB, thus clearly demonstrating the feasibility of these analog compression schemes in real environments. For SNR values above 20 dB there is a performance degradation caused by the limited number of resolution bits of the DAC and ADC, and also by the high PAPR of the transmitted signals.

In Chapter 6 we tackle the problem of the performance assessment of SCLDGM capacity approaching channel codes over MIMO channels using the GTEC MIMO testbed in indoor scenarios. The evaluation reports that the EXtrinsic Information Transfer (EXIT) function of the channel code can significantly influence the final performance exhibited by the channel code. Such a result motivated us to introduce the so-called EXIT-based Adaptive Coding (EAC) method as a means of helping to achieve channel capacity. The results obtained, however, showed that the available gain to be exploited by the EAC is heavily dependent on the type of wireless channel. In our case, we were able to achieve almost 75 % of the attainable gain.

Chapters 7 and 8 are dedicated to the research activities carried out in collaboration with the Institute of Communications and Radio-Frequency Engineering at the Vienna University of

Technology, Austria. We make use of the Vienna MIMO Testbed to carry out measurements in downtown Vienna, constituting a very realistic, urban, outdoor environment. More specifically, we investigate the influence of transmit antenna spacing and polarization on the closed-loop throughput of standard-compliant 2×2 MIMO High-Speed Downlink Packet Access (HSDPA) transmissions. Using the channel coefficients extracted from the measurement data, we were able to estimate the water-filling channel capacity, the unconstrained capacity (also referred to as mutual information in the literature) and the functional capacity as performance bounds. The results show the existence of a large gap between the actual throughput exhibited by the system and the maximum attainable throughput (i.e. the functional capacity) offered by the wireless channel. This difference is clearly more significant than that observed from the transmit antenna spacing. In the two standard HSDPA modes analyzed, the resulting throughput remains approximately constant over the transmit antenna spacing, thus opening the door for small base station construction. Finally, Chapter 8 explores the feasibility of the antenna selection applied at the receiver side of a single and dual transmit antenna HSDPA system. We propose a selection criterion that takes into account the entire communications system design, including the receiver, rather than only the wireless channel properties. We also show the feasibility of taking advantage of the diversity gain available at the receiver side of the communications link. We emphasize the suitability of antenna selection for HSDPA-like systems because most of the implementation issues can be overcome. The obtained throughput gains due to antenna selection are especially remarkable when only one receive antenna is selected out of the four available, in which case the gains vary from 5 dB to 4.5 dB when one or two transmit antennas are used, respectively. Such throughput gains increase to up to 6.3 dB when two receive antennas are used out of the four available. These results show that antenna selection should be considered as a low-cost approach to improve the throughput in HSDPA.

9.1 Future Work

Once a research group starts out along the road of the wireless communications systems assessment, the end of the road will never be reached. In other words, this section could be longer than the previous chapters of the thesis because the experimental evaluation of communications systems has just started. Until now, we have been able to measure single-user, closed-loop, multiple-antenna, downlink transmissions. However, the complexity of wireless communications systems is growing continuously and at an exponential pace. This means that the evaluation of these complex systems, as well as needing to be carried out in more complete and also realistic scenarios, requires more complicated set-ups. For example, the realistic evaluation of MIMO precoded systems in mobile scenarios requires real-time signal processing capabilities that are still not available in our testbed. Evaluation of multiuser techniques

demands at least three testbed nodes that have to be coordinated accordingly. Moreover, a multiuser scheme with several nodes, including real feedback channels for each user, represents an important challenge from the testbed point of view. Fortunately, very promising solutions have started to appear to help in the testbed improvement process.

9.1.1 Multinode Testbeds

The possibility of experimentally evaluating state of the art techniques to improve the efficiency and reliability of wireless multiuser systems is very attractive for a small research group like ours. For this purpose, it is necessary to build a multinode testbed in which several nodes can act as a transmitter or as a receiver. In collaboration with the GTAS group from the University of Cantabria, we have started to build a multinode testbed made up of heterogeneous hardware nodes. To date we have been able to emulate a multiuser broadcast channel with one transmit node and three receive nodes. A picture of the resulting scenario is shown in Figure 3.8, page 41.

In the context of multinode testbeds, several types of experiments can be carried out. For example, experimentally evaluating the performance of single and multiple-antenna techniques in the so-called multiple-access channel in which several users transmit simultaneously towards the same receiver. Another example consists in designating a testbed node to be used as a relay. Consequently, cooperative communications can be explored by means of testbed measurements. Finally, a very active topic in the research community is the so-called interference alignment, in which signals are designed so that they overlap at receivers, where they cause interference, while remaining distinguishable at receivers where they are desired [57, 58, 302].

9.1.2 Precoding

A very interesting topic in multiple-antenna and multiuser communications systems is the so-called precoding, in which a centralized transmitter (e.g. a base station) is equipped with multiple antennas to communicate with several single-antenna decentralized receivers (e.g. the mobile stations) [64]. The receivers demand limited power consumption, size and, consequently, reduced processing capabilities, and will thus be limited to single-antenna devices. On the contrary, at the base station such requirements can be relaxed, thus making it feasible to allow multiple antennas as well as high computational capabilities. For this reason, it is very interesting to transfer the complexity present in current communications systems from the receivers to the transmitter (in the downlink). This idea perfectly fits with the concept of Multiple-Input Single-Output (MISO) precoding as it is addressed in [64]. The problem of the experimental evaluation of MISO precoding schemes with limited feedback in real-world channels can be tackled using the GTEC MIMO testbed. To date we have carried out

some preliminary trials in which all operations were carried out off-line and with floating point precision.

9.1.3   GNU Radio and the USRP

With the advent of GNU Radio [7], a revolution in software-defined radio technologies is foreseen that will greatly reduce development costs in terms of hardware, money, and manpower. GNU Radio is a free and open software toolkit for the development of software-defined radio systems, for example, testbeds. GNU Radio provides the signal processing blocks for implementing reconfigurable software radios using the Universal Software Radio Peripheral (USRP). The USRP (and its successor, the USRP2) is a low-cost external device (see Figure 2.11, page 22) manufactured by Ettus Research LLC [3] and containing the digital hardware as well as pluggable RF front-ends named daughterboards. The available set of daughterboards covers a wide range of RF bands (from 50 MHz to 2.9 GHz, and from 4.9 to 5.85 GHz). Although Ettus claims that the designs of all daughterboards are free and open [5, 8], only the schematics are available for download. The main advantages of the GNU Radio approach are summarized below [247]:

- Low-cost solution. Compared to commercial solutions, GNU Radio is a free software platform and you only pay for the hardware manufacturing expenses.
- Low-cost software implementation. GNU Radio platform provides the programmer with a very flexible and sophisticated software-defined radio programming environment.
- Hardware and software components are open source[1], thus allowing customization to meet specific requirements.
- GNU Radio is platform-independent. The only requirement is a USB library and it is available on Windows, GNU/Linux, and Mac OS X systems.
- The available set of pluggable daughterboards covers the most commonly used RF bands, from 50 MHz to 2.9 GHz, and from 4.9 GHz to 5.85 GHz.
- A common external reference oscillator can be attached to multiple USRP and USRP2 boards.

Unfortunately, GNU Radio also has its limitations [247]:

- The main disadvantage of the first-generation USRP hardware is the use of a low-cost limited USB 2.0 port. The maximum sustainable net throughput is limited to 32 MB/s. Given that interleaved I/Q samples are mandatory, the sample rate is reduced to 8 Msample/s. Consequently, the maximum effective bandwidth is 8 MHz. This limitation is overcome in the second-generation of the USRP.

---

[1]With respect to the GNU Radio hardware, only the daughterboards offer open designs.

- MIMO is limited to two antennas at each side of the communications link unless several USRP units are synchronized using external devices.

- Real-time implementations are not supported in the USRP. However, the USRP2 allows real-time interconnection with Field Programmable Gate Array (FPGA) motherboards.

- Both USRP and USRP2 buffers cannot be used to store the samples off-line to be transferred later in real-time because they are too small.

Given the main advantages and limitations exhibited by the GNU Radio and the USRP, it constitutes a very attractive approach for complementing high-performance testbed nodes as well as for the experimental evaluation of sensor networks in which a great number of nodes is required.

9.1.4   Graphics Processing Units

Recently, the utilization of Graphics Processing Units (GPUs) for signal processing and software-defined radios has been considered [11, 172, 259]. Given that usually the testbed hardware (at least the digital section) is allocated in ordinary Personal Computers (PCs), it is cheap and straightforward to add graphics processing units to PCs to boost the signal processing operations. Recently, AccelerEyes presented a solution known as Jacket [11] that enables GPU computing using MATLAB. Additionally, well-known MIMO algorithms such as the sphere detector can be speeded up by exploiting parallelism in GPU cards [259]. All the above-mentioned examples make signal processing by means of GPUs a very attractive approach for speeding up signal processing tasks enormously while keeping high-level programming and floating point precision. Although the implementation of software-defined radio systems using GPUs is being considered in the literature [172], there are still many open questions regarding the feasibility of such approach for real-time systems currently based on Digital Signal Processors (DSPs) and FPGAs.

128

Appendix A

List of Acronyms

ADC Analog-to-Digital Converter

AMC Adaptive Modulation and Coding

API Application Program Interface

ASS Antenna Subset Selection

AWGN Additive White Gaussian Noise

BER Bit Error Ratio

BLER BLock Error Ratio

COFDM Coded Orthogonal Frequency Division Multiplexing

COTS Commercial Off-The-Shelf

CSI Channel State Information

DAC Digital-to-Analog Converter

DDC Digital Down Converter

DSP Digital Signal Processor

DSTBC Differential Space-Time Block Code

D-TxAA Double Transmit Antenna Array

DUC Digital Up Converter

EAC EXIT-based Adaptive Coding

EVM Error Vector Magnitude

EXIT EXtrinsic Information Transfer

FEC Forward Error Correction

FM Frequency Modulated

FPGA Field Programmable Gate Array

GPU Graphics Processing Unit

HARQ Hybrid Automatic Repeat reQuest

HDTV High Definition TV

HOS Higher-Order Statistics

HSDPA High-Speed Downlink Packet Access

IF Intermediate Frequency

iid independent and identically-distributed

ISM Industrial, Scientific and Medical

JADE Joint Approximate Diagonalization of Eigenmatrices

LDGM Low Density Generator Matrix

LDPC Low Density Parity Check

LMMSE Linear Minimum Mean Square Error

LS Least Squares

LTE Long Term Evolution

MAP Maximum A-Posteriori

MIMO Multiple-Input Multiple-Output

MISO Multiple-Input Single-Output

ML Maximum Likelihood

ML-EM Maximum Likelihood Expectation-Maximization

MMSE Minimum Mean Squared Error

MRC Maximum Ratio Combining

MSE Mean Squared Error

MVC Model View Controller

MWL Middleware Layer

OFDM Orthogonal Frequency-Division Multiplexing

OPTA Optimal Performance Theoretically Attainable

OSTBC Orthogonal Space-Time Block Code

PAPR Peak-to-Average Power Ratio

PC Personal Computer

PCA Principal Component Analysis

PN Pseudo Noise

PSD Power Spectral Density

RF Radio Frequency

RX Receiver

SCLDGM Serially-Concatenated Low Density Generator Matrix

SDR Signal-to-Distortion Ratio

SER Symbol Error Ratio

SHB Sundance High-Speed Bus

SIMO Single-Input Multiple-Output

SINR Signal to Interference and Noise Ratio

SISO Single-Input Single-Output

SNR Signal to Noise Ratio

SOS Second-Order Statistics

SPL Signal Processing Layer

STBC Space-Time Block Code

SVD Singular Value Decomposition

TCP Transmission Control Protocol

TIL Testbed Interface Layer

TX Transmitter

TxAA Transmit Antenna Array

UMTS Universal Mobile Telecommunications System

USB Universal Serial Bus

USRP Universal Software Radio Peripheral

VoD Video on Demand

VoIP Voice over Internet Protocol

Bibliography

[1] "3L Diamond, 3L Ltd." URL: http://www.3l.com/

[2] "Analog Devices, Inc." URL: http://www.analog.com

[3] "Ettus Research LLC." URL: http://www.ettus.com

[4] "The Spaniard Julio Cervera Baviera, and not Marconi, was the inventor of the radio, according to professor Ángel Faus. University of Navarra." URL: http://www.unav.es/english/news/38.html

[5] "The free software definition by GNU." URL: http://www.gnu.org/philosophy/free-sw.html

[6] "GE Fanuc." URL: http://www.gefanucembedded.com

[7] "GNU radio." URL: http://www.gnuradio.org

[8] "The GNU general public license (GPL)." URL: http://www.gnu.org/licenses/gpl.html

[9] "Hunt Engineering." URL: http://hunteng.co.uk

[10] "Innovative Integration." URL: http://www.innovative-dsp.com

[11] "Jacker, GPU computing using Matlab. accelereyes." URL: http://www.accelereyes.com/

[12] "KATHREIN-Werke KG Antenna No. 800 10543," 2010. URL: http://www.nt.tuwien.ac.at/fileadmin/data/testbed/kat-ant.pdf

[13] "KATHREIN-Werke KG Antenna No. 800 10629," 2010. URL: http://www.nt.tuwien.ac.at/fileadmin/data/testbed/kat-ant.pdf

[14] "NI LabVIEW, National Instruments." URL: http://www.ni.com/labview/

[15] "Lyrtech." URL: http://www.lyrtech.com

[16] "Maxim." URL: http://www.maxim-ic.com/

[17] "Merrian-Webster dictionary." URL: http://m-w.com

[18] "Nallatech." URL: http://www.nallatech.com

[19] "National Instruments." URL: http://www.ni.com

[20] "Pentek." URL: http://www.pentek.com

[21] "Software communication architecture (SCA)." URL: http://sca.jpeojtrs.mil/

[22] "SDR forum." URL: http://www.sdrforum.org/

[23] "Sundance Multiprocessor." URL: http://www.sundance.com

[24] "L-Com Antenna No. HG2458RD-SM," 2010. URL: http://www.l-com.com/item.aspx?id=22199

[25] "Xilinx System Generator for DSP." URL: http://www.xilinx.com/tools/sysgen.htm

[26] "Hydra: a wireless multihop testbed." URL: http://users.ece.utexas.edu/~rheath/research/prototyping/mimoadhoc/docs/Hydra_WNCG_2005_web.pdf

[27] "Open Air Interface, EURECOM," 2010. URL: http://www.openairinterface.org/

[28] "Technical specification group radio access network; physical layer procedures (FDD) (Tech. Spec. 25.214 V7.7.0)," Nov. 2007. URL: http://www.3gpp.org/ftp/Specs/html-info/25214.htm

[29] 3GPP, "Technical specification group radio access network; (e-utra) and(e-utran); overall description; stage 2," 3GPP, Tech. Rep., Sep. 2008. URL: http://www.3gpp.org/ftp/Specs/html-info/36300.htm

[30] A. Adjoudani, E. Beck, A. Burg, G. Djuknic, T. Gvoth, D. Haessig, S. Manji, M. Milbrodt, M. Rupp, D. Samardzija, A. Siegel, I. Sizer, T., C. Tran, S. Walker, S. Wilkus, and P. Wolniansky, "Prototype experience for MIMO BLAST over third-generation wireless system," *IEEE Journal on Selected Areas in Communications*, vol. 21, no. 3, pp. 440–451, Apr. 2003, doi: 10.1109/JSAC.2003.809724.

[31] S. M. Alamouti, "A simple transmit diversity technique for wireless communications," *IEEE Journal on Selected Areas in Communications*, vol. 16, no. 8, pp. 1451–1458, Oct. 1998, doi: 10.1109/49.730453.

[32] N. Ammar and Z. Ding, "On blind channel identifiability under space-time coded transmission," in *Conference Record of the Thirty-Sixth Asilomar Signals, Systems and Computers*, vol. 1, 2002, pp. 664–668, doi: 10.1109/ACSSC.2002.1197264.

[33] J. Andrews, S. Shakkottai, R. Heath, N. Jindal, M. Haenggi, R. Berry, D. Guo, M. Neely, S. Weber, S. Jafar, and A. Yener, "Rethinking information theory for mobile ad hoc networks," *IEEE Communications Magazine*, vol. 46, no. 12, pp. 94–101, Dec. 2008, doi: 10.1109/MCOM.2008.4689214.

[34] F. Azami, A. Ghorssi, H. Hemesi, A. Mohammadi, and A. Abdipour, "Design and implementation of a flexible 4x4 MIMO testbed," in *International Symposium on Telecommunications (IST)*, Aug. 2008, pp. 268–272, doi: 10.1109/ISTEL.2008.4651312.

[35] D. Bates, S. J. Henriksen, B. Ninness, and S. Weller, "A 4x4 FPGA-based wireless testbed for LTE applications," in *Proc. IEEE International Symposium on Personal, Indoor and Mobile Radio Communications (PIMRC 2008)*, Cannes, France, Sep. 2008, p. 5, doi: 10.1109/PIMRC.2008.4699820. URL: http://sigpromu.org/reports/Field65_277.pdf

[36] A. Behzad, *Wireless LAN Radios*. Hoboken, New Jersey, USA: John Wiley & Sons, 2007. ISBN: 978-0471-70964-0.

[37] I. Berenguer, X. Wang, and V. Krishnamurthy, "Adaptive MIMO antenna selection," *Conference Record of the Thirty-Seventh Asilomar Conference on Signals, Systems and Computers*, vol. 1, pp. 21–26, Nov. 2003, doi: 10.1109/ACSSC.2003.1291856.

[38] ——, "Adaptive MIMO antenna selection via discrete stochastic optimization," *IEEE Transactions on Signal Processing*, vol. 53, no. 11, pp. 4315–4329, Nov. 2005, doi:

10.1109/TSP.2005.857056.

[39] E. Beres and R. Adve, "Blind channel estimation for orthogonal STBC in MISO systems," *IEEE Transactions on Vehicular Technology*, vol. 56, no. 4, pp. 2042–2050, Jul. 2007, doi: 10.1109/TVT.2007.897639.

[40] T. Berger and D. Tufts, "Optimum pulse amplitude modulation–I: Transmitter-receiver design and bounds from information theory," *IEEE Transactions on Information Theory*, vol. 13, no. 2, pp. 196–208, Apr. 1967.

[41] C. Berrou, A. Glavieux, and P. Thitimajshima, "Near Shannon limit error-correcting coding and decoding: Turbo-codes," in *Proc. IEEE International Conference on Communications (ICC)*, vol. 2, May 1993, pp. 1064–1070, doi: 10.1109/ICC.1993.397441.

[42] K. S. Bialkowski, A. Postula, A. Abbosh, and M. E. Bialkowski, "2x2 MIMO testbed for dual 2.4ghz/5ghz band," in *Proc. International Conference on Electromagnetics in Advanced Applications (ICEAA 2007)*, Torino, Italy, Sep. 2007, pp. 1–4, doi: 10.1109/ICEAA.2007.4387223.

[43] D. Borkowski, L. Brühl, C. Degen, W. Keusgen, G. Alirezaei, F. Geschewski, C. Oikonomopoulos, and B. Rembold, "SABA: A testbed for a real-time MIMO system," *EURASIP Journal on Applied Signal Processing*, vol. 2006, Article ID 56061, p. 15, 2006, doi: 10.1155/ASP/2006/56061.

[44] C. Budianu and L. Tong, "Channel estimation for space-time orthogonal block codes," *IEEE Transactions on Signal Processing*, vol. 50, no. 10, pp. 2515–2528, Oct. 2002, doi: 10.1109/TSP.2002.803340.

[45] A. Burg and M. Rupp, *EURASIP Book on Smart Antennas*. EURASIP, 2006, ch. Demonstrators and Testbeds.

[46] F. Buschmann, R. Meunier, H. Rohnert, P. Sommerlad, and M. Stal, *Pattern-oriented software architecture: a system of patterns*. Wiley & Sons, 1996. ISBN: 978-0471958697.

[47] ——, *Pattern-oriented software architecture: a system of patterns, volume 1*. Wiley India Pvt. Ltd., 2008.

[48] S. Caban and M. Rupp, "Impact of transmit antenna spacing on 2x1 Alamouti radio transmission," *Electronics Letters*, vol. 43, no. 4, pp. 198–199, Feb. 2007, doi: 10.1049/el:20073153.

[49] S. Caban, C. Mehlführer, R. Langwieser, A. L. Scholtz, and M. Rupp, "Vienna MIMO testbed," *EURASIP Journal on Applied Signal Processing*, vol. 2006, 2006, doi: 10.1155/ASP/2006/54868.

[50] S. Caban, C. Mehlführer, L. W. Mayer, and M. Rupp, "2x2 MIMO at variable antenna distances," in *Proc. Vehicular Technology Conference Spring (VTC)*, Singapore, May 2008, doi: 10.1109/VETECS.2008.276.

[51] S. Caban, C. Mehlfuhrer, L. W. Mayer, and M. Rupp, "2x2 MIMO at variable antenna distances," in *Proc. IEEE Vehicular Technology Conference (VTC Spring)*, May 2008, pp. 1311–1315, doi: 10.1109/VETECS.2008.276.

[52] S. Caban, C. Mehlführer, G. Lechner, and M. Rupp, "Testbedding MIMO HSDPA and WiMAX,"

in *Proc. IEEE 70th Vehicular Technology Conference Fall (VTC)*, Sep. 2009, pp. 1–5, doi: 10.1109/VETECF.2009.5378995.

[53] S. Caban, J. A. García-Naya, L. Castedo, and C. Mehlführer, "Measuring the influence of TX antenna spacing and transmit power on the closed-loop throughput of IEEE 802.16-2004 WiMAX," in *Proc. IEEE International Instrumentation and Measurement Technology Conference*, Austin, Texas, USA, May 2010.

[54] S. Caban, J. A. García-Naya, C. Mehlführer, L. Castedo, and M. Rupp, "Measuring the closed-loop throughput of 2x2 HSDPA over TX power and TX antenna spacing," in *Proc. 2nd International ICST Conference on Mobile Lightweight Wireless Systems*, Barcelona, Spain, May 2010.

[55] S. Caban, "Testbed-based evaluation of mobile communication systems," Ph.D. dissertation, Vienna University of Technology, Sep. 2009.

[56] S. Caban, C. Mehlführer, G. Lechner, and M. Rupp, "Testbedding MIMO HSDPA and WiMAX," in *Proc. IEEE 70th Vehicular Technology Conference (VTC2009-Fall)*, Anchorage, AK, USA, Sep. 2009, doi: 10.1109/VETECF.2009.5378995.

[57] V. R. Cadambe and S. A. Jafar, "Interference alignment and degrees of freedom of the k-user interference channel," *IEEE Transactions on Information Theory*, vol. 54, no. 8, pp. 3425–3441, Aug. 2008, doi: 10.1109/TIT.2008.926344.

[58] ——, "Interference alignment and spatial degrees of freedom for the k user interference channel," in *Proc. IEEE International Conference on Communications (ICC)*, 2008, pp. 971–975, doi: 10.1109/ICC.2008.190.

[59] G. Caire and K. R. Kumar, "Information theoretic foundations of adaptive coded modulation," *Proceedings of the IEEE*, vol. 95, no. 12, pp. 2274–2298, Dec. 2007, doi: 10.1109/JPROC.2007.904444.

[60] H. Cao, C. Konig, A. Wilzeck, and M.-D. Perez Guirao, "Cognitive agile networking testbed," in *IEEE Radio and Wireless Symposium (RWS)*, Jan. 2010, pp. 296–299, doi: 10.1109/RWS.2010.5434169.

[61] J. F. Cardoso and A. Souloumiac, "Blind beamforming for non-gaussian signals," *IEE Proceedings-F Radar and Signal Processing*, vol. 140, no. 6, pp. 362–370, Dec. 1993.

[62] A. Carro-Lagoa, P. Suárez-Casal, A. Morales-Méndez, J. Camas-Albar, and L. Castedo, "Prototipado SDR de la capa física OFDMA del estándar IEEE 802.16e," in *Proc. XXIV Simposium Nacional de la Unión Científica Internacional de Radio (URSI)*, Cantabria, Spain, Sep. 2008.

[63] A. Carro-Lagoa, P. Suárez-Casal, J. A. García-Naya, L. Castedo, J. M. Camas, and A. Morales, "Reconfigurable SDR architecture for an OFDMA realtime PHY layer," in *Proc. European Reconfigurable Radio Technologies Workshop and Product Exhibition*, Jun. 2010.

[64] P. M. Castro-Castro, "Design of limited feedback for robust MMSE precoding in multiuser MISO systems," Ph.D. dissertation, University of A Coruña, Jun. 2009. URL:

https://www.educacion.es/teseo/mostrarRef.do?ref=839175

[65] J. Chen, W. Zhu, B. Daneshrad, J. Bhatia, H.-S. Kim, K. Mohammed, S. Sasi, and A. Shah, "A real time 4x4 MIMO-OFDM SDR for wireless networking research," in *Proc. 15th European Signal Processing Conference (EUSIPCO 2007)*, Sep. 2007, pp. 1151–1155, ISBN: 978-83-921340-2-2. URL: http://www.eurasip.di.uoa.gr/eurasip/Proceedings/Eusipco/Eusipco2007/Papers/C1L-A05.pdf

[66] R. Chen, Q. Cai, K. Alecke, O. Lazar, and T. Kaiser, "A real-time PRE-MIMO-LTE software radio testbed," in *Proc. 15th European Signal Processing Conference (EUSIPCO 2007)*, Poznań, Poland, Sep. 2007, pp. 1844–1849, ISBN: 978-83-921340-2-2. URL: http://www.eurasip.di.uoa.gr/eurasip/Proceedings/Eusipco/Eusipco2007/Papers/D1L-A03.pdf

[67] Z. Chen and H. Suzuki, "Performance of 802.11n WLAN with transmit antenna selection in measured indoor channels," in *Proc. Australian Communications Theory Workshop (AusCTW)*, Feb. 2008, pp. 139–143, doi: 10.1109/AUSCTW.2008.4460836.

[68] Z. Chen, I. B. Collings, Z. Zhou, and B. Vucetic, "Transmit antenna selection schemes with reduced feedback rate," *IEEE Transactions on Wireless Communications*, vol. 8, no. 2, pp. 1006–1016, Feb. 2009, doi: 10.1109/TWC.2009.080296.

[69] C. Y. Chiu, C. H. Cheng, Y. S. Wan, C. R. Rowell, and R. D. Murch, "Design of a flat fading 4 x 4 MIMO testbed for antenna characterization using a modular approach," in *Proc. IEEE Wireless Communications and Networking Conference (WCNC 2007)*, Hong Kong, Mar. 2007, pp. 2913–2918, doi: 10.1109/WCNC.2007.540.

[70] D. Chizhik, F. Rashid-Farrokhi, J. Ling, and A. Lozano, "Effect of antenna separation on the capacity of BLAST in correlated channels," *IEEE Communications Letters*, vol. 4, no. 11, pp. 337–339, Nov. 2000, doi: 10.1109/4234.892194.

[71] D. Chizhik, J. Ling, P. W. Wolniansky, R. A. Valenzuela, N. Costa, and K. Huber, "Multiple-input-multiple-output measurements and modeling in Manhattan," *IEEE Journal on Selected Areas in Communication*, vol. 21, no. 3, pp. 321–331, Apr. 2003, doi: 10.1109/JSAC.2003.809457.

[72] S.-Y. Chung, "On the construction of some capacity-approaching coding schemes," Ph.D. dissertation, Dept. EECS, Massachusetts Institute of Technology, 2000.

[73] S.-Y. Chung, J. Forney, G. D., T. J. Richardson, and R. Urbanke, "On the design of low-density parity-check codes within 0.0045 db of the shannon limit," *Communications Letters, IEEE*, vol. 5, no. 2, pp. 58–60, Feb. 2001, doi: 10.1109/4234.905935.

[74] M. Collados and A. Gorokhov, "Antenna selection for MIMO-OFDM WLAN systems," vol. 3, Sep. 2004, pp. 1802–1806.

[75] ——, "Antenna selection for MIMO-OFDM WLAN systems," *International Journal of Wireless Information Networks*, vol. 12, no. 4, pp. 205–213, Dec. 2005, doi: 10.1007/s10776-005-0007-9.

[76] J. P. Coon and M. Sandell, "Combined bulk and per-tone transmit antenna selection in OFDM systems," *IEEE Communications Letters*, vol. 14, no. 5, pp. 426–428, May 2010, doi: 10.1109/LCOMM.2010.05.100055.

[77] D. Cox, *Planning of Experiments*. John Wiley & Sons, 1958.

[78] O. Damen, A. Chkeif, and J.-C. Belfiore, "Lattice code decoder for space-time codes," *IEEE Communications Letters*, vol. 4, no. 5, pp. 161–163, May 2000, doi: 10.1109/4234.846498.

[79] A. Das, F. Khan, A. Sampath, and H.-J. Su, "Performance of hybrid ARQ for high speed downlink packet access in UMTS," in *Proc. 62th IEEE Vehicular Technology Conference Fall (VTC)*, vol. 4, 2001, pp. 2133–2137, doi: 10.1109/VTC.2001.957121.

[80] R. de Lacerda, L. S. Cardoso, R. Knopp, D. Gesbert, and M. Debbah, "EMOS platform: Real-time capacity estimation of MIMO channels in the UMTS-TDD band," in *Proc. IEEE 4th International Symposium on Wireless Communication Systems (ISWCS 2007)*, Trondheim, Norway, Oct. 2007, pp. 782–786, doi: 10.1109/ISWCS.2007.4392447.

[81] A. P. Dempster, N. M. Laird, and D. B. Rubin, "Maximum likelihood from incomplete data via the EM algorithm," *Journal of the Royal Statistical Society. Series B (Methodological)*, vol. 39, no. 1, pp. 1–38, 1977.

[82] V. Desai, J. F. Kepler, E. Stone, J. W. Thomas, and T. A. Thomas, "An experimental 8x8 system used to characterize the spatial channel at 3.5 GHz," in *Proc. IEEE 68th Vehicular Technology Conference (VTC 2008-Fall)*, Calgary, Canada, Sep. 2008, pp. 1–5, doi: 10.1109/VETECF.2008.38.

[83] J. Dowle, S. H. Kuo, K. Mehrotra, and I. V. McLoughlin, "An FPGA-based MIMO and space-time processing platform," *EURASIP Journal on Applied Signal Processing*, vol. 2006, Article ID 34653, p. 14, 2006, doi: 10.1155/ASP/2006/34653.

[84] B. Efron and D. V. Hinkley, *An Introduction to the Bootstrap (CRC Monographs on Statistics & Applied Probability)*, 1st ed. Chapman & Hall, 1994. ISBN: 0412042312.

[85] V. Erceg, L. Schumacher, P. Kyritsi, A. Molisch, D. Baum, A. Gorokhov, C. Oestges, Q. Li, K. Yu, and N. Tal, "TGn channel models," IEEE P802.11, Wireless LANs, Tech. Rep. URL: http://www.802wirelessworld.com/8802

[86] A. G. Fabregas, M. Guillaud, D. T. M. Slock, G. Caire, K. Gosse, S. Rouquette, A. R. Dias, P. Bernardin, X. Miet, J. M. Conrat, Y. Toutain, A. Peden, and Z. Li, "A MIMO-OFDM testbed for wireless local area networks," *EURASIP Journal on Applied Signal Processing*, vol. 2006, 2006, doi: 10.1155/ASP/2006/18083.

[87] G. Femenias, "BER performance of linear STBC from orthogonal designs over MIMO correlated nakagami-m fading channels," *IEEE Transactions on Vehicular Technology*, vol. 53, no. 2, pp. 307–317, Mar. 2004, doi: 10.1109/TVT.2004.823475.

[88] O. Fernandez, M. Domingo, and R. Torres, "Empirical analysis of the correlation of MIMO channels in indoor scenarios at 2 GHz," *IEE Proceedings-Communications*, vol. 152, no. 1, pp. 82–88, Feb. 2005, doi: 10.1049/ip-com:20041019.

[89] T. M. Fernández-Caramés, M. González-López, and L. Castedo, "FPGA-based vehicular channel emulator for real-time performance evaluation of IEEE 802.11p transceivers," *EURASIP Journal on Wireless Communications and Networking*, vol. 2010, pp. 1–18, 20010, doi:

10.1155/2010/607467.

[90] T. M. Fernández-Caramés, J. A. García-Naya, M. González-Lopez, and L. Castedo, "MIMO testbed middleware for transmission automation," in *Proc. 50th International Symposium ELMAR*, vol. 1, Zadar, Croatia, Sep. 2008, pp. 215–218.

[91] T. M. Fernández-Caramés, J. A. García-Naya, M. González-López, and L. Castedo, "FlexVehd: a flexible testbed for vehicular radio interfaces," in *Proc. Intelligent Transport Systems Telecommunications (ITST)*, Phuket, Thailand, Oct. 2008.

[92] T. M. Fernández-Caramés, M. González-López, and L. Castedo, "FPGA-based vehicular channel emulator for evaluation of IEEE 802.11p transceivers," in *Proc. Intelligent Transport Systems Telecommunications (ITST)*, Lille, France, Oct. 2009.

[93] U. Fincke and M. Pohst, "Improved methods for calculating vectors of short length in a lattice, including a complexity analysis," *Mathematics of computation*, vol. 44, no. 170, pp. 463–471, Apr. 1985.

[94] R. Fisher, *The Design of Experiments*. New York: Wiley, 1935.

[95] P. A. Floor, "On the theory of Shannon-Kotelnikov mappings in joint source-channel coding," Ph.D. dissertation, 2008.

[96] P. A. Floor and T. A. Ramstad, "Dimension reducing mappings in joint source-channel coding," in *Proc. 7th Nordic Signal Processing Symposium (NORSIG)*, Jun. 2006, pp. 282–285, doi: 10.1109/NORSIG.2006.275256.

[97] G. J. Foschini, "Layered space-time architecture for wireless communication in a fading environment when using multi-element antennas," *Bell Labs Technical Journal*, vol. 1, no. 2, pp. 41–59, 1996.

[98] G. J. Foschini and M. J. Gans, "On limits of wireless communications in a fading environment when using multiple antennas," *Wireless Personal Communications*, vol. 6, no. 3, pp. 311–335, 1998, doi: 10.1023/A:1008889222784.

[99] A. Fuldseth and T. A. Ramstad, "Bandwidth compression for continuous amplitude channels based on vector approximation to a continuous subset of the source signal space," in *Proc. IEEE International Conference on Acoustics Speech and Signal Processing (ICASSP)*, vol. 4, Apr. 1997, pp. 3093–3096, doi: 10.1109/ICASSP.1997.595446.

[100] R. Gallager, "Low-density parity-check codes," *IRE Transactions on Information Theory*, vol. 8, no. 1, pp. 21–28, Jan. 1962, doi: 10.1109/TIT.1962.1057683.

[101] E. Gamma, R. Helm, R. Johnson, and J. Vlissides, *Design patterns: elements of reusable object-oriented software*. Addison-Wesley, 1994. ISBN: 978-0201633610.

[102] G. Ganesan and P. Stoica, "Space-time block codes: a maximum SNR approach," *IEEE Transactions on Information Theory*, vol. 47, no. 4, pp. 1650 –1656, May 2001, doi: 10.1109/18.923754.

[103] J. Garcia-Frias and W. Zhong, "Approaching shannon performance by iterative decoding of linear

codes with low-density generator matrix," *IEEE Communications Letters*, vol. 7, no. 6, pp. 266–268, Jun. 2003, doi: 10.1109/LCOMM.2003.813816.

[104] J. A. García-Naya, T. M. Fernández-Caramés, H. J. Pérez-Iglesias, M. González-Lopez, L. Castedo, D. Ramírez, I. Santamaría, J. Pérez, J. Vía, and J. M. Torres-Royo, "Performance of STBC transmissions with real data," in *16th IST Mobile and Wireless Communications Summit*, Jul. 2007, pp. 1–5, doi: 10.1109/ISTMWC.2007.4299296.

[105] J. A. García-Naya, T. M. Fernández-Caramés, H. J. Perez-Iglesias, M. González-López, and L. Castedo, "Arquitectura multicapa distribuida para demostradores MIMO," in *Proc. XXIII Simposium Nacional de la Unión Científica Internacional de Radio (URSI)*, Madrid, Spain, Sep. 2008.

[106] J. A. García-Naya, M. González-López, and L. Castedo, "An overview of MIMO testbed technology," in *Proc. 4th International Symposium on Image/Video Communications over fixed and mobile networks (ISIVC)*, Bilbao, Spain, Jul. 2008.

[107] J. A. García-Naya, H. J. Pérez-Iglesias, A. Dapena, and L. Castedo, "A comparative study of blind channel identification methods for alamouti coded systems over indoor transmissions at 2.4 GHz," in *Proc. IEEE 5th Sensor Array and Multichannel Signal Processing Workshop (SAM)*, Jul. 2008, pp. 1–4, doi: 10.1109/SAM.2008.4606811.

[108] J. A. García-Naya, H. J. Perez-Iglesias, T. M. Fernández-Caramés, M. González-López, and L. Castedo, "A distributed multilayer architecture enabling end-user access to MIMO testbeds," in *Proc. IEEE 19th International Symposium on Personal, Indoor and Mobile Radio Communications*, Cannes, France, Sep. 2008, pp. 1–5, doi: 10.1109/PIMRC.2008.4699692.

[109] J. A. García-Naya, C. Mehlführer, S. Caban, M. Rupp, and L. Castedo, "Throughput-based antenna selection measurements," in *IEEE 70th Vehicular Technology Conference Fall (VTC)*, Sep. 2009, pp. 1–5, doi: 10.1109/VETECF.2009.5378992.

[110] J. A. García-Naya, M. González-López, and L. Castedo, *Radio Communications*. In-Tech, Apr. 2010, ch. A Distributed Multilayer Software Architecture for MIMO Testbeds, ISBN: 9789533070919.

[111] J. A. García-Naya, H. J. Pérez-Iglesias, A. Dapena, and M. González-López, "Digital communications learning tools - gtTAL: Graphical tool for testbed-assisted learning," in *Proc. 2nd International Conference on Computer Supported Education (CSEDU)*, Valencia, Spain, Apr. 2010.

[112] D. Garlan and M. Shaw, "An introduction to software architecture," *Advances in software engineering and knowledge engineering*, vol. 1, pp. 1–40, 1993.

[113] M. Gastpar, B. Rimoldi, and M. Vetterli, "To code, or not to code: lossy source-channel communication revisited," *IEEE Transactions on Information Theory*, vol. 49, no. 5, pp. 1147–1158, May 2003, doi: 10.1109/TIT.2003.810631.

[114] A. B. Gershman and N. D. Sidiropoulos, *Space-Time Processing for MIMO Communications*. John Wiley & Sons, 2005. ISBN: 978-0470010020.

[115] D. Gesbert, M. Shafi, D. shan Shiu, P. J. Smith, and A. Naguib, "From theory to practice: an overview of mimo space-time coded wireless systems," *Selected Areas in Communications, IEEE Journal on*, vol. 21, no. 3, pp. 281–302, Apr. 2003, doi: 10.1109/JSAC.2003.809458.

[116] D. Gesbert, M. Shafi, D. Shiu, P. Smith, and A. Naguib, "From theory to practice: an overview of MIMO space-time coded wireless systems," *IEEE Journal on Selected Areas in Communications*, vol. 21, no. 3, pp. 281–302, Apr. 2003, doi: 10.1109/JSAC.2003.809458.

[117] M. Gharavi-Alkhansari and A. B. Gershman, "Fast antenna subset selection in MIMO systems," *IEEE Transactions on Signal Processing*, vol. 52, no. 2, pp. 339–347, Feb. 2004, doi: 10.1109/TSP.2003.821099.

[118] A. Ghrayeb, "A survey on antenna selection for MIMO communication systems," *in Proc. 2nd Information and Communication Technologies (ICTTA 2006)*, vol. 2, pp. 2104–2109, 2006, doi: 10.1109/ICTTA.2006.1684727.

[119] A. Ghrayeb and T. M. Duman, "Performance analysis of MIMO systems with antenna selection over quasi-static fading channels," *IEEE Transactions on Vehicular Technology*, vol. 52, no. 2, pp. 281–288, Mar. 2003, doi: 10.1109/TVT.2003.808792.

[120] T. J. Goblick, "Theoretical limitations on the transmission of data from analog sources," *IEEE Transactions on Information Theory*, vol. 11, no. 4, pp. 558–567, Oct. 1965.

[121] C. Gomez-Calero, L. Garcia-Garcia, and L. de Haro-Ariet, "New test-bed for evaluation of antenna and system performance for MIMO systems," in *First European Conference on Antennas and Propagation (EuCAP)*, Nov. 2006, pp. 1–5, doi: 10.1109/EUCAP.2006.4585036.

[122] M. González-López, "Técnicas avanzadas de procesado de señal para sistemas multiple-intput multiple-output (MIMO)," Ph.D. dissertation, University of A Coruña, Feb. 2004. URL: https://www.educacion.es/teseo/mostrarRef.do?ref=319464

[123] M. González-López, L. Castedo, and J. Frias, "BICM for MIMO systems using low-density generator matrix (LDGM) codes," in *Proc. IEEE International Conference on Acoustics, Speech, and Signal Processing (ICASSP)*, vol. 4, May 2004, pp. 677–680, doi: 10.1109/ICASSP.2004.1326917.

[124] M. González-López, L. Castedo, and J. Garcia-Frias, "Low density generator matrix codes for bit-interleaved coded modulation," in *Proc. IEEE 59th Vehicular Technology Conference (VTC)*, vol. 1, May 2004, pp. 338–342.

[125] M. Gonzalez-Lopez, F. J. Vazquez-Araujo, L. Castedo, and J. Garcia-Frias, "Optimized serially-concatenated LDGM and Alamouti codes for approaching MIMO capacity," in *Proc. IEEE 17th International Symposium on Personal, Indoor and Mobile Radio Communications*, Sep. 2006, pp. 1–5, doi: 10.1109/PIMRC.2006.253959.

[126] M. González-López, F. J. Vázquez-Araújo, L. Castedo, and J. Garcia-Frias, "Serially-concatenated low-density generator matrix (SCLDGM) codes for transmission over AWGN and Rayleigh fading channels," *IEEE Transactions on Wireless Communications*, vol. 6, no. 8, pp. 2753–2758, Aug. 2007, doi: 10.1109/TWC.2007.05283.

[127] M. Gonzalez-Lopez, F. J. Vazquez-Araujo, L. Castedo, and J. Garcia-Frias, "Turbo-like MIMO systems with and without space-time codes," in *Proc. 9th International Symposium on Signal Processing and Its Applications (ISSPA)*, Feb. 2007, pp. 1–6, doi: 10.1109/ISSPA.2007.4555628.

[128] A. Gorokhov, "Antenna selection algorithms for MEA transmission systems," *Proc. IEEE International Conference on Acoustics, Speech, and Signal Processing (ICASSP)*, vol. 3, pp. 2857–2860, 2002, doi: 10.1109/ICASSP.2002.1005282.

[129] A. Gorokhov, D. Gore, and A. Paulraj, "Receive antenna selection for MIMO flat-fading channels: theory and algorithms," *IEEE Transactions on Information Theory*, vol. 49, no. 10, pp. 2687–2696, Oct. 2003, doi: 10.1109/TIT.2003.817458.

[130] ——, "Performance bounds for antenna selection in MIMO systems," *Proc. IEEE International Conference on Communications (ICC)*, vol. 5, pp. 3021–3025, May 2003, doi: 10.1109/ICC.2003.1203962.

[131] P. Goud Jr., C. Schlegel, W. Krzymień, and R. Hang, "Multiple-antenna communication systems: an emerging technology," *Canadian Journal of Electrical and Computer Engineering*, vol. 29, no. 1/2, pp. 51–59, Jan. 2004, doi: 0.1109/CJECE.2004.1425797.

[132] T. Gucluoglu and T. Duman, "Performance analysis of transmit and receive antenna selection over flat fading channels," *IEEE Transactions on Wireless Communications*, vol. 7, no. 8, pp. 3056–3065, Aug. 2008, doi: 10.1109/TWC.2008.061087.

[133] T. Gucluoglu, T. M. Duman, and A. Ghrayeb, "Antenna selection for space time coding over frequency-selective fading channels," *Proc. IEEE International Conference on Acoustics, Speech, and Signal Processing (ICASSP)*, vol. 4, pp. 709–712, May 2004, doi: 10.1109/ICASSP.2004.1326925.

[134] S. Haene, D. Perels, and A. Burg, "A real-time 4-stream MIMO-OFDM transceiver: System design, FPGA implementation, and characterization," *IEEE Journal on Selected Areas in Communications*, vol. 26, no. 6, pp. 877–889, Aug. 2008, doi: 10.1109/JSAC.2008.080805.

[135] M. Hajiaghayi and C. Tellambura, "Antenna selection for unitary space-time modulation over correlated Rayleigh channels," *Proc. IEEE International Conference on Communications (ICC)*, pp. 3824–3828, May 2008, doi: 10.1109/ICC.2008.718.

[136] J. Heath, R. W. and D. J. Love, "Multimode antenna selection for spatial multiplexing systems with linear receivers," *IEEE Transactions on Signal Processing*, vol. 53, no. 8, pp. 3042–3056, Aug. 2005, doi: 10.1109/TSP.2005.851109.

[137] M. Heikkila and K. Majonen, "Increasing HSDPA throughput by employing space-time equalization," in *Proc. 15th IEEE International Symposium on Personal, Indoor and Mobile Radio Communications*, vol. 4, Sep. 2004, pp. 2328–2332. URL: http://ieeexplore.ieee.org/stamp/stamp.jsp?tp=&arnumber=1368735

[138] F. Hekland, G. E. Oien, and T. A. Ramstad, "Using 2:1 Shannon mapping for joint source-channel coding," in *Proc. Data Compression Conference (DCC)*, Mar. 2005, pp. 223–232, doi: 10.1109/DCC.2005.92.

[139] F. Hekland, P. A. Floor, and T. A. Ramstad, "Shannon-Kotel'nikov mappings in joint source-channel coding," *IEEE Transactions on Communications*, vol. 57, no. 1, pp. 94–105, Jan. 2009, doi: 10.1109/TCOMM.2009.0901.070075.

[140] W. Hirt and J. L. Massey, "Capacity of the discrete-time Gaussian channel with intersymbol interference," *IEEE Transactions on Information Theory*, vol. 34, no. 3, pp. 380–388, May 1988, doi: 10.1109/18.6015.

[141] B. M. Hochwald and T. L. Marzetta, "Unitary space-time modulation for multiple-antenna communications in Rayleigh flat fading," *IEEE Transactions on Information Theory*, vol. 46, no. 2, pp. 543–564, Mar. 2000, doi: 10.1109/18.825818.

[142] B. M. Hochwald and W. Sweldens, "Differential unitary space-time modulation," *IEEE Transactions on Communications*, vol. 48, no. 12, pp. 2041–2052, Dec. 2000, doi: 10.1109/26.891215.

[143] B. M. Hochwald, T. L. Marzetta, T. J. Richardson, W. Sweldens, and R. Urbanke, "Systematic design of unitary space-time constellations," *IEEE Transactions on Information Theory*, vol. 46, no. 6, pp. 1962–1973, Sep. 2000, doi: 10.1109/18.868472.

[144] B. Hochwald and S. ten Brink, "Achieving near-capacity on a multiple-antenna channel," *IEEE Transactions on Communications*, vol. 51, no. 3, pp. 389–399, Mar. 2003, doi: 10.1109/TCOMM.2003.809789.

[145] H. Holma and J. Reunanen, "3GPP release 5 HSDPA measurements," in *Proc. EEE International Symposium on Personal, Indoor and Mobile Radio Communications (PIMRC)*, Sep. 2006, doi: 10.1109/PIMRC.2006.254116.

[146] H. Holma, A. Toskala, K. Ranta-aho, and J. Pirskanen, "High-speed packet access evolution in 3GPP release 7 [topics in radio communications]," *IEEE Communications Magazine*, vol. 45, no. 12, pp. 29–35, Dec. 2007, doi: 10.1109/MCOM.2007.4395362.

[147] A. Honda, I. Ida, Y. Oishi, Q. T. Tran, S. Hara, and J.-i. Takada, "Experimental evaluation of MIMO antena selection system using RF-MEMS switches on a mobile terminal," *Proc. IEEE 18th International Symposium on Personal, Indoor and Mobile Radio Communications (PIMRC)*, pp. 1–5, Sep. 2007, doi: 10.1109/PIMRC.2007.4394576.

[148] A. Hottinen, M. Kuusela, K. Hugl, J. Zhang, and B. Raghothaman, "Industrial embrace of smart antennas and MIMO," *IEEE Wireless Communications*, vol. 13, no. 4, pp. 8–16, Aug. 2006, doi: 10.1109/MWC.2006.1678161.

[149] J. Hou, P. H. Siegel, L. B. Milstein, and H. D. Pfister, "Capacity-approaching bandwidth-efficient coded modulation schemes based on low-density parity-check codes," *IEEE Transactions on Information Theory*, vol. 49, no. 9, pp. 2141–2155, Sep. 2003, doi: 10.1109/TIT.2003.815777.

[150] J. Hou, P. Siegel, and L. Milstein, "Design of multi-input multi-output systems based on low-density parity-check codes," *IEEE Transactions on Communications*, vol. 53, no. 4, pp. 601–611, Apr. 2005, doi: 10.1109/TCOMM.2005.844972.

[151] Y. Hu, J. Garcia-Frias, and M. Lamarca, "MMSE decoding for analog joint source channel

coding using Monte Carlo importance sampling," in *Proc. IEEE 10th Workshop on Signal Processing Advances in Wireless Communications (SPAWC)*, Jun. 2009, pp. 682–686, doi: 10.1109/SPAWC.2009.5161872.

[152] ——, "Analog joint source channel coding using space-filling curves and MMSE decoding," in *Proc. Data Compression Conference (DCC)*, Mar. 2009, pp. 103–112, doi: 10.1109/DCC.2009.45.

[153] B. L. Hughes, "Differential space-time modulation," *IEEE Transactions on Information Theory*, vol. 46, no. 7, pp. 2567 –2578, Nov. 2000, doi: 10.1109/18.887864.

[154] R. M. M. Hunukumbure and M. A. Beach, "Outdoor MIMO measurements for UTRA applications," in *Proc. of EURO-COST 2002*, 2002. URL: http://hdl.handle.net/1983/887

[155] "IEEE standard for local and metropolitan area networks; part 16: Air interface for fixed broadband wireless access systems, IEEE Std. 802.16-2004," Oct. 2004. URL: http://standards.ieee.org/getieee802/download/802.16-2004.pdf

[156] "IEEE standard for local and metropolitan area networks; part 16: Air interface for fixed broadband wireless access systems, IEEE Std. 802.16-2004," Feb. 2006. URL: http://standards.ieee.org/getieee802/download/802.16e-2005.pdf

[157] A. Intarapanich, P. Kafle, R. Davies, A. Sesay, and J. McRory, "Spatial correlation measurements for broadband MIMO wireless channels," in *Proc. IEEE Vehicular Technology Conference Fall (VTC)*, vol. 1, Sep. 2004, pp. 52–56, doi: 10.1109/VETECF.2004.1399919.

[158] T. Isotalo and J. Lempiäinen, "HSDPA measurements for indoor DAS," in *Proc. IEEE Vehicular Technology Conference Spring (VTC)*, Apr. 2007, pp. 1127–1130, doi: 10.1109/VETECS.2007.239.

[159] V. J., S. I., and P. J., "A sufficient condition for blind identifiability of MIMO-OSTBC channels based on second order statistics," in *Proc. IEEE 7th Workshop on Signal Processing Advances in Wireless Communications (SPAWC)*, Jul. 2006, pp. 1–5, doi: 10.1109/SPAWC.2006.346374.

[160] H. Jafarkhani, *Space-time coding: theory and practice*. Cambridge University Press, Oct. 2005. ISBN: 0521842913.

[161] J. Jalden, C. Martin, and B. Ottersten, "Semidefinite programming for detection in linear systems - optimality conditions and space-time decoding," in *Proc. 2003 IEEE International Conference on Acoustics, Speech, and Signal Processing (ICASSP)*, vol. 4, Apr. 2003, pp. 9–12.

[162] C. Jandura, P. Marsch, A. Zoch, and G. P. Fettweis, "A testbed for cooperative multi cell algorithms," in *Proc. 4th International Conference on Testbeds and research infrastructures for the development of networks & communities (TridentCom'08)*, Innsbruck, Austria, Mar. 2008, pp. 1–5, ISBN: 978-963-9799-24-0. URL: http://portal.acm.org/citation.cfm?id=1390576.1390600

[163] B. Johansson and T. Sundin, "LTE test bed," Ericsson, Tech. Rep., 2007. URL: http://www.ericsson.com/ericsson/corpinfo/publications/review/2007_01/files/2_lte_web.pdf

[164] V. Jungnickel, V. Pohl, and C. von Helmolt, "Capacity of MIMO systems with closely spaced antennas," *IEEE Communications Letters*, vol. 7, no. 8, pp. 361–363, Aug. 2003, doi:

10.1109/LCOMM.2003.815644.

[165] V. Jungnickel, S. Jaeckel, L. Thiele, U. Krueger, A. Brylka, and C. Helmolt, "Capacity measurements in a multicell MIMO system," in *IEEE Global Telecommunications Conference (GLOBECOM)*, Dec. 2006, pp. 1–6, doi: 10.1109/GLOCOM.2006.645.

[166] T. Kaiser, A. Wilzeck, M. Berentsen, and M. Rupp, "Prototyping for MIMO systems - an overview," in *Proc. 12th European Signal Processing Conference (EUSIPCO)*, 2004.

[167] C. G. Kakoyiannis and P. Constantinou, "Co-design of antenna element and ground plane for printed monopoles embedded in wireless sensors," in *Proc. 2nd International Conference on Sensor Technologies and Applications (SENSORCOMM)*, 2008, pp. 413–418.

[168] C. G. Kakoyiannis, S. V. Troubouki, and P. Constantinou, "Design and implementation of printed multi-element antennas on wireless sensor nodes," in *Proc. 3rd International Symposium on Wireless Pervasive Computing (ISWPC)*, 2008, pp. 224–228.

[169] F. Kaltenberger, R. Ghaffar, R. Knopp, and C. Anouar, H. nad Bonnet, "Design and implementation of a single-frequency mesh network using OpenAirInterface," *EURASIP Journal on Wireless Communications and Networking*, vol. 2010, pp. 1–16, 2010, doi: 10.1155/2010/719523.

[170] P.-S. Kildal and K. Rosengren, "Correlation and capacity of MIMO systems and mutual coupling, radiation efficiency, and diversity gain of their antennas: simulations and measurements in a reverberation chamber," *IEEE Communications Magazine*, vol. 42, no. 12, pp. 104–112, Dec. 2004, doi: 10.1109/MCOM.2004.1367562.

[171] D. Kim and M. Torlak, "Rapid prototyping of a cost effective and flexible 4x4 mimo testbed," in *Proc. 5th IEEE Sensor Array and Multichannel Signal Processing Workshop (SAM 2008)*, Darmstadt, Germany, Jul. 2008, pp. 5–8, doi: 10.1109/SAM.2008.4606812.

[172] J. Kim, S. Hyeon, and S. Choi, "Implementation of an SDR system using graphics processing unit," *IEEE Communications Magazine*, vol. 48, no. 3, pp. 156–162, Mar. 2010, doi: 10.1109/MCOM.2010.5434388.

[173] J. Kivinen, X. Zhao, and P. Vainikainen, "Empirical characterization of wideband indoor radio channel at 5.3 GHz," *IEEE Transactions on Antennas and Propagation*, vol. 49, no. 8, pp. 1192–1203, Aug. 2001, doi: 10.1109/8.943314.

[174] J. Koivunen, P. Almers, V.-M. Kolmonen, J. Salmi, A. Richter, F. Tufvesson, P. Suvikunnas, A. F. Molisch, and P. Vainikainen, "Dynamic multi-link indoor MIMO measurements at 5.3 GHz," in *Proc. The Second European Conference on Antennas and Propagation (EuCAP 2007)*, Edinburgh, UK, Nov. 2007, pp. 1–6, ISBN: 978-0-86341-842-6. URL: http://ieeexplore.ieee.org/stamp/stamp.jsp?arnumber=4458444&isnumber=4458235

[175] D. Kühling, A. Ibing, and V. Jungnickel, "12x12 MIMO-OFDM realtime implementation for 3GPP LTE+ on a cell processor," in *Proc. 14th European Wireless Conference (EW 2008)*, Prague, Czech Republic, Jun. 2008, pp. 1–5, doi: 10.1109/EW.2008.4623917.

[176] J. Kunze, C. Schmits, A. Bilgic, and J. Hausner, "Receive antenna diversity architectures for

HSDPA," in *Proc. IEEE Vehicular Technology Conference Spring (VTC)*, May 2008, pp. 2071–2075, doi: 10.1109/VETECS.2008.465.

[177] J.-B. Landre and A. Saadani, "HSDPA 14.4 Mbps mobiles - realistic throughputs evaluation," in *Proc. IEEE Vehicular Technology Conference Spring (VTC)*, May 2008, pp. 2086–2090, doi: 10.1109/VETECS.2008.468.

[178] S. Lang and B. Daneshrad, "The development and applications of a dual-band, 8x8 MIMO testbed with digital IF and DDFS," in *Proc. International Conference on Wireless Broadband and Ultra Wideband Communications (Auswireless 2006)*, Sydney, Australia, Mar. 2006, p. 6. URL: http://hdl.handle.net/2100/92

[179] S. Lang, R. M. Rao, and B. Daneshrad, "Design and development of a 5.25 GHz software defined wireless OFDM communication platform," *IEEE Communications Magazine*, vol. 42, no. 6, pp. 6–12, Jun. 2004, doi: 10.1109/MCOM.2004.1304225.

[180] E. G. Larsson, P. Stoica, and G. Ganesan, *Space-Time Block Coding for Wireless Communications*. New York, USA: Cambridge University Press, 2003.   ISBN: 0521824567.

[181] C. Lau and C. Leung, "Antenna selection in a multi-sector packet radio network," in *Proc. IEEE International Conference on Communications (ICC)*, vol. 1, Jun. 1989, pp. 188–192, doi: 10.1109/ICC.1989.49691.

[182] C. T. Lau and C. Leung, "A slotted ALOHA packet radio system with multiple antennas and receivers," *IEEE Transactions on Vehicular Technology*, vol. 39, no. 3, pp. 218–226, Aug. 1990, doi: 10.1109/25.131003.

[183] W. Lee, "Effects on correlation between two mobile radio base-station antennas," *IEEE Transactions on Communications*, vol. 21, no. 11, pp. 1214–1224, Nov. 1973.

[184] J. C. Liberti, J. C. Koshy, T. R. Hoerning, C. C. Martin, J. L. Dixon, A. A. Triolo, R. R. Murray, and T. G. McGiffen, "Experimental results using a MIMO test bed for wideband, high spectral efficiency tactical communications," in *Proc. IEEE Military Communications Conference (MILCOM 2005)*, vol. 3, Atlantic City, USA, Oct. 2005, pp. 1340–1345, doi: 10.1109/MILCOM.2005.1605864.

[185] H. S. Lichte, S. Valentin, F. Eitzen, M. Stege, C. Unger, and H. Karl, "Integrating multiuser dynamic OFDMA into IEEE 802.11a and prototyping it on a real-time software-defined radio testbed," in *Proc. 3rd International Conference on Testbeds and Research Infrastructure for the Development of Networks and Communities (TridentCom 2007)*, Orlando, Florida, USA, May 2007, pp. 1–9, doi: 10.1109/TRIDENTCOM.2007.4444671.

[186] R. Love, K. Stewart, R. Bachu, and A. Ghosh, "MMSE equalization for UMTS HSDPA," in *Proc. 58th IEEE Vehicular Technology Conference Fall (VTC)*, vol. 4, Oct. 2003, pp. 2416–2420, doi: 10.1109/VETECF.2003.1285963.

[187] B. Lu, X. Wang, and K. Narayanan, "LDPC-based space-time coded OFDM systems over correlated fading channels: Performance analysis and receiver design," *IEEE Transactions on Communications*, vol. 50, no. 1, pp. 74–88, Jan. 2002, doi: 10.1109/26.975756.

[188] B. Lu, G. Yue, and X. Wang, "Performance analysis and design optimization of LDPC-coded MIMO OFDM systems," *IEEE Transactions on Signal Processing*, vol. 52, no. 2, pp. 348–361, Feb. 2004, doi: 10.1109/TSP.2003.820991.

[189] P. Luethi, M. Wenk, T. Koch, W. Fichtner, M. Lerjen, and N. Felber, "Multi-user MIMO testbed," in *Proc. Third ACM international workshop on Wireless network testbeds, experimental evaluation and characterization (WiNTECH'08)*, San Francisco, California, USA, Sep. 2008, pp. 109–110, ISBN: 978-1-60558-187-3, doi: 10.1145/1410077.1410104.

[190] J. Luo, J. R. Zeidler, and S. McLaughlin, "Performance analysis of compact antenna arrays with MRC in correlated nakagami fading channels," *IEEE Transactions on Vehicular Technology*, vol. 50, no. 1, pp. 267–277, Jan. 2001, doi: 10.1109/25.917940.

[191] Q. Ma and C. Tepedelenlioglu, "Antenna selection for unitary space-time modulation," *IEEE Transactions on Information Theory*, vol. 51, no. 10, pp. 3620–3631, Oct. 2005, doi: 10.1109/TIT.2005.855602.

[192] D. MacKay and R. Neal, "Good codes based on very sparse matrices," *Cryptography and coding*, pp. 100–111, Jan. 1995, doi: 10.1007/3-540-60693-9.

[193] D. J. C. MacKay, "Good error-correcting codes based on very sparse matrices," in *Information Theory. 1997. Proceedings., 1997 IEEE International Symposium on*, Jun. 1997, doi: 10.1109/ISIT.1997.613028.

[194] M. Malkowski, "Link-level comparison of IP-OFDMA (mobile WiMAX) and UMTS HSDPA," in *Proc. 18th IEEE International Symposium on Personal, Indoor and Mobile Radio Communications (PIMRC)*, Sep. 2007, pp. 1–5, doi: 10.1109/PIMRC.2007.4394134.

[195] K. Mandke, S.-H. Choi, G. Kim, R. Grant, R. C. Daniels, W. Kim, R. W. Heath Jr., and S. M. Nettles, "Early results on hydra: A flexible MAC/PHY multihop testbed," in *Proc. IEEE 65th Vehicular Technology Conference, 2007 (VTC 2007-Spring)*, Dublin, Ireland, Apr. 2007, pp. 1896–1900, doi: 10.1109/VETECS.2007.393.

[196] J. Medbo, F. Harrysson, H. Asplund, and J.-E. Berger, "Measurements and analysis of a MIMO macrocell outdoor-indoor scenario at 1947 MHz," in *Proc. IEEE Vehicular Technology Conference Spring (VTC)*, vol. 1, May 2004, pp. 261–265. URL: http://ieeexplore.ieee.org/stamp/stamp.jsp?tp=&arnumber=1387954

[197] J. Medbo, M. Riback, and J.-E. Berg, "Validation of 3GPP spatial channel model including WINNER wideband extension using measurements," in *Proc. Vehicular Technology Conference Fall (VTC)*, Sep. 2006, pp. 1–5, doi: 10.1109/VTCF.2006.36.

[198] C. Mehlführer, M. Rupp, F. Kaltenberger, and G. Humer, "A scalable rapid prototyping system for real-time MIMO OFDM transmissions," in *Proc. The 2nd IEE/EURASIP Conference on DSPenabledRadio (Ref. No. 2005/11086)*, Southhampton, UK, Sep. 2005, p. 7. URL: http://publik.tuwien.ac.at/files/pub-et_10207.pdf

[199] C. Mehlführer, S. Caban, M. Wrulich, and M. Rupp, "Joint throughput optimized CQI and precoding weight calculation for MIMO HSDPA," *Conference Record of the Fourtysecond*

Asilomar Conference on Signals, Systems and Computers, 2008, pp. 1320–1325, Oct. 2008, doi: 10.1109/ACSSC.2008.5074632.

[200] C. Mehlführer, "Measurement-based performance evaluation of WiMAX and HSDPA," Ph.D. dissertation, Vienna University of Technology, Sep. 2009. URL: http://www.nt.tuwien.ac.at/fileadmin/data/testbed/diss-mc.pdf

[201] C. Mehlführer, S. Caban, and M. Rupp, "Experimental evaluation of adaptive modulation and coding in MIMO WiMAX with limited feedback," *EURASIP Journal on Advances in Signal Processing*, vol. 2008, 2008, doi: 10.1155/2008/837102.

[202] C. Mehlführer, S. Caban, J. A. García-Naya, and M. Rupp, "Throughput and capacity of MIMO WiMAX," in *Conference Record of the 43rd Asilomar Conference on Signals, Systems and Computers*, Pacific Grove, CA, USA, Nov. 2009. URL: http://publik.tuwien.ac.at/files/PubDat_178050.pdf

[203] C. Mehlführer, S. Caban, and M. Rupp, "MIMO HSDPA throughput measurement results in an urban scenario," in *Proc. 70th IEEE Vehicular Technology Conference (VTC2009-Fall)*, Anchorage, AK, USA, Sep. 2009, doi: 10.1109/VETECF.2009.5378994.

[204] M. Mendicute, J. Altuna, G. Landaburu, and V. Atxa, "Platform for joint evaluation of FPGA-implemented and matlab algorithms in real MIMO transmissions," in *Proc. The 2nd IEE/EURASIP Conference on DSPenabledRadio (Ref. No. 2005/11086)*, Southhampton, UK, Sep. 2005, p. 6. URL: http://ieeexplore.ieee.org/stamp/stamp.jsp?arnumber=1575329&isnumber=33305

[205] I. Mitola, J., "Software radios-survey, critical evaluation and future directions," in *Proc. National Telesystems Conference (NTC)*, May 1992, pp. 13/15 –13/23, doi: 10.1109/NTC.1992.267870.

[206] ——, "Software radio architecture: a mathematical perspective," *IEEE Journal on Selected Areas in Communications*, vol. 17, no. 4, pp. 514–538, Apr. 1999, doi: 10.1109/49.761033.

[207] J. Mitola, "The software radio architecture," *IEEE Communications Magazine*, vol. 33, no. 5, pp. 26–38, May 1995, doi: 10.1109/35.393001.

[208] A. F. Molisch, "MIMO systems with antenna selection – an overview," *Proc. Radio and Wireless Conference (RAWCON)*, pp. 167–170, Aug. 2003, doi: 10.1109/RAWCON.2003.1227919.

[209] A. F. Molisch and M. Z. Win, "MIMO systems with antenna selection," *IEEE Microwave Magazine*, vol. 5, no. 1, pp. 46–56, Mar. 2004, doi: 10.1109/MMW.2004.1284943.

[210] A. F. Molisch and X. Zhang, "FFT-based hybrid antenna selection schemes for spatially correlated MIMO channels," *IEEE Communications Letter*, vol. 8, no. 1, pp. 36–38, Jan. 2004, doi: 10.1109/LCOMM.2003.822512.

[211] A. F. Molisch, M. Z. Win, and J. H. Winters, "Capacity of MIMO systems with antenna selection," *Proc. IEEE International Conference on Communications (ICC)*, vol. 2, pp. 570–574, 2001, doi: 10.1109/ICC.2001.937004.

[212] A. F. Molisch, M. Z. Win, Y.-S. Choi, and J. H. Winters, "Capacity of MIMO systems with antenna selection," *IEEE Transactions on Wireless Communications*, vol. 4, no. 4, pp. 1759–1772, Jul.

2005, doi: 10.1109/TWC.2005.850307.

[213] A. F. Molisch, N. B. Mehta, H. Zhang, P. Almers, and J. Zhang, "Implementation aspects of antenna selection for MIMO systems," *Proc. 1st International Conference on Communications and Networking in China (ChinaCom)*, pp. 1–7, Oct. 2006, doi: 10.1109/CHINACOM.2006.344916.

[214] T. K. Moon and W. C. Stirling, *Mathematical Methods and Algorithms for Signal processing*, 1st ed. Upper Saddle River, NJ: Prentice Hall, 2000. ISBN: 9780201361865.

[215] G. E. Moore, "Cramming more components onto integrated circuits," *Proceedings of the IEEE*, vol. 86, no. 1, pp. 82–85, Jan. 1998, doi: 10.1109/JPROC.1998.658762.

[216] R. Morawski, T. Le-Ngoc, and O. Naeem, "Wireless and wireline MIMO testbed," in *Proc. IEEE Canadian Conference on Electrical and Computer Engineering (CCECE)*, vol. 3, May 2003, pp. 1913–1916.

[217] R. Mostafa, R. Gozali, R. C. Palat, M. Robert, W. G. Newhall, B. D. Woerner, and J. H. Reed, "Design and implementation of a DSP-based MIMO system prototype for real-time demonstration and indoor channel measurements," *EURASIP Journal on Applied Signal Processing*, vol. 2005, no. 16, pp. 2673–2685, 2005, doi: 10.1155/ASP.2005.2673.

[218] P. Murphy, A. Sabharwal, and B. Aazhang, "Design of WARP: a wireless open-access research platform," in *Proc. 14th European Signal Processing Conference (EUSIPCO 2006)*, Florence, Italy, Sep. 2006, p. 5. URL: http://scholarship.rice.edu/bitstream/handle/1911/20129/Mur2006Sep5DesignofWA.PDF?sequence=1

[219] M. Myllyla, M. Juntti, M. Limingoja, A. Byman, and J. R. Cavallaro, "Performance evaluation of two LMMSE detectors in a MIMO-OFDM hardware testbed," in *Proc. Fortieth Asilomar Conference on Signals, Systems and Computers (ACSSC'06)*, PACIFIC GROVE, CALIFORNIA, USA, Oct. 2006, pp. 1161–1165, doi: 10.1109/ACSSC.2006.354937.

[220] A. F. Naguib, V. Tarokh, N. Seshadri, and A. R. Calderbank, "A space-time coding modem for high-data-rate wireless communications," *IEEE Journal on Selected Areas in Communications*, vol. 16, no. 8, pp. 1459 –1478, Oct. 1998, doi: 10.1109/49.730454.

[221] A. F. Naguib, N. Seshadri, and A. R. Calderbank, "Increasing data rate over wireless channels," *IEEE Signal Processing Magazine*, vol. 17, no. 3, pp. 76–92, May 2000, doi: 10.1109/79.841731.

[222] M. Nakamura, Y. Awad, and S. Vadgama, "Adaptive control of link adaptation for high speed downlink packet access (HSDPA) in W-CDMA," in *Proc. 5th International Symposium on Wireless Personal Multimedia Communications*, vol. 2, Oct. 2002, pp. 382–386, doi: 10.1109/WPMC.2002.1088198.

[223] Nanyang Technological University, "MIMO-OFDM testbed for mobile WiMAX," Nanyang Technological Universit, Positioning and Wireless Technology Centre, Tech. Rep., 2008. URL: http://users.rsise.anu.edu.au/~bradyu/Work/MIMO-OFDM%20Project%20PWTC%20NTU.pdf

[224] X. Nieto, L. Ventura, and A. Mollfulleda, "GEDOMIS: a broadband wireless MIMO-OFDM testbed, design and implementation," in *Proc. 2nd International Conference on Testbeds and*

Research Infrastructures for the Development of Networks and Communities (TRIDENTCOM 2006), Barcelona, Spain, Mar. 2006, p. 10, doi: 10.1109/TRIDNT.2006.1649135.

[225] K. Nishimori, R. Kudo, N. Honma, Y. Takatori, O. Atsushi, and K. Okada, "Experimental evaluation using 16x16 multiuser MIMO testbed in an actual indoor scenario," in *Proc. IEEE Antennas and Propagation Society International Symposium (AP-S 2008)*, San Diego, California, USA, Jul. 2008, pp. 1–4, doi: 10.1109/APS.2008.4619160.

[226] H.-T. Pai, "Limited feedback for antenna selection in MIMO-OFDM systems," in *3rd IEEE Consumer Communications and Networking Conference (CCNC)*, vol. 2, Jan. 2006, pp. 052–1056.

[227] T. Pande, D. J. Love, and J. V. Krogmeier, "Reduced feedback MIMO-OFDM precoding and antenna selection," *IEEE Transactions on Signal Processing*, vol. 55, no. 5, pp. 2284–2293, May 2007, doi: 10.1109/TSP.2006.890936.

[228] C. S. Park and K. B. Lee, "Statistical multimode transmit antenna selection for limited feedback MIMO systems," *IEEE Transactions on Wireless Communications*, vol. 7, no. 11, pp. 4432–4438, Nov. 2008, doi: 10.1109/T-WC.2008.060213.

[229] J. Park, K. woo Kim, T. Song, S. M. Lee, J. Hur, K. Lim, and J. Laskar, "A cross-layer cognitive radio testbed for the evaluation of spectrum sensing receiver and interference analysis," in *3rd International Conference on Cognitive Radio Oriented Wireless Networks and Communications (CrownCom)*, May 2008, pp. 1–6, doi: 10.1109/CROWNCOM.2008.4562483.

[230] A. J. Paulraj, D. A. Gore, R. U. Nabar, and H. Bolcskei, "An overview of MIMO communications - a key to gigabit wireless," *Proceedings of the IEEE*, vol. 92, no. 2, pp. 198–218, Feb. 2004, doi: 10.1109/JPROC.2003.821915.

[231] "Increasing capacity in wireless broadcast systems using distributed transmission/directional reception (DTDR)," Sep. 1994, US Patent 5,345,599.

[232] A. Paulraj, R. Nabar, and D. Gore, Eds., *Introduction to Space-Time Wireless Communications*, 1st ed. Cambridge University Press, 2003. ISBN: 0-521-82615-2.

[233] K. Pedersen, P. Mogensen, and B. Fleury, "Spatial channel characteristics in outdoor environments and their impact on BS antenna system performance," in *Proc. IEEE Vehicular Technology Conference (VTC)*, vol. 2, May 1998, pp. 719–723, doi: 10.1109/VETEC.1998.683676.

[234] K. Pentikousis, E. Piri, J. Pinola, F. Fitzek, T. Nissilä, and I. Harjula, "Empirical evaluation of VoIP aggregation over a fixed WiMAX testbed," in *Proc. 4th International Conference on Testbeds and research infrastructures for the development of networks & communities (TridentCom'08)*, Innsbruck, Austria, Mar. 2008, pp. 1–10, ISBN: 978-963-9799-24-0. URL: http://portal.acm.org/citation.cfm?id=1390599#

[235] H. J. Pérez-Iglesias, A. Dapena, L. Castedo, and V. Zarzoso, "Blind channel identification for Alamoutis coding systems based on eigenvector decomposition," in *Proc. 13th European Wireless Conference*, Apr. 2007.

[236] H. J. Pérez-Iglesias, J. A. García-Naya, and A. Dapena, "A blind channel estimation strategy

for the 2x1 Alamouti system based on diagonalising 4th-order cumulant matrices," in *IEEE International Conference on Acoustics, Speech and Signal Processing (ICASSP)*, Apr. 2008, pp. 3329–3332, doi: 10.1109/ICASSP.2008.4518363.

[237] H. J. Pérez-Iglesias, J. A. García-Naya, A. Dapena, L. Castedo, and V. Zarzoso, "Blind channel identification in Alamouti coded systems: a comparative study of eigendecomposition methods in indoor transmissions at 2.4 GHz," *European Transactions on Telecommunications. Special Issue: European Wireless 2007*, vol. 19, no. 7, pp. 751–759, Nov. 2008, doi: 10.1002/ett.1321.

[238] J. G. Proakis, *Digital Communications*.   McGraw-Hill, 4th edition, Aug. 2000.   ISBN: 978-0072321111.

[239] G. G. Raleigh and J. M. Cioffi, "Spatio-temporal coding for wireless communication," *IEEE Transactions on Communications*, vol. 46, no. 3, pp. 357–366, Mar. 1998, doi: 10.1109/26.662641.

[240] D. Ramírez, I. Santamaría, J. Pérez, J. Vía, A. Tazón, J. A. García-Naya, T. M. Fernández-Caramés, M. González López, H. J. Pérez-Iglesias, and L. Castedo, "A flexible testbed for the rapid prototyping of MIMO baseband modules," in *Proc. 3rd International Symposium on Wireless Communication Systems (ISWCS)*, Sep. 2006, pp. 776–780, doi: 10.1109/ISWCS.2006.4362407.

[241] D. Ramírez, I. Santamaría, J. Pérez, J. Vía, J. A. García-Naya, T. M. Fernández-Caramés, H. J. Pérez-Iglesias, M. González López, L. Castedo, and J. M. Torres-Royo, "A comparative study of STBC transmissions at 2.4 GHz over indoor channels using a 2x2 MIMO testbed," *Wireless Communications and Mobile Computing*, vol. 8, no. 9, pp. 1149–1164, Nov. 2008, doi: 10.1002/wcm.558.

[242] T. A. Ramstad, "Shannon mappings for robust communication," *Telektronikk*, vol. 98, no. 1, pp. 114–128, 2002.

[243] R. Rao, W. Zhu, S. Lang, C. Oberli, D. Browne, J. Bhatia, J.-F. Frigon, J. Wang, P. Gupta, H. Lee, D. Liu, S. Wong, M. Fitz, B. Daneshrad, and O. Takeshita, "Multi-antenna testbeds for research and education in wireless communications," *IEEE Communications Magazine*, vol. 42, no. 12, pp. 72–81, Dec. 2004, doi: 10.1109/MCOM.2004.1367558.

[244] S.-B. Rhee and G. Zysman, "Results of suburban base station spatial diversity measurements in the UHF band," *IEEE Transactions on Communications*, vol. 22, no. 10, pp. 1630–1636, Oct. 1974.

[245] M. Riback, S. Grant, G. Jongren, T. Tynderfeldt, D. Cairns, and T. Fulghum, "MIMO-HSPA testbed performance measurements," in *Proc. EEE International Symposium on Personal, Indoor and Mobile Radio Communications (PIMRC)*, Sep. 2007, doi: 10.1109/PIMRC.2007.4394434.

[246] J. Rinas and K.-D. Kammeyer, "MIMO measurements of communication signals and application of blind source separation," in *Proc. 3rd IEEE International Symposium on Signal Processing and Information Technology (ISSPIT 2003)*, Darmstadt, Germany, Dec. 2003, pp. 94–97, doi: 10.1109/ISSPIT.2003.1341068. URL:

http://www.ant.uni-bremen.de/sixcms/media.php/102/4647/ISSPIT_2003_rinas.pdf

[247] J. Rodas, J. A. García-Naya, C. J. Escudero, and L. Castedo, "GNU Radio: A new paradigm for software defined radio," in *Proc. 49th FYTCE European Congress*, Sep. 2010.

[248] T. J. Rouhpael, *RF and Digital Signal Processing for Software-Defined Radio. A Multi-Standard Multi-Mode Approach.* USA: Elsevier, 2009. ISBN: 978-0-7506-8210-7.

[249] S. Roy, J.-F. Boudreault, and L. Dupont, "An end-to-end prototyping framework for compliant wireless LAN transceivers with smart antennas," *Computer Communications*, vol. 31, no. 8, pp. 1551–1563, 2008, doi: 10.1016/j.comcom.2008.01.016.

[250] D. Rudd, "Spectrum pricing's uncertain future," *Electronics world*, vol. 108, no. 1796, pp. 24–5, 2002.

[251] M. Rupp, A. Burg, and E. Beck, "Rapid prototyping for wireless designs: the five-ones approach," *Signal Processing*, vol. 83, no. 7, pp. 1427–1444, 2003.

[252] M. Rupp, C. Mehlführer, S. Caban, R. Langwieser, L. W. Mayer, and A. L. Scholtz, "Testbeds and rapid prototyping in wireless system design," *EURASIP Newsletter*, vol. 17, no. 3, pp. 32–50, Sep. 2006.

[253] M. Rupp, S. Caban, and C. Mehlführer, "Challenges in building MIMO testbeds," in *Proc. of the 13th European Signal Processing Conference (EUSIPCO 2007)*, Poznan, Poland, Sep. 2007.

[254] M. Rupp, J. A. García-Naya, C. Mehlführer, S. Caban, and L. Castedo, "On mutual information and capacity in frequency selective wireless channels," in *Proc. International Conference on Communications (ICC)*, May 2010.

[255] J. Salz, "Digital transmission over cross-coupled linear channels," *AT&T Technical Journal*, vol. 64, pp. 1147–1159, 1985.

[256] D. Samardzija, A. Lozano, and C. Papadias, "Experimental validation of MIMO multiuser detection for UMTS high-speed downlink packet access," in *Proc. IEEE Global Telecommunications Conference (GLOBECOM)*, vol. 6, Dallas, Texas, USA, Nov. 2004, pp. 3840–3844, doi: 10.1109/GLOCOM.2004.1379087.

[257] S. Sanayei and A. Nosratinia, "Antenna selection in MIMO systems," *IEEE Communications Magazine*, vol. 42, no. 10, pp. 68–73, Oct. 2004, doi: 10.1109/MCOM.2004.1341263.

[258] S. Sandhu and A. Paulraj, "Space-time block codes: a capacity perspective," *IEEE Communications Letters*, vol. 4, no. 12, pp. 384–386, Dec. 2000, doi: 10.1109/4234.898716.

[259] M. Sayed Khairy, C. Mehlführer, and M. Rupp, "Proc. boosting sphere decoding speed through graphic processing units," in *16th European Wireless Conference*, Lucca, Italy, Apr. 2010. URL: http://publik.tuwien.ac.at/files/PubDat_184823.pdf

[260] S. Shahbazpanahi, A. B. Gershman, and J. H. Manton, "Closed-form blind MIMO channel estimation for orthogonal space-time block codes," *IEEE Transactions on Signal Processing*, vol. 53, no. 12, pp. 4506–4517, Dec. 2005, doi: 10.1109/TSP.2005.859331.

[261] C. E. Shannon, "A mathematical theory of communication," *The Bell System Technical Journal*,

vol. 7, pp. 379–423, 1948.

[262] C. E. Shannon and W. Weaver, *The Mathematical Theory of Communication*. Urbana, Illinois, USA: The University of Illinois Press, 1949. ISBN: 0-252-72548-4.

[263] M. Shaw and D. Garlan, *Software architecture: perspectives on an emerging discipline*. Prentice Hall Englewood Cliffs, NJ, 1996. ISBN: 978-0131829572.

[264] D.-S. Shiu, G. J. Foschini, M. J. Gans, and J. M. Kahn, "Fading correlation and its effect on the capacity of multielement antenna systems," *IEEE Transactions on Communications*, vol. 48, no. 3, pp. 502–513, Mar. 2000, doi: 10.1109/26.837052.

[265] N. Skentos, A. Kanatas, G. Pantos, and P. Constantinou, "Capacity results from short range fixed MIMO measurements at 5.2 GHz in urban propagation environment," in *Proc. IEEE International Conference on Communications (ICC)*, vol. 5, Jun. 2004, pp. 3020–3024, doi: 10.1109/ICC.2004.1313086.

[266] S. St. Lauren, J. Johnston, E. Dumbill, and D. Winer, *Programming Web Services with XML-RPC*. O'Reilly Media; 1st edition, 2001. ISBN: 978-0596001193.

[267] P. Stoica and G. Ganesan, "Space-time block codes: trained, blind, and semi-blind detection," *Digital Signal Processing*, vol. 13, no. 1, pp. 93–105, Jan. 2003.

[268] G. L. Stüber, J. R. Barry, S. W. McLaughlin, Y. Li, M. A. Ingram, and T. G. Pratt, "Broadband MIMO-OFDM wireless communications," *Proceedings of the IEEE*, vol. 92, no. 2, pp. 271–294, Feb. 2004, doi: 10.1109/JPROC.2003.821912.

[269] R. Stuhlberger, L. Maurer, G. Hueber, and A. Springer, "The impact of RF-impairments and automatic gain control on UMTS-HSDPA-throughput performance," in *Proc. IEEE 64th Vehicular Technology Conference Fall (VTC)*, Sep. 2006, pp. 1–5, doi: 10.1109/VTCF.2006.389.

[270] P. Suárez-Casal, A. Carro-Lagoa, T. M. Fernández Caramés, and L. Castedo, "Diseño FPGA de un emulador de canal para WiMAX," in *Proc. XXIII Simposium Nacional de la Unión Científica Internacional de Radio (URSI)*, Madrid, Spain, Sep. 2008.

[271] P. Suárez-Casal, A. Carro-Lagoa, J. A. García-Naya, L. Castedo, J. M. Camas, A. Morales, and A. Quintana, "OFDMA PHY layer real-time implementation using SDR and COTS modules," in *SDR Forum*, 2009.

[272] P. Suárez-Casal, A. Carro-Lagoa, J. A. García-Naya, and L. Castedo, "A multicore SDR architecture for reconfigurable WiMAX downlink," in *Proc. 13th EUROMICRO Conference on Digital System Design (DSD)*, Lille, France, Sep. 2010.

[273] P. Sudarshan, N. Mehta, A. Molisch, and J. Zhang, "Antenna selection with RF pre-processing: robustness to RF and selection non-idealities," *Radio and Wireless Conference, 2004 IEEE*, pp. 391–394, Sep. 2004.

[274] P. Sudarshan, N. B. Mehta, A. F. Molisch, and J. Zhang, "Channel statistics-based RF pre-processing with antenna selection," *IEEE Transactions on Wireless Communications*, vol. 5, no. 12, pp. 3501–3511, Dec. 2006, doi: 10.1109/TWC.2006.256973.

[275] J. Sun, L. Wei, X. Du, and D. Yuan, "Development of a DSP and FPGA based real time MIMO prototyping testbed," in *5th International Conference on Wireless Communications, Networking and Mobile Computing (WiCom)*, Sep. 2009, pp. 1–4, doi: 10.1109/WICOM.2009.5301760.

[276] H. Suzuki, B. Murray, A. Grancea, R. Shaw, J. Pathikulangara, and I. B. Collings, "Real-time wideband MIMO demonstrator," in *Proc. International Symposium on Communications and Information Technologies (ISCIT'07)*, Sydney, Australia, Oct. 2007, pp. 284–289, doi: 10.1109/ISCIT.2007.4392031.

[277] Z. Tang, H. Suzuki, and I. B. Collings, "Performance of antenna selection for MIMO-OFDM systems based on measured indoor correlated frequency selective channels," *Proc. Australian Telecommunication Networks and Applications Conference (ATNAC)*, Dec. 2006.

[278] V. Tarokh and H. Jafarkhani, "A differential detection scheme for transmit diversity," *IEEE Journal on Selected Areas in Communications*, vol. 18, no. 7, pp. 1169–1174, Jul. 2000, doi: 10.1109/49.857917.

[279] V. Tarokh, H. Jafarkhani, and A. R. Calderbank, "Space-time block codes from orthogonal designs," *IEEE Transactions on Information Theory*, vol. 45, no. 5, pp. 1456 –1467, Jul. 1999, doi: 10.1109/18.771146.

[280] I. Telatar, "Capacity of multi-antenna Gaussian channels," *European Transactions on Telecommunications*, vol. 10, no. 6, pp. 585–596, 1999.

[281] S. ten Brink, G. Kramer, and A. Ashikhmin, "Design of low-density parity-check codes for modulation and detection," *IEEE Transactions on Communications*, vol. 52, no. 4, pp. 670–678, Apr. 2004, doi: 10.1109/TCOMM.2004.826370.

[282] T. A. Thomas, V. Desai, and J. F. Kepler, "Experimental MIMO comparisons of a 4-element uniform linear array to an array of two cross polarized antennas at 3.5 GHz," in *Proc. IEEE 70th Vehicular Technology Conference Fall (VTC)*, Sep. 2009, doi: 10.1109/VETECF.2009.5378996.

[283] D. A. Thushara, A. K. Rodney, and T. Jaunty, "On capacity of multi-antenna wireless channels: Effects of antenna separation and spatial correlation," in *3rd Australian Communications Theory Workshop (AusCTW)*, Feb. 2002. URL: http://citeseerx.ist.psu.edu/viewdoc/download?doi=10.1.1.18.6688&rep=rep1&type=pdf

[284] Q. T. Tran, S. Hara, A. Honda, Y. Nakaya, I. Ida, and Y. Oishi, "A receiver side antenna selection method for MIMO-OFDM system," *in Proc. 64th IEEE Vehicular Technology Conference (VTC 2006 Fall)*, pp. 1–5, Sep. 2006, doi: 10.1109/VTCF.2006.103.

[285] U. Trautwein, C. Schneider, and R. Thomä, "Measurement-based performance evaluation of advanced MIMO transceiver designs," *EURASIP Journal on Applied Signal Processing*, vol. 2005, no. 11, pp. 1712–1724, 2005, doi: 10.1155/ASP.2005.1712.

[286] Y. N. Trivedi and A. K. Chaturvedi, "Performance analysis of Alamouti scheme with transmit antenna selection in MISO systems," in *National Conference on Communications (NCC)*, 2010, pp. 1–5, doi: 10.1109/NCC.2010.5430237.

[287] F. J. Vázquez-Araújo, "Design of serially-concatenated LDGM codes," Ph.D. dissertation,

University of A Coruña, Oct. 2008. URL: https://www.educacion.es/teseo/mostrarRef.do?ref= 514926

[288] F. J. Vázquez-Araújo, M. González-López, L. Castedo, and J. Garcia-Frfas, "BICM for MIMO channels using LDGM codes and sphere detection," in *Proc. IEEE 5th Workshop on Signal Processing Advances in Wireless Communications (SPAWC)*, Jul. 2004, pp. 313–317, doi: 10.1109/SPAWC.2004.1439255.

[289] F. J. Vázquez-Araújo, M. González-López, L. Castedo, and J. Garcia-Frias, "Serially-concatenated LDGM codes for MIMO channels," *IEEE Transactions on Wireless Communications*, vol. 6, no. 8, pp. 2860–2871, Aug. 2007, doi: 10.1109/TWC.2007.05651.

[290] J. M. Vazquez Burgos, E. Gago-Cerezal, V. A. Gracia, and L. M. Campoy Cervera, "DEMIURGO, an SDR testbed for distributed MIMO," in *Proc. 3rd International Symposium on Wireless Communication Systems (ISWCS)'06*, Valencia, Spain, Sep. 2006, pp. 210–213, doi: 10.1109/ISWCS.2006.4362289.

[291] J. Vía, "Estima e igualación ciega de canales MIMO con y sin redundancia espacial," Ph.D. dissertation, University of Cantabria, Jul.

[292] J. Via and I. Santamaria, "On the blind identifiability of orthogonal space time block codes from second-order statistics," *IEEE Transactions on Information Theory*, vol. 54, no. 2, pp. 709–722, Feb. 2008, doi: 10.1109/TIT.2007.913561.

[293] J. Via, I. Santamaria, J. Perez, and D. Ramirez, "Blind decoding of MISO-OSTBC systems based on principal component analysis," in *Proc. IEEE International Conference on Acoustics, Speech and Signal Processing (ICASSP)*, May 2006, doi: 10.1109/ICASSP.2006.1661026.

[294] C. Waldschmidt, C. Kuhnert, S. Schulteis, and W. Wiesbeck, "Analysis of compact arrays for MIMO based on a complete RF system model," in *IEEE Topical Conference on Wireless Communication Technology*, Oct. 2003, pp. 286–287, doi: 10.1109/WCT.2003.1321527.

[295] J. Wallace, B. Jeffs, and M. Jensen, "A real-time multiple antenna element testbed for MIMO algorithm development and assessment," in *IEEE Antennas and Propagation Society International Symposium*, vol. 2, Jun. 2004, pp. 1716–1719, doi: 10.1109/APS.2004.1330527.

[296] M. Wenk, P. Luethi, T. Koch, P. Maechler, N. Felber, W. Fichtner, and M. Lerjen, "Hardware platform and implementation of a real-time multi-user MIMO-OFDM testbed," in *IEEE International Symposium on Circuits and Systems (ISCAS)*, May 2009, pp. 789–792, doi: 10.1109/ISCAS.2009.5117872.

[297] A. Wilzeck, M. El-Hadidy, Q. Cai, M. Amelingmeyer, and T. Kaiser, "MIMO prototyping test-bed with off-the-shelf plug-in RF hardware," in *IEEE Workshop on Smart Antennas*, Ulm, Germany, 2006.

[298] A. Wilzeck, P. Pan, and T. Kaiser, "Transmit and receive antenna subset selection for MIMO SC-FDE in frequency selective channels," *Proc. European Signal Procesing Conference (EUSIPCO)*, Sep. 2006.

[299] J. H. Winters, "On the capacity of radio communication systems with diversity in a Rayleigh fading environment," *IEEE Journal on Selected Areas in Communications*, vol. 5, no. 5, pp. 871–878, Jun. 1987.

[300] M. Wouters, T. Huybrechts, R. Huys, S. D. Rore, S. Sanders, and E. Umans, "PICARD: platform concepts for prototyping and demonstration of high speed communication systems," in *Proc. 13th IEEE International Workshop on Rapid System Prototyping (RSP 2002)*, Darmstadt, Germany, Jul. 2002, pp. 166–170, doi: 10.1109/IWRSP.2002.1029753.

[301] W. Xiang, P. Richardson, B. Walkenhorst, X. Wang, and T. Pratt, "A high-speed four-transmitter four-receiver MIMO OFDM testbed: Experimental results and analyses," *EURASIP Journal on Applied Signal Processing*, vol. 2006, Article ID 45401, p. 10, 2006, doi: 10.1155/ASP/2006/45401.

[302] C. M. Yetis, T. Gou, S. A. Jafar, and A. H. Kayran, "Feasibility conditions for interference alignment," in *Proc. IEEE Global Telecommunications Conference (GLOBECOM)*, Nov. 2009, pp. 1–6, doi: 10.1109/GLOCOM.2009.5425326.

[303] J. Ylioinas, K. Hooli, K. Kiiskila, and M. Juntti, "Interference suppression in MIMO HSDPA communication," in *Proc. 6th Nordic Signal Processing Symposium (NORSIG)*, 2004, pp. 228–231.

[304] H. Yu, M.-S. Kim, E. young Choi, T. Jeon, and S. kyu Lee, "Design and prototype development of MIMO-OFDM for next generation wireless LAN," *IEEE Transactions on Consumer Electronics*, vol. 51, no. 4, pp. 1134–1142, Nov. 2005, doi: 10.1109/TCE.2005.1561835.

[305] X. N. Zeng and A. Ghrayeb, "Performance bounds for combined channel coding and space-time block coding with receive antenna selection," *IEEE Transactions on Vehicular Technology*, vol. 55, no. 4, pp. 1441–1446, Jul. 2006, doi: 10.1109/TVT.2006.877459.

[306] P. Zetterberg, "Software and hardware support functionality for first selection of schemes to be implemented," Royal Institute of Technology (KTH), Stockholm, Tech. Rep. COOPCOM project. Number: D3.1., 2007. URL: http://www.coopcom.eu.org/public_deliverables.php

[307] H. Zhang, A. F. Molisch, and J. Zhang, "Applying antenna selection in WLANs for achieving broadband multimedia communications," *IEEE Transactions on Broadcasting*, vol. 52, no. 4, pp. 475–482, Dec. 2006, doi: 10.1109/TBC.2006.884831.

[308] X. Zhang, A. F. Molisch, and S.-Y. Kung, "Variable-phase-shift-based RF-baseband codesign for MIMO antenna selection," *IEEE Transactions on Signal Processing*, vol. 53, no. 11, pp. 4091–4103, Nov. 2005, doi: 10.1109/TSP.2005.857024.

[309] X. Zhao, J. Kivinen, P. Vainikainen, and K. Skog, "Propagation characteristics for wideband outdoor mobile communications at 5.3 GHz," *IEEE Journal on Selected Areas in Communications*, vol. 20, no. 3, pp. 507–514, Apr. 2002, doi: 10.1109/49.995509.

[310] K. Zheng, L. Huang, G. Li, H. Cao, W. Wang, and M. Dohler, "Beyond 3G evolution," *IEEE Vehicular Technology Magazine*, vol. 3, no. 2, pp. 30–36, Jun. 2008, doi: 10.1109/MVT.2008.923968.

[311] L. Zheng and D. N. C. Tse, "Diversity and multiplexing: a fundamental tradeoff in multiple-antenna channels," *IEEE Transactions on Information Theory*, vol. 49, no. 5, pp. 1073–1096, May 2003, doi: 10.1109/TIT.2003.810646.

[312] W. Zhong and J. Garcia-Frias, "LDGM codes for channel coding and joint source-channel coding of correlated sources," *EURASIP Journal on Applied Signal Processing*, vol. 2006, no. 6, pp. 942–953, 2005, doi: 10.1155/ASP.2005.942.

[313] W. Zhu, D. Browne, and M. Fitz, "An open access wideband multiantenna wireless testbed with remote control capability," in *Proc. First International Conference on Testbeds and Research Infrastructures for the Development of Networks and Communities (Tridentcom 2005)*, Trento, Italy, Feb. 2005, pp. 72–81, doi: 10.1109/TRIDNT.2005.12.

[314] X. Zhu and D. Yuan, "Performance analysis of adaptive modulation in MIMO system using transmit antenna selection with Alamouti scheme," in *Proc. 4th International Conference on Wireless Communications, Networking and Mobile Computing (WiCOM)*, 2008, pp. 1–4, doi: 10.1109/WiCom.2008.118.